Aléa sismique et gravitaire en zone de montagne : application au Cachemire (Pakistan)

Mohammad Tahir

Aftershock properties and its triggering mechanism

Lucilla de ARCANGELIS
Department of Information Engineering and CNISM, Second University of Naples, Rapporteur
Alon ZIV
Ben-Gurion University of the Negev, Rapporteur
David MARSAN
ISTerre, Université de Savoie, Examinateur
Clement NARTEAU
IPGP, Paris, Examinateur
Jean-Robert GRASSO
ISTerre, Grenoble, Directeur de thèse
Michel BOUCHON
ISTerre, Grenoble, Co-directeur de thèse

Aftershock properties and

its triggering mechanism

Abstract

On the last decades, progresses on the understanding of clustering seismicity in time, size and space have been driven by two parallel approaches. From the one hand studies on the mechanics of faulting in an elastic medium argue for the static stress triggering to dominate in the near field, i.e within distance less than 10 fault length. From the other hand, mean field properties of the triggering are reproduced using cascading effects in point process models. In this study we try to reconcile these approaches by emphasizing the importance of faulting style on average properties of seismicity. Starting with the study of the seismicity rate triggered by the Muzaffarabad, Kashmir, 2005 $M_w = 7.6$, $M_s = 7.7$ earthquake, which appears as above the average when analysing the aftershocks sequences in the India-Asia collision belt, we resolve the strike slip event productivity to be on average 4 times smaller than the thrust faulting productivity. Using global earthquake catalog, we further extend this result as all the parameters of the Omori law (p, K, α, $N(t)$) being dependent on faulting styles. Within the ETAS model strong K, N and low α values are driven by high branching ratio (n). As consequences of the relative high $n - value$ of the thrust events, it also predicts a lower $p - value$ for thrust event as compare to strike slip and normal events as the $p_N > p_{SS} > p_T$ we observe. Within rate and state friction framework it implies a change in stress heterogeneity patterns. We do not resolve any robust changes in foreshocks rate, $p' - value$, whereas our analysis allow us to extend Båths law in time, space and focal mechanism. For reverse faults, both the magnitude difference and the distance from the mainshock to the largest aftershock are somewhat less than for strike slip faults. The distribution of time intervals between mainshocks and their

largest aftershocks is consistent with Omori's law but with a somewhat faster rate of decay than for aftershocks in general. This implies that the largest aftershock is more likely to occurs earlier than later in a given sequence of aftershocks. Moreover, this finding argues for going beyond the branching point model, with implications for short term forecasts. Also we resolve unambiguous dependency of $p - value$ of Omori law to mainshock magnitude for the aftershock within 10 days after the mainshock occurrence, this dependency being lost when using complete cascade sequences. We find this time threshold also corresponds to a change in diffusion patterns, all these changes synchronize with the occurrence of the largest aftershock. Accordingly, our results converge toward the key role of the secondary aftershocks on the mechanics of size, time and space pattern of cascading processes.

Résumé

Au cours des dernières décennies, des progrés ont été réalisés sur la compréhension des répliques de séismes dans les domaines spatio-temporels. D'une part des études sur la mécanique dune faille dans un milieu élastique montrent que le déclenchement statique domine le déclenchement des répliques dans le champ proche, i.e., une distance de moins de 5-10 $*L$, (L, longueur de la faille sismique). D'autre part les propriétés du champ moyen du déclenchement sont reproduites à l'aide de cascade dans des modèles de branchement. Au cours de cette thése, nous avons tenté de concilier ces 2 approches en mettant en évidence l'importance du type de faille sur les propriétés moyennes de la sismicité déclenchée, i.e. les répliques de séismes. En commenant par l'étude du taux de sismicité déclenché par le séisme de Muzaffarabad, au Cachemire, 2005, Mw = 7.6, ce dernier apparaissant comme un évènement extrme, par comparaison avec les séquences de répliques des grands séismes de la collision Inde-Asi, on est amené à montrer que la quantité de répliques produites par les failles inverses dans cette collision est en moyenne 4 fois supérieure à celle produite par les séismes en coulissage. En utilisant le catalogue de sismicité global, nous étendons ce résultat à tous les paramètres de la loi d'Omori ($N(t) = \frac{K}{(c+t)^p}$, $N(t)$ taux de répliques), montrant que ces derniers dépendent du type de mécanisme au foyer. Dans un modéle de cascade par branchement (ETAS), la dépendance du taux de répliques au mécanisme au foyer est pilotée par le taux de branchement. Ce taux de branchement, supérieur pour les séismes en faille inverse, prédit aussi la faible valeur observée de l'exposant p de la décroissance en fonction du temps du taux de répliques (loi d'Omori) pour les séismes en faille inverse $p_N > p_{SS} > p_T$. Dans un modele de la frottement rate and state, nos observations sont

correspondent à un changement dans les hétérogénéités de contraintes induites par les différents types de mécanismes aux foyers. Notre analyse nous permet aussi de prédire les propriétés des plus fortes répliques dans le temps et l'espace (extension de la loi de Bath) en fonction du mécanisme au foyer du choc principal. Pour des failles inverses, la différence de magnitude et la distance entre le choc principal et la plus grande réplique sont plus petites que pour les séismes en coulissage. La distribution des intervalles de temps entre le choc principal et leur plus forte réplique est elle aussi en loi de puissance. Ceci implique que la plus grande réplique est plus susceptible de survenir plus tt que plus tard dans une séquence de répliques. Par ailleurs, la dépendance au mécanisme au foyer du choc principal suggére d'aller au-delà des modèles de branchement ponctuel, avec des implications pour les prévisions à court terme. Nous trouvons aussi une dépendance (univoque) de la valeur p de la loi d'Omori à la magnitude du choc principal, pour les 10 jours suivant le choc principal, cette dépendance étant perdue lors de l'utilisation des séquences de répliques complète. Nous trouvons également que cette limite en temps (occurrence de la réplique majeure) correspond à un changement dans les schémas de diffusion. Ces changements étant synchrone de l'apparition de la plus forte réplique, nos résultats convergent vers le rôle clé de la plus forte réplique, comme brisure spatio-temporel majeure dans le processus en cascade utilisé pour simuler la sismicité.

Acknowledgement

First and foremost I want to thank my advisor Dr. Jean Robert Grasso. I appreciate all his contributions of time, ideas, and funding to make my Ph.D. experience productive and stimulating. The joy and enthusiasm he has for his research was contagious and motivational for me, even during tough times in the Ph.D. pursuit. I am also thankful for the excellent example he has provided as a successful physicist and professor.

I am also indebted to Dr. Michel Bouchon who co-supervised this work. His advice and effective guidance was always source of motivation. Without his extended help and guidance this research work was far to complete successfully.

The members of the mécanique des failles group have contributed immensely to my personal and professional time at Isterre. The group has been a source of friendships as well as good advice and collaboration. I am especially grateful of: David marsan, David Amitrano, François Thouvenot and Mai-Linh Doan for scientific discussion with them. Especially David Marsan suggestions and discussion are very helpful in advancing this work. I would like to acknowledge other past and present students of Jean Robert Grasso that I have had the pleasure to work with, Agnès Helmstetter, Lucille Tatard, Paola Traversa, Daniel Amorese, Lacroix pascal and Agathe Schmid. I am especially grateful for conversations with Agnès Helmstetter as she help me and provide me her code for ETAS simulation.

In my attempted of corrections of this work, i thank the following people for helpful discussions with us: Virginie Durand, Andrew Rathbun, Julie Richard and Abbas.

For this dissertation I would like to thank my reading committee members: Lucilla de

Contents

General introduction

Large earthquakes and burst of its aftershock are threat to society and human beings. They are rare due to their low recurrence rates but most of them are highly hazardous giving up to approximately 50 percent of the total loss in human life and 30 percent of economic losses over the last 50 years (Woessner and Wiemer (2005)). The October 2005, Kashmir earthquake caused severe damage to cultivable land, physical infrastructure, social infrastructure, provision of public goods, water quality and its sources, sanitation and sewerage, health and nutrition in the Azad Jammu & Kashmir and northern area of Pakistan. The total economic loss due to damage and destruction is estimated to be about U.S. $5 billion (Maqsood and Schwarz (2010)). More than 73,000 people lost their lives, with another 128,000 people injured during the earthquake (according to the National Disaster Management Authority of Pakistan (NDMA 2007), http://ndma.gov.pk).

Scientists, engineers and decision makers are responsible to mitigate earthquake risk in order to reduce casualties and financial losses in future. The most important from a scientific point of view, is understanding the physics of the earthquake, its triggering mechanism and implementation of triggering dependent hazard models in seismic risk area. To contribute scientific efforts to these hazard models, statistical methods based on spatio-temporal analysis of near field seismicity have been modified, improve link between earthquake physics and triggering mechanism, which may further used in earthquake prediction models.

As it is difficult to deal all problems of hazard models, we focus on earthquake triggering mechanism considering larger earthquakes and its clustered quakes that is aftershock which

sometime pose more hazard than the mainshock, because of its broad range of frequencies, different sizes and occurred in hugh number in very small time. Aftershocks define regions which failed during earthquake and further suggest the details of fault complexity (e.g., Reasenberg and Ellsworth (1982); Okubo and Aki (1987)). The principles questions to be address in this research were;

- Which spatio-temporal parameters control aftershocks productivity ?

- Is clustered seismicity parameters dependent on faulting style ?

- When, how far and where the strongest aftershock occur ?

- Is the largest aftershock controlling diffusion regimes ?.

- Is there any magnitude dependency of p, $\alpha - value$, duration and stress heterogeneity.

- Is global aftershocks triggering mainly driven by static or dynamic mechanism?

Earthquakes are the brittle response of the earth crust to the applied stresses (e.g, Lee (2003); Rundle et al. (2003)). Significant deformations are required to develop a fracture in the brittle environment (Lee (2003)). Deformation across these fractures generates faults (Lee (2003)). Clearly these faults or fractures processes in the earth crust are complex and occur on a wide range of scales (e.g., Mandelbrot (1983)). In general, the seismically active regions are dissected by a number of fault arrays which exhibit fractal statistics both in the distribution of surface roughness and in their length distribution (e.g., Okubo and Aki (1987)). Kagan (1993) further suggested that earthquakes occurs on a fractal structures of many closely related faults rather than single fractal. One approach to earthquake analysis is to assume the slips and displacements on a a single active fault in a region rather than considering all faults. Under this assumption, great earthquakes on the master fault occur on a periodic basis and the period of no earthquake is called as seismic gaps. An alternative approach to earthquake mechanics is to assume that the crust is a complex self-organizing system that can be treated by statistical techniques (e.g., Lee, 2003).

Aftershocks are the common observation after every large earthquakes. Generally every earthquake interacts with other structures by applying some load on neighboring and far faults, which eventually rupture. Relaxation of tectonic strain is therefore complex and involves large sets of different size of earthquakes, over spatial and time scale (Marsan (2003)). Numerous physical models have been proposed to explain earthquake triggering process (e.g., Scholz, 1968; Nur and Booker, 1972; Stein and Lisowski, 1983; Oppenheimer et al., 1988; Mendoza and Hartzell, 1988; Reasenberg and Simpson, 1992b; Stein et al., 1992; King et al., 1994; Boatwright and Cocco, 1996; Stein et al., 1997; Dieterich, 1994; Gomberg et al., 1998; Harris, 1998; Kagan and Jackson, 1998; Stein, 1999; Toda et al., 1998; Gomberg et al., 2000; Toda and Stein, 2000; Freed and Lin, 2001; Gomberg et al., 2001b; Kilb et al., 2002; Helmstetter et al., 2002; Steacy et al., 2005; Toda et al., 2005). Generally aftershocks triggering mechanism has been modeled by using either static stress transfer calculation, in which aftershocks occur in area of positive co-seismic stress changes (King et al., 1994; Stein, 2003), or dynamic triggering process, caused by passing seismic waves (Voisin, 2002; Perfettini et al., 2003), or relaxation due to viscoelastic effects (Romanowicz, 1993; Piersanti et al., 1995, 1997; Zeng, 2001), or rate and state friction model (Dieterich (1994)), and damage rheology (Ben-Zion and Lyakhovsky (2006)). Hence, at short time scale both dynamic and static stress changes are very important while at large time scale visco-elastic changes may lead to temporally delayed earthquakes occurrence. Other factors such as rupture type and small scale slip heterogeneity may also have effect on the resultant seismicity patterns (e.g., Marsan (2006))

The triggering of the another large earthquake can happen rapidly, such as in case of Big bear earthquake following only one hour after the Lander earthquake or several decades such as Kobe earthquake thought to have been triggered by 1944, Tonankai and 1946, Nankaido earthquakes (e.g., Pollitz and Selwyn Sacks (1997); Freed (2005)). Because of this complexity, there is a clear need in earthquake physics for more integrative observations, modeling, and statistical analyses. Understanding the earthquake triggering models will greatly help us to provide the inside physics of the earthquakes cycle and most importantly, may greatly help our ability of seismic hazard mitigation by pointing the zone where the

next large earthquake may occur (e.g., Freed (2005)). Physics-based models are useful to understand the physical processes, while statistical earthquake models can be very successful in fitting observed data.

The interdependence of spatio-temporal parameters of aftershocks and its systematic changes with various tectonics has been observed in many studies (e.g., Wiemer and Katsumata, 1999; Schorlemmer et al., 2005; Narteau et al., 2009; Peixoto et al., 2010). Based on these findings, i have dedicated a large fraction of my thesis work to develop some correlations of spatio-temporal parameters of aftershocks test their dependency on the rake angle and under the nature of triggering mechanism.

The main motivation of chapter 1, is to find answer for the highest aftershocks productions of Kashmir, 2005 earthquake, when compare with larger ($M_s \geq 7.0$) aftershock sequences occurred nearly 20° around the Kashmir earthquake epicenter. Normalized rate, duration, Omori law parameters and average aftershock density of 18 aftershock sequences, have been calculated. Correlations between these parameters have been tested, when there is an open debate on this topics. Dieterich (1994) and Ziv (2006a) show that duration is independent of mainshock magnitude but higher for large events as compare to smaller one. In contrast Marsan and Lengline (2008) observed that duration of aftershocks sequence is very well correlated with mainshock size for dressed aftershocks of the sequences. Drakatos and Latoussakis (2001) resolve a similar correlation between duration and mainshock size using Greece data. Dependency of spatio-temproal parameters on faulting styles are also being observed although we use 18 aftershock sequences, which consist 4 strike slip, 13 thrusts and 1 normal events. This work has been submitted in *Bulletin of the Seismological Society of America*.

In chapter 2, i apply role of faulting style as that observed for small data scale in chapter (1) with to change, develop and update on global scale data. Schorlemmer et al. (2005) show that b-value is dependent on faulting style, using California and Global data. In similar way Gulia and Wiemer (2010) use Italy data and show that earthquake size is dependent on rake angle. Narteau et al. (2009) show that c-value is dependent on rake angle of the fault, but there is no model for aftershock production, $p-value$ and rate.

Like b-value, $p - value$ is also strongly effected by the mechanism of stress relaxation and frictions laws in seismogenic zone (Mikumo and Miyatake (1979); Dieterich (1986)).

I show, average values of different spatio-temporal parameters (rate, p, $K - value$ and H) are dependent on faulting styles. Thrust events have higher diffusion, rate, duration and background rate as compare to strike slips events. Higher duration in the environment of high background rate is driven by high branching ratio and low $p - value$ of thrust events as compare to that of strike slip. For normal events to limited data we only analysis its $p - value$. Which has highest $p - value$ as compare to other faulting styles. Density rate diffusion of thrust events are different as compare to strike slips events, which further implies different diffusion of faulting styles. This work has been submitted in *Journal of Geophysical Research*.

In chapter 3, we analyse largest aftershock patterns. Average magnitude ΔM, time ΔT and normalize distance ΔD^* between mainshock and its corresponding largest aftershock is independent of mainshock magnitude. The largest aftershock is bounded on average by -1.2 magnitude from the mainshock. Thirty years of the global earthquake catalogue allow us to extend Båth's law in the time and space domains, as the largest aftershocks are closer in size (mode value : $\Delta M_r = 0.95$, $\Delta M_{ss} = 1.51$) and distance (mode value : $\Delta D_r^* = 0.11$, $\Delta D_{ss}^* = 0.22$) to the triggering shock, for ($_r$) reverse slip than for ($_{ss}$) strike slip events. The faster power law decay in time relative to regular aftershocks implies that the largest aftershocks are more prone to occur at the onset of any aftershock sequence. This pattern is the only to be reproduced by a branching point model. This work has been submitted in *Geophysical Research Letters*.

In chapter 4, We analysis spatio-temporal parameters of the global stacked data. Aftershocks productivity increases with that of mainshock magnitude $\sim 10^{\alpha m}$, with $\alpha = 0.82 \pm 0.06$. $p - value$ is a function of mainshock magnitude for direct aftershock, whereas correlation is lost when we have both direct and indirect aftershock. Duration has a positive correlation with mainshock magnitude. Stress step and duration decreases as distance from mainshock increases. We also observed that linear density obeys power law and its peak density distance from the mainshock is dependent on mainshock size. We resolve

static stress triggering is the main responsible mechanism for global earthquake triggering process. This work has been submitted in *Journal of Geophysical Research.*

In chapter 5, We analyzed Omori's law exponent ($p - value$ from $N(t) = \frac{K}{(t+c)^p}$) and diffusion exponent (H from $R(t) = t^H$) of foreshocks and aftershocks. $p - value$ of the stack aftershocks is higher than that of the foreshocks, whereas the same pattern observed for the decay slope of linear density.

Previously, earthquake scale invariance are shown either in space or in time. But limited or negligible work has done on scale invariance of both time and space. This link between space and time would help us in better understanding the triggering mechanism of the fault systems. We observe that seismicity rate (number/km/day) as a function of distance obey as power law ($\Phi(t) \sim \frac{1}{(d+r)^{1+\mu}}$). The exponent μ decreases and finally reaches to the background level at long time (> 2000 day) window with $\mu \sim 0$. Aftershocks density rate (number/km/day) expansion toward the background is slower as compare to the foreshocks inverse expansion (from background toward the mainshock). Initially (upto 5 days), aftershocks migrate slowly away from the mainshock than that of the foreshocks ($H_{aft.} = 0.07$ and $H_{fore.} = 0.20$). But for time (> 5 days) contemporary to the occurrence of largest aftershock, the migration of aftershocks becomes fast ($H_{aft.} = 0.38$). Linear density show aftershock diffusion that is different from that of foreshock, whereas background have nearly same value of the exponent. This work will be submitted in *Geophysical Research Letters.*

INTRODUCTION GÉNÉRALE

Les grands séismes et leurs répliques sont une menace pour la société et les êtres humains. Ils sont rares en raison de leur faible récurrence, mais la plupart d'entre eux sont très dangereux, causant environ 50 pour cent de la perte totale dans des la vie humaine et 30 pour cent des pertes économiques au cours des 50 dernières années (Woessner and Wiemer (2005)). Le séisme d'octobre 2005, au Cachemire a gravement endommagé les terres cultivables, les infrastructures physiques, l'infrastructure sociale, la fourniture de biens publics, la qualité de l'eau et ses sources, les systèteme d'assainissement et d'égouts, de santé et de nutrition dans l'Azad Jammu et Cachemire et la zone nord du Pakistan. Les pertes économiques totales dues à des dommages et des destructions sont estimées à environ 5 milliards dollars américains (Maqsood and Schwarz (2010)). Plus de 73,000 personnes ont perdu la vie, et 128 000 personnes ont été blessées lors du séisme (selon l'Autorité nationale de gestion des catastrophes du Pakistan (NDMA 2007), http://ndma.gov.pk).

Les scientifiques, les ingénieurs et les autorités sont responsables pour atténuer le risque sismique afin de réduire les pertes humaines et financières à l'avenir. Le plus important d'un point de vue scientifique, est de comprendre la physique du tremblement de terre, son mécanisme de déclenchement et de mettre en œuvre des modèles de risque. Pour contribuer à ces efforts scientifiques dans les modèles de risque, les méthodes statistiques basées sur l'analyse spatio-temporelle de la sismicité en champ proche donnent accès un le lien entre la physique et le mécanisme de déclenchement du tremblement de terre, pouvant en outre être utilisé dans les modèles de prévision des séismes.

Comme il est difficile de traiter l'ensemble de la prolemetique du risque, nous nous

concentrons sur le mécanisme de déclenchement du tremblement de terre en considérant les grands tremblements de terre et leurs répliques en essaim, ces devenirs parfois posent plus de risques que le choc principal, en raison de leur large gamme de fréquences, de leurs différentes tailles et du fait leur grand nombre en peu de temps (e.g., Reasenberg and Ellsworth (1982); Okubo and Aki (1987)). Les questions principales lois de cette recherche ont été;

- quel paramétres contrôle la prodcutivité spatio-temporelle des répliques?

- comment les répliques dépendent elles du type de failles?

- Quand, à quelle distance et oú les plus fortes répliques se produisent-elles?

- est-ce que la plus grande réplique contrôle les régimes de diffusion?

- y at-il une dépendance á la magnitude de p, de α, de la durée de et l'hétérogénéité des contraintes.

- est-ce quelle le déclenchant des réliques est contrôlé principalement par un mécanisme statique ou dynamique?

Les tremblements de terre sont la réponse cassante de la croûte terrestre à des contraintes appliquées (e.g., Lee (2003); Rundle et al. (2003)). Les déformations significatives sont nécessaires pour développer une fracture dans l'environnement fragile (Lee (2003)). Les déformations à travers ces fractures génères des hétérogénéité défauts (Lee (2003)). Manifestement, ces tailles ou ces fractures dans la croûte terrestre sont complexes et se produisent sur une large gamme d'échelles (e.g., Mandelbrot (1983)). En général, les régions sismiquement actives sont découpées par un certain nombre de réseaux de failles, qui présentent des statistiques fractales tant dans la distribution de rugosité de surface et dans leur distribution de longueur (e.g., Okubo and Aki (1987)). Kagan (1993) suggère en outre que les séismes se produisent sur les structures fractales de nombreuxs failles étroitement liées plutôt que sur une faille unique. Une approche pour l'analyse des tremblements de terre est de supposer les glissments et les déplacements sur une faille active

unique dans une région plutôt que de considérer toutes les failles. Sous cette hypothèse, les gros séismes sur la faille principale se produisent sur une base périodique et la période durant laquelle il n'y a aucun tremblement de terre est appelée lacune sismique. Une approche alternative à la mécanique du tremblement de terre est de supposer que la croûte est un système complexe auto-organisé qui peut être traité par des techniques statistiques (e.g., Lee (2003)).

Les répliques sont couramment observée après chaque grand tremblement de terre. Généralement chaque tremblement de terre interagit avec d'autres structures en appliquant certaines charges sur les failles voisines et lointaines, qui cassent. La relaxation des contraints tectoniques est donc complexe et implique de grands ensembles de tremblements de terre de taille différente, sur l'échelle spatiale et temporelle (Marsan (2003)). De nombreux modèles physiques ont été proposés pour expliquer le processus de déclenchement des tremblements de terre (e.g., Scholz, 1968; Nur and Booker, 1972; Stein and Lisowski, 1983; Oppenheimer et al., 1988; Mendoza and Hartzell, 1988; Reasenberg and Simpson, 1992b; Stein et al., 1992; King et al., 1994; Boatwright and Cocco, 1996; Stein et al., 1997; Dieterich, 1994; Gomberg et al., 1998; Harris, 1998; Kagan and Jackson, 1998; Stein, 1999; Toda et al., 1998; Gomberg et al., 2000; Toda and Stein, 2000; Freed and Lin, 2001; Gomberg et al., 2001b; Kilb et al., 2002; Helmstetter et al., 2002; Steacy et al., 2005; Toda et al., 2005).

Généralement le mécanisme de déclenchement des répliques a été modélisé en utilisant soit le calcul de transfert de contrainte statique, dans lequel les répliques se produisent dans la zone des changements positifs de la contrainte co-sismique (King et al., 1994; Stein, 2003), ou comment un processus dynamique de déclenchement dynamique, causée par le passage des ondes sismiques (Voisin, 2002; Perfettini et al., 2003), ou par la relaxation due aux effets viscoélastiques (Romanowicz, 1993; Piersanti et al., 1995, 1997; Zeng, 2001), ou le modèle de friction de rate and state ((Dieterich (1994)), et la rhéologie (Ben-Zion and Lyakhovsky (2006)). Ainsi, à courte échelle de temps, à la fois les changements des contraintes dynamiques et statiques sont très importants tandis que à grande échelle les changements viscoélastiques peuvent conduire à l'occurrence de tremblements de terre

temporellement retardée. D'autres facteurs comme le type de rupture et de glissement de petites hétérogénéité d'échelle peuvent aussi avoir un effet sur la distribution des séismes (e.g., Marsan (2006)).

Le déclenchement d'un grande séisme peut arriver rapidement, comme dans le cas du Big bear earthquake, suivant seulement d'une heure le tremblement de terre "Lander" (e.g., Pollitz and Selwyn Sacks (1997); Freed (2005)). En raison de cette complexité, il ya un besoin évident en physique du tremblement de terre d'observations plus intégratives, de modélisation et d'analyses statistiques. Comprendre les modèles de déclenchement va nous aider à déceive la physique du cycle de tremblements de terre et, surtout, peut grandement aider notre capacité d'atténuation des risques sismiques en pointant la zone où le prochain grand tremblement peut se produire (e.g., Freed (2005)). Les modèles basés sur la physiques sont utiles pour comprendre les processus physiques, tandis que les modèles statistiques du tremblement de terre peuvent être très utiles pour extraire des dans les domain taille, space et temp.

L'interdépendance des paramètres spatio temporelles des répliques et de ses changements systématiques avec différentes tectoniques a été observée dans de nombreuses études (e.g., Wiemer and Katsumata, 1999; Schorlemmer et al., 2005; Narteau et al., 2009; Peixoto et al., 2010). Basé sur ces résultats, j'ai consacré une grande partie de mon travail de thèse à développer certaines corrélations spatio-temporelles des paramètres de répliques pour tester leur dépendance à l'angle de glissement et à la nature du mécanisme de déclenchement.

La motivation principale du chapitre 1 est de trouver réponses pour les productions des répliques les plus élevées du tremblement de terre du Cachemire en 2005, comparé aux grandes séquences de répliques ($M_m \geq 7.0$) survenues a près de 20° autour de l'épicentre du tremblement de terre du Cachemire. Les taux normalisés, la durée, les paramètres de la loi d'Omori et la densité moyenne de 18 séquences de répliques, ont été calculés. Les corrélations entre ces paramètres ont été testées, quand il ya un débat ouvert sur ces sujets. En revanche Marsan and Lengline (2008) ont observé que la durée de la séquence de répliques est très bien corrélée avec la taille du choc principal. Drakatos and Latoussakis (2001) résolvent une corrélation similaire entre la durée des réliques et la taille du choc prin-

cipal en utilisant des données de Grèce. Des dépendances des paramètres spatio-temproal aux styles de failles sont également observées, bien que nous utilisions 18 séquences de répliques, qui consistent en quatre coulissage, 13 faille inverse et 1 événement en faille normale. Ce travail a été présenté dans le *Bulletin of the Seismological Society of America*.

Dans le chapitre 2, j'applique le rôle styles de failles à comme observé pour les petits volumes de données dans le chapitre (1) des données à l'échelle mondiale. Schorlemmer et al. (2005) montrent que la $b - valeur$ est dépendante du type de faille, en utilisant la Californie et des données mondiales. De la même manière Gulia and Wiemer (2010) utilisent des données d'Italie montrent et que la taille du tremblement de terre dépend du orientation du glissement sismique. Narteau et al. (2009) montrent que la valeur c est dépendante du rake de langle d'inclinaison de la faille. Il n'existe pas de modèle pour la production des réplique, la valeur p et le taux de rélique. Comme la valeur b, la $p - valeur$ est également fortement affectée par le mécanisme de relaxation les contraintes et des lois de friction dans la zone sismogéne (Mikumo and Miyatake (1979); Dieterich (1986)).

Je montre que les valeurs moyennes des différents paramètres spatio-temporels (taux, p, K et H) sont dépendants des types de failles. Des événements en faille inverse ont une durée, un taux, une sismicité de fond et une diffusion plus élevés, comparé aux événements en coulissage. Les plus grandes durées dans un environnement de bruit de fond élevé sont contrôllées par le fort rapport de branchement et la faille valeur p des événements en faille inverse comparé á des coulissage. La diffusion du taux de densité d'événements en faille inverse est différente de celle des événements coulissage, ce qui implique en outre des diffusions différent suivant le type de faille. Ce travail a été soumis au Journal of Geophysical Research.

Dans le chapitre 3, nous avons analysé les modèles des plus grandes répliques. La magnitude moyenne ΔM, le temps ΔT et la distance normalisée ΔD^* entre le choc principal et sa plus grande réplique sont indépendant de la magnitude du choc principal. La plus grande réplique est limitée en moyenne à -1.2 de la magnitude du choc principal. Trente ans du catalogue des séismes mondiaux nous permettent d'étendre la loi de Båth's dans les

domaines du temps et de l'espace, car les plus grande répliques sont plus proches en taille (valeur mode: $\Delta M_r = 0.95$, $\Delta M_{ss} = 1.51$) et distance (valeur en mode: $\Delta D_r^* = 0.11$, ΔD_{ss}^* $= 0.22$) du choc de déclenchant, pour ($_r$) un glissement inverse que pour des événements en coulissage($_{ss}$). La décroissance rapide de la loi puissance dans le temps par rapport aux répliques régulières implique que les plus grandes répliques sont plus probable au début de n'importe quelle séquence de répliques. Cette observation est le seule à être reproduite par un modèle de point de branchement. Ce travail a été présenté dans Geophysical Research Letters.

Dans le chapitre 4, nous faisons une analyse spatio-temporelle des paramètres des données globales stackées. La productivité de répliques augmente avec la magnitude du choc principal $\sim 10^{\alpha m}$, avec $\alpha = 0.82 \pm 0.06$. La valeur p est fonction de la magnitude du choc principal pour les répliques directes, alors que la corrélation est perdue lorsque nous avons à la fois des répliques directes et indirectes. La durée a une corrélation positive avec la magnitude du choc principal. Nous avons également observé que la densité linéaire obéit à la loi de puissance et que la distance de son pic de densité au choc principal dépend de la taille du choc principal. Nous suggérons que le déclenchement par la contrainte statique est le principal mécanisme responsable des processus de déclenchement des tremblements de terre mondiaux. Ce travail a été soumis au Journal of Geophysical Research.

Dans le chapitre 5, nous avons analysé l'exposant de loi d'Omori ($p - valeur$ de $N(t) = \frac{K}{(t+c)^p}$) et la diffusion de l'exposant (H de $R(t) = t^H$) pour des précurseurs et des répliques. La valeur p des répliques stackées est plus élevée que celle des précurseurs, alors que le même schéma est observé pour la pente de la décroissance de densité linéaire.

Auparavant, l'invariance d'échelle du tremblement de terre a été indiquée dans l'espace ou dans le temps. Le lien entre l'espace et le temps peut nous aider à mieux comprendre le mécanisme de déclenchement des systémes de failles. Nous observons que le taux de sismicité (nombre / km / jour) en fonction de la distance obéit à une loi de puissance ($H(t) \sim \frac{1}{(D+R)}^{1+\mu}$). L'exposant μ diminue et atteind le niveau de fond à long terme ($>$ 2000 jours) avec $\mu \sim 0$. L'expansion de taux de densité de répliques (nombre / km / jour) vers le niveau de fond est plus lent comparé à la contraction des précurseurs (à partir du

niveau de fond vers le choc principal). Initialement (jusqu'à 5 jours), des répliques migrent plus lentement á partir du choc principal que pour les précurseurs ($H_{aft.} = 0.07$ et de $H_{fore.} = 0.20$). Mais pour le temps (> 5 jours) contemporain de l'apparition de la plus grande réplique, la migration des répliques devient rapide ($H_{aft.} = 0.38$). La diffusion linéaire des réplique est différente de celle des précurseurs, alors que la sismicité de fond à presque la même valeur dans les 2 cas. Ce travail sera présenté dans Geophysical Research Letters.

Chapter 1

Aftershocks patterns in the Asian continental collision belt and the Muzafffarabad, Kashmir, 2005, sequence.

M. Tahir [1], JR Grasso[1]

[1]Institut des sciences de la Terre (ISTerre)

University Joseph Fourier - Grenoble I, FRANCE

Abstract

The seismicity rate triggered by the Muzaffarabad, Kashmir, 2005 $M_w = 7.6$, $M_s = 7.7$ earthquake appears as above the average when analysing the aftershocks sequences in the India-Asia collision belt for period of 1973-2008. To quantify this pattern we compare the aftershock patterns triggered by the 18 $M_s \geq 7.0$ earthquakes which occurred in $20°$ latitude and $40°$ longitude box size, centered on the Muzaffarabad (Kashmir, 2005) earthquake epicenter. Such area, stands as the major region in which continental plates interact, worldwide. After normalizing by the mainshock size and by the magnitude range of observation, the $M_s = 7.7$ Kashmir, the $M_s = 7.0$ Khurgu (Iran, 1977) and the $M_s = 7.6$ Southern Xinjiang (China, 1985) aftershocks rates are above the 1-2 standard deviations of the 18 aftershocks rates. We test how Omori's law parameters, background rate, space and time patterns of the sequences interplay to produce the huge aftershock productivity for Kashmir earthquake. This anomaly of Kashmir sequence rate is not driven by a single Omori law parameter. It appears as a combination of many parameters that leads to a relatively longer sequence duration, higher density, in a higher background rate setting (pre stress conditions) than the others western Asia sequences, respectively. For the Khurgu Iran sequence, the anomaly in large rate emerges as driven by a large aftershocks productivity, as measured from the normalized $K - value$ of the Omori law. Also this aftershock cascade develops further away in space, above a two standard deviation significance level, than for the other sequences respectively. Normalization by earthquake sizes allow us to identify anomalies in aftershock sequence, i.e. above two times of standard deviation, for the productivity and rate of Khurgu earthquake, aftershock density for Kashmir sequences, high background rate for Southern Keriya sequence and long duration for Gazli (1976b) and Qaenat earthquakes. The other major result we robustly quantify for Western Asia $M_s > 7.0$ events, is the dependence of aftershock productivity on faulting styles, for all of the Omori law parameters. We resolved the strike slip event productivity to be on average 4 times smaller than the thrust faulting productivity.

Les taux normalisés, la durée, les paramètres de la loi d'Omori et la densité moyenne de 18 séquences de répliques, ont été calculés. Les corrélations entre ces paramètres ont été testées, quand il y a un débat ouvert sur ces sujets. En revanche Marsan and Lengline (2008) ont observé que la durée de la séquence de répliques est très bien corrélée avec la taille du choc principal. Drakatos and Latoussakis (2001) résolvent une corrélation similaire entre la durée des réliques et la taille du choc principal en utilisant des données de Grèce. Des dépendances des paramètres spatio-temproal aux styles de failles sont également observées, bien que nous utilisions 18 séquences de répliques, qui consistent en quatre coulissage, 13 faille inverse et 1 événement en faille normale.

1.1   Introduction

The Muzaffarabad earthquake, October, 8th 2005, Kashmir, Pakistan, $M_w = 7.6$ is one of the rare, if any, Himalayan quakes that produced a surface faulting in the past centuries (Avouac et al. (2006); Grasso and Mughal (2006); Pathier et al. (2006)). It was followed by relatively large number of aftershocks, as compare to the other mainshock ($M_s \geq 7.0$) situated in the Indian-Asia collision belt (figure 1.1). The aftershock activity was particularly intense beyond the NW termination of the fault rupture (Avouac et al. (2006)). The largest aftershock with magnitude ($M_w = 6.5$) occurred on December 12th 2005 and located (latitude = $36.36N$, longitude = $71.09E$) ~ 305 km from the mainshock location. The second largest aftershock with magnitude ($M_w = 6.4$) occurred on the same day of the mainshock and located (latitude = $34.73N$, longitude = $73.10E$) very close (~ 50 km) to the mainshock location. The difference between Kashmir mainshock and its largest aftershock magnitude obeys Båth's law i.e., $\Delta M = 1.2$. We aim to quantify and to understand the specificity of the Muzaffarabad earthquake sequence, by comparing the aftershock spatial and temporal patterns of this event to the one of $M_s \geq 7.0$ events in the surrounding regions. In particular, we seek a physically based relationship between the causative faulting parameters and the aftershocks density in space and time.

Aftershocks production is the brittle response of the crust to the stress or strain, or

stress-strain rate changes triggered by any given earthquake. Because aftershocks exist for every earthquake, it is suggested by this property to go beyond the a-priori definition of foreshock-mainshock-aftershock time dependance as conditioned on the earthquake size (e.g., Helmstetter et al. (2002); Helmstetter and Sornette (2003a)). It is suggested that aftershocks production depend on rock type, ambient temperature and fluid content (Ben-Zion (2008); Yang and Ben-Zion (2009)). Previous studies show that cold continental regions have high aftershock productivity and long duration of aftershock sequences, whereas hot continental regions and oceanic lithosphere have low aftershock productivity and short sequence (e.g., Mogi (1967); Davis and Frohlich (1991); Kisslinger and Jones (1991); Utsu et al. (1995); McGuire et al. (2005)).

In the near field, i.e., within a couple of fault length from the trigger shock, the seismic rate globally increases where the co-seismic stress change, i.e., the Coulomb Stress Change, is positive (Mendoza and Hartzell (1988); Boatwright and Cocco (1996); Stein et al. (1997); Gomberg et al. (1998); Harris (1998); Stein (1999); Gomberg et al. (2000); Toda and Stein (2000); Kilb et al. (2002)). Because of the few bar changes that are resolved to increase the seismicity rate after each given shock, aftershocks are suggested as triggered slips on faults that are already close to instability threshold (Console and Catalli (2005); Ziv (2006a)). Thus in the near field i.e., 1-3 fault length, the static stress change is suggested to drive the aftershock triggering (e.g., Parsons et al. (2006); Hainzl et al. (2010b)). At large distances static stress changes is suggested to be too low to trigger aftershocks (e.g., Hill et al. (1993)) then the distant triggered slips could be related to the dynamic stress changes (Freed (2005); Felzer and Brodsky (2006)).

Reasenberg and Simpson (1992a) show that the aftershocks production rate are dependent on the background rate with using the seismicity rate changes in central California occurring at the time of Loma Prieta earthquake. Similarly Toda et al. (2005) used southern California data for period of 1986-2003, suggest that background seismicity is the key parameter for the aftershock production, coulomb stress changes efficiently being amplified by the background seismicity. These authors validated this model by using Big Bear, Barstow and Hector Mine seismicity which became active immediately after the Landers

earthquake despite experiencing only small static stress increases. Accordingly, small stress changes are suggested to produce large changes in the seismicity rate in the areas of high background seismicity (Toda et al. (2005)). Following Dieterich (1994) using rate and state friction law, the seismicity and background rate are linearly proportional and similar scaling exists between aftershock production and stress step. When the stress step is high, the higher will be the aftershock production and vice versa. The rate of production of earthquake changes through time after a stress step is reproduced by a rate and state friction law (Dieterich (1994)). In this model, the duration of the aftershock sequence, i.e., the time when the aftershock rate decline down to the background seismcity rate, is a characteristic feature of earthquake recurrence time. Dieterich model further shows that aftershock duration is stress step dependent (Dieterich, 1994). Drakatos and Latoussakis (2001) show for aftershock sequences in Greece (1971–1997) that duration and magnitude have correlation even though their residual square is poor, i.e., 30%. In a similar way Marsan and Lengline (2008) show that duration and aftershock production is very well correlated with mainshock magnitude for dressed (direct + indirect) aftershock sequence. Kagan (2002a) correlates the size of aftershock zone with mainshock magnitude (≥ 7.0) using global data, aftershocks being defined as events that occur within 7 days after the mainshock.

In this study we made an attempt toward a comprehensive analysis of aftershocks patterns in space and time for the Kashmir events as compared to the others 17 $M_s \geq 7$ events occurring within thousand kilometer square on the 1973 - 2008 period and centered at the 2005 Kashmir event. We first normalized the aftershock production rate by the mainshock sizes and catalogue completeness. Using these normalized data allows us to cross analyse the density, the rate, the duration and the size of aftershock zone for 18 aftershock sequences. We correlate these parameters with the one of the Omori law, the background rate and the mainshock faulting style. We extract earthquake outliers as event for which parameters are above or below 1-2 standard deviations, as computed for the values of 18 sequences, respectively. Finally we discuss the physical processes that are possible candidates to reproduce the observation.
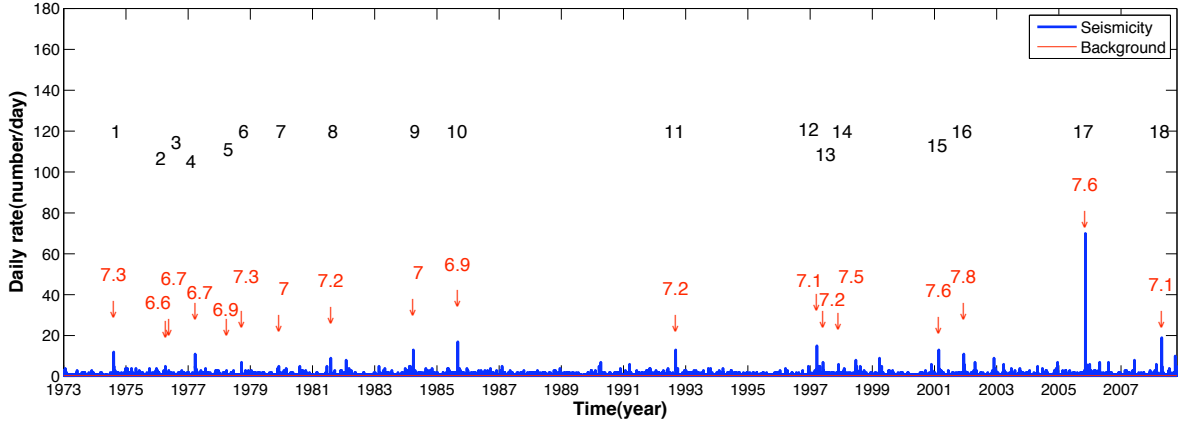
Figure 1.1: Daily seismicity rate, within $\pm$ 10° (latitude) and $\pm$ 20° (longitude), box centered on Kashmir earthquake. Black numbers show the sequence number (table 2.1) and red numbers are mainshock magnitude (M_w). Data are taken from USGS (http://earthquake.usgs.gov)

1.2   Mainshocks and Aftershocks selection

We have selected $M_s \geq 7.0$ earthquakes that are located within 10° of latitude and within 20° longitude relatively to the Muzaffarabad, October 8th 2005 epicenter. Such a box, centered on Kashmir 2005 earthquake, stands as the major region in which continental plates interact, worldwide (figure 1.2). The data we use are from USGS (http://earthquake.usgs.gov) and global harvard CMT catalogs (http://www.globalcmt.org-/CMTsearch.html). For the 18 ($M_s \geq 7.0$) earthquakes in the study area we use as mainshocks, there are large fluctuations between M_s and M_w (figure 1.3, table 2.1).

We used [$\pm$ 5 yr, $5L$] window from the mainshock, to estimate the m_c completeness value of each sequence. The fault length (L) for each event is estimated using Wells and Coppersmith (1994) formula. Then, we impose the aftershock magnitudes to be larger than the completeness m_c value, this later being estimated for each sequence by using maximum curvature technique (Wiemer and Wyss (2000); Woessner and Wiemer (2005)) (figure 1.4, table 1.2). We tested the results are stable on [1, 5, 10]*L set of normalized aftershock distances to the mainshock. On the 18 aftershocks sequences from $M_s \geq 7.0$, 1973-2008, there is one normal, 4 strike-slip and 13 thrust faulting mainshocks, respectively (table 2.1).

One of these events, the Kulun Shan, 2001 earthquake is suggested to have a supershear rupture velocity (Bouchon and Vallée (2003)). This later appears to trigger aftershocks at larger distance from the mainshcoks epicenter and to have only few aftershocks in the epicentral region relatively to the other events (Bouchon and Karabulut (2008)).
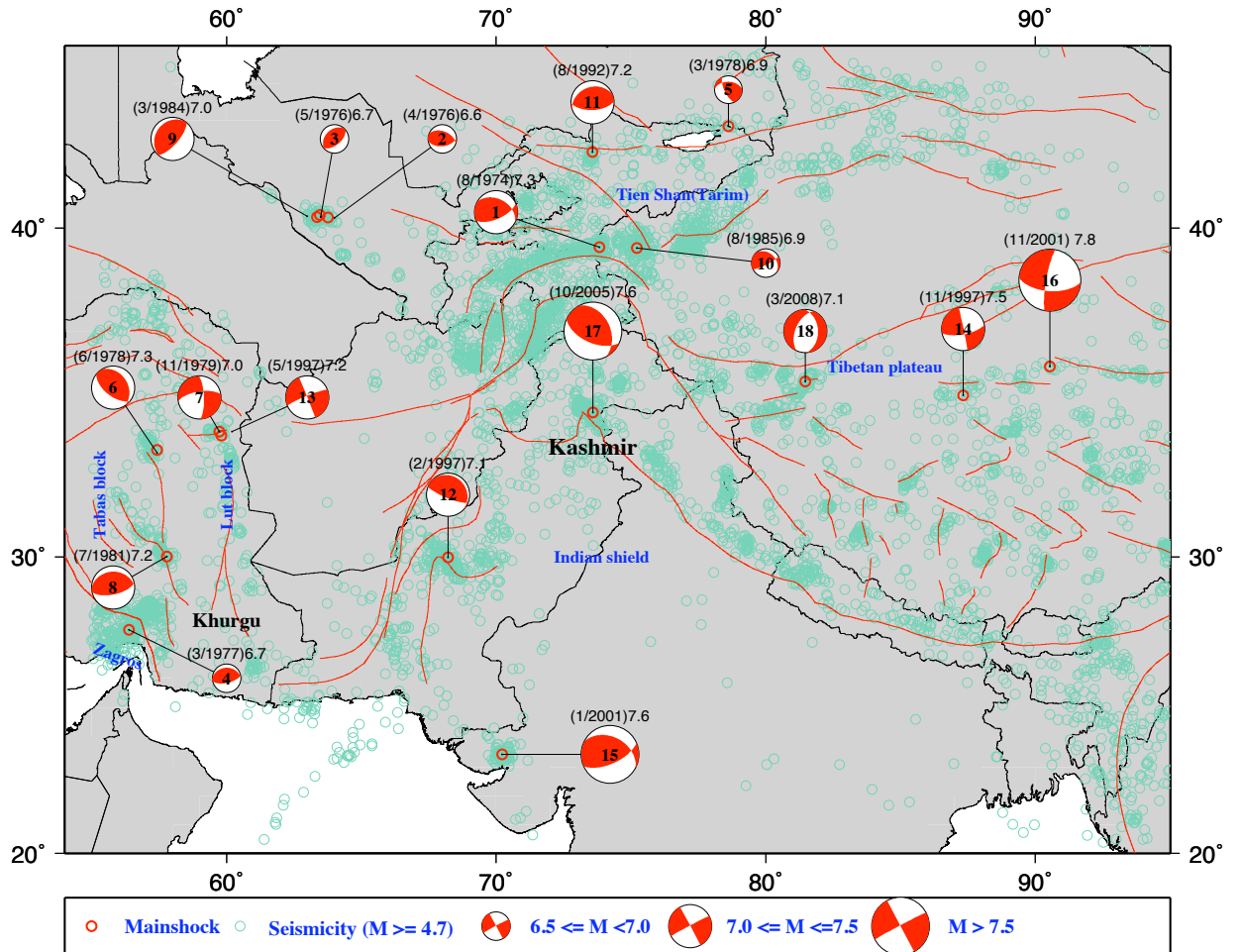
Figure 1.2: Shallow earthquakes with magnitude greater than threshold magnitude($m_c \geq 4.7$) red circle are mainshocks ($M_s \geq 7.0$). Red lines are major faults in the area (Peltzer and Saucier (1996);Hatzfeld and Molnar (2010);Replumaz (1999)). All blue labels are major tectonic blocks (Hatzfeld and Molnar (2010)).

Figure 1.3: M_s (surface wave magnitude) versus M_w (moment magnitude) of 18 major events ($M_s \geq 7.0$) of the Eurasia collision zones with time period of 1973-2008. 1 normal event (red), 13 thrust (blue) and 4 strike slip (green) events are seleceted. Events number are from table 2.1.

Num	Name	Date	Magnitude		Location		Mech	Depth(km)	L(km)	Surface Rupture(km)
			M_s	M_w	Longitude	Latitude				
1	Markansu,Tajikistan	11/08/1974	7.3	7.1	73.83	39.46	Thrust	9	65.6	NI
2	Gazli, Uzbekistan	08/04/1976	7.0	6.6	63.77	40.31	Thrust	33	21.6	No
3	Gazli, Uzbekistan	17/05/1976	7.0	6.7	63.47	40.38	Thrust	10	25.3	No
4	Khurgu, Iran	21/03/1977	6.9	6.7	56.39	27.61	Thrust	29	25.3	No
5	Zhalanash Tyup, Kazakhstan	24/03/1978	7.1	6.9	78.61	42.84	Thrust	33	34.8	NI
6	Tabas, Iran	16/09/1978	7.4	7.3	57.43	33.39	Thrust	33	65.6	85 km[1]
7	Ghanenat(Qaenat), Iran	27/11/1979	7.1	7.0	59.73	33.96	Strike Slip	10	40.7	60 km[2]
8	Sirch(Kerman), Iran	28/07/1981	7.1	7.2	57.79	30.01	Thrust	33	56.0	5 km[3]
9	Gazli, Uzbekistan	19/03/1984	7.0	7.0	63.35	40.32	Thrust	14	40.7	NI
10	Southern Xinjiang, China	23/08/1985	7.6	6.9	75.22	39.43	Thrust	6	34.8	NI
11	Susamyr, Kyrgyzstan	19/08/1992	7.4	7.2	73.57	42.14	Thrust	27	56.0	50 km[4]
12	Quetta, Pakistan	27/02/1997	7.3	7.1	68.21	29.98	Thrust	33	47.8	NI
13	Qaenat, Iran	10/05/1997	7.3	7.2	59.81	33.83	Strike Slip	10	56.0	150 km[5]
14	Mani, China	08/11/1997	7.9	7.5	87.32	35.07	Strike Slip	33	90.2	NI
15	Bhuj, India	26/01/2001	8.0	7.6	70.23	23.42	Thrust	16	105.7	NO
16	Kulun shan, China	14/11/2001	8.0	7.8	90.54	35.95	Strike Slip	10	145.2	400 km[6]
17	Kashmir, Pakistan	08/10/2005	7.7	7.6	73.59	34.54	Thrust	26	105.7	70 km[7]
18	southern Keriya, China	20/03/2008	7.3	7.1	81.47	35.49	Normal	10	47.8	NI

M_s=Surface wave Magnitude
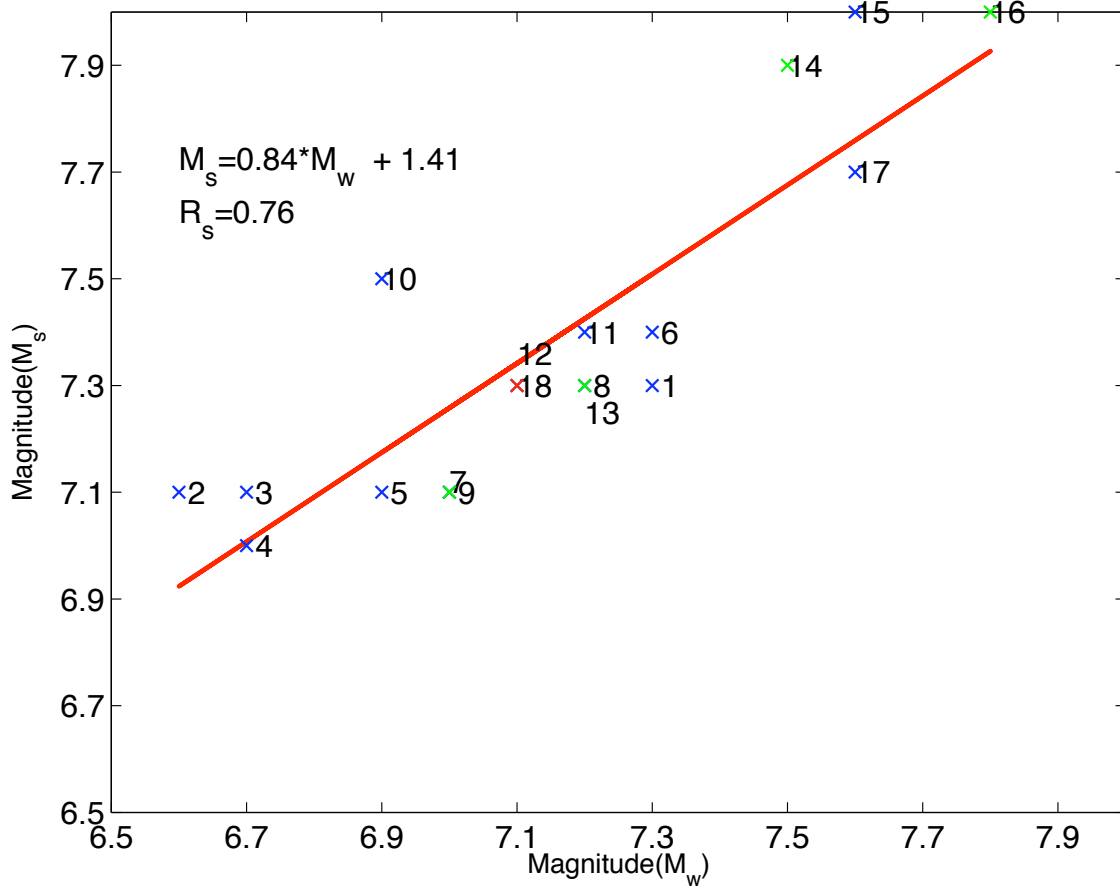M_w= Moment Magnitude
NI = No information available
NO= No Surface rupture observed
Mech=Mechanism
L=Rupture length calculated from Wells and Coppersmith (1994)
Surface Rupture = Surface rupture reported in literature
[1] Berberian (1979),[2] Haghipour and Amidi (1980), [3] Adeli (1982),[4] Ghose et al. (1997),[5] Berberian and Yeats (1999),[6] Lin et al. (2002),[7] Kaneda et al. (2008),

Table 1.1: Mainshocks parameters

1.3 Analysis of aftershock patterns in time and space

1.3.1 Normalised aftershock rate

The number of aftershocks ($m \geq m_c$) for each of the mainshock were calculated using a fixed distance, 5*L (L is fault length calculated from Wells and Coppersmith (1994)) and time window as 24, 48 and 72 hours after the mainshock, respectively. These time windows allow to withdraw any possible finite size effect induced by the difficulty to pinpoint the onset and the end of the aftershocks sequence. The relative ranking of daily rate productivity of the 18 events are stable for 24, 48 and 72 hours respectively (figure 1.5). Always the Kashmir sequence is the most productive. The same analysis is repeated for 1*L and 10*L, but the results are still stable. Number of aftershocks $n(m_m)$ of a mainshock of magnitude (m_m) is proposed as;

$$n(m_m) \sim 10^{\alpha(m_m - m_c)} \qquad (1.1)$$
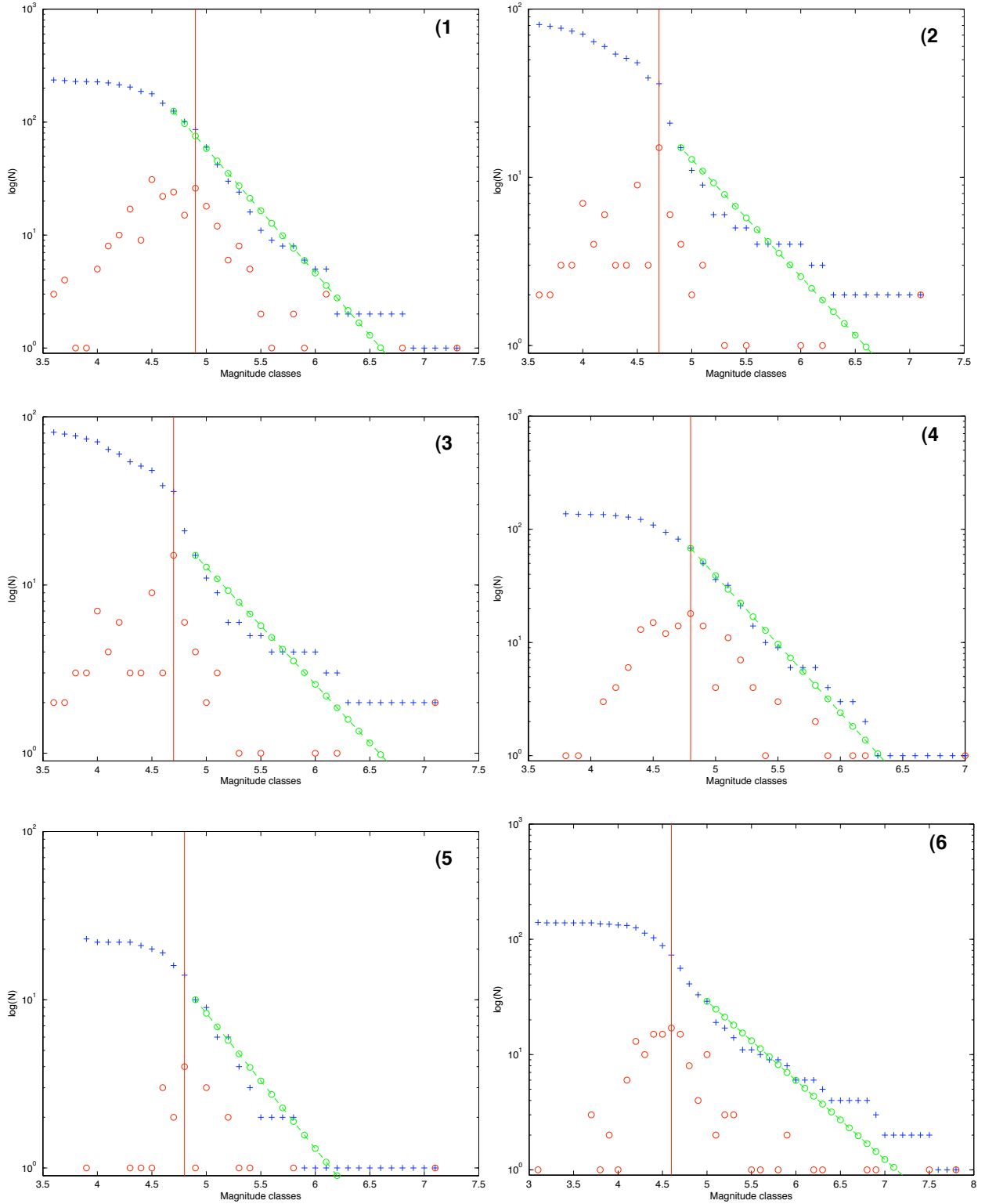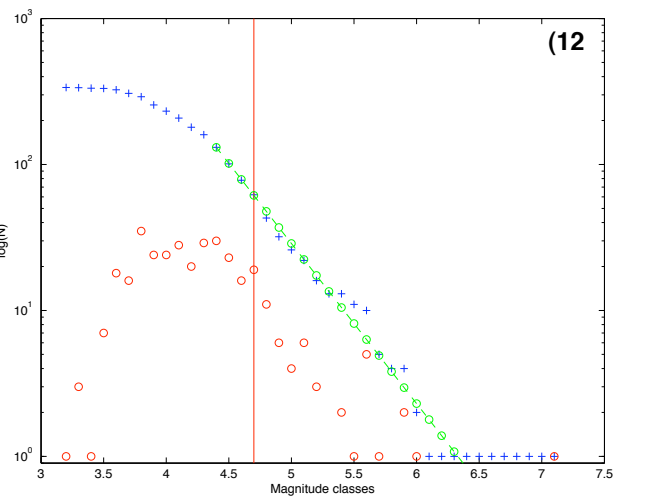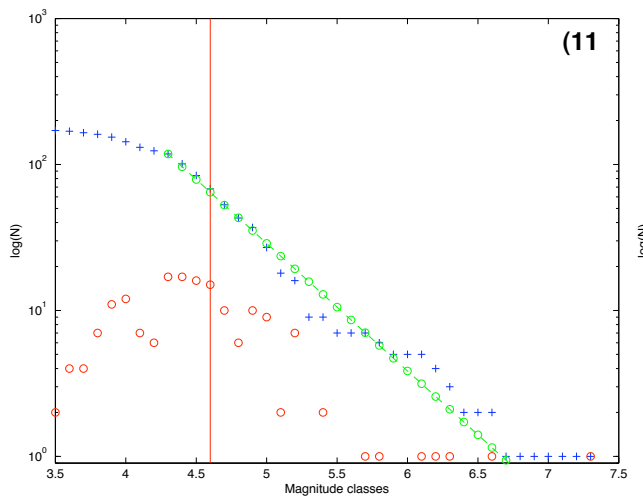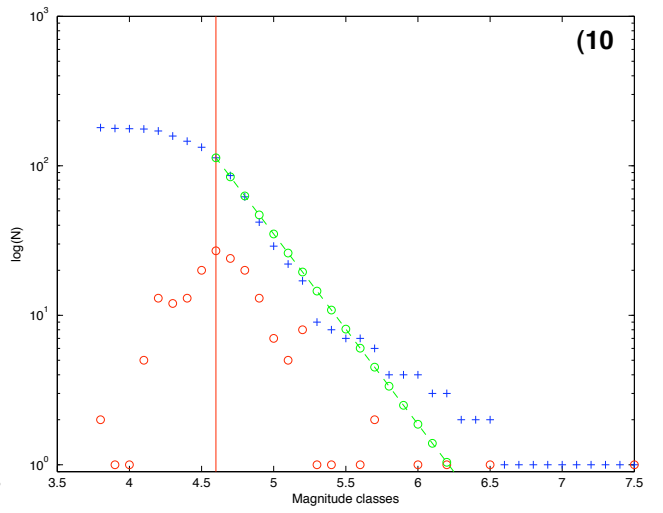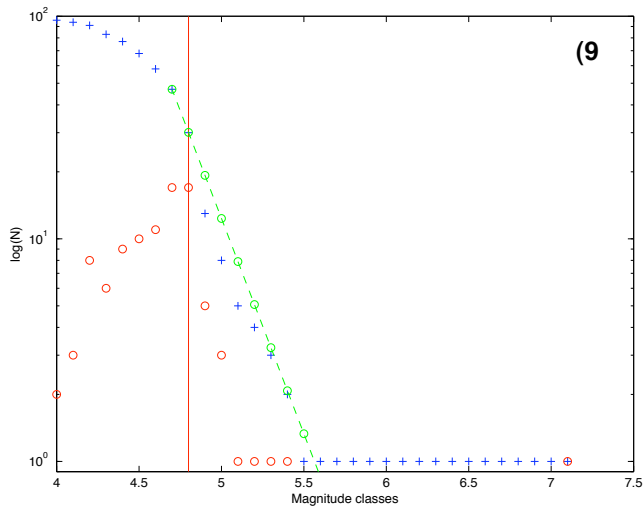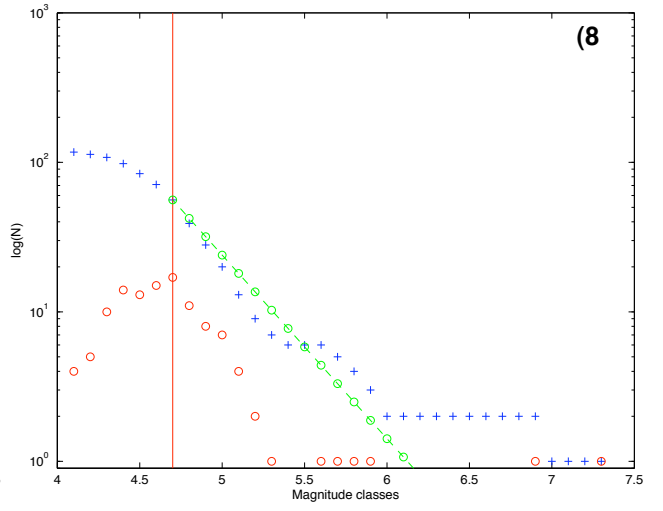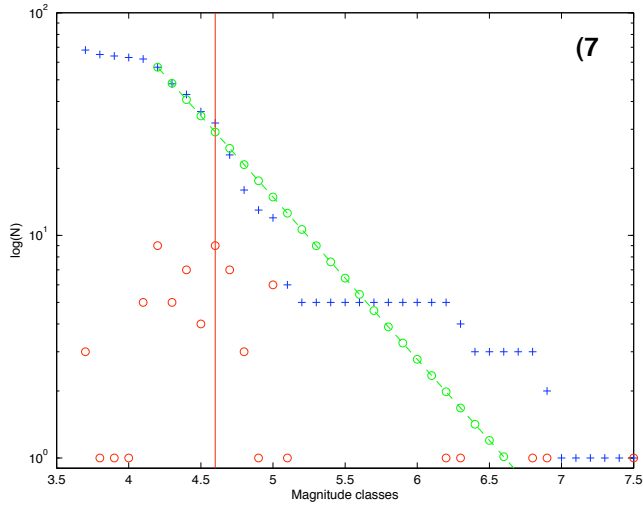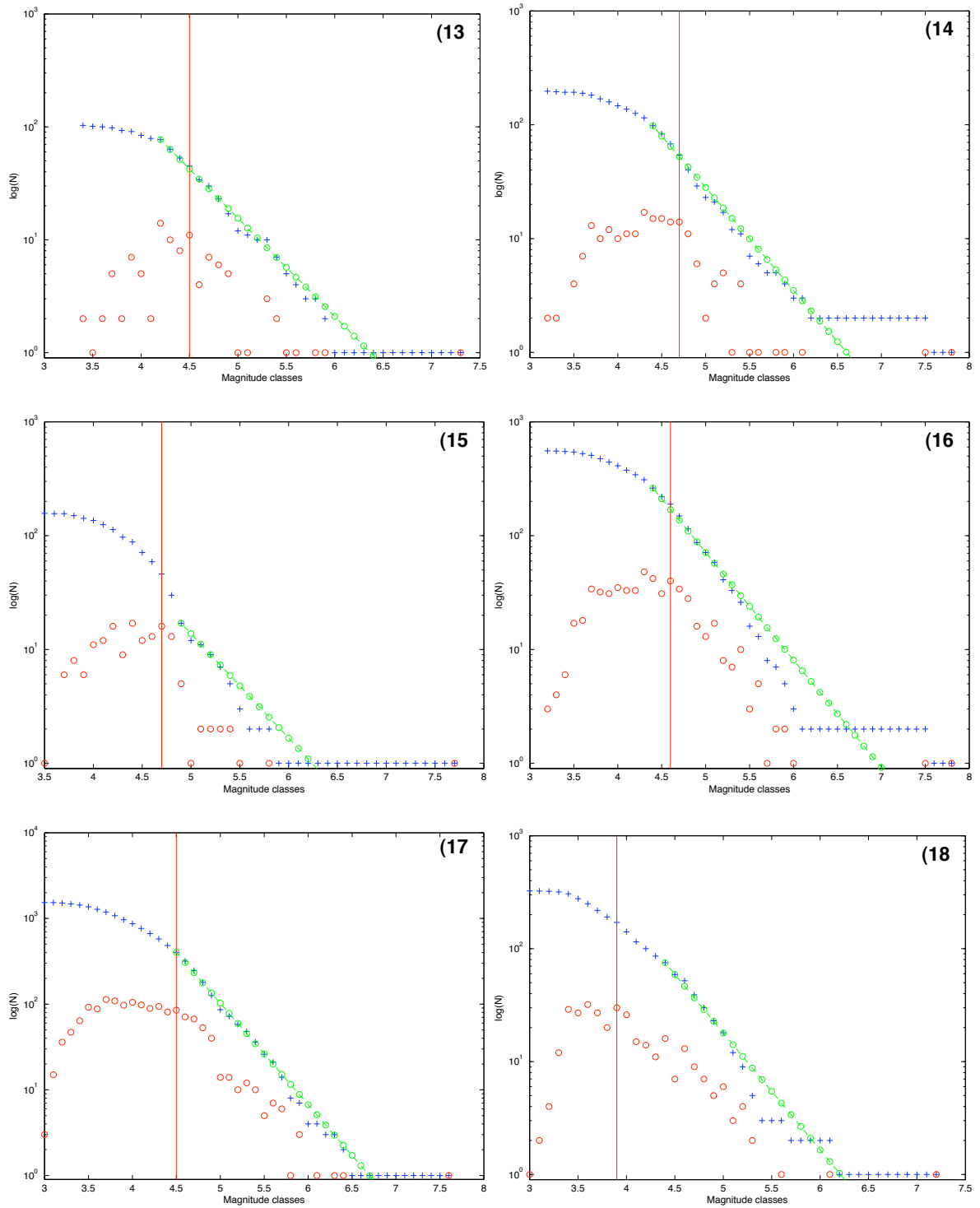
Figure 1.4: Frequency magnitude of aftershock sequences with data used 5 years before and after the mainshock, aftershocks are taken within distance=5*L arround the mainshock. Blue cross is cummulative number, red circle is discrete number. Red straight line is m_c calculated from maximum curvature of frequency magnitude plot.

where $\alpha \sim 0.9 - 1$ for California catalog (Helmstetter (2003); Felzer et al. (2002b)). To remove the effects of mainshock magnitude (m_m) and threshold magnitude (m_c), which is different for each sequences we normalize $n(m_m)$ as;

$$n^*(m_m) = \frac{n(m_m)}{10^{\alpha(m_m - m_c)}} \tag{1.2}$$

We found the $n^*(m_m)$ is still high for Kashmir earthquake, with the emergence, above one σ value, of the Khurgu (# 4) and Southern Xinjiang (# 10) sequences. The Khurgu earthquake sequence is more productive than that of the Kashmir sequence. We also tested the normalized rates for $1*L$, $10*L$. Again we find very small variations in the normalized rates, for different time and space windows (figure 1.6).

1.3.2 Background Seismicity and Duration of Aftershock Sequences

The average background daily rate is computed by using the seismicity that occurred within one year before the mainshock time and distance as $5*L$ around the mainshock (figure 1.7). If there is no event upto one year before the mainshock then we increase the time window such as two year for average background daily rate.

The duration of each aftershocks sequences is defined as the first return point to the background rate. Duration is estimated by using three different techniques. Firstly the duration is defined as the first return time of the weekly seismicity rate to the weekly background rate (figure 1.7c). When data sets are small, this technique give a lower bound estimate of duration, because it is sensitive to the empty bins. Secondly we compute duration using nearest neighbor technique (Silverman (1986)), in which daily rate is estimated by taking inverse of the width of the box contain k neighboring points. Smoothing is controlled by k. The advantage of this technique is that smoothing is uniform and there are no empty bin (Felzer and Brodsky (2006)). We use $k = 2$, but the test was also performed for different $k - values$. This duration is defined as the time when the daily rate computed using nearest neighbor method ($k = 2$) reaches the average daily background rate (figure 1.8–1.9, table 1.2). Thirdly we calculate duration using Omori law parameters (see section
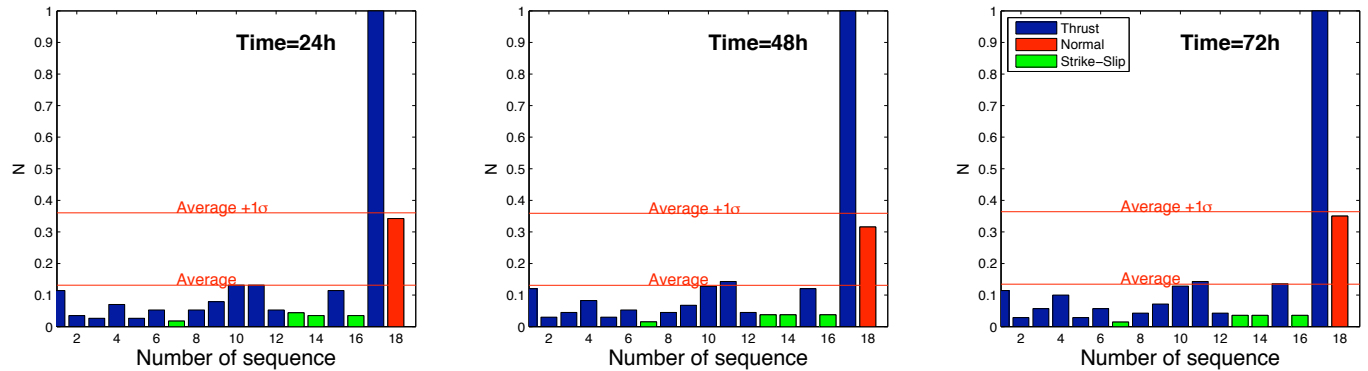
(a) Aftershocks rate in 24, 48 and 72 hours after the mainshock time and for distance as 1*L arround mainshock.
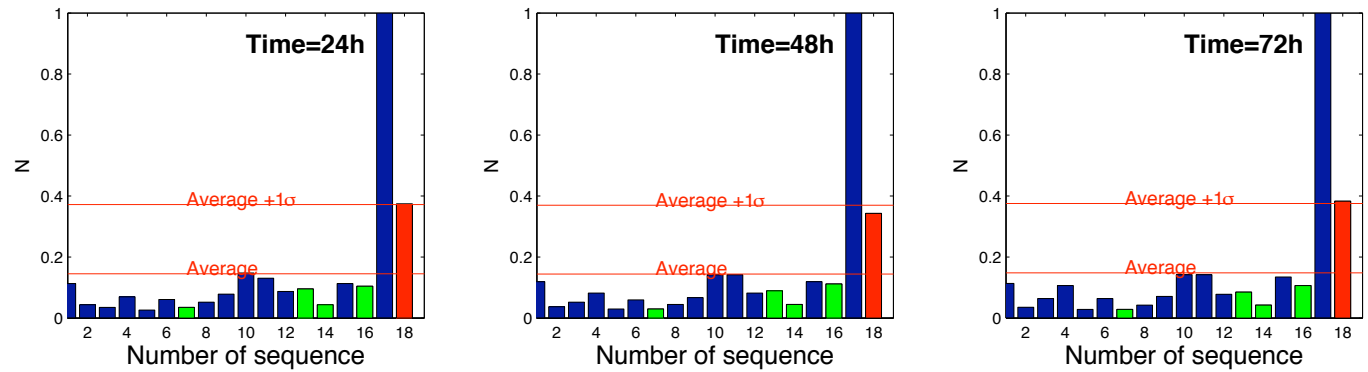
(b) Aftershocks rate in 24, 48 and 72 hours after the mainshock time and for distance as 5*L arround mainshock.
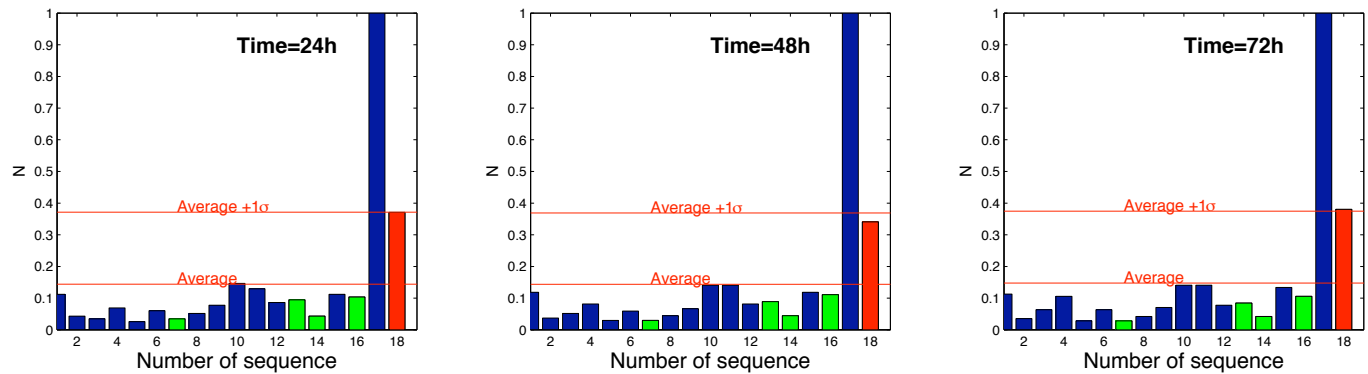
(c) Aftershocks rate in 24, 48 and 72 hours after the mainshock time and for distance as 10*L arround mainshock.

Figure 1.5: Aftershocks rate, for time and distance window. (a) 1*L (b) 5*L (c) 10*L arround mainshock. N=(Number of aftershocks)/Nmax, Nmax=maximum number of aftershocks.
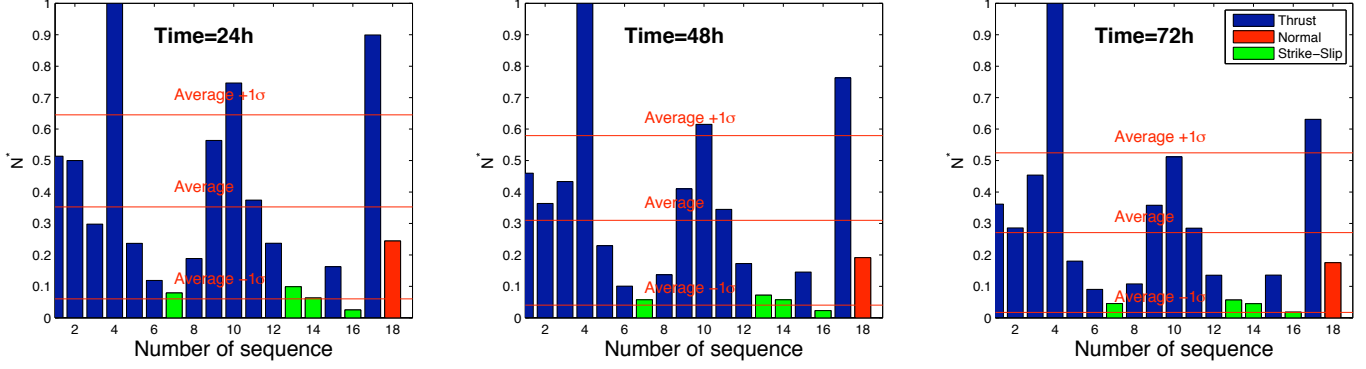
(a) Normalized rate of aftershocks in 24, 48 and 72 and distance as 1*L.
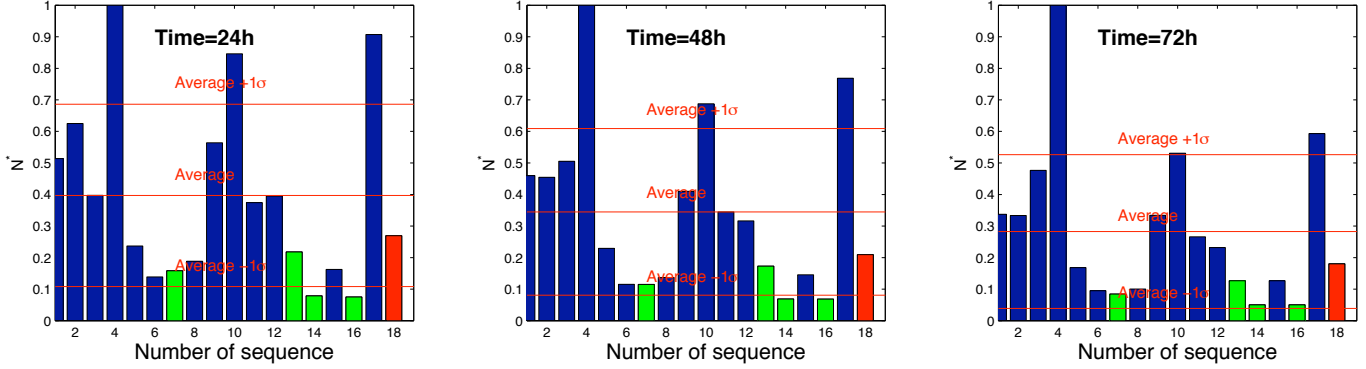
(b) Normalized rate of aftershocks in 24, 48 and 72 and distance as 5*L.
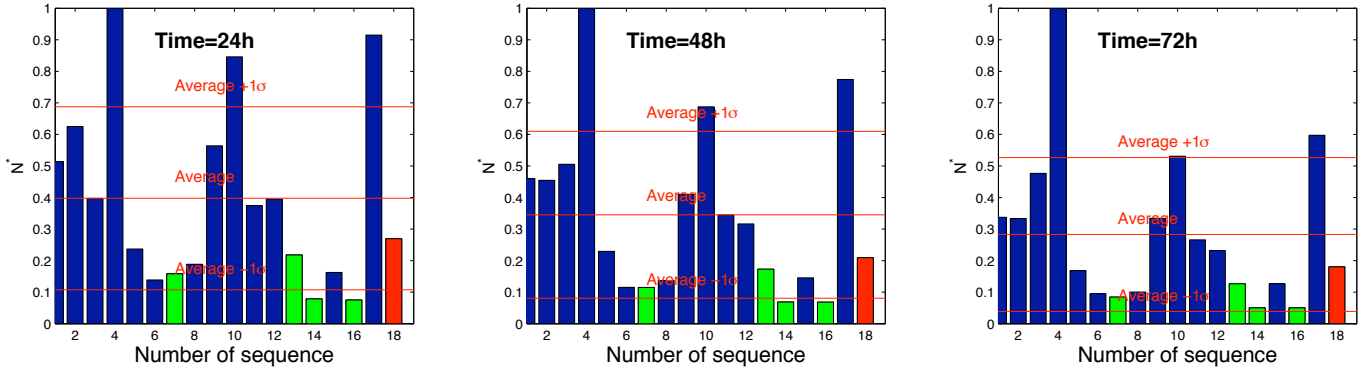
(c) Normalized rate of aftershocks in 24, 48 and 72 and distance as 10*L.

Figure 1.6: Normalized aftershocks rate, for time and distance window. (a) 1*L (b) 5*L (c) 10*L. $N^* = \frac{N}{N_{max}10^{m_m - m_c}}$, Nmax=maximum number of aftershocks, m_m is mainshock magnitude (M_w), m_c is thereshold magnitude.
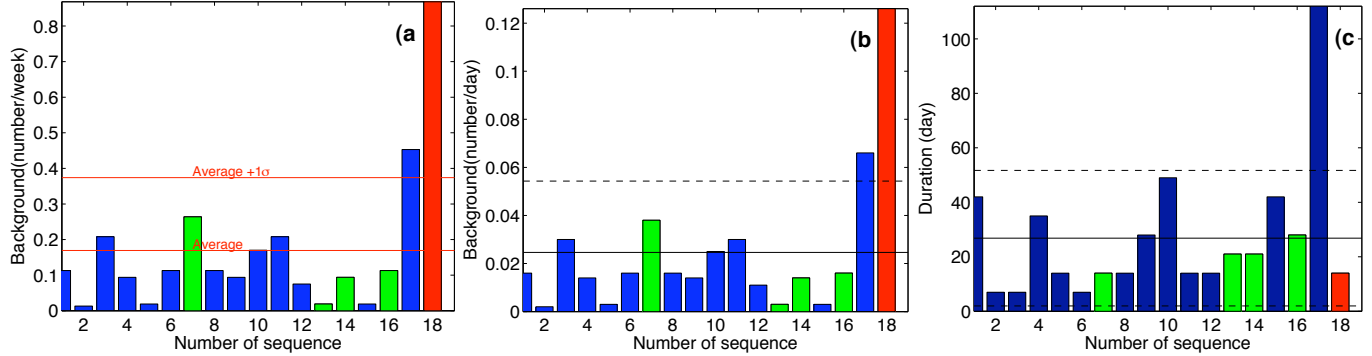
Figure 1.7: Background rate and duration of 18 aftershock sequences. Background rate is estimated using one year data before the mainshock, but if there is no event within this time period then we increase the time window to 2 years. (a) Background rate calculated from weekly rate. (b) Background rate calculated from daily rate. (c) Duration estimated from weekly rate.

4.3.3).

1.3.3   Omori Law Parameters

The change in time of seismicity rate following a mainshock is well reproduced by

$$N(t) = \frac{K}{(t+c)^p} \tag{1.3}$$

$N(t)$ is the seismicity rate, t is the time that start from the mainshock time, p, c and K are constants (Utsu et al. (1995); Utsu (1961)). A median $p-value \sim 1.1$ is reported for the aftershock sequences in the various parts of the world, with $\sim$0.6 - 2.5 range (Utsu et al. (1995)). K is the productivity of aftershocks sequences. Because $K-value$ is a function of mainshock size, so we normalize K as;

$$K^* = \frac{K}{10^{\alpha(m_m - m_c)}} \tag{1.4}$$

We used maximum likelihood method of Ogata (1983) to calculate, K, p, c, the modified Omori law parameters. The error in these parameters is strongly dependent on the number of aftershocks used to calculate these parameters (figure (1.10, 1.11)).

50
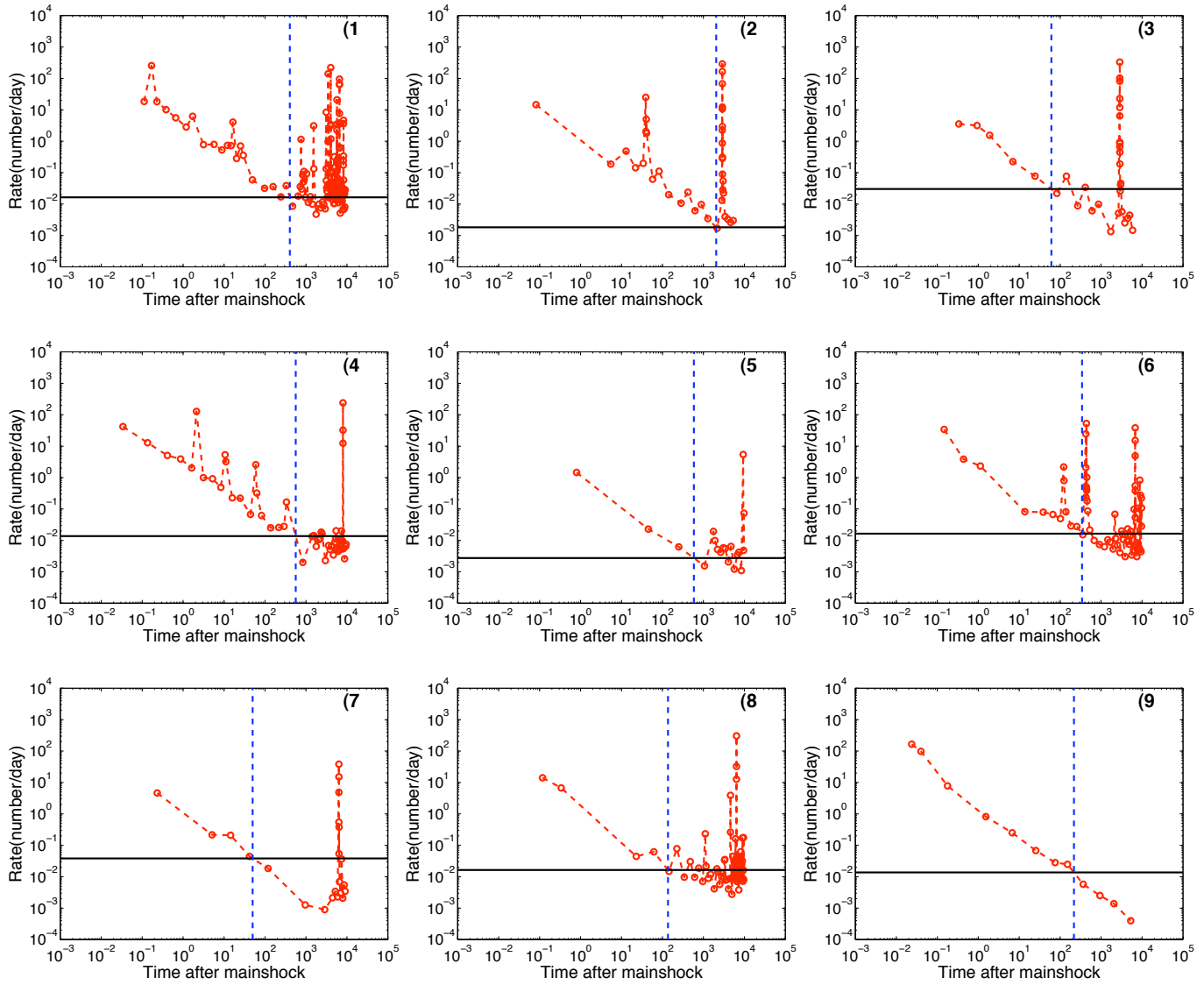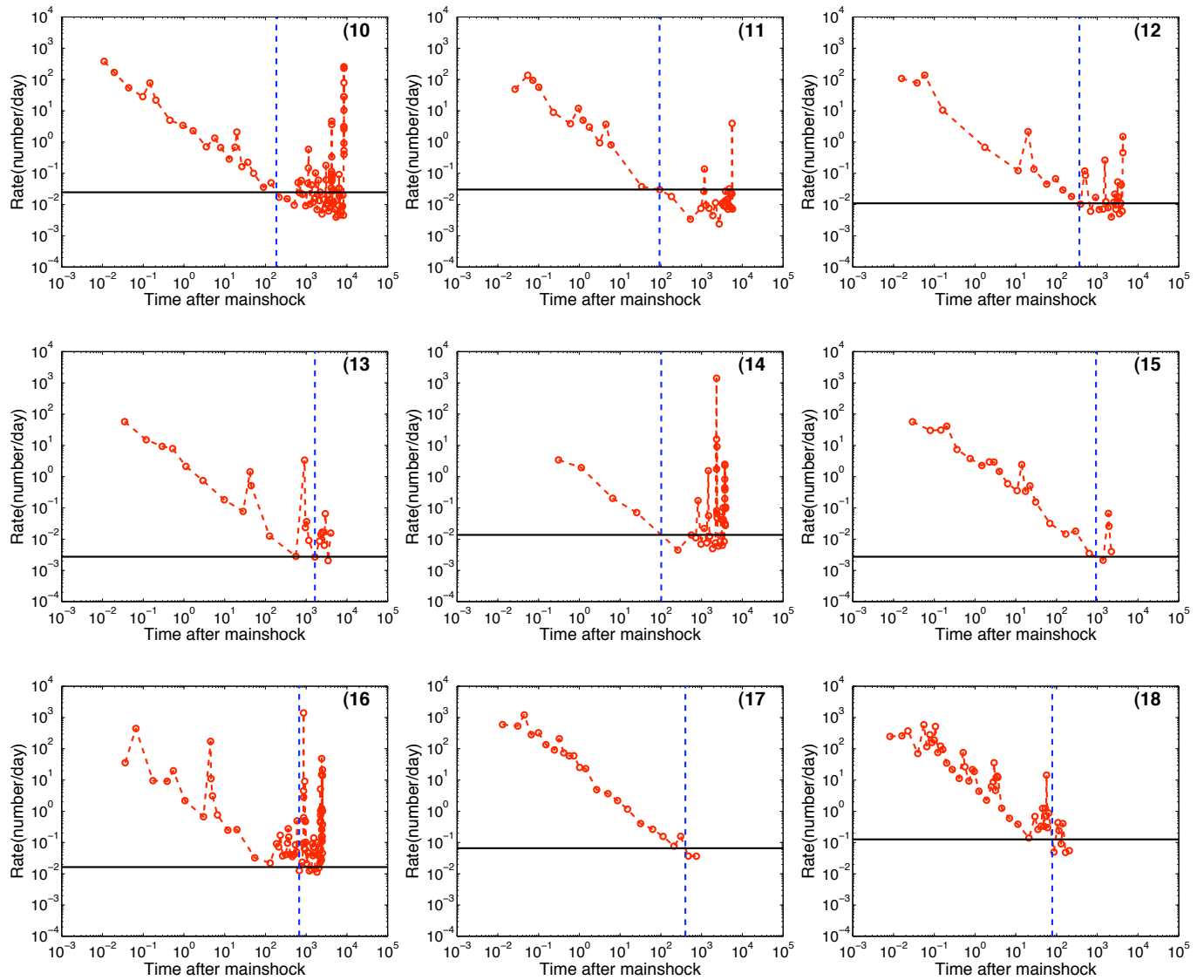
Figure 1.8: Duration of aftershock sequences estimated by using nearest neighbour method. Aftershocks are taken within distance = 5*L around mainshock. Blue dotted line shows the position where daily rate (red) first time goes to average daily background rate (black). Average background rate is calculated using events 1yr, 5L around the mainshock.
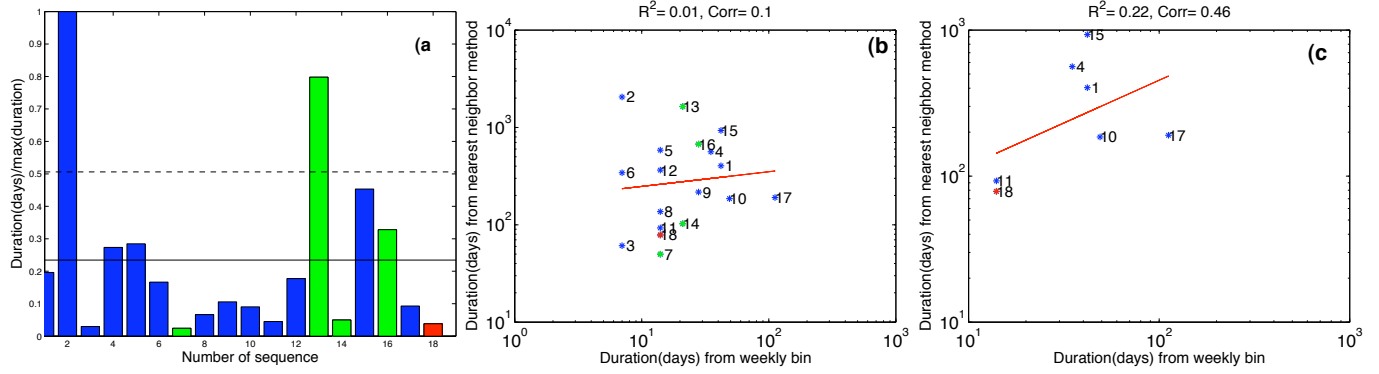
Figure 1.9: Duration (days) estimated from daily rate. (a) Duration estimated by using nearest neighbor method with smoothing factor $k = 2$, k is the number of points taken inside the bin used to calculate the rate, higher k the more will be smooth the data, but for small data higher k cannot be used. (b) Comparison between the duration calculated from nearest neighbor method and weekly bin method. (c) The same comparison as in (a), but in this case we have only those sequences with number of aftershock greater then 20.

Using Omori law parameters we estimate duration as the time when the rate reaches the background rate (figure (1.10, 1.12a)). Then we compare these duration estimates with that deduced from nearest neighbor method (figure 1.12b).

1.3.4 Size of Aftershock zone and average aftershock density

Following Kagan (2002a) we estimated the size of the aftershock zone as;

$$S_k = 4\sigma_j \tag{1.5}$$

$$\sigma_j = \sqrt{\frac{1}{2(N-1)}(xx + yy + \sqrt{(xx - yy)^2 + 4\rho_a^2 * xx * yy})} \tag{1.6}$$

$$\sigma_n = \sqrt{\frac{1}{2(N-1)}(xx + yy - \sqrt{(xx - yy)^2 + 4\rho_a^2 * xx * yy})} \tag{1.7}$$

whereas

$$\rho_a = \frac{xy}{\sqrt{xx * yy}}$$
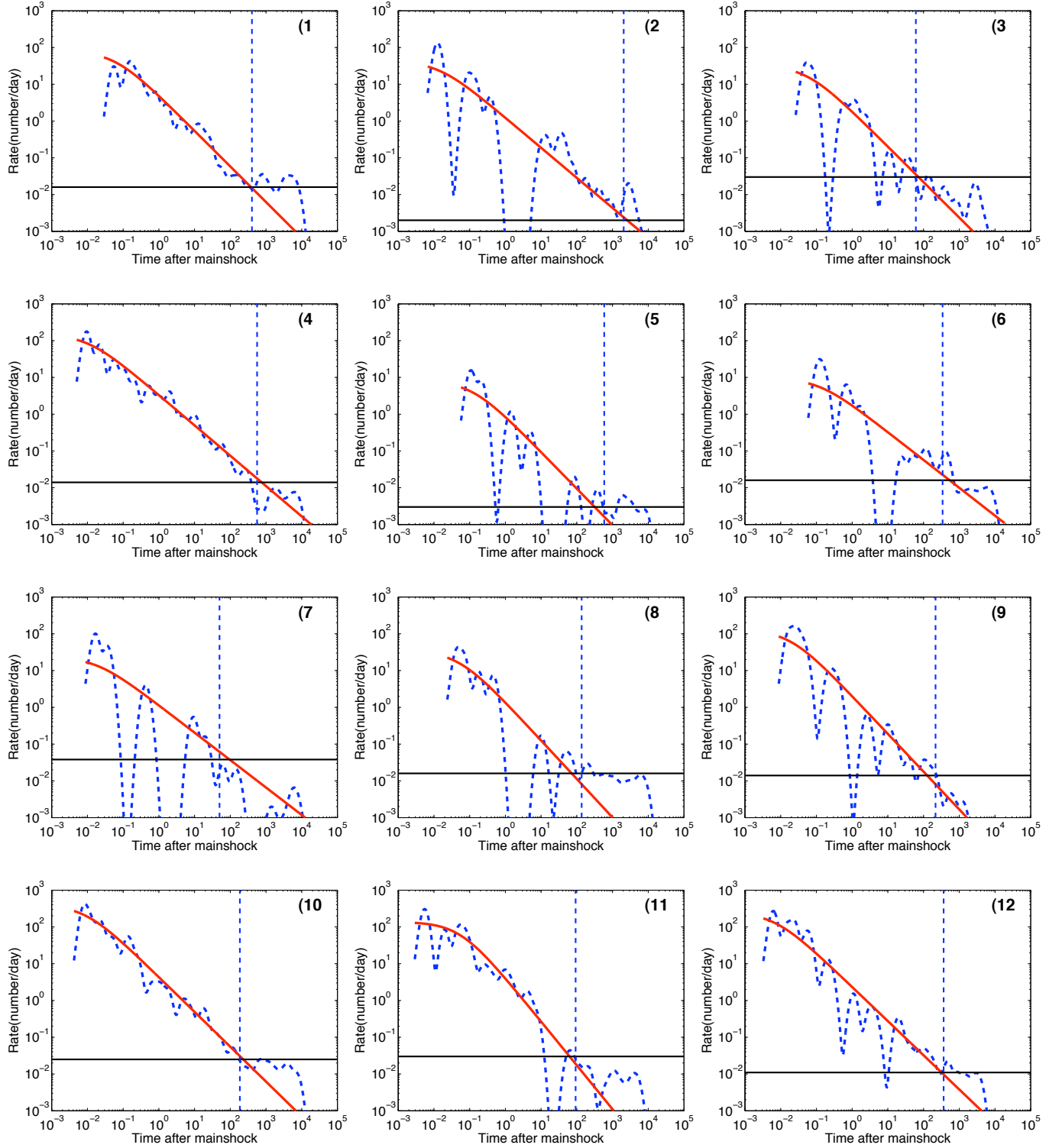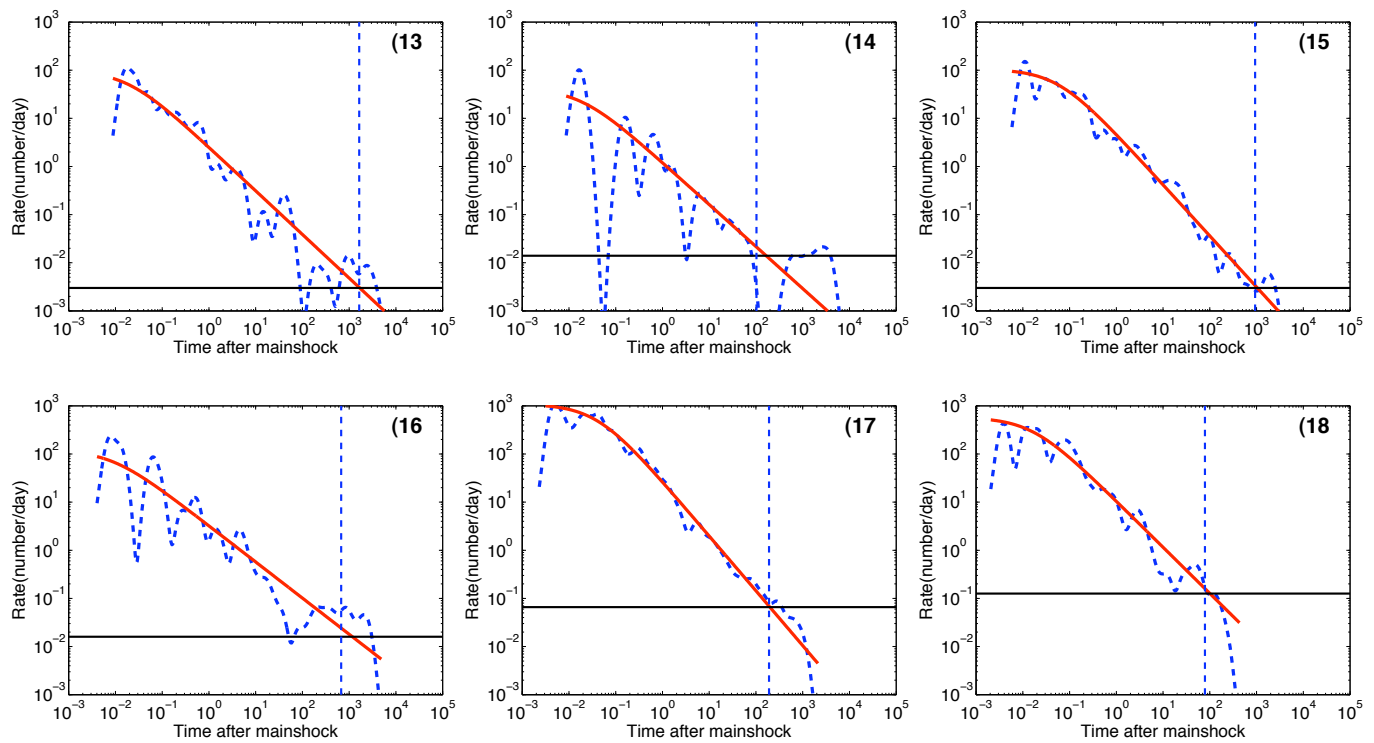
Figure 1.10: Modified Omori Law parameters of all aftershock sequences, with aftershocks are taken within distance = 5*L around mainshock. Blue line is the gaussian smoothed daily rate. Red line is the Omori's law parameters as estimated using maximum likelihood method of Ogata (1983). Blue dotted vertical line is duration calculated using nearest neighbor method.
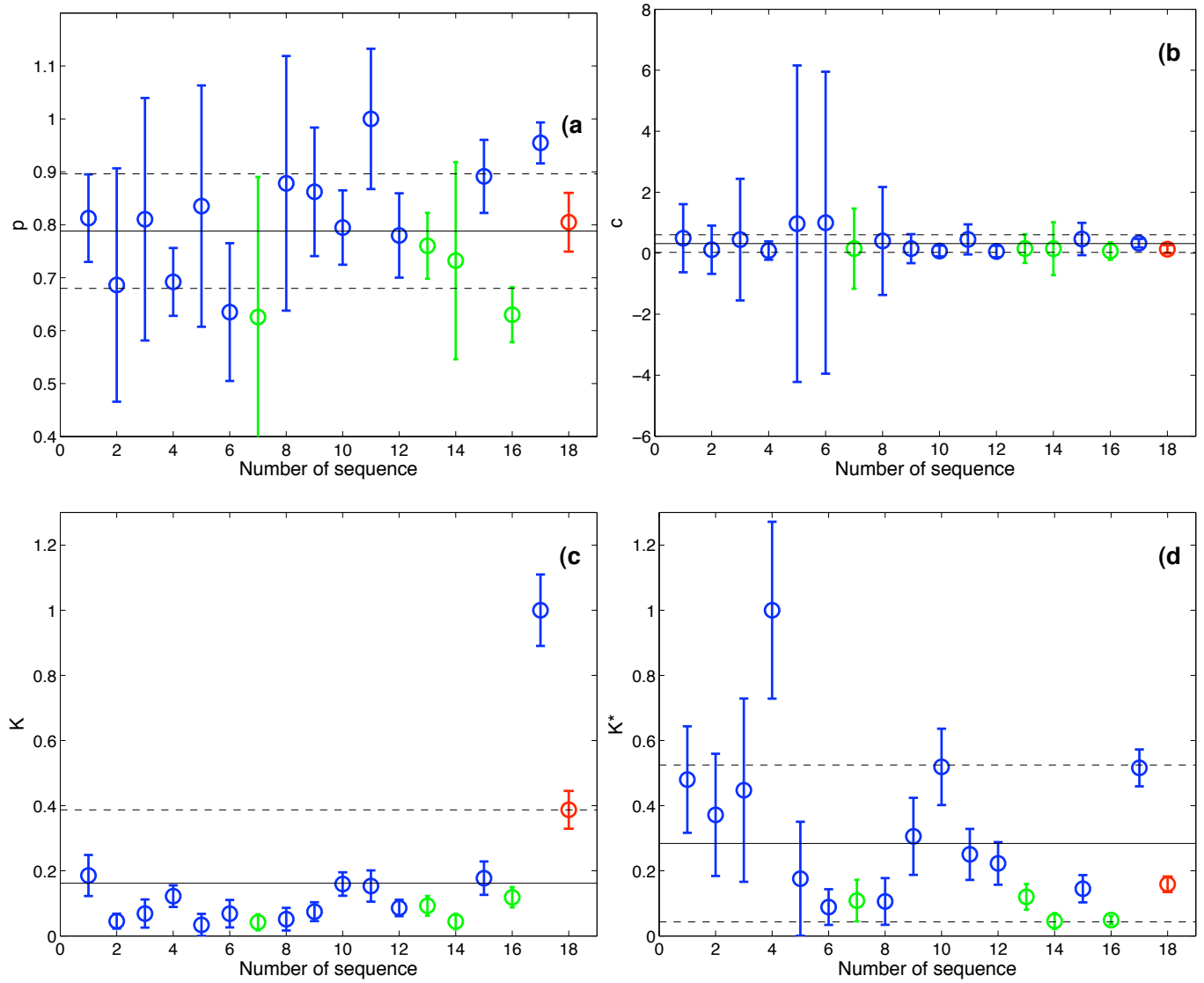
Figure 1.11: For all parameters we show normalized value as, $p = p-value/max(p-value)$. For the 18 aftershock sequences (a) $p-value$ (b) $c-value$ (c) $k-value$ (d) $K*-value$.
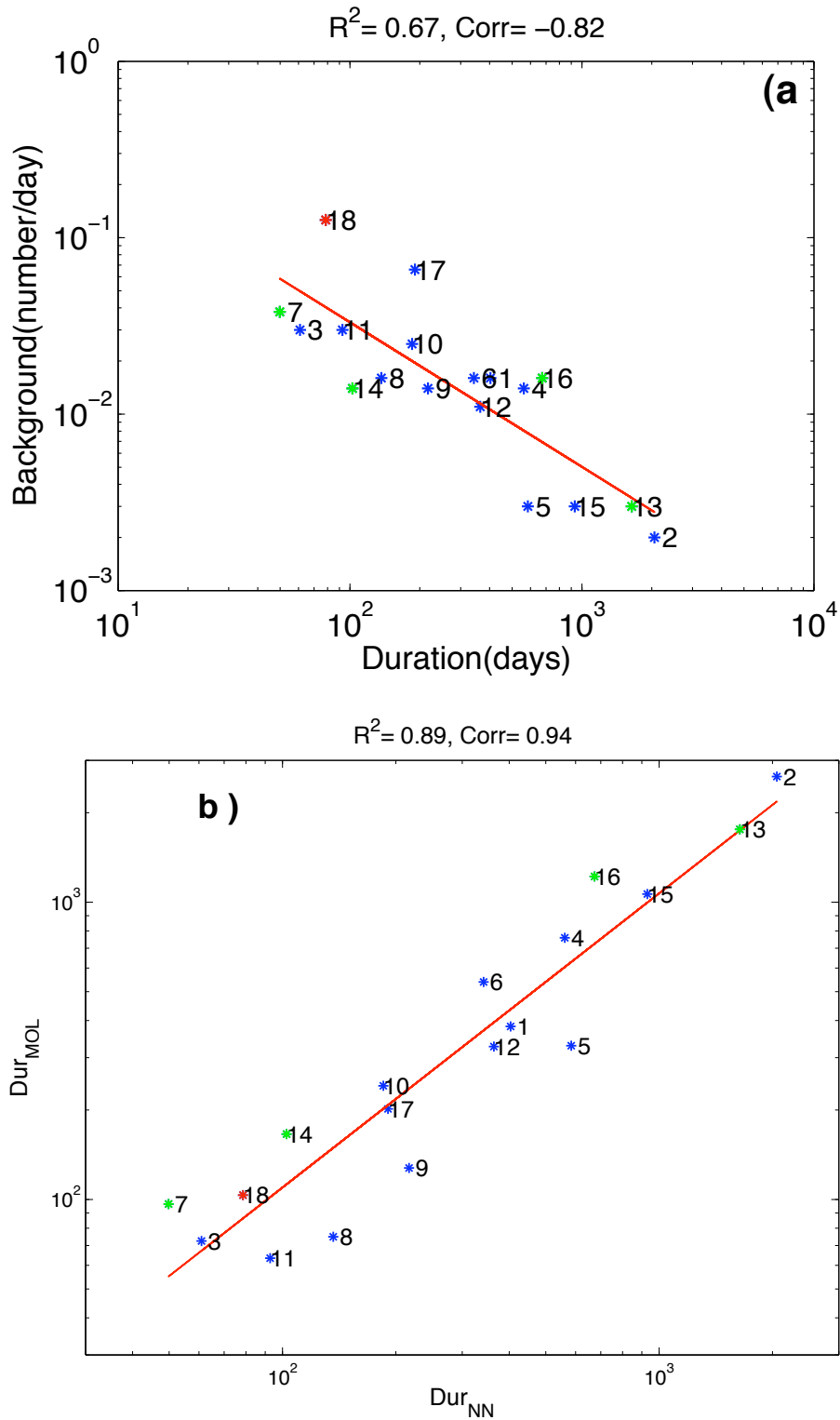
Figure 1.12: Duration (Dur_{MOL}) calculated from Omori law parameters as a function of nearest neighbor method (Dur_{NN}). (a) Duration calculated from Omori parameters. (b) Correlation between duration calculated from Omori law parameters and that from nearest neighbor method.

$$xx = \sum_{i=1}^{N_7}(x_i - \bar{x})^2$$

$$yy = \sum_{i=1}^{N_7}((y_i - \bar{y})cos(\bar{x}))^2$$

$$xy = \sum_{i=1}^{N_7}(x_i - \bar{x})(y_i - \bar{y})cos(\bar{x})$$

whereas σ_j and σ_n are major and minor axis of an ellipse, N_7 is the total number of aftershocks (above m_c) that occur upto $t = 7$ days after the mainshock time (similar with that of Kagan (2002a)) and within $5*L$ around the mainshock. X_i, y_i is the latitude and longitude respectively of the ith aftershock, $\bar{x}$ is the average latitude for aftershock sequence and $\bar{y}$ is the average longitude. Estimate of S_k are plotted on map view using focal mechanism strikes (figure 1.13)

Average aftershock density (figure 1.14) is defined as;

$$\langle d \rangle = \frac{N_7}{S_k} \tag{1.8}$$

1.4   Results and discussion

1.4.1   Temporal Analysis

From the crude analysis of the daily seismicity rate on the 1973-2008 period, the 2005 Kashmir sequence of aftershocks appears as the major event for the Eurasia collision zones (figure 1.1).

The high seismicity rate following the $M_w = 7.6$ *October* 8th 2005 event remains within the highest top 3 rates of the region when normalizing the rate by the mainshock size and the catalogue completeness (figure 1.6). These top peak values are stable when using 1-5-10 fault length distances around the mainshock and 24-48-72 hrs time window after the trigger shocks.

After normalization event # 4, $M_w = 6.7$ Khurgu Iran earthquake and event # 10, $M_w = 6.9$ Southern Xinjiang China earthquake also emerge with rates above of one standard deviation as computed from the average of the 18 event values. Khurgu earthquake
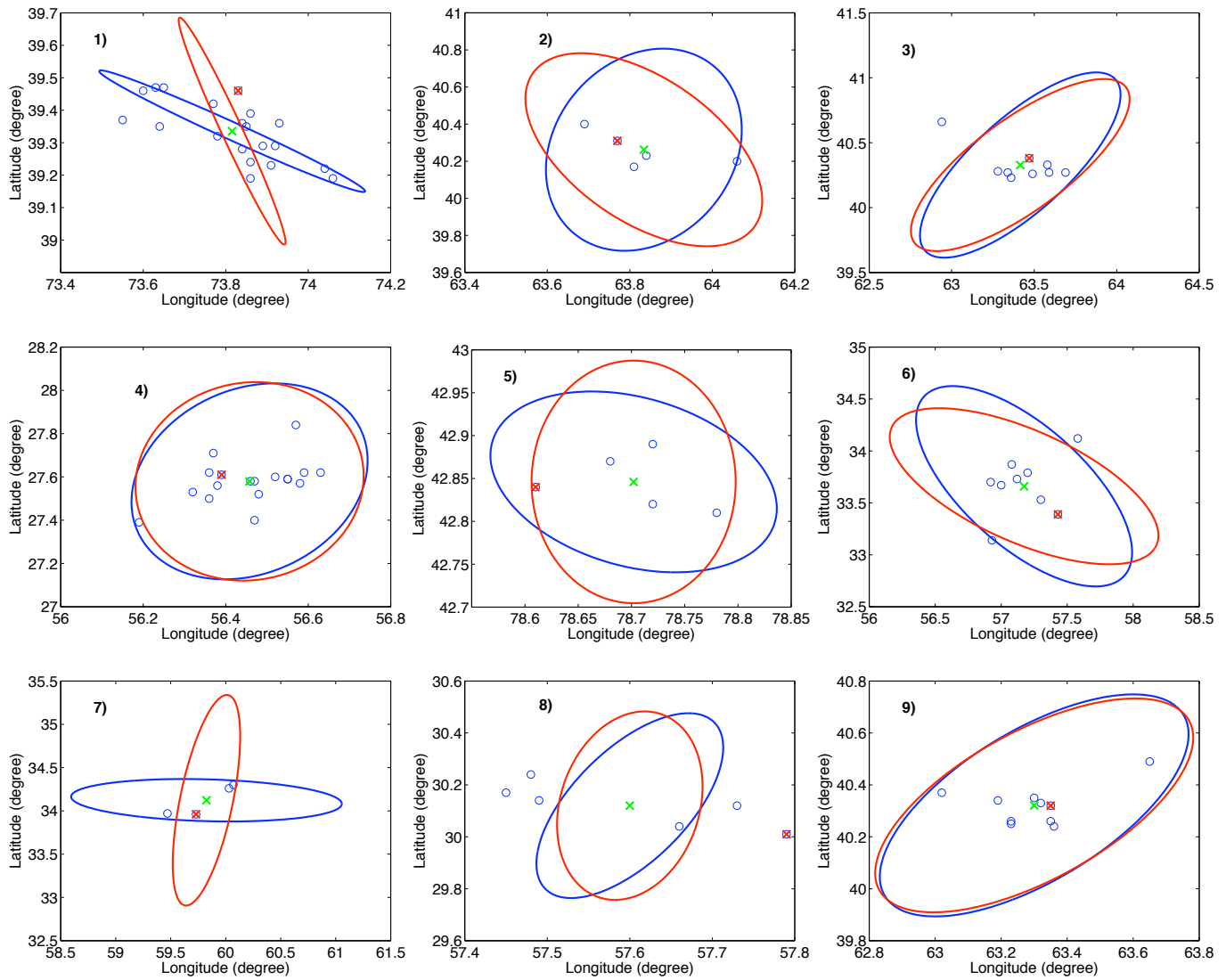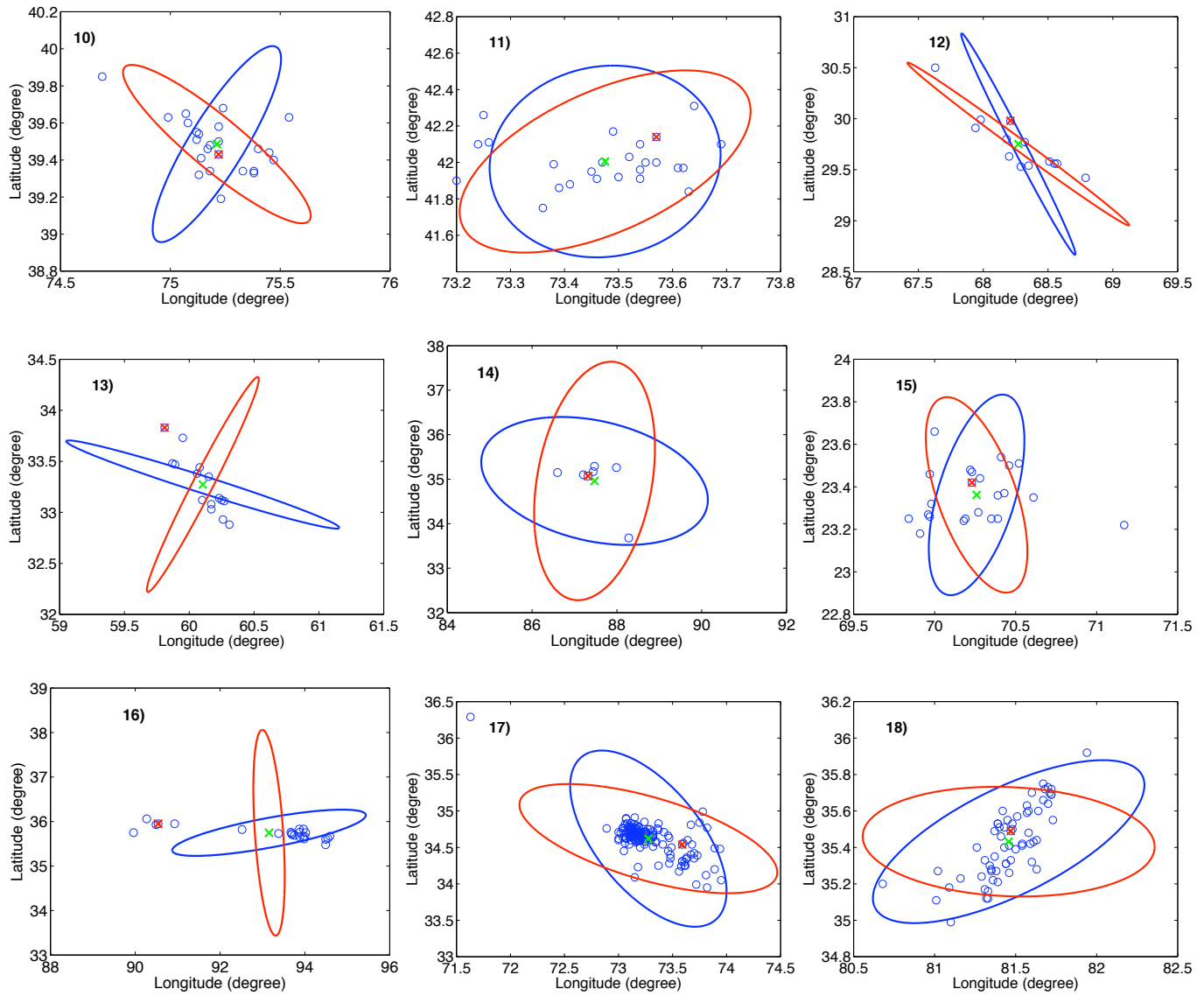
Figure 1.13: Aftershock zone length with aftershocks within time = duration and 5*L around the mainshock. Note that red ellipse is the trend taken from strike 1 of the focal mechanism, whereas blue ellipse is the trend of strike 2.
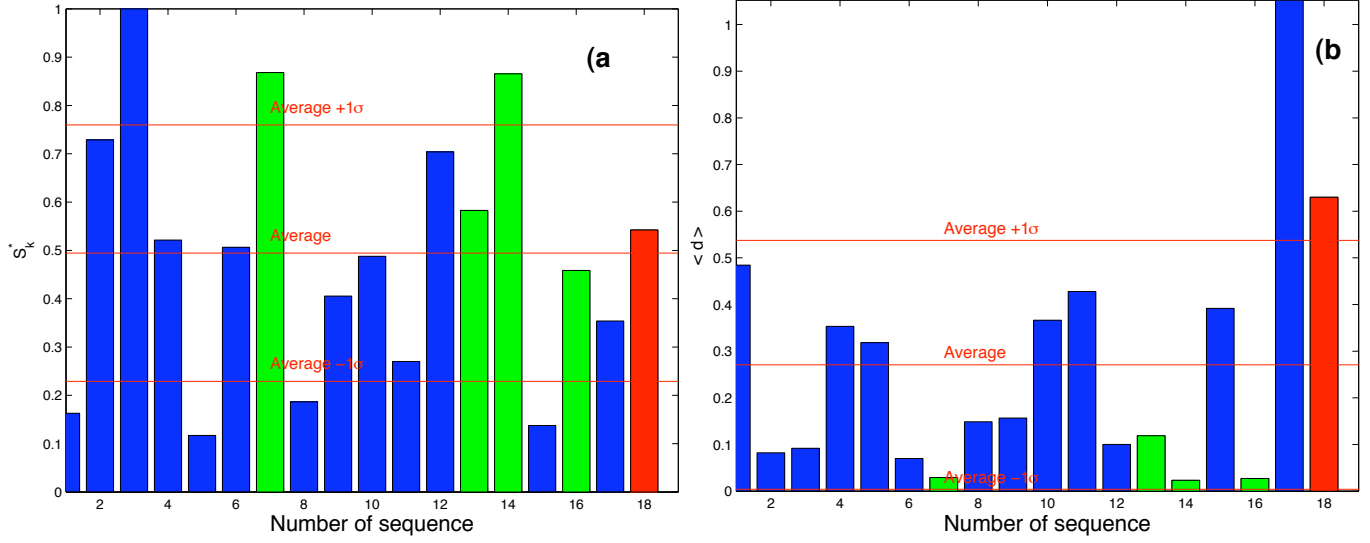
Figure 1.14: Aftershock sequences size and density (a) Normalized aftershock zone length S_k^* ($\frac{S_k}{L}$) (b) Average density $\langle d \rangle = \frac{Total\,number\,in\,aftershock\,zone}{S_k}$.

rate overpasses the Kashmir sequence for 72 hours duration and 5-10 fault length distance to the mainshock. To try to understand the large production rate we observed for these 3 mainshocks we analyze in the following section how space and time patterns of the aftershock sequences interact. In the analysis section we have demonstrated that the rate are stable when using 1-5-10 fault length distances. By increasing distance we slightly increase the background level. Accordingly, in the following we present results corresponding to the use a of trade off distance, i.e., $5*L$.

We use three aftershock duration estimates. First, using weekly seismicity rate, the duration of Kashmir event # 17 emerges as an outlier in the distribution of the 18 event durations (figure 1.7c). These estimates are sensitive to empty bins. To remove the effect of these empty bins due to the small number of aftershocks (table 1.2), the duration is also calculated using neighbor points e.g., nearest neighbor techniques (Silverman (1986)). These duration estimates for 18 aftershock sequences differ from that calculated using weekly rate as (figure (1.7c, 1.9a). Duration is also being calculated using Omori law parameters (figure 1.10). The correlation between the later two duration estimates is strong (figure 1.12b). From these duration estimates event 2 (Gazli), event 13 (Qaenat

earthquake) and event 15 (Bhuj earthquake) emerge as the longest durations as compare to other sequences.

Thus the first technique which uses constant weekly bin rate, works well when number of data points are high and there is no empty bin as shown for our results of event 17, but gives small values when there are some empty bins in aftershock sequences data.

We tentatively test how the higher duration for Gazli and Qaenat earthquake and higher number of aftershocks than the average for the Kashmir and Khurgu earthquake, can emerge from K, p Omori's law parameters.

Because the relatively long duration for Gazli and Qaenat earthquake does not correspond to either small $p-value$ or higher $K-value$, it suggests the lower duration may be driven by their small background rate.

We further resolve a correlation between duration and background (figure **??**), as (Dur $\sim \frac{1}{Bg^{0.8}}$). This correlation is consistent with rate and state model. For aftershocks which predicts $Dur \sim Bg^{-1}$, with Dur $\sim \frac{A\sigma}{\dot{\tau}}$. Accordingly, $\dot{\tau} \sim \frac{1}{Bg}$, where $\dot{\tau}$ is the reference stressing rate, σ is the normal stress and A is the fault constitutive parameter. Earthquake recurrence rate is dependent on duration, small duration will have higher recurrence rate and vice versa (Dieterich, 1994).

The high rate for Khugru sequence is driven by large $K-value$ whereas for Kashmir earthquake it is driven by strong density and high $p-value$ (table (1.5, 1.6)).

1.4.2   Spatial Analysis

To estimate the spatial impact each of the aftershock sequences we follow Kagan (2002a) technique to estimate the size of the aftershocks zone (figure 1.13, 1.14a). Kagan uses the earliest aftershocks, 1-3 days from the mainshocks and a gaussian kernel to extract (S_k) the size of the aftershocks swarm at the 95% confidence level (Kagan (2002a)). Aftershock normalized sizes $(S_k^* = S_k/L)$ are the highest for event 3, 7 and 14 (figure 1.13, 1.14b). Note that all these events have a small duration and are preceded by large event as 2 of them are compound earthquakes. Aftershocks average density is the highest for event #

17 and # 18 (figure 1.14).

1.4.3   Compound earthquake

Event 2, 3, 9 and event 6, 7, 13 are compounds earthquakes, that occur close in space and in time (Scholz (2002)). Event 2 and 3 have 39 days time gap and event 6 and 7 have 431 days time gap, all being located within distance $5L$ distance (figure 1.15).

We observed that $p-value$ increases from first mainshock to the last mainshocks i.e., $p_2 < p_3 < p_9$, $p_6 \sim p_7 < p_{13}$ (table 1.2), which is consistent with the results of Daniel et al. (2008). They observed higher $p-value$ of the second as compare to first, in the case of case of doublet earthquakes. It supports the stress perturbation of the first event impacts on the next event in the same region.

The simplest candidate to drive the longer duration of event 2 is its compound cascading nature. Because event 3 (second sequence) occurs within the stress relaxation of event 2, Gazli, it drive a longer sequence for event 2 and a higher background rate for event 3. This later induces a shorter duration for this event.

The same pattern holds for # 9 event, the third event of the sequence. Similarly to # 2, way event # 13 has no background data for one year before the mainshock, so we go for two years and thus its average background rate is small, similar to # 2 event. Number 13 event is characterized by the second longest duration, and # 6-7 events, which occur in the vicinity in time and space of # 13 have small durations (figure 1.15 − 1.17). These observations further support the duration is dependent on pre-stress condition, as demonstrated by compound earthquake analysis.

The second characteristics of compound earthquake appears as a higher normalized size (S_k^*) of aftershock sequence for the following earthquakes, i.e., #3, 7 event. Because these (#3, 7) events occur in the stress relaxation period of the event 2 and 6 respectively, our analysis may mixed aftershock in space of both compound earthquakes.
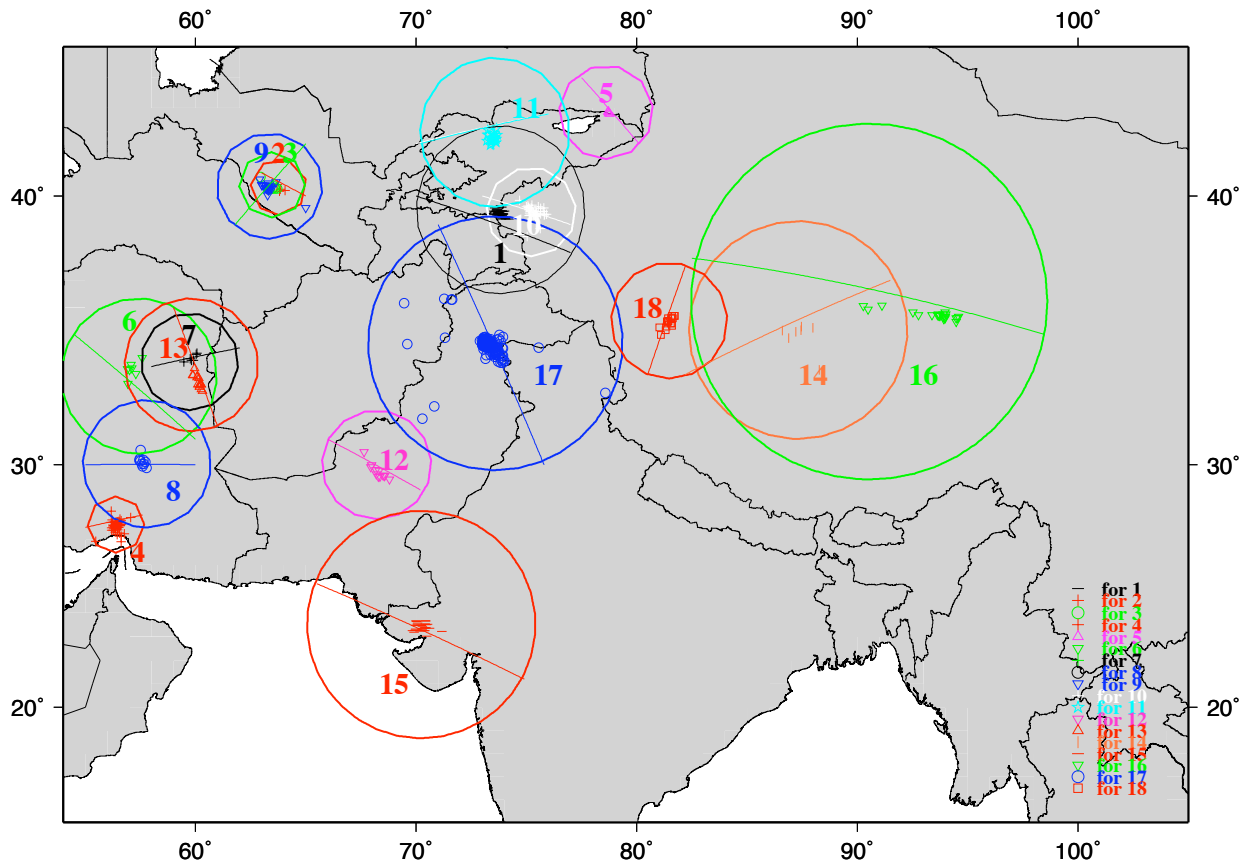
Figure 1.15: Aftershock sequences, aftershocks are within time = duration (calculated from nearest neighbor method, figure 1.9) of the sequence and distance = 5*L (surface rupture length) arround the mainshock. Circle is 5*L. Straight line is the fault orientation from focal mechanim solution. Note that events 2, 3, 9 and events 6, 7, 13 are compound earthquakes, event 16 is super shear earthquake.
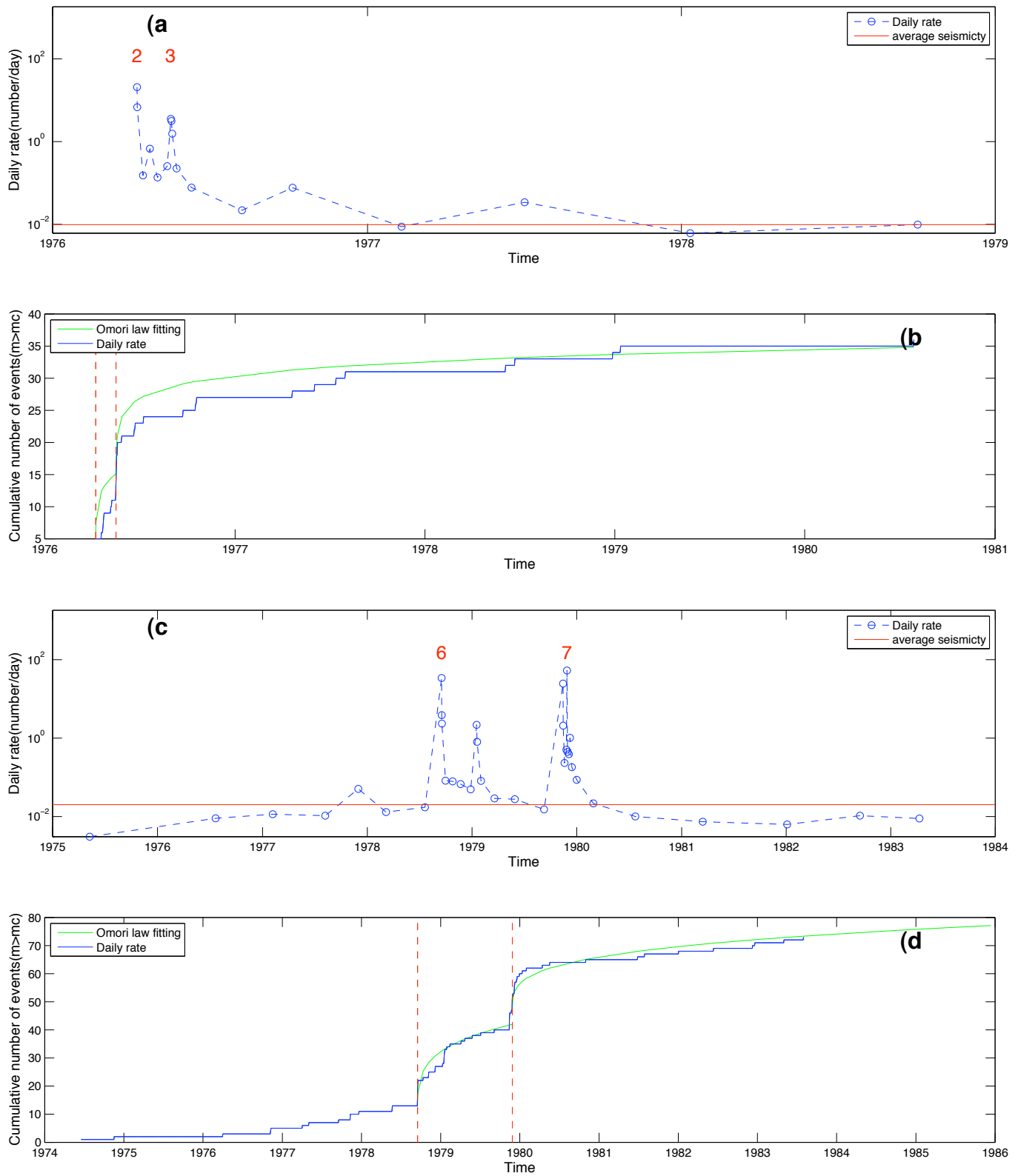
Figure 1.16: Daily rate of events occurring within distance 5*L around. (a) Gazli sequence
(b) Gazli sequence (c) Tabas sequence. (d) Cumulative number
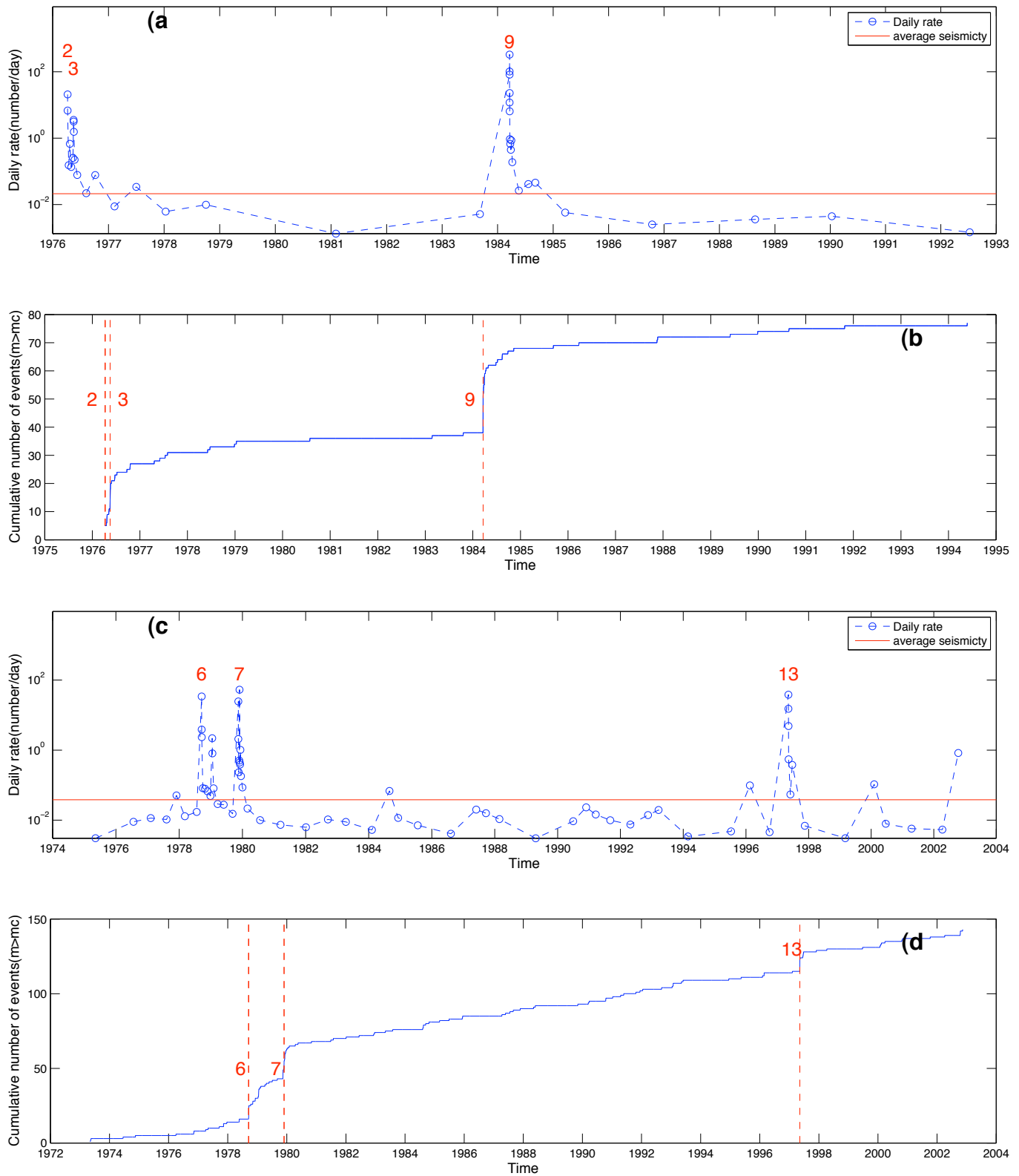
Figure 1.17: Daily rate of events occurring within distance 5*L around. (a) Gazli sequence (b) Gazli sequence (c) Tabas sequence. (d) Cumulative number

1.4.4 Correlation between $Ms \geq 7.0$ aftershock patterns in the Eurasia collision belt

Normalizing rate by the magnitude range of observations for each aftershocks sequences shows that the $M_s = 7.7$ Kashmir (Pakistan), $M_s = 7.6$ Southern Xinjiang (China) and the $M_s = 7.0$ Khurgu (Iran, 1977) aftershock rates are above 1 standard deviations of the 18 aftershocks rates. The anomaly of Kashmir sequence corresponds to high (above 1σ) aftershock production, background rate and density. For the Khurgu sequence, the anomaly in large rate emerges from a large aftershocks productivity, as measured from the normalized $K - value$ of the Omori law.

To understand how Omori law parameters duration and background rate interacts, we estimate correlations between these patterns. Duration and background have strong inverse relationship (1.3, 1.4). This pattern is also predicted by rate and state friction model, when we assume constant $p - value$. Duration is strongly dependent of stress step, which is the rate normalize by average background rate. Duration scales with $1/\tau$ which is the reference stressing rate. Duration has direct relationship with earthquake recurrence time (Dieterich (1994)). Accordingly our results suggest the background rate stands for a stressing rate proxy. The large duration of the Gazli sequence, e.g., the low recurrence rate of the 1976a Gazli earthquake support the possible human triggering (Grasso, 1992; Bossu et al., 1996; McGarr et al., 2002)

The variation of $p - value$ has been related to crustal temperature (Mogi (1962)), heat flow (Kisslinger and Jones (1991)), degree of heterogeneity in the fault zone (Mikumo and Miyatake (1979)), static fatigue (Scholz (1968); Narteau et al. (2002)), pore fluid flow (Nur and Booker (1972)) and fractal dimension of the pre-existing fault system (Nanjo et al. (1998)). However we observed that $p - value$ is dependent on aftershocks size zone and aftershocks density (figure 1.20). $p - value$ decrease as aftershocks normalize zone size (S_k^*) increases suggests that stress heterogeneity decreases with distance from the mainshock (Helmstetter and Shaw, 2006; Ziv et al., 2003). Others correlation are week as seen in table (1.3, 1.4).
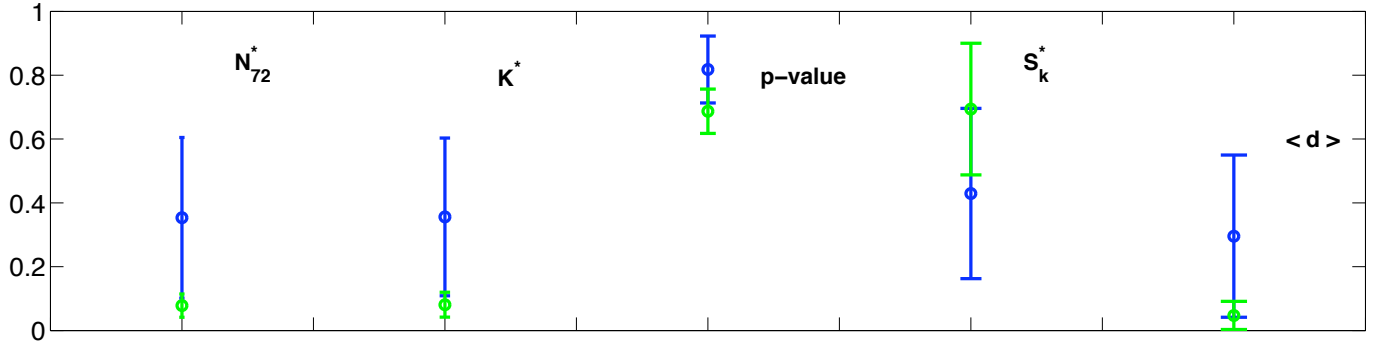
Figure 1.18: Average rate, p-value, $K^* - value$, aftershock size, aftershock density of thrust (blue) and strike slip (green) mechanism. note that each value is being normalized by it maximum value.

The other major result we robustly quantify for Western Asia $M_s \geq 7.0$ events, is the dependence of aftershock spatio temporal parameters on the faulting style. We resolved average rate (N^*), productivity (K^*), $p - value$ and aftershock density ($\langle d \rangle$) to be higher for thrust events than for strike slip events (figure 1.18 – 1.19). Average aftershock size (S_k) is higher for strike slip events than for thrust events. Similar results emerge from the analysis of thrust and strike slip stacked sequences (figure 1.19). $K - value$ and duration are higher for thrust events as compare to strike slip whereas $p - value$ of both mechanism are within errorbars. Figure 1.19 suggests an higher average rate and higher average duration for thrust events than strike slip events. Density of strike slip aftershocks appear as a rough constant value as a function of distance, respectively lower and higher than thrust events for short and long distance, respectively. The higher linear density of strike slip at larger distance is primarily driven by super shear rupture sequence which trigger aftershock upto 300 km (e.g., Bouchon and Karabulut (2008)). As a second possible effect is the co-seismic static stress changes which imply, most of strike-slip aftershock epicenters are observed to be clustered at fault edge, i.e., at larger distance and more clustered than the rough plateau density of reverse aftershock epicenters which expend within the whole hanging wall (King et al. (1994); Stein (1999); Freed (2005)).
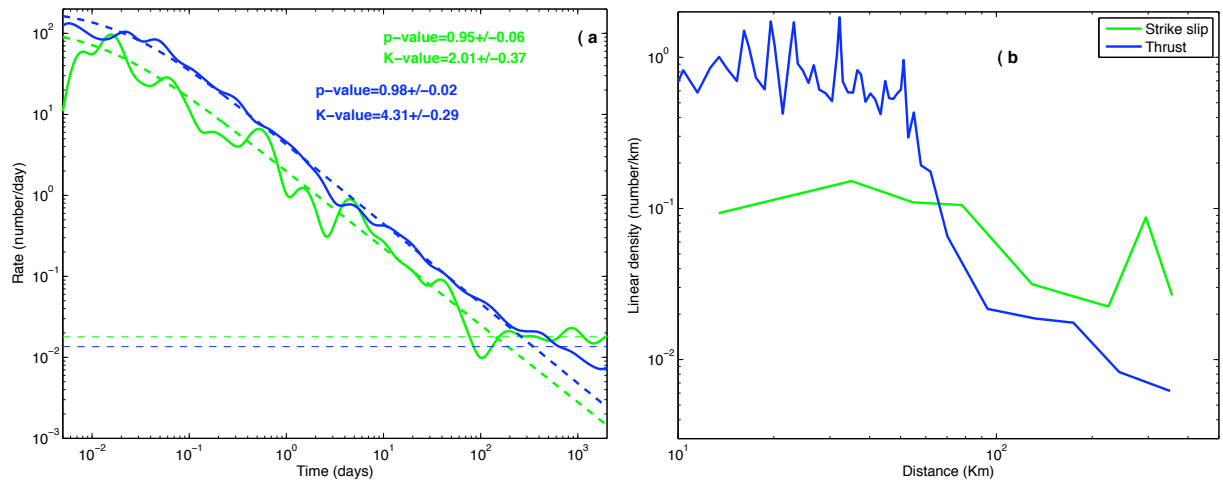
Figure 1.19: Stack aftershocks rate and linear density for thrust and strike slip events (a) Aftershocks rate of thrust (# 1:6,8:12,15,17) and strike slip (# 7,13,14,16) events. Omori law fitted is the dashed line. Horizontal dash line is the average daily background rate calculated by using 5 years data before the mainshock. (b) Linear density of stack thrust and strike slip events. Using nearest neighbor method (Silverman (1986)) with neighboring points (k) taken as 10.
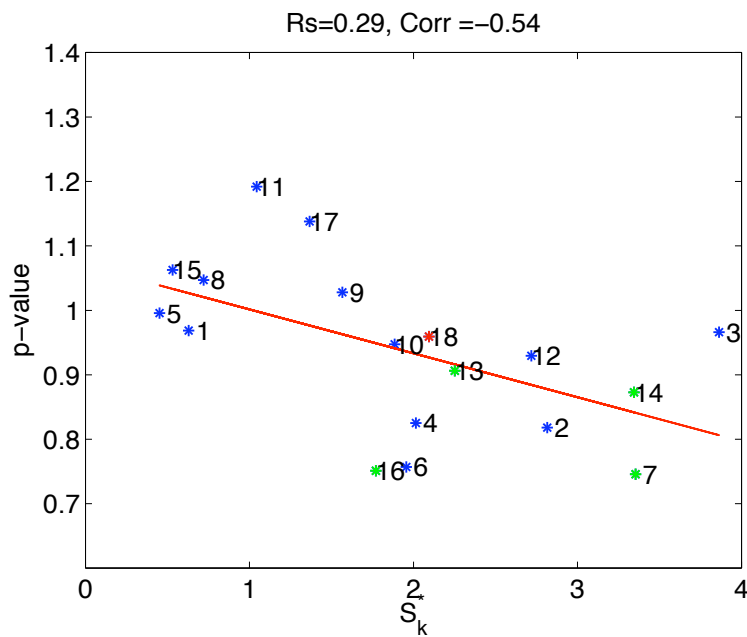
Figure 1.20: Correlation between $p - value$ and aftershocks normalize size.

1.5   Conclusions

Using USGS data for $M \geq 7.0$ events of the Eurasia collision zones with 1973-2008 period, we explore the aftershocks patterns at two scale. On the one hand global patterns for all sequences emerge as background and duration to be anti-correlated ($Dur \sim \frac{1}{Bg}$). On the other hand, specific results appears as compound earthquakes have larger normalized aftershock zone (S_k^*) and , longer duration for afterschock sequence. It further suggests the role of indirect aftershocks to help the ongoing sequence to develop. Following rate and state friction law prediction (Dieterich (1994)) it supports a larger recurrence rate for intracontinental events (Gazli 1976, Bhuj 2001). We also resolve $p - value$ increases with aftershocks density. Strong $p - value$ implies the sequence to be shortened, event cannot expend in space and accordingly density increases. Thrust and strike slip sequence patterns for most Omori law parameters are rejected to be same in space and size domains.

Num	Date	M_c	Rate				Dur(days)	MOL Parameters				Size(km)		b-value	Bg(N/day)
			N_{24}	N_{48}	N_{72}	N_{Dur}		p	c	k	k*	S_k	S_k^*		
1	08/11/74	4.9	13	16	16	37	403.30	0.97±0.10	0.06±0.13	5.04±1.72	0.020±0.007	41.3	0.63	-1.31±0.26	0.016
2	04/08/76	4.7	4	4	4	4	2053.61	0.82±0.26	0.01±0.09	1.23±0.62	0.016±0.008	60.8	2.82	-0.82±0.40	0.002
3	05/17/76	4.7	3	6	8	12	60.94	0.97±0.27	0.05±0.24	1.87±1.18	0.019±0.012	97.7	3.86	-1.24±0.64	0.030
4	03/21/77	4.8	8	11	14	28	561.71	0.83±0.08	0.01±0.04	3.32±0.90	0.042±0.011	51.0	2.01	-1.20±0.22	0.014
5	03/24/78	4.8	3	4	4	5	584.41	1.00±0.27	0.11±0.61	0.92±0.92	0.007±0.007	15.7	0.45	-0.97±0.59	0.003
6	09/16/78	4.6	6	7	8	19	342.04	0.76±0.16	0.12±0.58	1.86±1.14	0.004±0.002	128.4	1.96	-0.98±0.30	0.016
7	11/27/79	4.6	2	2	2	7	49.86	0.75±0.32	0.02±0.16	1.14±0.67	0.005±0.003	136.6	3.35	-0.73±0.37	0.038
8	07/28/81	4.7	6	6	6	9	136.46	1.05±0.29	0.05±0.21	1.40±0.95	0.004±0.003	40.3	0.72	-1.06±0.65	0.016
9	03/19/84	4.8	9	9	10	18	216.81	1.03±0.14	0.02±0.06	2.03±0.78	0.013±0.005	63.8	1.57	-1.53±0.70	0.014
10	08/23/85	4.6	15	17	18	34	185.33	0.95±0.08	0.01±0.02	4.33±0.98	0.022±0.005	65.5	1.88	-1.18±0.26	0.025
11	08/19/92	4.6	15	19	20	28	92.76	1.19±0.16	0.05±0.06	4.17±1.30	0.010±0.003	58.4	1.04	-0.77±0.16	0.030
12	02/27/97	4.7	6	6	6	18	364.17	0.93±0.09	0.01±0.02	2.34±0.68	0.009±0.003	129.8	2.72	-1.02±0.28	0.011
13	05/10/97	4.5	5	5	5	7	1638.50	0.91±0.07	0.02±0.06	2.52±0.82	0.005±0.002	126.0	2.25	-0.90±0.18	0.003
14	11/08/97	4.7	4	5	5	9	102.53	0.87±0.22	0.02±0.10	1.21±0.64	0.002±0.001	301.5	3.34	-0.88±0.50	0.014
15	01/26/01	4.7	13	16	19	41	930.76	1.06±0.08	0.05±0.06	4.82±1.39	0.006±0.002	56.2	0.53	-1.32±0.34	0.003
16	11/14/01	4.6	4	5	5	8	673.93	0.75±0.06	0.01±0.03	3.22±0.84	0.002±0.001	257.2	1.77	-0.98±0.14	0.016
17	10/08/05	4.5	114	133	140	198	190.55	1.14±0.05	0.04±0.02	27.15±2.98	0.022±0.002	144.5	1.37	-1.09±0.07	0.066
18	03/20/08	3.9	39	42	49	80	78.55	0.96±0.07	0.02±0.02	10.52±1.57	0.007±0.001	100.0	2.10	-0.76±0.08	0.126

Num=Sequence Number

M_c = Threshold magnitude

N_{24}=Total number events in 24 hours, calculated using hourly rate.

N_{48}=Total number events in 48 hours, calculated using hourly rate.

N_{72}=Total number events in 72 hours, calculated using hourly rate.

N_{Dur}=Total number events in time taken as duration of the aftershocks sequence, calculated using weekly rate.

Dur=Duration(days)

p= p-value calculated from Modified Omori Law

k= k-value calculated from Modified Omori Law

c= c-value calculated from Modified Omori Law

k*=k-value/10^{m-mc}

S_k= Aftershock zone length(km)

S_k^*=S_k/(L)

b-value = b-value calculated from Maximum Likelihood Method

Bg=background

Table 1.2: Overall parameters of aftershocks sequences

M^R	0.04	0.01	0.06	0.03	0.05	0.00	0.01	0.05	1.00
M_W	0.19	0.02	0.26	0.02	0.09	0.03	0.01	1.00	0.05
Bg	0.01	0.03	0.00	0.20	0.01	0.33	1.00	0.01	0.01
$\langle d \rangle$	0.25	0.39	0.16	0.05	0.22	1.00	0.33	0.03	0.00
S_k^*	0.00	0.29	0.00	0.00	1.00	0.22	0.01	0.09	0.05
Dur	0.01	0.07	0.00	1.00	0.00	0.05	0.20	0.02	0.03
K*	0.95	0.01	1.00	0.00	0.00	0.16	0.00	0.26	0.06
P	0.04	1.00	0.01	0.07	0.29	0.39	0.03	0.02	0.01
N*	1.00	0.04	0.95	0.01	0.00	0.25	0.01	0.19	0.03
	N*	P	K*	Dur	S_k^*	$<d>$	Bg	Mw	M^R

Table 1.3: Residual square of different spatio-temporal parameters, Note that N* is the total number of aftershocks within duration(time=duration) of the sequences and 5*L arround the mainshock

M^R	0.20	-0.10	0.25	0.17	0.23	0.00	-0.09	-0.22	1.00
M_w	-0.43	0.13	-0.51	-0.15	-0.30	0.18	0.08	1.00	-0.22
Bg	0.10	0.18	0.01	-0.44	0.10	0.58	1.00	0.08	-0.09
$\langle d \rangle$	0.50	0.62	0.40	-0.21	-0.47	1.00	0.58	0.18	0.00
S_k^*	-0.05	-0.54	-0.01	-0.00	1.00	-0.47	0.10	-0.30	0.23
Dur	-0.11	-0.26	-0.01	1.00	-0.00	-0.21	-0.44	-0.15	0.17
K*	0.98	0.09	1.00	-0.01	-0.01	0.40	0.01	-0.51	0.25
P	0.20	1.00	0.09	-0.26	-0.54	0.62	0.18	0.13	-0.10
N*	1.00	0.20	0.98	-0.11	-0.05	0.50	0.10	-0.43	0.18
	N*	P	K*	Dur	S_k^*	$<d>$	Bg	Mw	M^R

Table 1.4: co-relation co-efficients of different spatio-temporal parameters, Note that N* is the total number of aftershocks within duration(time=duration) of the sequences and 5*L arround the mainshock

M^R=Ms/Mw(Surface wave magnitude/moment magnitude)

M_w=Moment Magnitude

Bg=average Background(number/week) using one year foreshock data

S_k^* = Normalized aftershock zone length(aftershock zone length/L)

$\langle d \rangle$ =Average density (total number/aftershock zone length)

Dur=Duration(days)

K*=k-value/10^{m-mc}

P=p-value

N*=Total number/10^{m_m-mc}

Aftershock Parameters	Sub Parameters	1	2	3	4	5	6	7	8	9	10	11	12	13	14	15	16	17	18
N*					+						+				-		-	+	
	P						-	-				+						-	+	
	K*				+															
Dur														+		+			
	S_k^*	-		+		-		+	-					+	+	+			
	$< d >$														+	-		+	+
Tectonic Setting	Bg		-															+	+
	Ms/Mw		+						-	-	+								
	F.M	T	T	T	T	T	T	SS	T	T	T	T	T	SS	SS	T	SS	T	N
	S.R	NI	No	No	No	NI	85km[1]	60km[2]	5km[3]	NI	50km[4]	NI		150km[5]	NI	No	400km[6]	70km[7]	NI
Score		-1	+1/-1	+1	+2	-1	-1	-1/+1	-2	-1	+2	+1		+1	+1/-1	+1/-1	-2	+4	+2

N*=Total number/10^{m-mc}
P=p-value
K*=k-value/10^{m-mc}
Dur=Duration(days)
S_k^* = Normalized aftershock zone length(aftershock zone length/L)
$< d >$ =Average density (total number/aftershock zone length)
Bg=Background(number/week)
MS/MW=(Surface wave magnitude)/(Moment magnitude)
F.M=Focal mechanism
S.R=Surface Rupture
T=Thrust
SS=Strike Slip
N=Normal
NI=No informations
No= No Rupture observed

[1] Berberian,1979, [2] Haghipour & amidi,1980, [3] Adeli, 1982, [4] Ghose et al., 1997, [5] Berberian et al., 1999, [6] Lin et al., 2002 [7] Heitaro et al., 2008

Table 1.5: All spatio-temporal parameters with above/below the mean+1σ, Note that N* is the total number of aftershocks within duration(time=duration) of the sequences and 5*L arround the mainshock

Aftershock Parameters	Sub Parameters	1	2	3	4	5	6	7	8	9	10	11	12	13	14	15	16	17	18
N*					+														
	P																		
	K*				+														
Dur														+					
	S_k^*																		
	$<d>$																	+	
Tectonic Setting	Bg																		
	Ms/Mw										+								
	F.M	T	T	T	T	T	T	SS	T	T	T	T	T	SS	SS	T	SS	T	N
	S.R	NI	No	No	No	NI	85km[1]	60km[2]	5km[3]	NI	NI	50km[4]	NI	150km[5]	NI	No	400km[6]	70km[7]	NI
Score					+2						+1			+1				+1	+1

N*=Total number/10^{m-mc}
P=p-value
K*=k-value/10^{m-mc}
Dur=Duration(days)
S_k^* = Normalized aftershock zone length(aftershock zone length/L)
$<d>$ =Average density (total number/aftershock zone length)
Bg=Background(number/week)
MS/MW=(Surface wave magnitude)/(Moment magnitude)
F.M=Focal mechanism
S.R=Surface Rupture
T=Thrust
SS=Strike Slip
N=Normal
NI=No informations
No= No Rupture observed

[1] Berberian,1979, [2] Haghipour & amidi,1980, [3] Adeli, 1982, [4] Ghose et al., 1997, [5] Berberian et al., 1999, [6] Lin et al., 2002 [7] Heitaro et al., 2008

Table 1.6: All spatio-temporal parameters with above/below the mean+2σ, Note that N* is the total number of aftershocks within duration(time=duration) of the sequences and 5*L arround the mainshock

Chapter 2

Faulting style controls on the aftershocks patterns: worldwide earthquake catalogue

M. Tahir [1], JR Grasso[1]

[1]Institut des sciences de la Terre (ISTerre)

University Joseph Fourier - Grenoble I, FRANCE

Abstract

Apart from the complexity to understand and thus to predict earthquake occurrence in size, time and space, seismicity patterns are characterized by two robust empirical laws: The exponential distribution of magnitude (Gutenberg Richter law; $\log (N) = a - bm$) and the power law decrease of aftershock rate over time (Omori law; $N(t) = \frac{K}{(t+c)^p}$, $K = K_\circ 10^{\alpha(m_m - m_c)}$). Recently the b-value, exponent of the GR distribution, and the $c - value$ (time constant of the Omori's law) have been suggested, using regional catalogs to be dependent on faulting styles. Using global earthquake catalogs, we resolve that on average all the parameters of the Omori law (p, K, α, $N(t)$) are dependent on faulting styles. Strike slip events, have lower aftershocks rate (N^*) and $K - value$ than thrust and normal events, with aftershocks productivity, $\alpha_{SS} > \alpha_T$. Within the ETAS model strong K, N^* and low α values are driven by high branching ratio(n), as estimated on the global USGS catalog ($\frac{n_T}{n_{SS}} \sim 1.4 \pm 0.05$). As consequences, a relatively higher n value of the thrust events, also predicts a lower $p - value$ for thrust events as compared to strike slip and normal events i.e., the $p_N > p_{SS} > p_T$ we observe. Furthermore we observed that earthquake interactions at various spatio-temporal scaling are different for both strike slip and thrust faulting mechanism. The exponent μ ($\Phi(t) \sim \frac{1}{r^\mu}$) of thrust event density evolves with time and distance and is always smaller than the one of strike slip events, i.e., $\langle \mu_T \rangle < \langle \mu_{SS} \rangle$. When Anderson faulting theory predicts thrust faulting requires a somewhat larger stresses, in absolute magnitude, that does normal faulting, within the framework of rate and state friction law, a change in the stress heterogeneity patterns drive the $p - value$ changes (e.g., Helmstetter and Shaw, 2006).

Schorlemmer et al. (2005) montrent que la $b - valeur$ est dépendante du type de faille, en utilisant la Californie et des données mondiales. De la même manière Gulia and Wiemer (2010) utilisent des données d'Italie montrent et que la taille du tremblement de terre dépend du orientation du glissement sismique. Narteau et al. (2009) montrent que la valeur c est dépendante du rake de langle d'inclinaison de la faille. Il n'existe pas de modèle pour

la production des réplique, la valeur p et le taux de rélique. Comme la valeur b, la $p-valeur$ est également fortement affectée par le mécanisme de relaxation les contraintes et des lois de friction dans la zone sismogéne (Mikumo and Miyatake (1979); Dieterich (1986)).

Je montre que les valeurs moyennes des différents paramètres spatio-temporels (taux, p, K et H) sont dépendants des types de failles. Des événements en faille inverse ont une durée, un taux, une sismicité de fond et une diffusion plus élevés, comparé aux événements en coulissage. Les plus grandes durées dans un environnement de bruit de fond élevé sont contrôllées par le fort rapport de branchement et la faille valeur p des événements en faille inverse comparé á des coulissage. La diffusion du taux de densité d'événements en faille inverse est différente de celle des événements coulissage, ce qui implique en outre des diffusions différent suivant le type de faille.

2.1   Introduction

Aftershocks are the response of a seismogenic zone to the stress perturbation, contemporary to any earthquake size (e.g., Helmstetter, 2003). Relaxation of this stress perturbation may contain information about lithology, rock type, temperature and fluid contents of the seismic zone (e.g., Ziv, 2006b; Yang and Ben-Zion, 2009). Several physical models have been proposed to reproduce the dependency of the aftershock rate relaxation with different factors such as, fluid flow (Nur and Booker, 1972), viscous relaxation (Mikumo and Miyatake, 1979) or aseismic slip (Benioff, 1951; Schaff et al., 1998; Peng et al., 2005; Zöller and Ben-Zion, 2005). A number of other processes are also able to reproduce earthquake triggering by stress changes, such as stress corrosion (Das and Scholz, 1981; Yamashita and Knopoff, 1987; Gomberg et al., 2001b), rate and state friction model (Dieterich, 1994), and damage rheology (Ben-Zion and Lyakhovsky, 2006).

In space, aftershocks triggering is also proposed to be spatially dependent on the faulting style. When the orientation of the fault plane and local effective coefficients of static friction are known, it is possible to predict the zone where aftershocks would preferentially occur (e.g., King et al., 1994). Spatial distribution of the triggered seismicity strongly depends

on local fault geometry, slip distribution of the mainshock and mechanical properties of the crustal volume surrounding the causative fault (e.g., Scholz, 2002; Marsan, 2003). Previous studies show that aftershock linear density decay with distance from mainshock can be adjusted with a range of functions, including power law and combination of power laws with constant and exponentials (Huc and Main, 2003; Felzer and Brodsky, 2006; Marsan and Lengliné, 2010; Richards-Dinger et al., 2010). Frohlich and Willemann (1987) and Michael (1989) report a correlation of aftershock hypocenter locations with respect to the focal mechanisms of the mainshock. Using shallow earthquakes they showed that aftershocks cluster along the closest nodal plane and in the direction of strike of the mainshock, whereas for the deeper earthquakes this phenomenon has not been observed (e.g., Michael, 1989). Similarly ? studied the spatial clustering of aftershocks with respect to the focal mechanism of the mainshock to conclude that normal stress has little or no influence on aftershocks occurrence.

Earthquake triggering as driven by static stress changes is suggested by many authors such as Stein et al. (1992); King et al. (1994); ?); Tosi et al. (2004); Freed (2005). Aftershocks away from the mainshock are delayed,and this pattern is suggested to be driven by a lower stress changes at large distances (Helmstetter and Sornette, 2002b). These interactions are usually mapped as either aftershocks migration or diffusion with time, through either viscous relaxation process (Rydelek and Sacks, 2001) or due to fluid transfer in the crust (Nur and Booker, 1972; Hudnut et al., 1989; Noir et al., 1997) or by rate and state dependent friction model (Dieterich, 1994), subcritical crack grow (Das and Scholz, 1981; Yamashita and Knopoff, 1987) or damage or static fatigue laws (Lee and Sornette, 2000). Many other models assuming stress weakening or failure time increase are also suggested to reproduce aftershocks productivity through time and space (e.g., Mogi, 1968; Imoto, 1981; Chatelain et al., 1983; Tajima and Kanamori, 1985b,a; Ouchi and Uekawa, 1986; Wesson, 1987; Jacques et al., 1999; Helmstetter and Sornette, 2002b; Godano and Pingue, 2005). Apart from stress diffusion, multiple triggering or secondary aftershocks has also been proposed to be responsible for aftershock diffusion (e.g., Ouchi and Uekawa, 1986; Marsan et al., 2000). Initially aftershocks are triggered by the mainshock, but then after-

shocks produce their own aftershocks as time increases (e.g., Marsan and Lengline, 2008), thus producing cascade process that leads to an expansion of the aftershock zone (e.g., Marsan et al., 2000). Helmstetter and Sornette (2002b) further observed that the diffusion exponent H depends on Omori's law exponent ($p = 1 \pm \theta$) and linear density exponent (μ) i.e., $H = \frac{\theta}{\mu}$. Diffusion should be observed if $p < 1$ and it predicts H decreases with either decreasing $p - value$ or increasing $\mu - value$ (Helmstetter and Sornette, 2002b).

The stress changes imparted by thrust faults are typically higher than those for normal and strike-slip faults (e.g., **?**Lin and Stein, 2004; **?**). Using the global Harvard CMT catalog Huc and Main (2003) show that thrust events rate dominates the worldwide seismicity as compared to normal and strike slip events. In the literature the role of faulting style on the statistics of triggered seismicity is analyzed either using $b - value$ from Gutenberg Richter law or using $c - value$ from Omori law. Frohlich and Davis (1993) and Kagan (2002b) using the CMT catalog for shallow earthquakes, report a correlation between the exponent of the size of earthquake and faulting style ($\beta = 2/3 \ b - value$) as $\beta_N > \beta_T > \beta_{SS}$; N, SS, T for normal, thrust and strike-slip faulting respectively. Schorlemmer et al. (2005) reported that the $b - value$ of the Harvard CMT, Japan, Southern California (SCSN) and Northern California (NCSN) catalogs have dependency on fault plane solutions as, $b_N > b_{SS} > b_T$. Recently similar results were reported by Narteau et al. (2009) for $c - value$ and by Gulia and Wiemer (2010) for $b - value$ using aftershock data from Italy. This dependency of $b - value$ or $c - value$ on the faulting style was interpreted by Narteau et al. (2009) as consequences of the vertical stress (σ_v) value, maximum in case of normal faulting and minimum for thrust faulting. According to Narteau et al. (2009), $\sigma_{vN} > \sigma_{vSS} > \sigma_{vT}$ mimics b and $c - value$ relationship to the faulting styles.

Here we analyses how all Omori law parameters, i.e., aftershocks productivity, rate and p and $\alpha - value$ are dependent on faulting style triggering. Enescu and Ito (2002) suggested that $p - value$ depends on the frictional heating produced during rupture. They found that larger $p - value$ correlated with the region of larger slip of the 2000, Tottori earthquake. A small $p - value$ was found in the region which did not experience significant rupture. Similar results, i.e., $p - value$ depending on the slip distribution of the mainshock

was observed by Wiemer and Katsumata (1999) for four aftershock sequences (Landers, Morgan Hill, Northridge and Kobe earthquake). Higher $p-values$ were also correlated with higher crustal temperature and faster stress relaxation (Mogi, 1962, 1967; Kisslinger, 1996; Klein et al., 2006). Kisslinger and Jones (1991) found that higher $p-values$ in Southern California are in area of high heat flow, whereas Klein et al. (2006) examined a number of aftershock sequences from Hawaii and associated the higher $p-value$ with higher temperatures and faster stress relaxation near magma reservoirs.

In this study we attempt to perform a comprehensive spatio-temporal analysis of the aftershock patterns in space and time. For $m_m \geq 7$, mainshocks m_m being surface wave magnitude, we use both USGS and Harvard CMT focal mechanisms. For aftershocks we only use the USGS catalog because its completeness is better than the one of the CMT catalog. For fault plane solution the CMT completeness is better than the USGS one.

First for each of the mainshock with available focal mechanism solution, we estimate rate, Omori law parameters ($K-value$, $p-value$) for aftershocks and aftershock durations. We defined normal event (-135° < rake <-45°), thrust event (45° < rake <135°) and the remaining as strike slip events (e.g., Aki and Richards, 2002). Values of each clustering parameter is averaged on rake bin.

Secondly, we analyse linear density patterns of the stacked aftershock sequences. Finally diffusion processes of different faulting styles are tentatively compared.

2.2 Data: Mainshocks, aftershocks and background (foreshocks) selection

A distinction between foreshock, mainshock and aftershock remains empirical. Some authors (such as Kagan and Knopoff, 1981; Shaw, 1993; Jones et al., 1995; Felzer et al., 2002a; Helmstetter and Sornette, 2003b) suggest this distinction as arbitrary and physically artificial. "Regular" foreshocks are earthquakes (above the background rate) preceding the larger earthquake (mainshock) which itself is followed by smaller earthquakes,

taken as aftershocks when they occur within specific space-time window. Different proce-
dures for the selection of mainshock and its corresponding aftershocks have been previously
proposed (e.g., Gardner and Knopoff, 1974; Reasenberg, 1985; Kagan, 1991; Knopoff, 2000;
Felzer et al., 2002a; Helmstetter, 2003; Felzer et al., 2004; Marsan, 2005; Helmstetter et al.,
2005; Marsan and Lengline, 2008). No definitive time, space window emerge for aftershock
selection (e.g., Bak et al., 2002).

In this study, we selected shallow (depth < 70 km) earthquake with $m_m \geq 7.0$ as a
mainshock when its focal mechanism solution are available either in USGS or CMT catalog.
This mainshock selection is similar to the one of Kagan (2002a); Parsons (2002); Tahir and
Grasso (2009). We also isolate the mainshock from the effect of the nearest largest shock
by ignoring mainshock which is either followed or preceded by a larger event with [1 yr,
$5L$] window. Foreshock and aftershocks data of the corresponding mainshocks are taken
from USGS (http://earthquake.usgs.gov). This catalog (USGS catalog) choice is driven by
the lower completeness magnitude than the global Harvard CMT catalog. USGS catalog
spans on a period of about 37 years (1973 - 2010).

CMT and USGS focal mechanism catalog start from 1977 and 1980 respectively. For the
same event the focal mechanism solution (http://earthquake.usgs.gov/earthquakes/eqarchives/sopar/)
are different in both (CMT and USGS) catalogs (figures (2.1 – 2.3)).

For the selection of aftershocks, the m_c completeness magnitude value is estimated
using maximum curvature technique (Wiemer and Wyss, 2000; Woessner and Wiemer,
2005). m_c is computed for the entire USGS catalog, 1973 – 2010. Only shock ($m > m_c$)
triggered 3, 7, 30 days after the mainshock are used. We further imposed $m < m_m$ and the
the aftershock to occur within $5*L$ distance. L is the fault length derived from magnitude
using Wells and Coppersmith (1994) formula. For the background event we select events
in the [5 yrs, $5L$] window around the mainshock. Although we have tested different space-
time windows, but we used $5*L$ as an optimized space window to have enough data for
backgrounds and aftershocks. For the analysis of spatio-temporal triggering (diffusions),
we extend the space window upto $10*L$ around the mainshock .
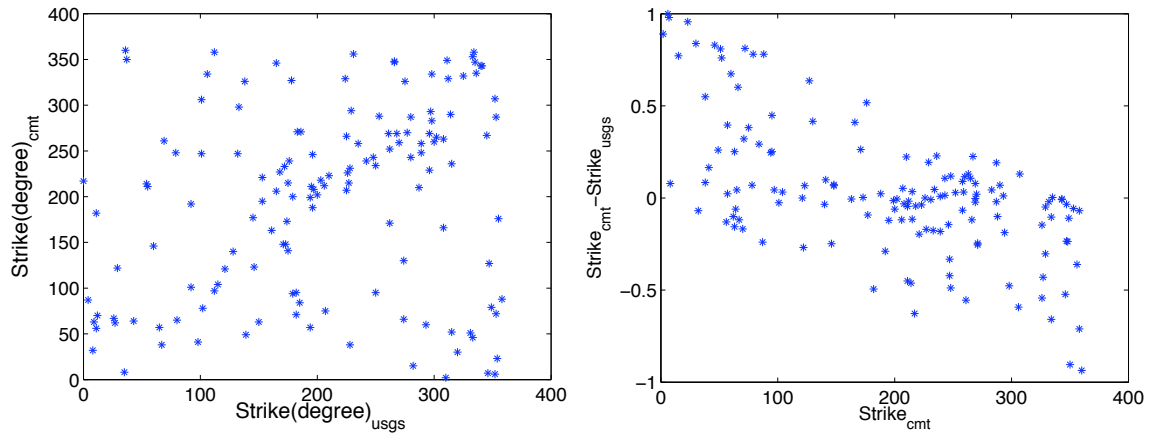
Figure 2.1: Strike of the mainshocks ($m_m \geq 7.0$) for the USGS and CMT catalogs.
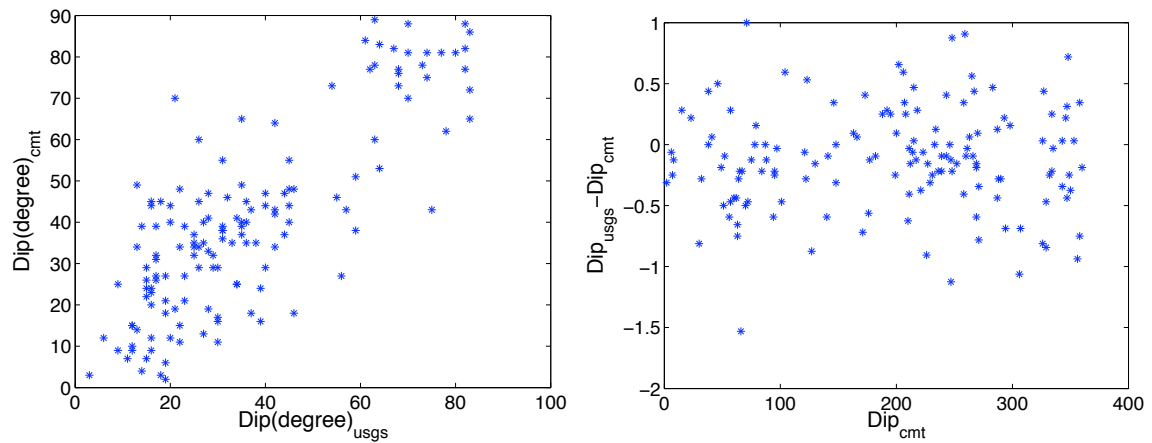
Figure 2.2: Dip of the mainshocks ($m_m \geq 7.0$) for the USGS and CMT catalogs.
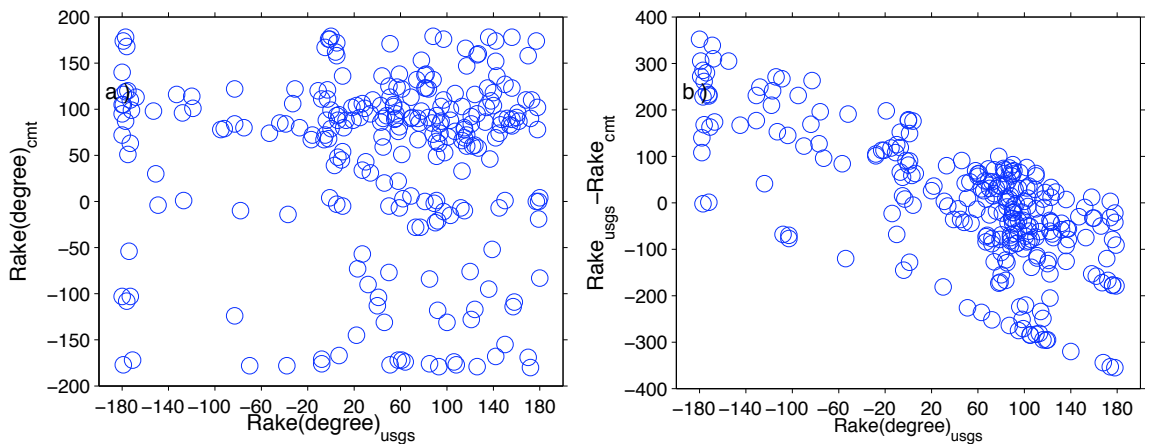
Figure 2.3: Rake of the mainshocks ($m_m \geq 7.0$) for the USGS and CMT catalogs.

2.3 Time and space aftershock patterns

2.3.1 Normalised aftershock rate

The number of aftershocks $n(m \geq m_c)$ for each of the corresponding mainshock are calculated using a fixed 5*L distance and 3, 7 and 30 days, time windows. $n(m_m)$ is proposed to be dependent on mainshock magnitude m_m i.e., $n(m_m) \sim 10^{\alpha(m_m - m_c)}$, where $\alpha \sim 0.8 - 1$ (e.g., Helmstetter (2003); Felzer et al. (2002b)). To correct for the effects mainshock magnitude (m_m) and threshold magnitude (m_c) on rate, this later being different for each sequences, we used the normalized aftershocks rate (N^*) (e.g., Helmstetter, 2003; Tahir and Grasso, 2009).

The normalized rate (N^*) of each sequence with N_i aftershocks within $t_w = [3, 7, 30]$ days window after the mainshock, is written as,

$$N^* = \frac{N_i}{t_w 10^{\alpha(m_m - m_c)}}; \quad t_w = [3, 7, 30]; \tag{2.1}$$

$$N^*_{20°} = N_r \bigcup_{r=-180°:20°:160°} N_{r+20°} \tag{2.2}$$

$N^*_{20°}$ is the union or stack of the normalized rate for each of the mainshocks in a corresponding 20° rake bin (figure 4.1(a,b,c)). For simiplicity α value is taken as 1, as suggested by Helmstetter et al. (2005). Discrete average normalize rate $\langle N^*_{20°} \rangle$ is defined as;

$$\langle N^*_{20°} \rangle = \frac{\sum_{j}^{N_l}(N^*_{20°})_j}{N_l} \tag{2.3}$$

Where N_l is the total number of mainshocks in the corresponding 20° rake bin.

Mainshocks are classified into different mechanisms (thrust, strike slip and normal) ac-

cording to their rake angle (Aki and Richards, 2002). Then global average rate ($\langle N^*_{20°}\rangle_{cmt/usgs}$) and standard deviation of each faulting style are calculated as;

$$\langle N^*_{20°}\rangle_{cmt/usgs} = \frac{\sum\langle N^*_{20°}\rangle}{Nr} \tag{2.4}$$

Where Nr is the number of events of the corresponding faulting style in a given bin. Finally normalized rate of each faulting style is further divided by it maximum value to obtain rate in [0 1] range (figure 4.1d).

2.3.2   Background Rate

Background rate is estimated using events within 5*L and 5 years before the mainshock. Normalized background rates per rake bin are computed in the same way as for aftershocks rates. Global average ($\langle Bg_{20°}\rangle_{cmt/usgs}$) and standard deviation for each faulting style are extracted, similar as equation (2.4). We explore background rate for 30 days, 1 year and 5 years time windows (figure 2.6(b,c,d)).
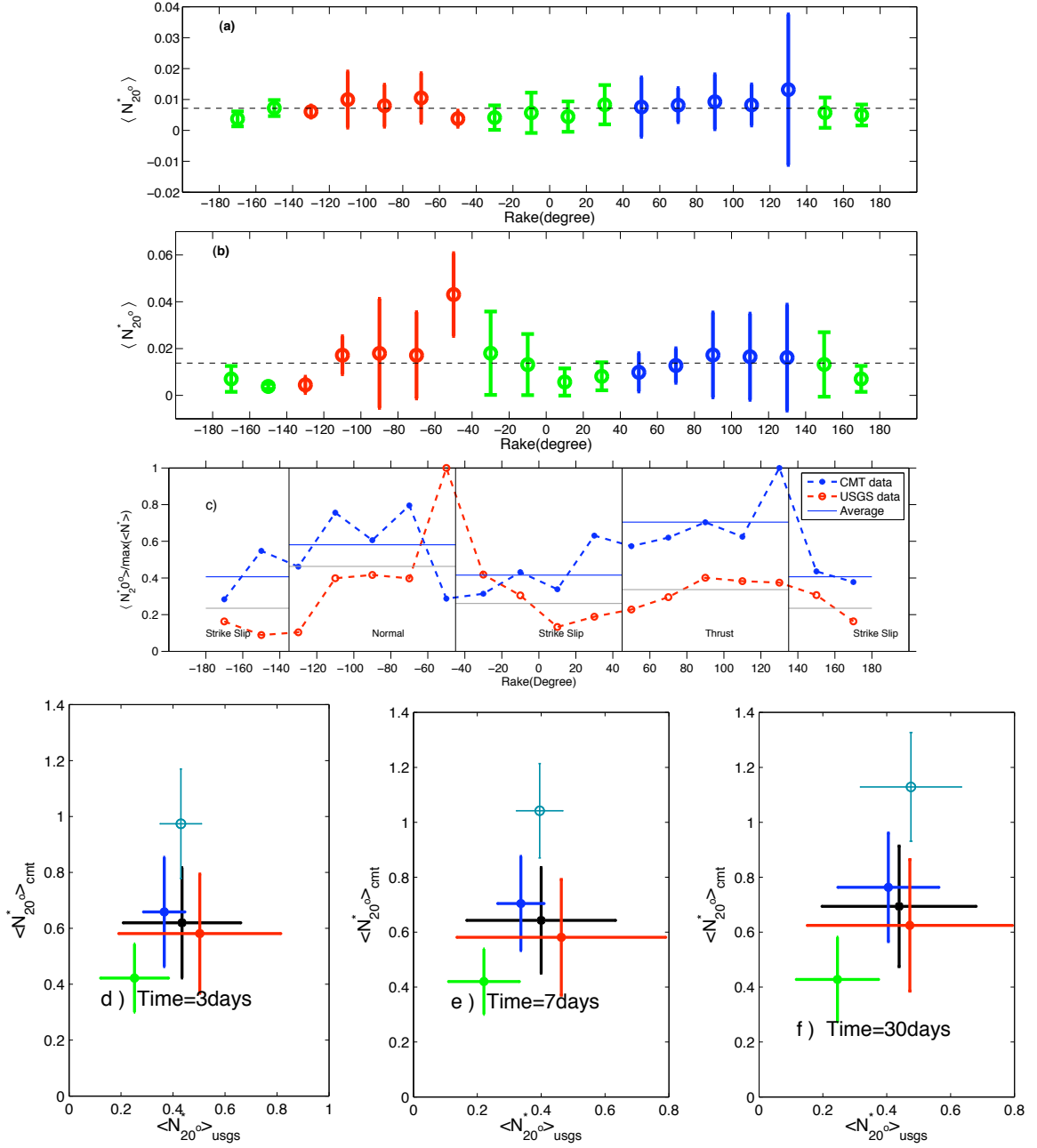
Figure 2.4: Average normalized aftershock rate as function of focal mechanism. Red normal event, blue thrust event, green strike slip, black dip slip. Global average normalize rate ($\langle N_{20°}^* \rangle_{cmt/usgs}$) for each faulting style is being computed using equation (2.4). (a) Discrete average normalize aftershocks rate ($\langle N_{20°}^* \rangle$) and standard deviation in 20° rake bin, calculated using 7 days aftershocks time window, with mainshock focal mechanism solution from CMT catalog; black dotted line is global average rate. (b) Same as (a) but focal mechanism solutions from USGS. (c) Comparison of discrete average normalize rate with focal mechanism solution from CMT (blue) and USGS (red) catalog; horizontal straight line is the global average value of the corresponding faulting style. (d - f) $\langle N_{20°}^* \rangle_{cmt}$ as function of $\langle N_{20°}^* \rangle_{usgs}$ for 3 (d), 7 (e) and 30 (f) days window.
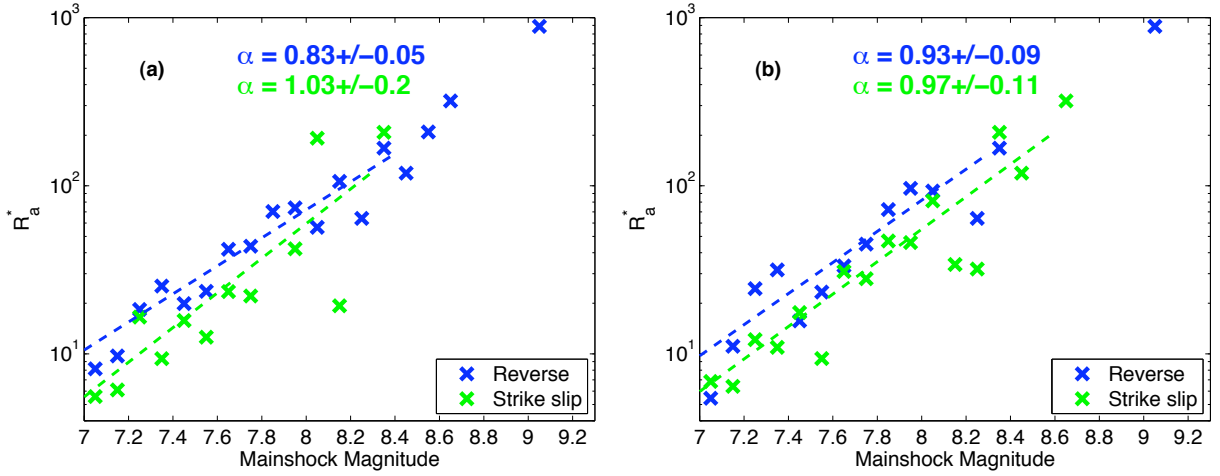
Figure 2.5: Comparison of α for different faulting style. Aftershocks are selected [1 yr, 1*L] window from the mainshock. Normalized aftershock rate ($R_a^* = \frac{R_a}{N_m}$) is the number of aftershocks, with mainshock magnitude $\in [M, M+0.1]$, divided by the number of mainshocks (N_m) in each class. Slope of the least square line is $\alpha - value$. (a) $\alpha - value$ calculated using CMT catalog; (b) $\alpha - value$ calculated using USGS catalog.

2.3.3 Omori Law Parameters

The change in time of seismicity rate following a mainshock is well reproduced by Omori's law;

$$N(t) = \frac{K}{(t+c)^p} \tag{2.5}$$

$N(t)$ is the seismicity rate, t is the time the mainshock occurrence, p, c and K are constants (Utsu et al., 1995; Utsu, 1961). A median $p - value$ of ~ 1.1 is reported for the aftershock sequences in the various parts of the world, with range of ~ 0.6 - 2.5 (Utsu et al., 1995). K is the productivity of aftershocks sequences.

We have used Maximum likelihood method of Ogata (1983) to estimate, K, p, c, the modified Omori law parameters. In order to reduce error bars, we only used aftershock sequences with number of aftershocks greater than 5 within distance = 5*L. Omori law parameters are calculated for the stack data.
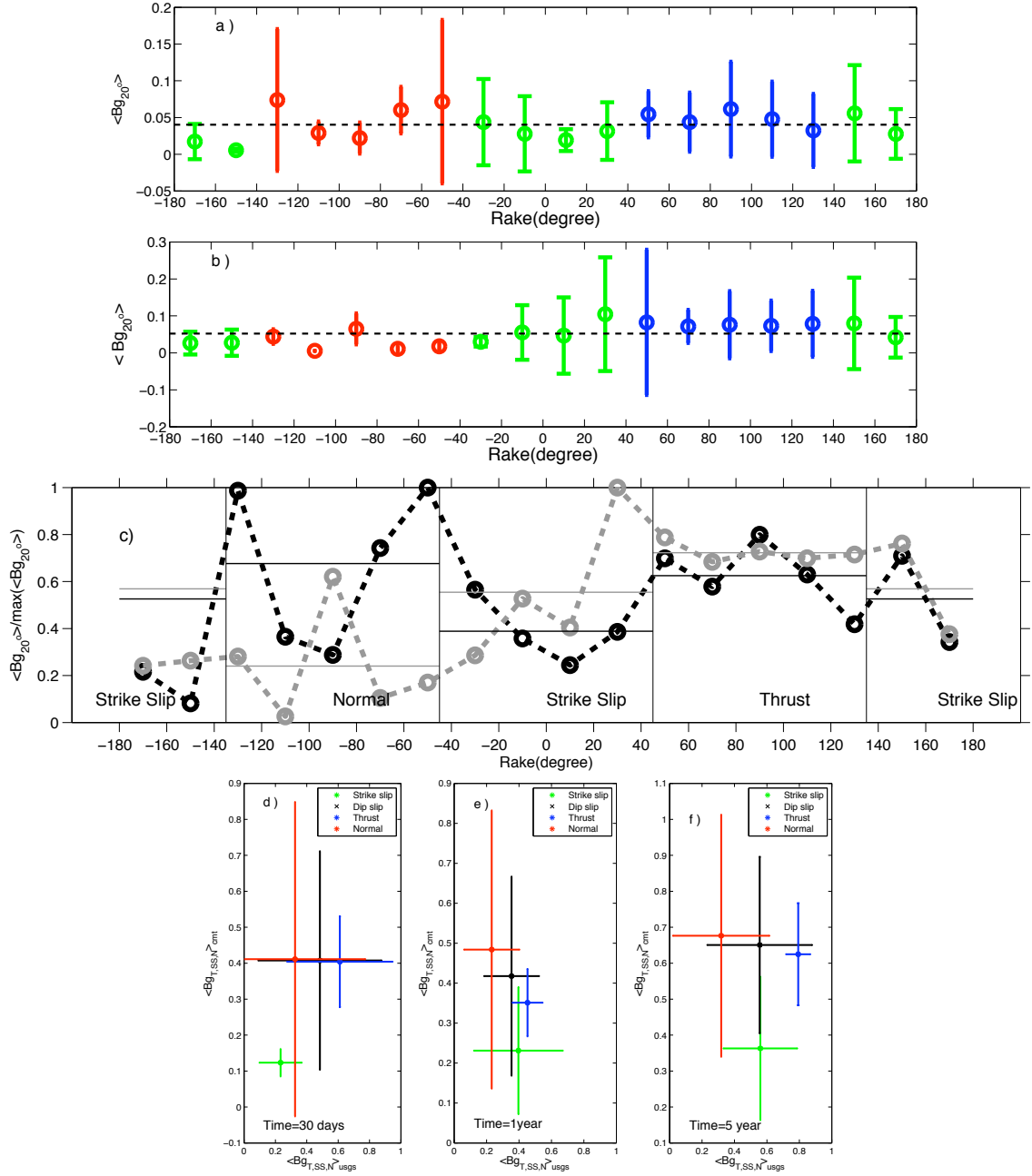
Figure 2.6: Average background rate and focal mechanism. Red normal event, blue thrust event, green strike slip, black dip slip. Global average background rate ($\langle Bg_{20°} \rangle_{cmt,usgs}$) for each faulting style is being computed using equation (2.4). (a) Discrete average background rate ($\langle Bg_{20°} \rangle$) and standard deviation in 20° rake bin, calculated using 5* yr events data before the mainshock, with mainshock focal mechanism solution from CMT catalog; black dotted line is global average rate. (b) Same as (a) but focal mechanism solutions from USGS. (c) Comparison of discrete average background rate with focal mechanism solution from CMT (black) and USGS (gray) catalog; horizontal straight line is the global average value of the corresponding faulting style. (d - f) $\langle Bg_{20°} \rangle_{cmt}$ as function of $\langle Bg_{20°} \rangle_{usgs}$ for 30 days (d), 1 yr (e) and 5 yr (f) time window.

$p - value$ for different faulting style using stacked data

To reach stable estimation of the variations of $p - value$ with respect to rake, we analyse $p - value$ of the stacked aftershock sequences. The stacking of the data smoothes out fluctuations associated with individual sequences and highlights the common features of all sequences (e.g., Helmstetter and Sornette, 2003b; Ouillon and Sornette, 2005; Yang and Ben-Zion, 2009).

Firstly we stack aftershock sequences for three rake bins values [-135°, -45°] as normal slip trigger, [45°, 135°] as thrust slip trigger and remaining as strike slip trigger.

$$R_N(t) = \bigcup_{-135:Rake:-45} T_i \tag{2.6}$$

$$R_T(t) = \bigcup_{45:Rake:135} T_i \tag{2.7}$$

Where T_i is the time series of each sequence, $R_T(t)$ and $R_N(t)$ are the stacked aftershocks time series for thrust and normal mechanism respectively. Then $p-value$ ($p-value_{cmt}/p-value_{usgs}$) of each faulting style is computed by fitting an Omori law to the stacked sequences (i.e., $R_T(t)$, $R_N(t)$ and $R_{SS}(t)$, figure 2.7).

Secondly we stack aftershock sequences within 20° rake bin as,

$$R_{20°} = T_i \bigcup_{i=-180°:20°:160°} T_{i+20°} \tag{2.8}$$

Where $R_{20°}$ is the stack of aftershock sequences (T) with mainshock rake angle in the corresponding 20° bin. $p - value$ is fitted upto 10 days of the stacked rate for each rake bin, but the $p - value$ is also estimated using the duration of sequence as time length. Average $p - value$ ($\langle p_{20°} \rangle_{cmt/usgs}$) and standard deviation are calculated for each faulting style similarly to equation (2.4).
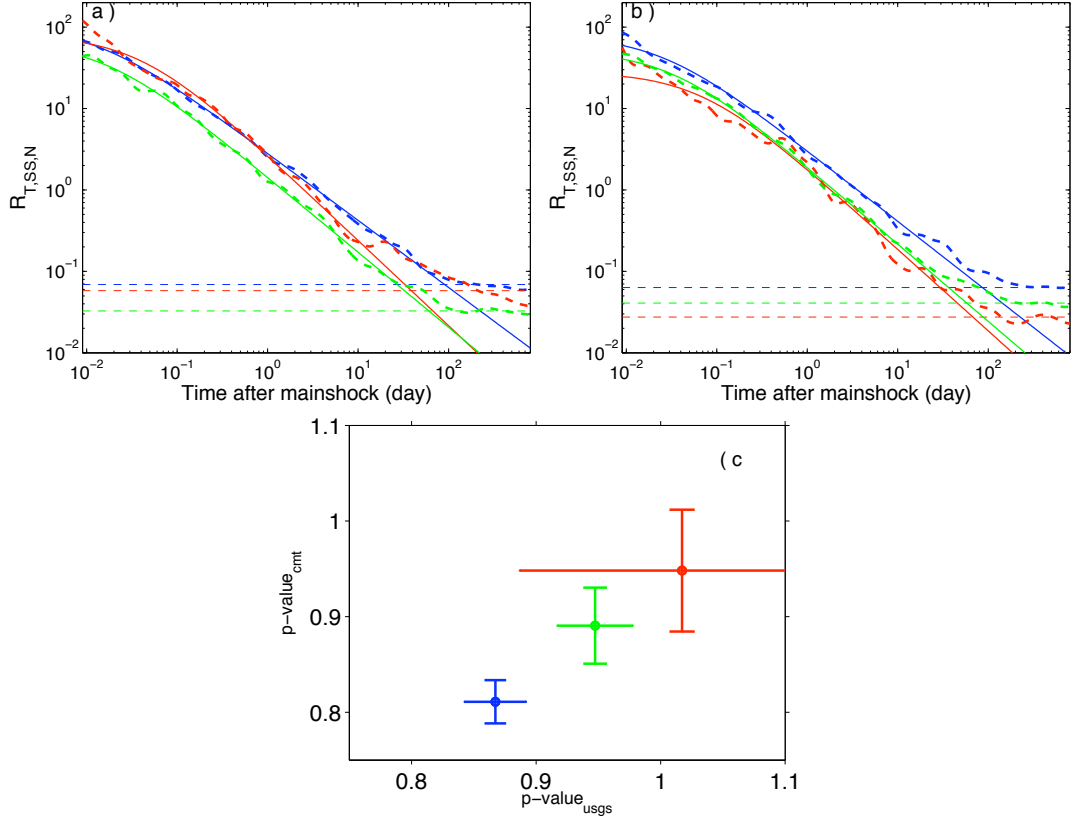
Figure 2.7: Stacked aftershocks daily rate for different focal mechanism. (a) Aftershocks rate with focal mechanism from CMT catalog (b) Aftershocks rate with focal mechanism from USGS catalog. Note that stack data is normalized by its corresponding number of mainshocks (c) Comparison of $p-value$ from CMT (vertical errorbar) and USGS (horizontal errorbar), see section 2.2 for mainshock selection. Omori law law parameters are calculated for the aftershocks data upto 10 days. Normal events (red), thrust events (blue), strike slip events (green). Solid line show Omori law fit to the stacked data (dash line). Note that stack aftershocks rate are calculated by using gaussian method (Helmstetter and Sornette, 2002b). Aftershocks are selected within [5 yr, 5*L] window. Horizontal dashed line is the average background rate within 5L, 5 yrs window before the mainshock.
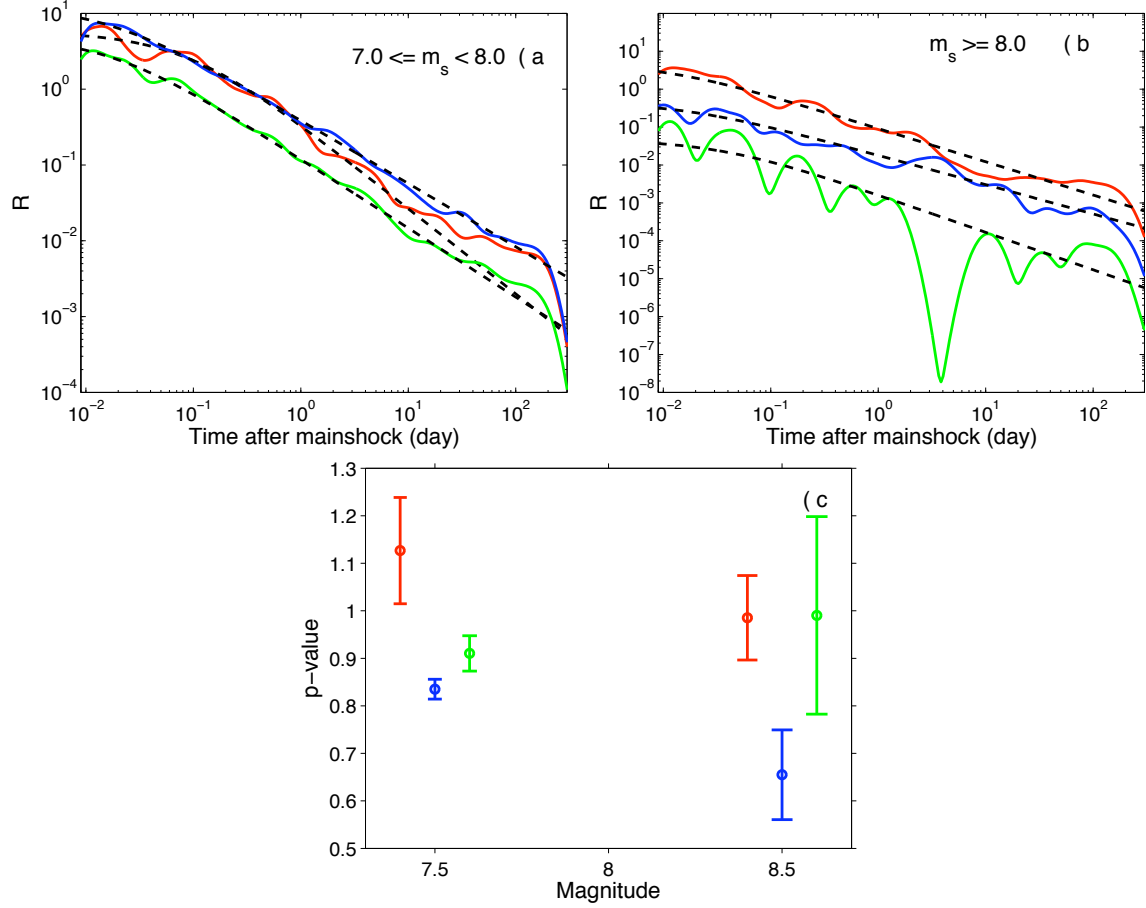
Figure 2.8: Aftershock rate (R) and mainshock magnitude. (a) Stacked aftershock rate with $7.0 \leq m_s < 8.0$, data is being smoothed with using Gaussian function (Helmstetter and Sornette, 2002b) (b) Stacked aftershock rate with $m_s \geq 8.0$ (c) comparison of the $p - value$ with mainshock $7.0 \leq m_s < 8.0$ and $m_s \geq 8.0$. Aftershocks are selected within 1 yr, 5*L time-space window. Dash black line shows Omori law fit to the stack data (red normal, blue thrust and green strike slip events). Note that each stacked sequences is normalize by its corresponding number of mainshock.

2.3.4   Aftershocks diffusion and faulting style

Aftershocks and foreshocks linear density have been observed to obey power law (e.g., Ogata, 1999; Felzer and Brodsky, 2006; Lippiello et al., 2009b; Brodsky, 2011);

$$\Phi(t) \sim \frac{1}{(r)^{\mu(t)}} \tag{2.9}$$

where $\Phi(t)$ is the linear density, r is the distance between mainshock and aftershock (e.g., Ogata, 1999; Helmstetter and Shaw, 2006). Helmstetter and Sornette (2002b) show that diffusion exponent H $(R(t) \sim t^H)$ can be written as $H = \frac{\theta}{\mu}$, where $\theta = 1 + p$. In order to test aftershocks migration toward background, we calculate $\Phi(t)$ within $10*L$ and ($[5 : 2 : 80]$ days) time window around the mainshock. Linear density of the stack sequence is calculated by using nearest neighbor method (Felzer and Brodsky, 2006). $\Phi(t)$ is further normalized by the duration of time window to get normalized linear density, $\Phi'(t)$ number/km/day. Slope ($\mu(t)$) of the power law decay part of linear density is computed using least square method. Because linear density have plateau upto 40 km, for power law fitting, we use data in the 40 - 500 km range (figure 2.15).

Furthermore, we also compute average distances between mainshock and it corresponding aftershocks at different time window from the mainshock. Similarly to $\Phi(t)$ we only use stack data of different faulting style.

2.4   Results

Space time characteristics of earthquake clustering have been tested for the dependency on faulting style, by defining a mainshock for magnitude ($m_m \geq 7.0$), shallow (< 70 km) depth. We ignore mainshock which is either followed or preceded by larger event within (1 yr, $5L$) window. We use threshold magnitude (m_c) as 5.0, which is estimated from frequency magnitude plot for the whole USGS catalog.
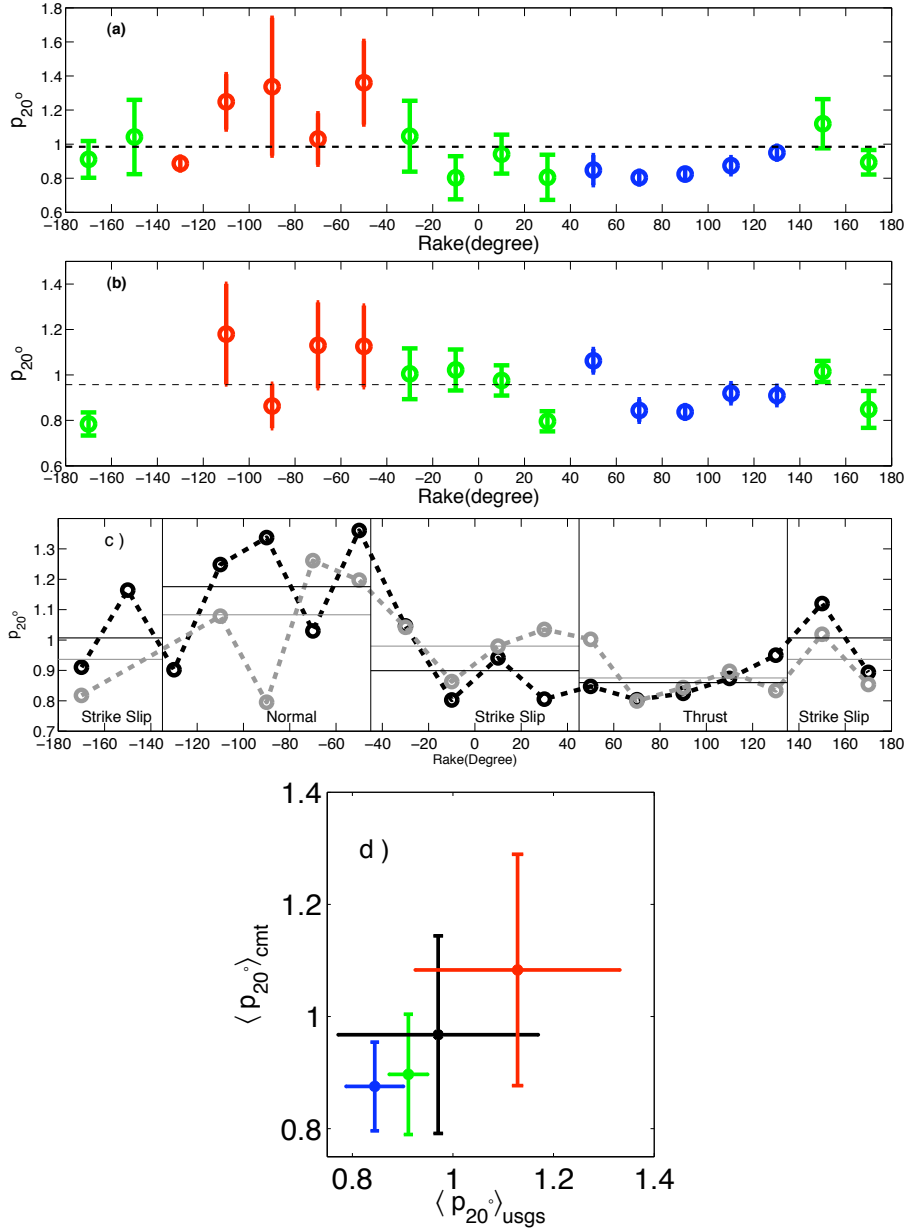
Figure 2.9: $p - value$ for $20°$ rake bin using stacked data. Aftershocks are within 10 days, $5*L$ window from the mainshock. (a) $p - value$ ($p_{20°}$) with focal mechanism solution from CMT catalog. (b) $p - value$ ($p_{20°}$) with focal mechanism solution from USGS catalog. (c) Comparison of $p - value$ from both CMT and USGS catalog as function of rake. (d) Average $p - value$ for CMT ($\langle p_{20°}\rangle_{cmt}$) and USGS ($\langle p_{20°}\rangle_{usgs}$) catalogs.
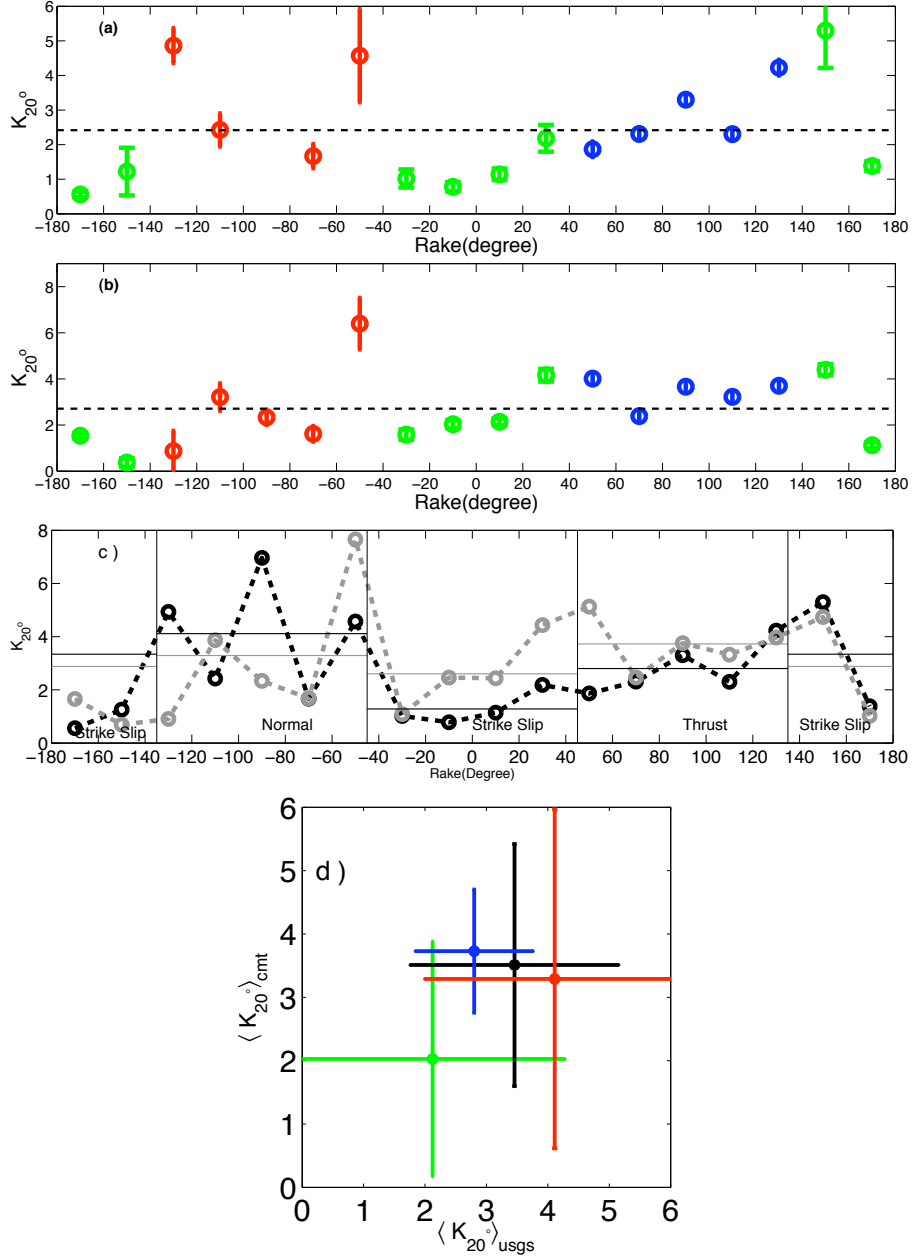
Figure 2.10: $K-value$ for $20°$ rake bin using stacked data. Aftershocks are within 10 days, $5*L$ window from the mainshock. (a) $K-value$ ($K_{20°}$) with focal mechanism solution from CMT catalog. (b) $K-value$ ($K_{20°}$) with focal mechanism solution from USGS catalog. (c) Comparison of $K-value$ from both CMT and USGS catalog as function of rake. (d) Average $K-value$ for CMT ($\langle K_{20°} \rangle_{cmt}$) and USGS ($\langle K_{20°} \rangle_{usgs}$) catalogs.

94

2.4.1   Temporal analysis

Earthquake rate, after and before the trigger shock

Discrete average normalized aftershock rate ($\langle N^*_{20°} \rangle$) changes with mainshock rake angle (figure 4.1). For thrust events the global averaged normalized rate is significantly higher than for strike slip events. We resolve dip slip events have higher global average normalize rate than the strike slip events. The results are robust with 3, 7 and 30 days time windows (figure 4.1). Although thrust events have higher global average aftershock rate than the strike slip events, but $\alpha - values$ show that $\alpha_{SS} > \alpha_T$ (figure 2.5). Note that this change in $\alpha - value$ is only resolve for CMT catalog.

Discrete average background rates ($\langle Bg_{20°} \rangle$) calculated for different faulting style using $20°$ rake bin data on $[5L, 5 \text{ yrs}]$ window before the mainshock display high error bars (figure 2.6(b,c,d)).

Global average background rate for thrust events emerges as always higher than strike slip events (figure 2.6 (b,c,d)). These results ($Bg_T > Bg_{SS}$) are confirmed from stacking all the pre-events seismicity rate for thrust and strike slip events within 5 yrs, $5L$ windows (figure 2.7). The results are robust and do not changes with changing time windows.

$p - value$

In order to analyze $p - value$ as a function of different faulting styles, we process the data in two different ways. First we use the stacked aftershocks sequence for each of the corresponding faulting style (i.e., thrust, strike slip and normal events). Using maximum likelihood method, we obtain $p_N > p_{SS} > p_T$ (figure (2.7)). The same results are confirmed for $7.0 \leq m_m < 8.0$ and $m_m \geq 8.0$ (figure (2.8)). The similarity between results demonstrates the pattern is not driven by mainshock magnitude.

Secondly, the same pattern again emerges from the average of $p_{20°}$ ($p - value$ from stacking $20°$ rake bin data, figure 2.9). Furthermore, the results are robust and do not change for $p - value$ estimated using with duration of the aftershock sequence as time window.

$K - value$

$\langle K_{20°} - value \rangle$ also highlights the dependency on the faulting style (figure 2.10 (a, b, c)). This pattern is in agreement with the one of average normalize rates ($\langle N_{20°}^* \rangle$), i.e., K_T, $K_N > K_{SS}$ (figure 2.10).

Foreshocks α', K' and $p' - value$

Because foreshocks rate is weak and fluctuating, so we only use 10 days window for Omori's law fitting. We resolve average thrust foreshock rate is higher than for strike slip, but foreshock productivity (α') as a function of mainshock magnitude displays no trend (figure 3.1). Similarly, we do not resolve any $p' - value$ dependency on faulting style (figure 2.12).

2.4.2 Spatial analysis

Normalize linear density ($\Phi'(t)$) of all type of faulting style does not always obey a power law, specifically for distance < 40 km from the mainshock epicenter. Initially density increases with distance from the mainshock epicenter upto a peak density value and then it decays as power law. Distance of the peak density from the mainshock depends on the size of the mainshock (e.g., Lippiello et al., 2009b). We observe both catalogs (CMT and USGS) have peak linear density ~ 40 km distance from mainshock epicenter. Accordingly we adjust a power law fit between 40 and 500 km for the stacked data (figure 2.13, 2.14). We performed our calculations upto 500 km distance because at large distances the uncorrelated events strongly interact with tails of aftershock sequences (e.g., Richards-Dinger et al., 2010).

To test for possible influence of different faulting style on aftershocks diffusion, we estimate linear density for 5 to 80 days with step size as 2 days. We further normalize the linear density by each corresponding time window. For normal events, it was difficult to adjust a power law on data due to limited data points and large error bars. So we only analyze thrust and strike slip events (figure (2.13, 2.14)). $\mu - value$ computed from
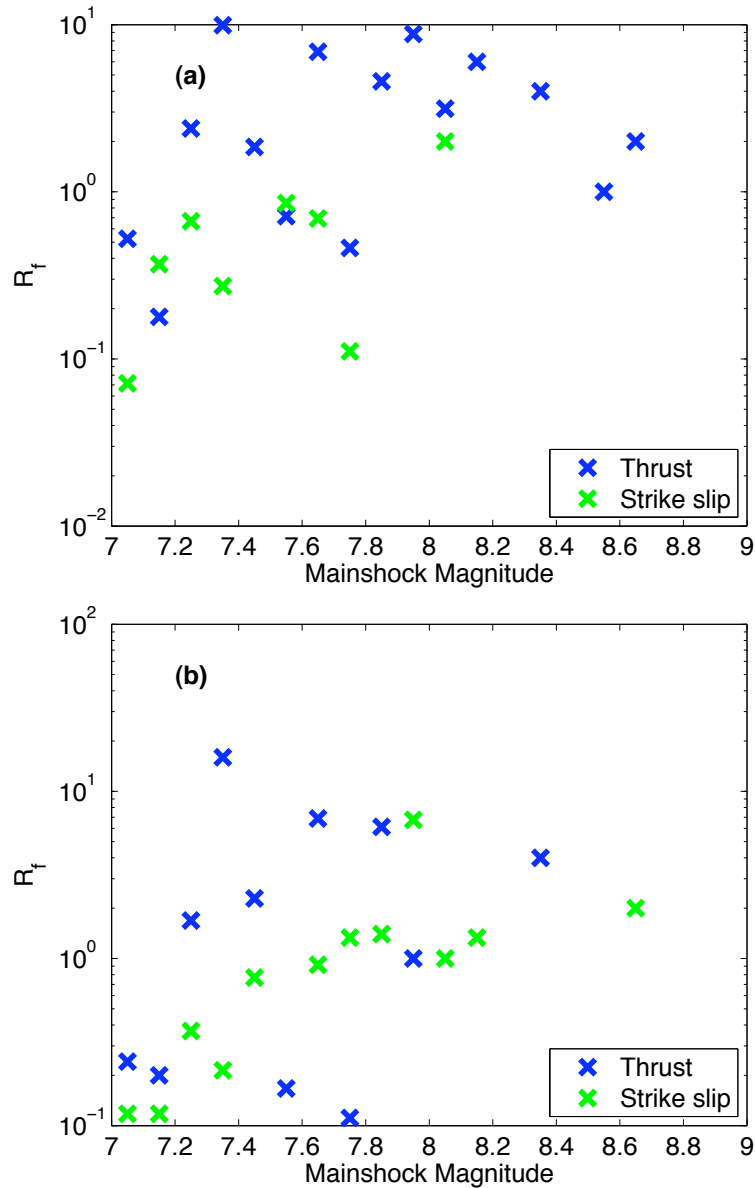
Figure 2.11: Foreshocks rate as a function of mainshock magnitude for different faulting style (CMT and USGS catalogs); Foreshocks are taken within 10 days, 1*L window around the mainshock. Normalize rate (R_f) is the number of foreshocks in a space time window, divided by number of mainshock (N) in each class. (a) Foreshock rates, CMT catalog (b) Foreshock rates, USGS catalog.
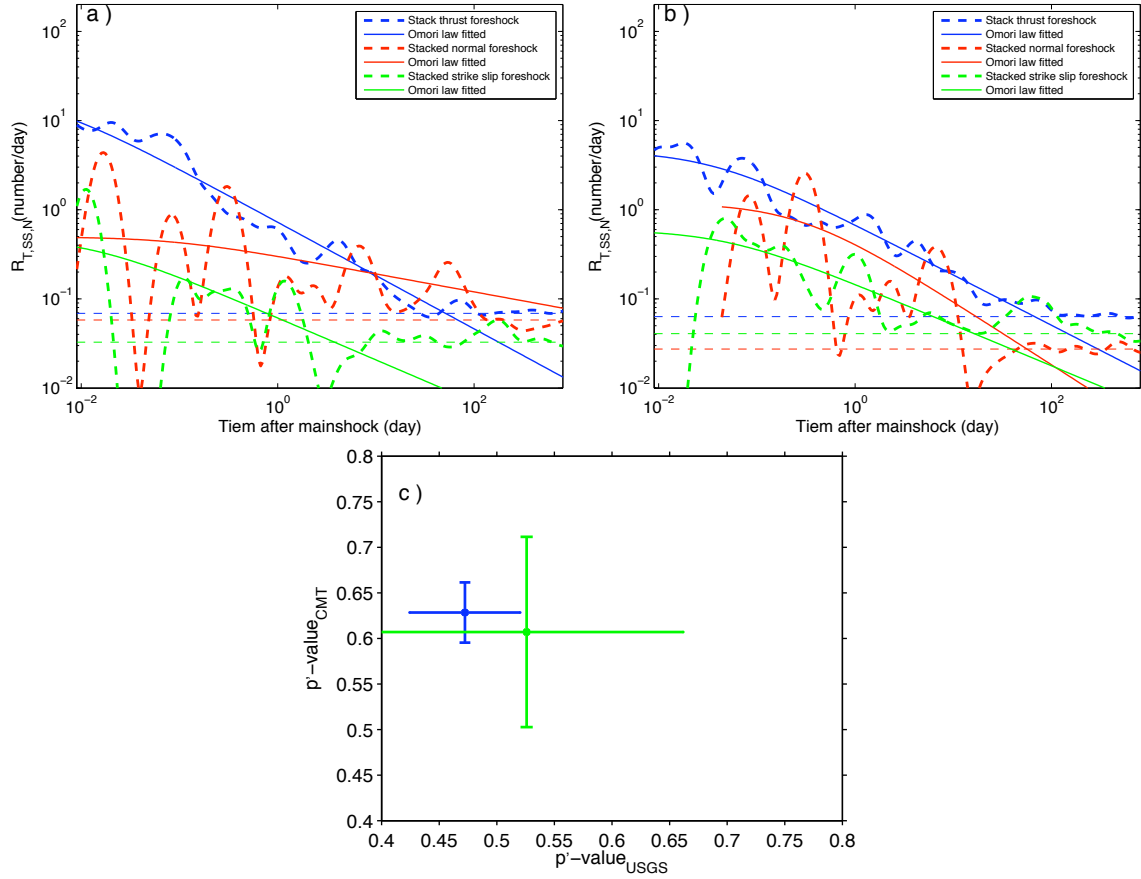
Figure 2.12: Stacked foreshocks daily rate; thrust (blue), strike slip (green) and normal (red). Events (above the background rate) occur before and within distance 5*L around the mainshock are taken as foreshocks. Solid line is Omori law fit to the stacked data (dash line) upto 10 days. Foreshocks are plotted on the same side of aftershocks by multiplying with -1. Horizontal dash line show average background rate. (a) Foreshocks rate using focal mechanism from CMT catalog (b) Foreshocks rate using focal mechanism from USGS catalog. (c) Comparison of $p' - value$ from CMT (vertical errorbar) and USGS (horizontal errorbar). Note that stacked data is normalize by its corresponding number of mainshocks.

equation (2.9) varies with time after the mainshock and its value is larger for strike slip events than for thrust events (figure 2.15). We fails to resolve change between thrust and strike slip driven diffusion style, when estimating (H_T, H_{SS}) exponent.

2.5 Discussion

Our analysis of aftershock sequences of $m_m \geq 7$, worldwide demonstrates all the Omori law parameters, and the exponent of linear density (μ) vary with the mainshock faulting style. On average the tectonic settings are playing an important role to control the trigerring processes in space time. Thrust events comparatively to the strike slip events have higher $K-value$ and aftershocks rates in the high background rate setting. These observations are consistent with the results of Toda et al. (2005). They show that active areas that is the region where the pre-seismic activity is higher have the higher aftershock rates, because of the Coulomb stress changes amplify the background seismicity (Toda et al., 2005). So, small stress changes produce large changes in the seismicity rate. Similarly Marsan (2006) performed an extensive numerical simulations and show that reference seismicity rate increases with multiple interactions which decrease the ratio of aftershock to background rates. Thus the same results i.e., higher background and aftershock rates emerge from thrust events, multiple interactions of thrust events are stronger than that of strike sip events. We show that the higher thrust event rates is driven by sequences of 7.0 $\leq m_m \leq 8.0$ (figure 2.5). Independently, the relative dependency on mainshock size drives an α value of strike slip which is greater than that of thrust events.

One possible candidate to reproduce our results, using the ETAS (epidemic type aftershock sequence) model, is the tuning of branching ratio (n). Its values depend on numerous parameters as, $n = \frac{Kbc^{1-p}(1-10^{(\alpha-b)(m_m-m_c)})}{(b-\alpha)(p-1)(1-10^{b(m_m-m_c)})}$ (Helmstetter and Sornette, 2002a; Hainzl et al., 2006). Using the he simplied form ($n = \frac{Kb}{\alpha-b}$) we estimate $\frac{n_T}{n_{SS}} = 1.4 \pm 0.05$ by using K, α and $b-value$ of the respective faulting styles (Table 2.1). Following (e.g., Helmstetter and Sornette, 2002a) interpretation of branching ratio, a lower branching ratio for strike slip event sequences suggests a more visco-elastic or ductile properties of the crust compliance

99
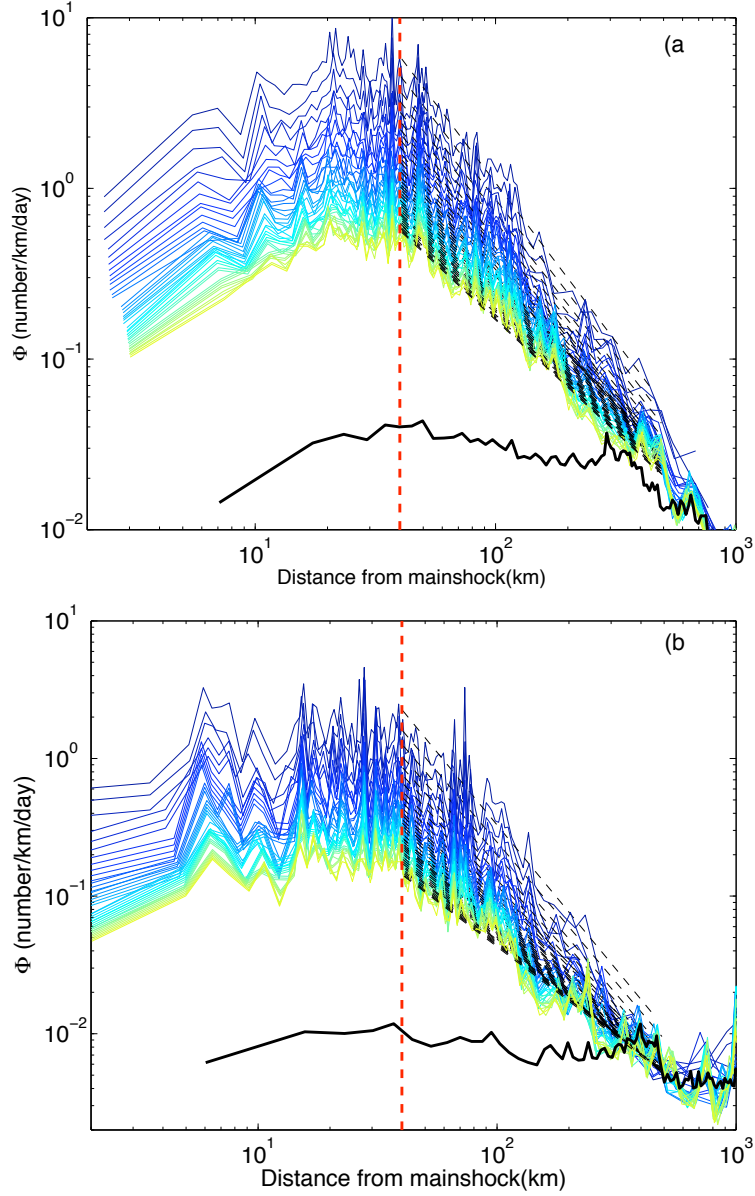
Figure 2.13: Normalized density rate $(\Phi'(t))$ of thrust (top) and strike slip (bottom) events, with its focal mechanism from CMT catalog. $\Phi(t)$ (equation 2.9) is calculated for time windows ranging from 5 (blue line, top) to 80 days (red line, bottom) with step size as 2 days for each calculation. The linear density $(\Phi(t))$ is further normalized by the duration of the time window used to estimate the normalized density rate $(\Phi'(t))$. (a) Density rate $(\Phi'(t))$ for thrust events, with least square line is fitted to the data between 40 to 500 km. (b) Density rate $(\Phi'(t))$ for strike slip events.
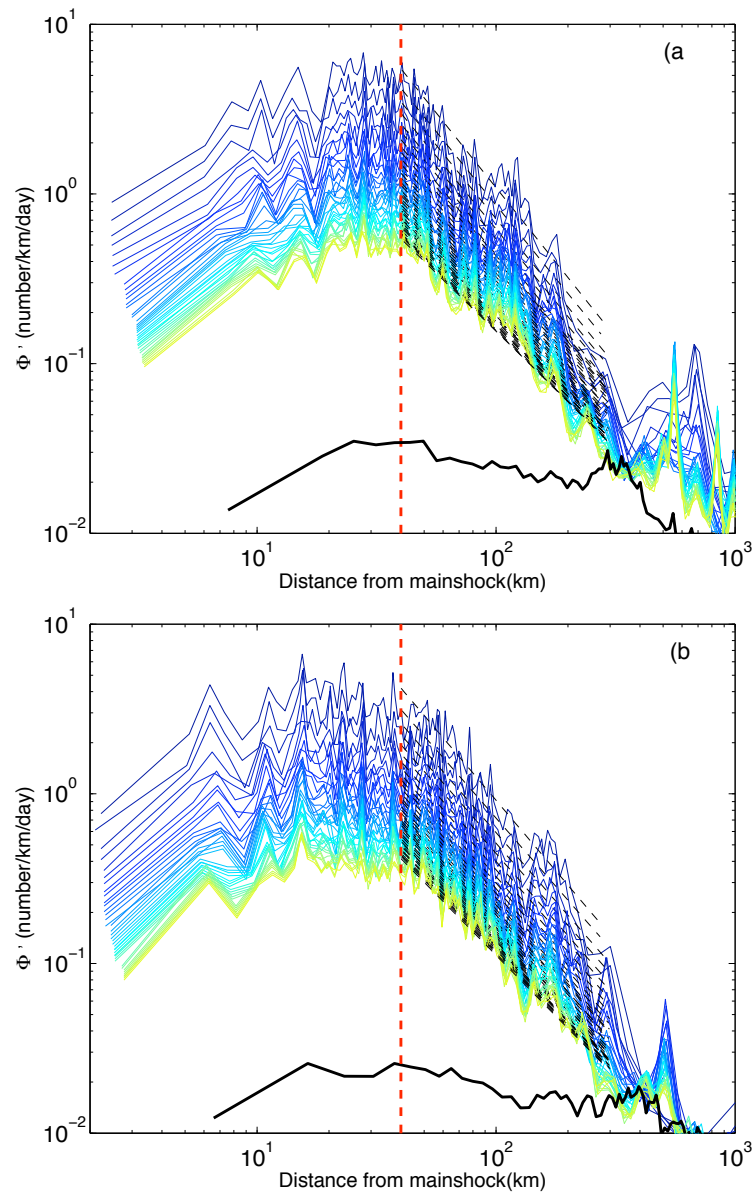
Figure 2.14: Same as figure 2.13, but for USGS catalog.
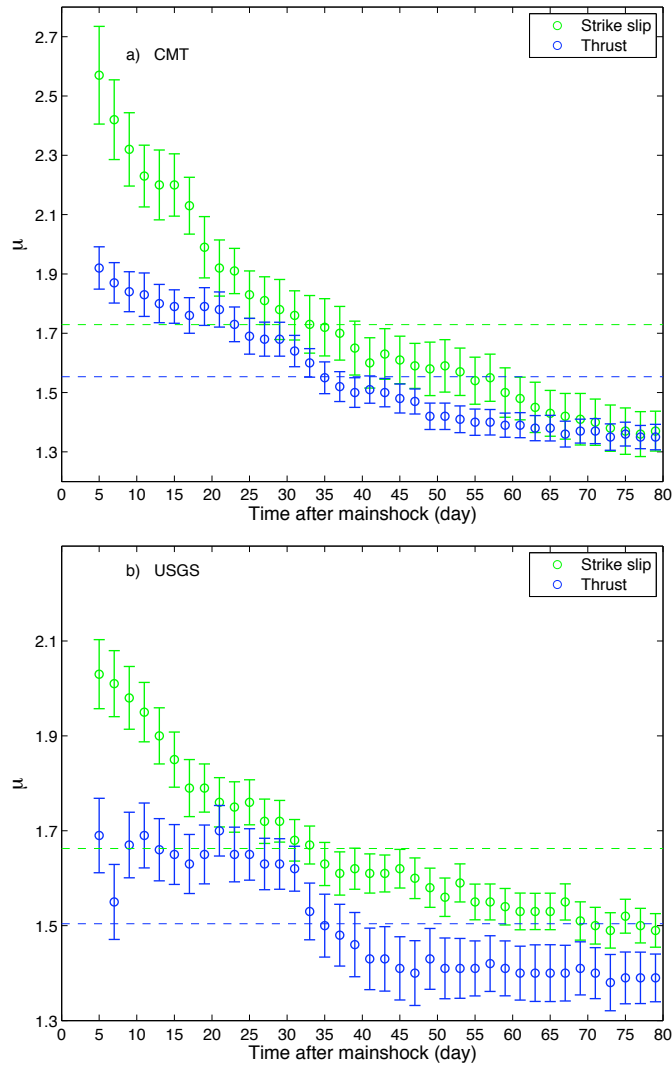
Figure 2.15: Exponent of the linear density as a function of time for CMT (top) and USGS (bottom), μ is the slope of the least square line fit to the stack linear density data at different time window as shown in figure (2.13, 2.14), (a) Exponent of linear density. For mainshock fault plane solution from CMT catalog (b) Exponent of linear density from USGS catalog.

around the strike slip trigger than the thrust trigger shocks respectively.

We also argue that the slower decay of thrust events may also be driven by its larger $n - value$ (Helmstetter and Sornette, 2002a,b). Our $p - value$ trend mimics that of the $b - value$ pattern (e.g., Schorlemmer et al., 2005; Gulia and Wiemer, 2010) and $c - value$ (e.g., Narteau et al., 2009). We checked we recover the $b_N > b_{SS} > b_T$ on the worldwide catalog (figure 2.16). This pattern is resolved only for CMT catalog, being within the error bars for the USGS catalog. It may argue that similarly to $b - value$, $c - value$, $p - value$ is possibly dependent on stress setting. Lin and Stein (2004) used moderate to large earthquakes (e.g., $M_w = 6.0$ Whittier narrows earthquake, $M_w = 9.5$ Chile earthquake, $M_w = 7.9$ Fort Tejon earthquake) from different parts of the world and concluded that the stress changes imparted by the thrust events are larger as compare to strike and normal events. They further show that the aftershocks of thrust events are sensitive to the normal stress changes and possess an intermediate friction due to high pore pressure and cumulative slip as compare to the strike slip with lower friction (e.g., Harris et al., 1995; Parsons et al., 1999; Toda and Stein, 2002). Accordingly, a larger stress change would induced a larger rate of triggered earthquakes. The possible role of cumulative slip and friction coefficient on the aftershock patterns remain open questions.

Parameters	CMT			USGS		
	Thrust	Strike slip	Normal	Thrust	Strike slip	Normal
Number of Events	144	89	23	113	137	14
$p - value$	0.82 ± 0.02	0.92 ± 0.03	1.04 ± 0.06	0.86 ± 0.02	0.95 ± 0.03	1.00 ± 0.12
$\langle K - value \rangle$	2.83 ± 0.07	1.44 ± 0.07	2.68 ± 0.21	3.05 ± 0.09	1.92 ± 0.07	1.88 ± 0.30
$\alpha - value$	0.91 ± 0.05	1.03 ± 0.2		0.96 ± 0.09	0.97 ± 0.11	
$b - value$	0.99 ± 0.06	1.12 ± 0.09		1.13 ± 0.1	1.09 ± 0.28	
$\langle Bg \rangle (\#/day)$	0.068	0.033	0.058	0.063	0.041	0.027
$\langle Duration(days) \rangle$	296	131	252	282	181	284
$\langle \mu \rangle$	1.55	1.72		1.50	1.66	

$\langle Bg \rangle$ = Average daily background rate

$\langle \mu \rangle$ = Exponent of linear density

Table 2.1: Spatio-temporal parameters

Helmstetter and Shaw (2006) used a rate and state model suggest that the $\Delta A \sigma_n$ heterogeneity drives an increase in $p - value$ and decreases the duration of the sequence. Thus a strong $\Delta A \sigma_n$ heterogeneity value of strike slip events may drive its higher $p - value$ and its lower duration than thrust events. It supports that earthquake triggering is not only controlled by average values of Coulomb stress change, or of effective of vertical stress but rather by their heterogeneity. To sum up, our observations of dependency of spatio-temporal parameters on faulting style can be reproduced by the ETAS model (change in branching ratio) and by the rate-and-state model (Dieterich, 1994) for a heterogeneous stress change along the fault plane (Helmstetter and Shaw, 2006; Marsan, 2006).

Normalized linear density $(\Phi'(t))$ decreases with time after the mainshock and finally at large time window becomes constant or merges toward the background.

Ziv (2003) also performed simulation based on quasi-static fault model to show that multiple interactions between earthquake modify the spatial distribution of aftershocks if the stress distribution induced by mainshock is non-uniform. Helmstetter and Sornette (2002b) observed that diffusion exponent H depends on Omori's law exponent $(p - value)$ and linear density exponent (μ) i.e., $H = \frac{\theta}{\mu}$. Diffusion should be observed if $p < 1$ and H decreases with increasing $p - value$ (Helmstetter and Sornette, 2002b). Using ETAS model simulations they concluded that aftershock diffusion is mainly driven by the secondary aftershocks. Thus our results of $p_T < p_{SS}$ and $\langle \mu_T \rangle < \langle \mu_{SS} \rangle$ predict higher diffusion for
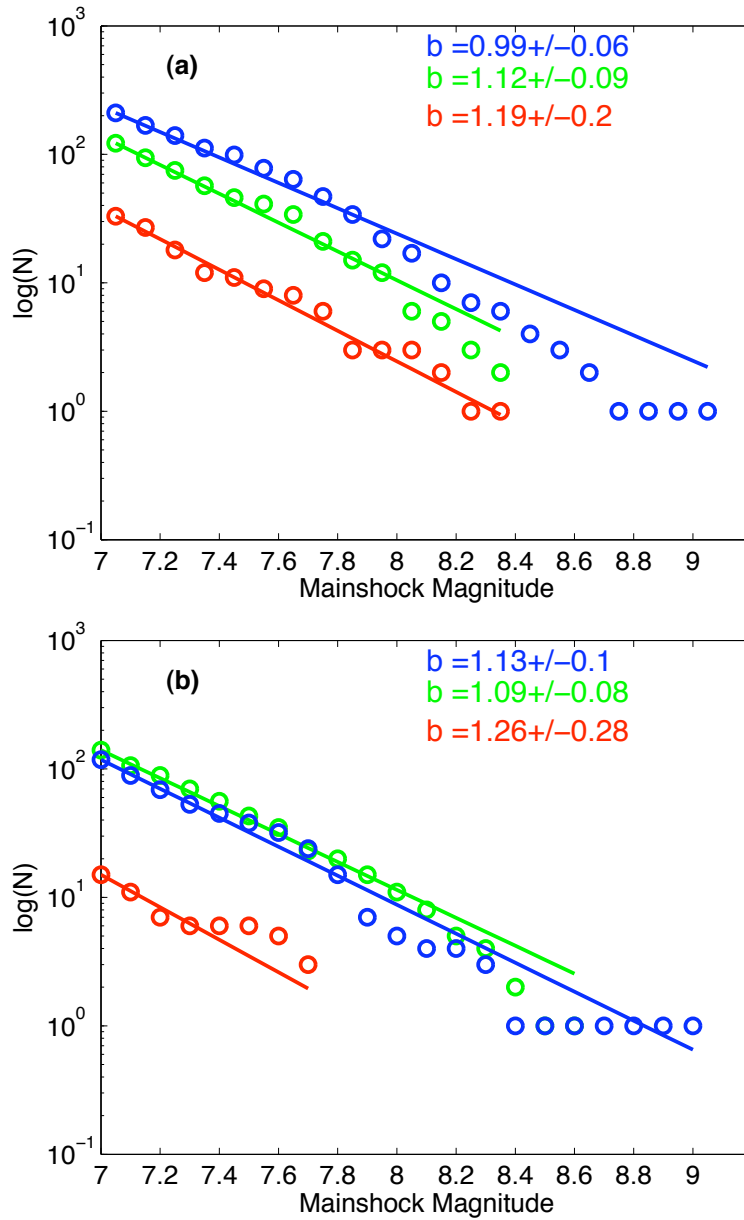
Figure 2.16: Comparison of $b - value$ for different faulting style; normal (red), strike slip (green) and thrust (blue) events. $b - value$ is calculated using maximum likelihood method of Aki (1965) for aftershocks within [1 yr, 1*L] window arround the mainshock. (a) $b - value$ for CMT catalog; (b) $b - value$ for USGS catalog.
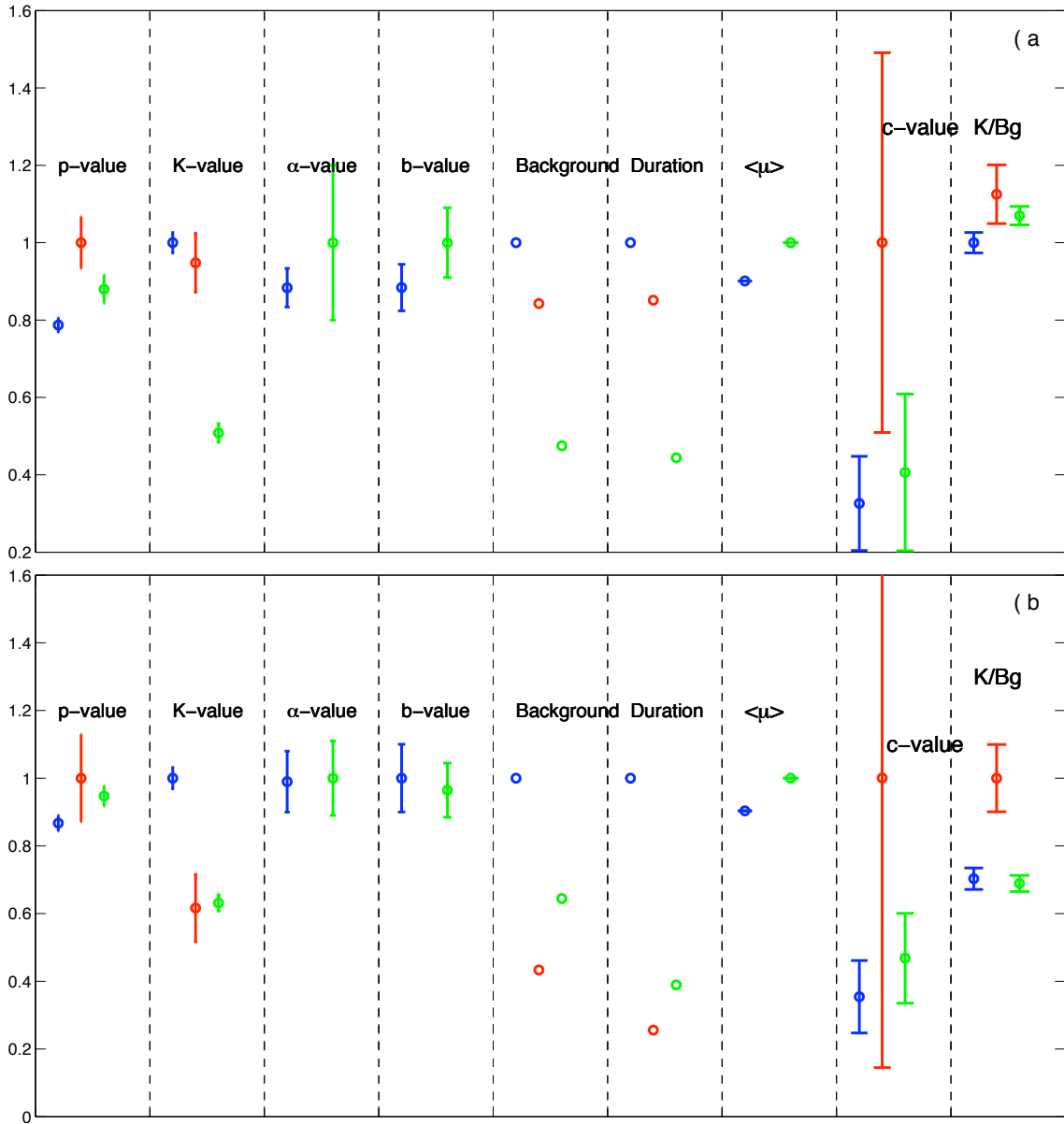
Figure 2.17: Spatio-temporal parameters of different faulting style, with fault plane solution taken from CMT (top) and USGS (bottom) catalog, calculated by stacking events with same faulting style, thrust (blue), strike slip (green), normal (red).

thrust events as compare to the strike slip events i.e., $H_T > H_{SS}$.

Exponent of linear density (μ) is also used to distinguish between dynamic and static stress triggering (e.g., Felzer and Brodsky, 2006; Lippiello et al., 2009a; Richards-Dinger et al., 2010). When $\mu + D - 1 = 1$ suggests dynamic triggering, whereas a value of 2 supports static stress triggering. Using D = 1 (Lippiello et al., 2009a), our results support static triggering for both thrust and strike slip events. D is the fractal dimensional of epicenters (Lippiello et al., 2009a).

2.6 Conclusion

In this study, we compared spatio-temporal parameters of aftershocks patterns in different tectonic settings. We described that the tectonic conditions drive its values. Empirically we observed that thrust events have higher K, aftershocks and background rate but lower $p-value$, $\langle\mu\rangle$ and $\alpha-value$ as compare to strike slip and normal events. We suggests that multiple interactions through higher branching ratio (n) of the thrust events drive its higher rates. Small $p-value$ and duration of the strike slip events suggests, within the rate and state context, stronger stress heterogeneity than for thrust events. In addition to provide new insight into the mechanics of earthquake interactions, our results also extends previous investigations, on importance of tectonics setting to all the parameters of both Gutenberg-Richter and Omori's laws. These findings will help, in the near future, to improve seismic hazard models.

Chapter 3

The largest aftershock: how strong, how far away, how delayed?

M. Tahir [1], JR Grasso[1] , D. Amorèse[2]

[1]Institut des sciences de la Terre (ISTerre)

University Joseph Fourier - Grenoble I, FRANCE

[2]Laboratoire M2C, Université de Caen Basse-Normandie, UMR CNRS/INSU 6143, FRANCE

Abstract

Proposed in the 1950's, Båth's law states that the largest aftershock has a magnitude that is typically 1.2 less than that of the mainshock. Thirty years of the global earthquake

catalog allow us to extend Båth's law in time, space and focal mechanism. On average, reverse faults have a smaller magnitude and distance from the mainshock to largest aftershock than strike-slip faults. The distribution of the time intervals between mainshocks and their largest aftershocks obeys power law, but with a somewhat faster rate of decay than for aftershocks, in general. This implies that the largest aftershocks are more likely to occur earlier rather than later in a given sequence of aftershocks.

La magnitude moyenne ΔM, le temps ΔT et la distance normalisée ΔD^* entre le choc principal et sa plus grande réplique sont indépendant de la magnitude du choc principal. La plus grande réplique est limitée en moyenne à -1.2 de la magnitude du choc principal. Trente ans du catalogue des séismes mondiaux nous permettent d'étendre la loi de Båth's dans les domaines du temps et de l'espace, car les plus grande répliques sont plus proches en taille (valeur mode: $\Delta M_r = 0.95$, $\Delta M_{ss} = 1.51$) et distance (valeur en mode: $\Delta D^*_r = 0.11$, $\Delta D^*_{ss} = 0.22$) du choc de déclenchant, pour ($_r$) un glissement inverse que pour des événements en coulissage($_{ss}$). La décroissance rapide de la loi puissance dans le temps par rapport aux répliques régulières implique que les plus grandes répliques sont plus probable au début de n'importe quelle séquence de répliques. Cette observation est le seule à être reproduite par un modèle de point de branchement.

3.1 Introduction

Earthquakes are the brittle response of the earth crust to stress-strain changes. These brittle seismic instabilities in the crust emerge as combined and complex effects of the response of heterogeneous media to small changes in loading rate which occur over a wide range of scales (e.g., Bak and Tang, 1989; Sornette and Sornette, 1989; Main, 1995; Rundle et al., 2003). These brittle deformations scale from dislocations and microcracks (~ 1 μm to 1 cm) to tectonic plate boundaries (10^3 - 10^4 km), whereas time scales range from a few seconds during dynamic rupture to 10^3 - 10^4 years (as the repeat times for the large $M > 7 - 8$ earthquakes) and to 10^7 - 10^8 years (evolution of the plate boundaries)

(e.g., Rundle et al., 2003). For earthquakes, Gutenberg and Richter (1944) suggested the frequency magnitude distribution as;

$$log_{10}N = a - bM \tag{3.1}$$

where N is the total number of earthquakes with magnitude M or greater, a and b are constants. Regional analyses (e.g., Utsu, 2002) suggest $b - values$ in the 0.8 – 1.2 range, including for aftershock sequences. Variation in $b - value$ across different stress regimes are suggested by Schorlemmer et al. (2005). Aftershocks also are observed to obey Omori's law (Utsu, 1961)

$$N(t) = \frac{K}{(t + c)^p}, \tag{3.2}$$

where $N(t)$ is the number of aftershock per unit time, t is the elapsed time since the mainshock, K, c and p are constants. A median $p - value$ of $\sim$1.1 is reported for the aftershock sequences in the various parts of the world, with a range of $\sim$0.6 - 2.5 (Utsu et al., 1995). Narteau et al. (2009) observed that $c - value$ varied with mainshock faulting styles. As proposed by Helmstetter and Sornette (2003c)

$$K = 10^{\alpha(M - M_c)} \tag{3.3}$$

M_c is threshold magnitude for catalog completeness, α is a parameter that controls the relative number of aftershocks triggered as a function of mainshock magnitude($\alpha = 0.66$ - 1.15, suggested by Hainzl and Marsan (2008) for the global catalog). Thirdly Båth's law for earthquake aftershocks is observed in many empirical and statistical studies. Initially reported by Richter (1958) as Båth's observation, it states the average magnitude difference (ΔM) between the mainshock and its largest aftershock is 1.2, regardless of mainshock magnitude (Båth, 1965). A number of studies have been conducted for the physical interpretation of Båth's law (e.g., Vere-Jones, 1969; Console et al., 2003a; Helmstetter and Sornette, 2003a; Shcherbakov et al., 2006; Vere-Jones, 2008, etc). Among them Helmstet-

ter and Sornette (2003a) using ETAS (epidemic type aftershock sequence for seismicity model) simulations provide a comprehensive analysis of the empirical Båth's law.

They suggest that Båth's law occurrence depends on both $\alpha - value$ of the mainshock and the relative difference, (M_m- M_c), between mainshock magnitude (M_m) and catalog completeness (M_c) value. When M_m-$M_c \geq 2$ and $\alpha = 0.8$ - 1.0, then Båth's law applies. In other cases, i.e., M_m-$M_c < 2$, α-value < 0.8, $\langle \Delta M \rangle$ is smaller than 1.2 (i.e., ranging between 0 and 1.2) and it increases rapidly with M_m.

In this latter case, the apparent increase in $\langle \Delta M \rangle$ is correlated with a low $\alpha - value$. A lower aftershock rate implies a lower picking rate in the Gutenberg-Richter law distribution, and thus a lower probability of a large magnitude occurrence (see equation 1 of Helmstetter and Sornette, 2003a). More recently Saichev and Sornette (2005) showed the relationship of Båth's $\Delta M = 1.2$ value to the branching ratio (n) of the ETAS point process model of earthquake interactions. For high n ($n \geq 0.8$), α ($\alpha \geq 0.9$) values, the ETAS model yields a constant value of $\Delta M = 1.2$ (Båth's law) and for low n ($n \leq 0.6$) and α ($\alpha \leq 0.5$) Båth's law does not apply.

In this paper we extend Båth's law, (i) to space and time patterns of the largest aftershocks, and (ii) we consider the earthquake faulting style as a possible control parameter on size and location of the largest aftershock. To do this, we explore $\Delta T = T_m - T_a$ ($T_m =$ mainshock time, $T_a =$ largest aftershock time) and $\Delta D^* = D_a^*$ is the normalized distance between the largest aftershock and the mainshock epicenter.

Using the USGS global earthquake catalog, we verify that the ΔM, ΔT and ΔD^* values are independent of mainshock magnitude. Second, we investigate density distributions of size, time and space patterns of aftershocks. Third, we analyse ΔM and ΔD^* values as functions of earthquake faulting styles, as defined according mainshock rake angle (e.g., Aki and Richards, 2002).

3.2 Data and Methods

We selected shallow (depth < 70 km) earthquakes of the available global earthquake catalog, (1973 - 2010, http://earthquake.usgs.gov) with M_s (surface wave magnitude) $\geq$ M_c (threshold magnitude). For the selection of aftershocks and mainshocks, the completeness magnitude M_c is computed for the entire USGS catalog containing all earthquakes. Using median-based analysis of the segment slope (MBASS) method (**?**), we derive $M_c = 5$, the same M_c value was previously reported by **?**. Focal mechanism solutions are taken from global harvard CMT catalog (http://earthquake.- usgs.gov/earthquakes/eqarchives/sopar/), $1977 - 2010$.

A number of declustering procedures are available to isolate aftershocks from background seismicity (e.g., Gardner and Knopoff, 1974; Reasenberg, 1985; Kagan, 1991; Knopoff, 2000; Felzer et al., 2004; Helmstetter et al., 2005; Marsan and Lengline, 2008). None of them being 100% robust, we instead focus in the near field by selecting aftershocks as events which occur within one fault length (L) distance from the mainshock. By using normalized distance to mainshock as $D^* = |D/L|$, D is the aftershock distance to the mainshock, which is measured as the arc length on the earth's surface. L is the earthquake rupture length, derived from the earthquake magnitude, $L \sim 10^{0.59 M_m}$ (Table 2A from, Wells and Coppersmith, 1994). We test how the patterns evolve when using $D^* = [1,2,...5]$ and $[1,2,....5]$ years for the space and time windows respectively (see auxiliary material).

For mainshock selection we follow Helmstetter and Sornette (2003a); Saichev and Sornette (2005) who observed that Båth's law only exists for events whose $\alpha - value$ is larger than 0.5 (see equation 3.3). This criterion corresponds to M_m-$M_c \geq 2$ (e.g., Helmstetter and Sornette, 2003a). Because $M_c = 5$ for the global data, we expect a constant ΔM with respect to mainshock magnitude for $M_m \geq 7$ (Figure 3.1, 3.2). To ensure the robustness of the M_m-$M_c \geq 2$ mainshock selection, we estimate $\alpha - value$ for the entire earthquake catalog and for the thrust, strike slip faulting styles (Figure 3.1a). We sum up the number of aftershocks within time = 1 year, $D^* = 1$ window with mainshock magnitude $\in [M_m$, M_m+0.1] bin and we further normalize by the number of mainshocks in each bin. The
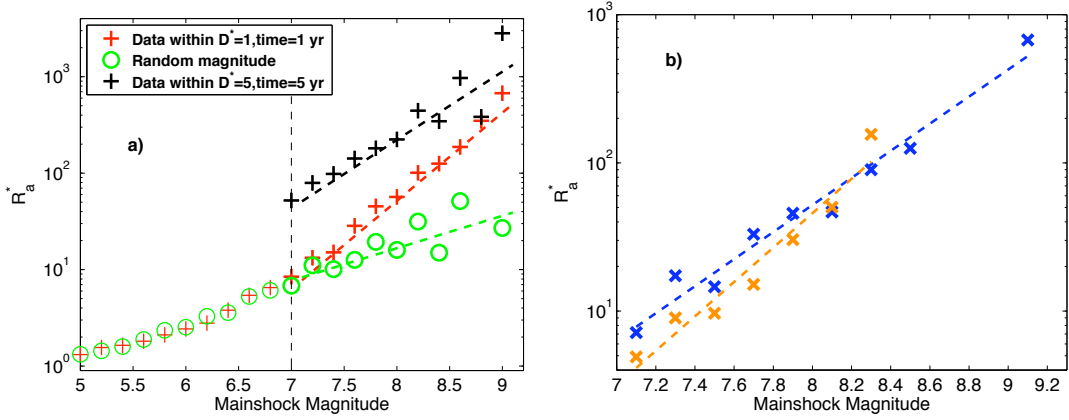
Figure 3.1: Aftershock normalised rate ($R_a^* = R_a/N_m$) as a function of mainshock size and faulting style: R_a is the number of aftershocks within mainshock magnitude class $\in$ [M, M+0.2] for $M \geq 5$, N_m is the number of mainshocks. (a) Aftershock within 1 yr and D^*=1 window (red cross), aftershock from randomly reshuffled magnitude catalogue (green circle), aftershocks (black cross) within 5 yr, $D^* = 5$ window. Note that the increase in productivity for M_m >7 events, correspond to M_m - $M_c \geq$2. The slope of the rate versus magnitude plot is defined as α the productivity value (e.g., (Helmstetter, 2003)). Below M_m=7 the slope is close to 0.38 $\pm$ 0.03 for random and real data. Above M_m=7, the slope value is 0.34 $\pm$ 0.08 and 0.91 $\pm$ 0.03 for random and real data respectively (see text for details). (b) Aftershock rate as a function of faulting style: (45<rake<135) reverse slip (blue cross, $\alpha = 0.91 \pm 0.06$); (-180$\leq$ $rake$ $\leq$-135, -45$\leq$ $rake$ $\leq$45, 135$\leq$ $rake$ $\leq$180) strike slip (orange cross, , $\alpha = 1.16 \pm 0.12$). Note that the aftershock rates is always larger for reverse slip aftershocks than for strike slip aftershocks for M_m <8. Slope of dotted lines are the α values. Data from http://earthquake.usgs.gov

least square estimate of the slope value is defined as the α value. Accordingly, Figure (3.1) suggests $M_m \geq 7$ as the threshold value for events with $\alpha \geq 0.5$.

First, we compute magnitude difference (ΔM), time (ΔT) and normalized distance (ΔD^*) between mainshock and largest aftershock as a function of mainshock magnitude classes [M_m, M_m+0.1] for M_m = 7 - 9.5. Then average, standard deviation and median with first and third quartiles (Q1,Q3) are being determined for each of the magnitude classes. Quartiles provide an interesting measure of the data dispersion since they are less susceptible than standard deviation when the data distribution is skewed or has many outliers. Because above $M = 8.3$ and for normal events, there is at most 1 single event per magnitude bin, we cannot compute error bars. Using $M_m \geq 7$, in the global catalog we only

have 26 normal faulting events for 100 and 191 strike slip and thrust events, respectively. Accordingly, we restrict the following analysis to $M \leq 8.3$ of strike slip and reverse faulting earthquakes.

Second, the density distribution of magnitude (ΔM), time (ΔT) and average linear density (e.g., Felzer and Brodsky, 2006) of normalized distance (ΔD^*) between mainshock and the largest aftershock are analyzed. In order to test the stability of the results, we compare each of ΔM, ΔT and ΔD^* outputs against the one derived from randomly reshuffled magnitude, time and location, respectively (i.e., either magnitude or time or location of events within the catalog are randomly interchanged with each other). Each reshuffled data are averaged results from 100 simulations.

3.3   Results and Discussion

For the global earthquakes catalog using $M_m \geq M_c + 2$, time ≤ 1 yr and $D^* \leq 1$ for time and space window, we observe $\alpha = 0.91 \pm 0.03$ (Figure 3.1). This value falls in the suggested range for Båth's law (e.g., Helmstetter and Sornette, 2003a; Saichev and Sornette, 2005).

We showed that the normalized aftershock rate of reverse events remains higher than for strike slip events for $M_m < 8.0$ (Figure 3.1b). This pattern indicate more aftershocks for reverse than strike slip events.

By selecting mainshock magnitude $\geq M_c + 2$, (Helmstetter and Sornette, 2003a; Saichev and Sornette, 2005) we first validated Båth's law for world wide earthquake catalog, i.e., average $\Delta M \sim 1.2$, independent of the mainshock magnitude (Figure 3.2) and second, we extend this empirical law to distance (ΔD^*) and time (ΔT), (Figure 3.3-3.4). The average density distribution of ΔM is not gaussian as it shows a fat tail, reminiscent of the Gutenberg Richter law (Figure 3.2b and S1e). Furthermore, the ΔM distribution is faulting style dependent i.e., mode of $\Delta M_{ss} > \Delta M_r$ (1.51, 0.95, ΔM_{ss}, ΔM_r being magnitude difference between mainshock and largest aftershock for strike slip and reverse events respectivley). Accordingly, we expect on average $\Delta M_{ss} - \Delta M_r = 0.24$, i.e., a
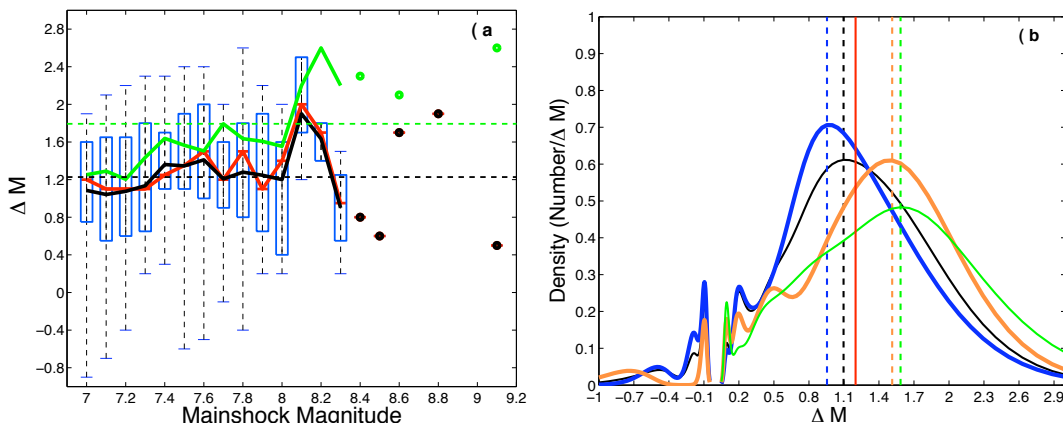
Figure 3.2: Magnitude difference (ΔM) between mainshock and its corresponding largest aftershock. (a) Average ΔM (black), median ΔM (red) and average ΔM for reshuffled magnitude (green). Horizontal dotted lines are global average $\langle \Delta M \rangle$, 1.23 and 1.79 for data and reshuffled magnitude, respectively (b) ΔM distribution for different faulting styles. All type of mainshock (black, mode $\Delta M = 1.1$), reverse events (blue, mode $\Delta M = 0.95$), strike slip (orange, mode $\Delta M = 1.51$) and reshuffled magnitude (green, mode $\Delta M = 1.58$). Dotted vertical lines are mode values, and red vertical line is Båths law. Aftershocks are selected within time = 1 year and $D^* = 1$. Because above $M = 8.3$ there is at most 1 single event per magnitude bin, we cannot compute error bars. Accordingly, we restrict the following analysis to $M \leq 8.3$ events.

0.24 magnitude decrease for the largest aftershock of strike slip mainshocks relatively to reverse events. This 0.24 average magnitude decrease is within the $\langle \Delta M \rangle = 0.19 - 0.33$ range of analytical ΔM estimates as a function of aftershock rate and $b - value$ (Feller, 1966; Helmstetter and Sornette, 2003a). From equation (1,4) in Helmstetter and Sornette (2003a) we derived $\langle \Delta M \rangle_r - \langle \Delta M \rangle_{ss} \sim \frac{1}{b_r} log_{10} \frac{N_r}{N_m} - \frac{1}{b_{ss}} log_{10} \frac{N_{ss}}{N_m}$. For these $\langle \Delta M \rangle$ estimates we use $b - value\ b_r = 0.99 \pm 0.06$, $b_{ss} = 1.12 \pm 0.09$ as estimated for global CMT catalog by Tahir and Grasso (2011).

The average linear density distribution of ΔD^* is strongly peaked at $\Delta D^* = 0.2$, with mode values for $\Delta D^*_{ss} > \Delta D^*_r$ (Figure 3.3). Accordingly, the largest aftershocks of strike slip mainshocks are on average, smaller than and occur at a larger distance from the mainshock than those triggered by reverse shocks (Figure 3.2 – 3.3).

For any magnitude bin, the rate of aftershocks is always larger for reverse triggers than for strike slip triggers (Figure 3.1b). Tahir and Grasso (2009, 2011) suggested this global

production of aftershock is driven by a lower $p-value$, larger $K-value$, for reverse events than that for strike slip events, respectively. For fixed $b-value$, a larger aftershock rate imply a greater probability to randomly pick a large earthquake from Gutenberg-Richter law (see Helmstetter et al., 2002, as predicted by ETAS model). Accordingly, the larger aftershock rate we resolve for $M_m \geq 7.0$ on Figure 3.1b drives the larger magnitude which emerges for the largest aftershocks of reverse events than for strike slip events, respectively. Also, one must note the lower α value we resolve for reverse earthquakes than for strike slip ones further re-enforces this pattern, with $\langle \Delta M \rangle =$ f(b - α/b, M_m, $K/1$-n) as derived from analytical solution of ETAS model (e.g. equation(5) from Helmstetter and Sornette, 2003a). For the distance patterns, it appears that in the near field, within 1– 3 fault length of the mainshock, the aftershocks are driven by the co-seismic static stress changes (Kanamori and Brodsky, 2004; Parsons and Velasco, 2009; Hainzl et al., 2010a; Marsan and Lengliné, 2010). Accordingly, most of strike-slip aftershock epicenters are observed to be clustered at the fault edges, i.e., at larger distance and more clustered than the rough plateau density of reverse aftershock epicenters which are located within the hanging wall (King et al., 1994; **?**; Freed, 2005).

We find that the ΔT distribution is independent of faulting style and obeys power law. The observed 0.2 slope difference between inter-event time of the largest aftershock and regular aftershock relaxation is found to emerge from synthetic catalogs (Figure 3.4b and inset) using epidemic cascading point process (ETAS) for earthquake interactions (e.g., Helmstetter et al., 2002).

3.4 Conclusions

Thirty years of the global earthquake catalog allow us to extend Båths law in time, space and focal mechanism. First, more aftershocks are observed for reverse than for strike slip events. Second, for reverse faults the ΔM of largest aftershock is in average larger than the one of strike slip events, all being independent of magnitude. Third the distance from the mainshock to the largest aftershock is somewhat less for reverse faults than for
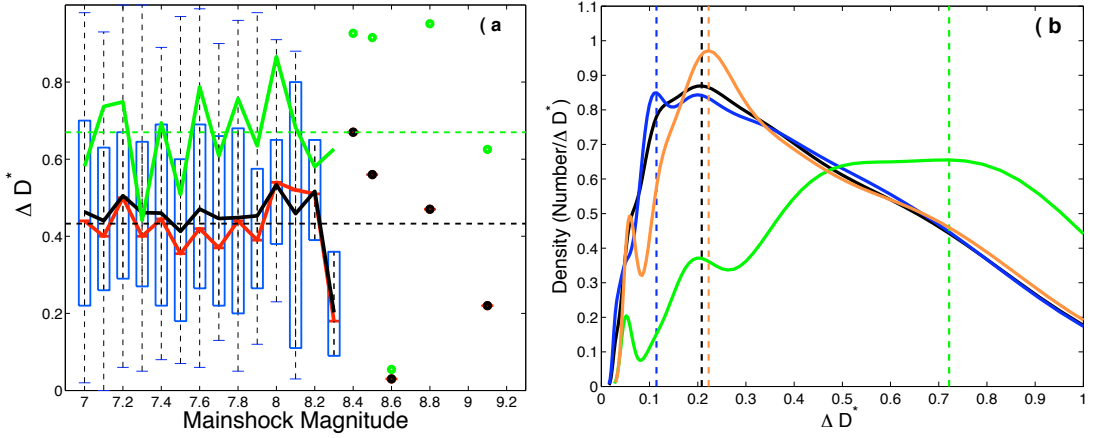
Figure 3.3: Normalized distance difference (ΔD^*) between mainshock and its corresponding largest aftershock. (a) Average ΔD^* (black), median ΔD^* (red) and average ΔD^* for reshuffled location (green). Dotted lines are global average of ΔD^*, 0.43 and 0.67 for data and reshuffled location, respectively. (b) ΔD^* distribution for different faulting styles, with all type (black, mode $\Delta D^* = 0.21$), reverse events (blue, mode $\Delta D^* = 0.11$), strike slip (orange, mode $\Delta D^* = 0.22$) and reshuffled location (green, mode $\Delta D^* = 0.72$). Dotted vertical lines are mode values. Aftershocks are selected within time = 1 year and $D^* = 1$. Because above $M = 8.3$ there is at most 1 single event per magnitude bin, we cannot compute error bars. Accordingly, we restrict the following analysis to $M \leq 8.3$ events.

strike slip faults. Fourth, the distribution of time intervals between mainshocks and their largest aftershocks is consistent with power law but with a somewhat faster rate of decay than for aftershocks in general. This implies that the largest aftershock is more likely to occur earlier than later in a given sequence of aftershocks (i.e., median $\Delta T \sim 3$ days).

These empirical results for, ΔM, ΔD^*, ΔT are robust patterns that are direct inputs to refine the current practice of early forecasts of earthquakes activity (http://www.cseptesting.org/).

On the one hand, these results provides quantitative probabilistic prediction tools for time space and size estimates of the largest aftershock. On the other hand these predictions, size and distance dependent on the faulting style, argue for going beyond the point process for the cascading model of earthquake interactions. Our analysis of the largest aftershock patterns confirms the role of static triggering as the main process to trigger earthquake in the near field, i.e., within 1 year and 1 fault length of mainshock.
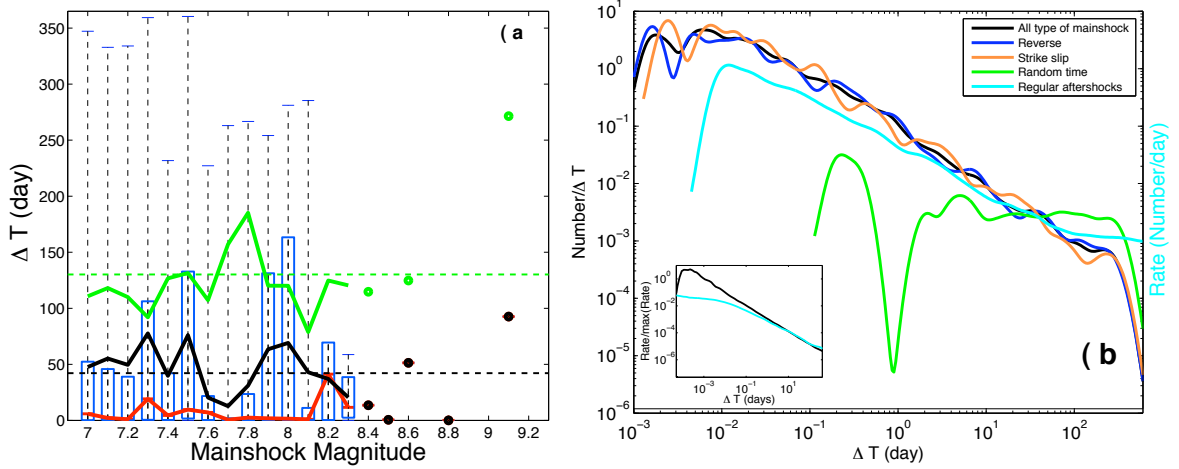
Figure 3.4: Time difference (ΔT) between mainshock and its corresponding largest after-shock. (a) Average (black), median (red) and average ΔT for reshuffled time (green), $\langle \Delta T \rangle$ as 42.17 day and 130.22 day for data and reshuffled time respectively. (b) ΔT distribution of largest aftershock for different faulting styles. All type ($p-value = 0.96 \pm 0.03$), reverse events ($p-value = 0.96 \pm 0.04$), strike slip ($p-value = 0.98 \pm 0.05$) and all aftershocks (not restricted to the largest one) ($p-value = 0.82 \pm 0.009$). Note that $p-value$ for "all aftershocks" is different from $p-value$ of largest aftershocks. Insert on (b) shows average of 1000 ETAS model simulation with input $p = 1.2$ and $n = 0.99$, (n is the branching ratio (e.g., Helmstetter and Sornette, 2003a)). Black line is the largest aftershock from synthetic catalog, $p = 0.85 \pm 0.027$ and and light blue are all aftershocks, $p = 1.05 \pm 0.0008$. The 0.2 $p-value$ increase for the largest aftershocks is the same for the ETAS simulation and the real data. Aftershocks are selected within 1 year, $D^* = 1$ window.

Chapter 4

How much the mainshock size controls the aftershock patterns ? a global catalogue analysis.

M. Tahir [1], JR Grasso[1]

[1]Institut des sciences de la Terre (ISTerre)

University Joseph Fourier - Grenoble I, FRANCE

Abstract

We investigate the spatio-temporal parameters of aftershocks as a function of the main-shock size. Aftershock productivity (α; $n(t) = 10^{\alpha m}$) as 0.82 ± 0.06 and 0.84 ± 0.05 estimated using two different techniques. Strong co-relation between $p - value$ of Omori's law and mainshock size exist for the aftershocks taken within first week after the mainshock occurrence (i.e., $0.09 - 10$ days). But the correlation becomes very weak when considering whole cascading sequence. The evolution of $p - value$ show that initially its value increases (~ 30 days) then start decrease and finally becomes constant. We observe that duration of the triggered earthquakes increases with triggering size, duration $\sim 10^{0.32 m_m}$. Normalized rate decrease with distance from mainshock but along with duration and $p - value$ also decrease as distance increases from the mainshock. We observe aftershocks linear density of the global data with large-to-moderate size mainshock exhibit a maximum peak density at certain distance from the mainshock, that depend on the mainshock size. Finally, fractal dimensionless behavior of linear density is shown due the static stress triggering.

La productivité de répliques augmente avec la magnitude du choc principal $\sim 10^{\alpha m}$, avec $\alpha = 0.82 \pm 0.06$. La valeur p est fonction de la magnitude du choc principal pour les répliques directes, alors que la corrélation est perdue lorsque nous avons à la fois des répliques directes et indirectes. La durée a une corrélation positive avec la magnitude du choc principal. Nous avons également observé que la densité linéaire obéit à la loi de puissance et que la distance de son pic de densité au choc principal dépend de la taille du choc principal. Nous suggérons que le déclenchement par la contrainte statique est le principal mécanisme responsable des processus de déclenchement des tremblements de terre mondiaux.

4.1   Introduction

Earthquake characteristics in space time are hypothesized as the interaction of stress, strain and fluid flow (e.g., Nur and Booker, 1972; Rice and Cleary, 1976; Li et al., 1987; Hudnut et al., 1989; Jaume and Sykes, 1992; Okada, 1992; Stein et al., 1992; King et al., 1994; Noir et al., 1997; Stein, 1999; King and Cocco, 2001, among several other authors). These interaction are responsible for earthquake triggering, which generally follow some specific empirical laws. For magnitude distribution, most of the earthquakes follows Gutenberg and Richter (1954) relation;

$$log_{10}N(m) = a - bm \tag{4.1}$$

where $N(m)$ is the total number of earthquakes with magnitude m; a, b are constant that depend on local activity rate (Gutenberg and Richter (1944)). The constant 1.2 magnitude difference between mainshock and the largest aftershock is known as Båth law (Båth (1965); Console et al. (2003a); Helmstetter and Sornette (2003a)).

It is also well known that earthquake of any magnitude can trigger their own aftershocks (Helmstetter (2003)) and that almost all triggered aftershock sequences decay with time as a power law (Omori (1894)), empirically well described by the modified Omori formula;

$$N(t) = \frac{K}{(t + c)^p} \tag{4.2}$$

Where $N(t)$ is the number of aftershock per unit time, t is the elapsed time since the mainshock, K, c and p are constants. A median $p-value$ of $\sim$1.1 is reported for the aftershocks sequences in the various parts of the world, with range of $\sim$0.6 - 2.5 (Utsu et al. (1995)), but $p-value$ may fluctuate for aftershock sequences (Wiemer and Katsumata (1999)). This variability of the $p-value$ is suggested to be related to the tectonic condition of the region such as structural heterogeneity, stress heterogeneity, fluid contents, heat flow, frictional heating, earthquake slip and temperature (e.g., Mogi (1962); Mogi (1967); Mikumo and Miyatake (1979); Kisslinger and Jones (1991); Utsu et al. (1995); Wiemer and

Katsumata (1999); Helmstetter and Shaw (2006)). Kisslinger (1996) provides an overview of the physical factors that may affect $p - value$. On the basis of rate and state friction model, Helmstetter and Shaw (2006) provide a link between $p - value$ and stress step. The faster the stress decay after the mainshock the higher the $p - value$ of aftershock (e.g., Helmstetter and Shaw (2006)). Helmstetter and Shaw (2006) and Peng et al. (2007) further show that $p - value$ increases with time after mainshock, as suggested to be driven by heterogeneous stress distribution over fault plane.

Ouillon and Sornette (2005) use California seismicity to show that $p - value$ depends on the size of earthquake as $p - value$ increases with increasing mainshock magnitude. They explain this pattern using multifractal model of stress interactions. Peng et al. (2007) and Marsan and Lengline (2008) used respectively JMA (Japna) and California catalog and observe no correlation between $p - value$ and mainshock magnitude. Hainzl and Marsan (2008) using ISC global earthquake catalog, observed that $p - value$ is dependent on mainshock magnitude. They explain that these observations within the framework of the rate and state friction model. More recently Ouillon et al. (2009) used California, Japan and world wide Harvard Centroid Moment Tensor (CMT) catalog, to suggest a correlation between $p - value$ and mainshock size.

Similar to $p - value$ it is also proposed by many studies that aftershock productivity (K) grows with mainshock magnitude (m_m) as $K = K_o 10^{\alpha(m_m - m_c)}$. α is a parameter that controls the relative number of aftershocks triggered as a function of mainshock magnitude. Its value varies from region to region (e.g., Utsu and Seki (1954); Solovev and Soloveva (1962); Papazachos et al. (1967); Utsu (1970); Singh and Suarez (1988); Yamanaka and Shimazaki (1990); Davis and Frohlich (1991); Molchan and Dmitrieva (1992); Shaw (1993); Drakatos and Latoussakis (2001)). In these studies, the largest event of a sequence was taken as mainshock, and the following events within specific space-time window around the main shock are taken as aftershocks. They further proposed α is in the [0.65, 1] range. Helmstetter (2003) using southern California seismicity, shows that whatever the size (3.0 $\leq m_m \geq 7.0$) of the earthquake can trigger their aftershocks with aftershocks productivity depends on the mainshock size. She found $\alpha = 0.8$, whereas an earthquake is selected

as mainshock if there is no event preceded by the mainshock with magnitude larger than the mainshock in a specific space-time window (distance = 50 km, time = 1 year). All events following within one rupture length and 1 year from the mainshock are taken as aftershocks. Felzer et al. (2004) use mainshock as an event that produce aftershock upto minimum 30 days after the mainshock and events following within 2.5 rupture length are taken as aftershocks. Using these aftershocks they suggest α =1, for the California seismicity. Helmstetter et al. (2005) use the same catalog and found $\alpha = 1.05 \pm 0.05$. Helmstetter et al. (2005) used a de-clustering algorithm similar with that of Reasenberg (1985).

Other studies measured the α exponent by using a statistical model of seismicity (e.g., Ogata (1989); Kagan (1991); Ogata (1992); Console et al. (2003b); Zhuang et al. (2004)). The α value is in the $[0.5 - 0.7]$ range (Console et al. (2003b); Zhuang et al. (2004)). When these models applied to individual aftershock sequences, Guo and Ogata (1997) conclude an α as 0.2 –1.9.

Hainzl and Marsan (2008) use ISC global earthquake catalog and apply different declustering approaches (e.g., Gardner and Knopoff (1974), Helmstetter (2003), Helmstetter et al. (2005) and Marsan and Lengline (2008)) to found α value in the [0.66, 1.15] range. They suggest that the variability in α value may be dependent on the tectonic settings of the region, but also due to the different procedures used to select main shocks and its corresponding aftershocks. They further tested the increase of $p - value$ and aftershocks productivity with mainshock size for different parameters such as Hurst exponent (H) of fractal slip distribution, co-efficient of variation (CV) of the stress distribution and mean stress drop on fault plane (e.g., Hainzl and Marsan (2008)). For larger stress heterogeneity ($CV = 8.0$) and H ($H = 0.9$), the correlation between $p - value$ and mainshock size becomes very weak and but aftershocks production remains same.

Previously number of studies have shown that coulomb stress changes decrease with distance from mainshock, with a decay rate as $\sim 1/\sqrt{r}$ in near field and $\sim 1/r^3$ in the far field (e.g., Dieterich (1994); Huc and Main (2003); Helmstetter et al. (2003); Helmstetter and Shaw (2006)). In time, Helmstetter and Shaw (2006) show that shear stress changes

decreases after mainshock, as estimated from seismicity rate using Dieterich et al. (2000) method. Dieterich (1994) further correlates aftershock rate and duration with shear stress step. In this context duration decreases when stress step decreases.

Furthermore, aftershocks density also decreases as distance increases from the mainshock (e.g., Dieterich (1994); Huc and Main (2003); Helmstetter et al. (2003); Helmstetter and Shaw (2006)). This decrease or decays of linear density with distance from mainshock have been observed to obey a range of functions, including power law and combination of power laws with constant and exponentials law (Huc and Main (2003); Felzer and Brodsky (2006); Marsan and Lengliné (2010); Richards-Dinger et al. (2010)). Slope of aftershocks linear density is used to distinguish between dynamic and static stress triggering respectively (e.g., Felzer and Brodsky (2006); Richards-Dinger et al. (2010); Lippiello et al. (2009a)). Linear density in both cases decay as $R^{-\mu}$, where $\mu + D$ -1 is 1 or 2 for dynamic or static stress triggering respectively. D is the fractal dimensionality of epicenter (Lippiello et al. (2009a)), R is the distance from the mainshock, μ is the exponent of the decay slope of linear density.

At different time window aftershocks spatial distributions yield to diffusion or migration. This behavior (aftershock expansion) has been observed in many studies (e.g., Tajima and Kanamori (1985b); Ouchi and Uekawa (1986); Eneva and Pavlis (1991); Dieterich (1994); Marsan et al. (2000); Huc and Main (2003); Helmstetter et al. (2003); Daniel et al. (2011)).

Previously CMT, California, Japan and ISC catalog have been used to observed a correlation between $p - value$ and mainshock size. Some studies (e.g., Ouillon and Sornette (2005), Hainzl and Marsan (2008); Ouillon et al. (2009)) suggest their dependency while other (e.g., Peng et al. (2007); Marsan and Lengline (2008)) have no evidence. In this paper first we will use global USGS data, to test the dependency of $p - value$ on mainshock size, as no one previously test this pattern on world wide USGS catalog.

Secondly, we focus on time dependent evaluation of $p - value$ for different mainshock sizes. Previously Peng et al. (2007) and Helmstetter and Shaw (2006) suggest $p - value$ increases with time after mainshock. Marsan and Lengline (2008) show a positive correlation

between duration of the cascade sequence (direct and indirect) and mainshock size.This correlation is lost when using only the direct aftershocks.

In this study we performed a detail spatio-temporal analysis of the global shallow (depth < 70 km) earthquakes, by calculating aftershock rate, $K-value$, $p-value$, duration and linear density as function of mainshock magnitude and distance from the mainshock.

4.2   Data Selection: Main Shocks and Aftershocks

We analyze shallow (depth < 70 km) earthquakes of the global USGS catalog (http://earthquake.usgs.gov). Events with magnitude $\geq m_c$ and that occur within the time span of the catalog (i.e., $1973 - 2010$) are considered in the analysis. Threshold magnitude is proposed as 5.0 for the global data (e.g., Kagan, 2004; Tahir and Grasso, 2009). The magnitude are generally available in m_s (Surface wave magnitude), but if m_s is not available then m_b (Body wave magnitude) is used instead.

Different declustering procedures are proposed to separate the non random earthquakes from that of random earthquake (e.g., Gardner and Knopoff (1974); Reasenberg (1985); Kagan (1991); Knopoff (2000); Felzer et al. (2002a); Helmstetter (2003); Felzer et al. (2004); Marsan (2005); Helmstetter et al. (2005)). In this study we follow a procedure which is close to that of Helmstetter (2003) and Ouillon and Sornette (2005). For selecting of mainshock and its corresponding aftershocks, these authors defined an event as mainshock if it is not preceded by an event with larger magnitude in a specified space time window. Helmstetter (2003) use time window as 1 year and distance as 50 km, whereas Ouillon and Sornette (2005) use the same time window but space window as 2*L. L is the earthquake rupture length, as calculated using Wells and Coppersmith (1994) relationship. We follow Ouillon and Sornette (2005) choice and define $D^* = \frac{D}{L}$ that allows a space window which scales with mainshock size. The space and time windows are chosen in order to minimize the influence of background activities. Practically, we select an event of magnitude m_m as mainshock if it does not impact on the space time window (time = 1 year, distance = 5*L) of any previous or following events of magnitude greater than m_m. This selection

aims to avoid overlap between large aftershocks sequences that occurs close in space time domain. Our procedure for mainshock selection differs from that of Helmstetter (2003) and Ouillon and Sornette (2005) in term (i) space window, (ii) they consider only those events preceded the larger earthquake and no constrain on the following events. But in our procedure mainshock is neither preceded nor followed by larger events. The events following the mainshock within space window as 5*L are taken as aftershocks whereas in the same space window the events preceding the mainshock are used to define foreshocks or background (foreshocks are the events above the background rate). We analyze aftershocks by exploring 10 – 100 days time window. Average daily background rate is calculated by using the events within [5*L, 5 yrs] space-time window before the mainshock.

4.3 Estimating Aftershock Patterns in Time and Space

To reach stable estimation of different spatio temporal parameters with respect to the mainshock magnitude and distance we use stacked aftershock sequences. The stacking of the data smoothes out fluctuations associated with individual sequences and highlights the common features of all sequences (e.g., Helmstetter (2003); Ouillon and Sornette (2005) Yang and Ben-Zion (2009) and several others authors).

Aftershocks sequences within distance = 5*L and time = 1 year are stacked for different mainshock magnitude classes, $m \in [m, m + 0.5]$ with $m = 5.5, 6.0, ... 9.5$. Each stacked sequences are normalized by its corresponding number of mainshocks.

4.3.1 Average aftershock rate

First we estimate number of aftershocks ($m_m \geq m_c$) for each of the corresponding mainshock using a fixed distance as 5*L and time window as 10 days. This time window is a trade off between small time window (as in Pegler and Das (1996)) that would diminish

the number of aftershocks available for analysis, and a longer time window which have complexify of the sequences due to possible compound earthquakes occurrences. We use 10 days aftershocks data which is close to the 7 days used by Kagan (2002a).

Using mainshock with magnitude class ($[5.5 : 0.5 : 9.5]$), magnitude class we define the average aftershock normalized rate (N^*) as;

$$N^1 = \sum_{i=1}^{10} N_i; \qquad i = 1, 10 \; days \tag{4.3}$$

$$N^s = N_r^1 \bigcup_{r=5.5:0.5:9.0} N_{r+0.5}^1; \qquad r \; mainshock \; magnitude \; class \tag{4.4}$$

$$N^* = \frac{\sum_{j=1}^{8} N_j^s}{length(N_j^s)}; \qquad j = 1, \; 8; \; mainshock \; magnitude \; class \tag{4.5}$$

N_i is the daily number of aftershocks, N^1 is the total number of aftershocks in 10 days, N^s is the stack number of aftershock for each magnitude class, N^* is the average number of aftershock of each magnitude class. Similar to the aftershocks average rate of each magnitude class, earthquake rate is estimated for the events that precede the mainshock upto 10 days. Least square line reproduced the aftershock rate versus magnitude plot, for $7.0 \leq m_m \leq 9.5$ (figure 4.1). This slope defines the α-value (Helmstetter (2003)), such as $K - value$ can be expanded as $K = K_0 10^{\alpha(m_m - m_c)}$.

4.3.2 Background Rate and Duration

The duration of each aftershocks sequences is defined as the first return point to the average background rate. Average daily background rate is being computed by using the events that occurred within five year before the mainshock and within distance as $5*L$ around the mainshock are being stacked.

Aftershocks rate of the stacked sequences for each magnitude class is being calculated by using nearest neighbor technique (Silverman (1986)), in which daily rate is estimated by
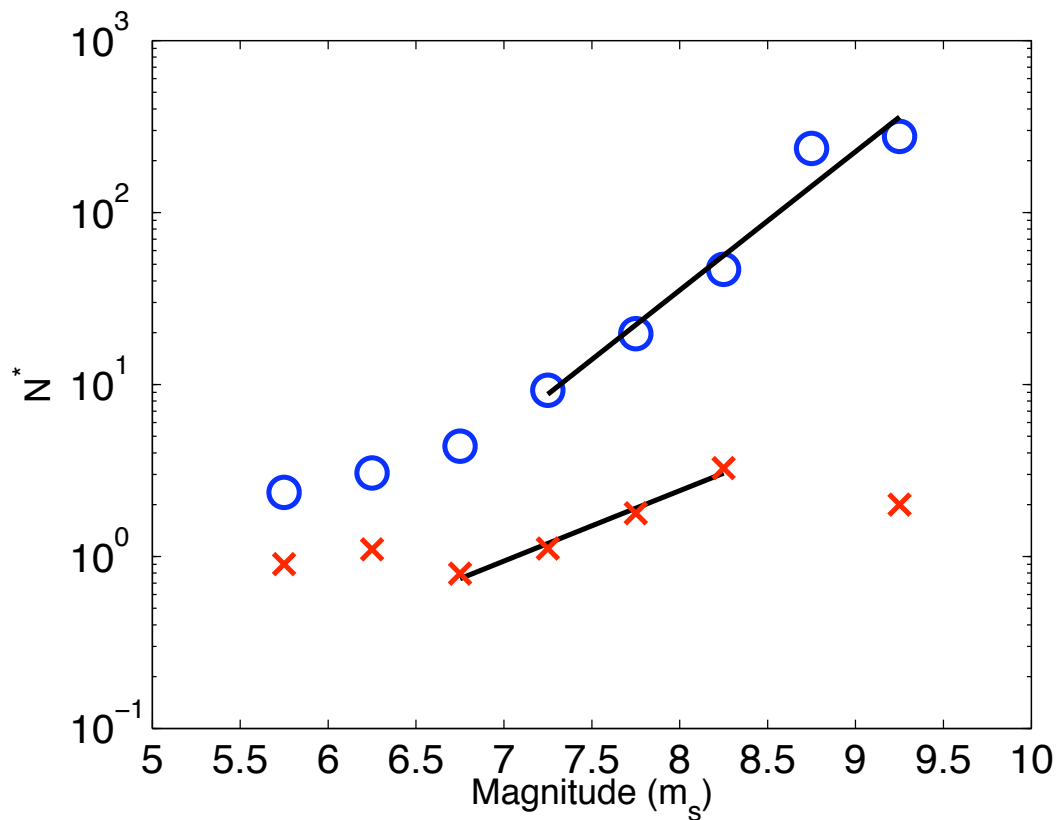
Figure 4.1: Average rate of the triggered earthquakes as a function of the triggering magnitude. Triggered events are selected within [10 days, 5*L] window around the triggering. Average aftershocks rate (blue circles) $\sim 10^{0.82 m_m}$, Average foreshocks rate (red cross) $\sim 10^{0.41 m_m}$. Least square line (black line) fit to the data between 7.0 to 9.5 magnitude.

taking inverse of the width of the box which contains k neighboring points. Smoothing is controlled by k. The advantage of this technique is the smoothing is uniform and there are no empty bins (Felzer and Brodsky (2006)). Instead of using fix number for all sequences we use variable k values as a function of the length of aftershocks data. We use $k = 5\%$ of the length of aftershocks data of the corresponding mainshock. Then the duration is taken as the time when daily rate computed using nearest neighbor method goes to average daily background rate as shown in figure (4.2 - 4.4).

According to Dieterich (1994), duration is stress stress step dependent. In order to test the dependency of duration with respect to stress step (as the stress step decreases with increasing distance from the mainshock), we further calculate duration of the stack aftershock data at different distance classes ($[0 : 0.5*L : 3*L]$) from the mainshock (see in section 4.3.4).

4.3.3   Omori's Law Parameters

We used maximum likelihood method of Ogata (1983) to calculate, K, p, c, the modified Omori's law parameters. The error in these parameters is strongly dependent on the number of aftershocks used to calculate these parameters, higher the number of aftershocks and smaller the errorbar in parameters estimates.

Omori law parameters are computed for 10 days of the stack data of figure (4.2). The computation is repeated for the stack data upto 80 days and for window starting time as 0.009 days and ending time varies between [10: 2: 100] days (figure (4.6, 4.7)).
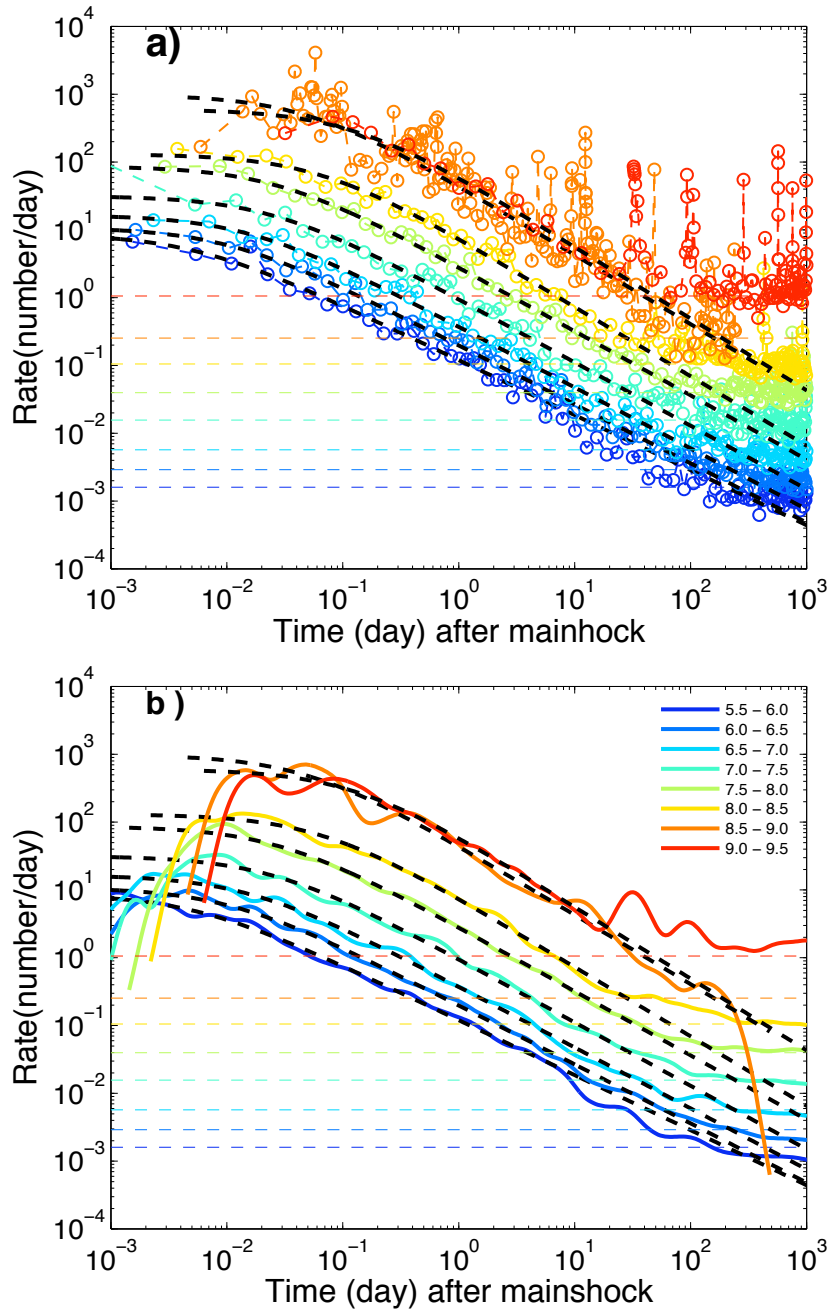
Figure 4.2: Average aftershocks rate as function of time after the mainshock, dash horizontal line is the average background rate of the triggering earthquake. Omori law fit to the data range $0.01 < t < 10$ days (a) rate for different values of the magnitude of the triggering earthquake increasing from 5.5 t o 9.5 with a step of 0.5 from bottom to top. Aftershock rate is calculated using nearest neighbor method with k = 5% of the total data of the corresponding sequence. (b) Same as (a) but aftershocks rate is calculated using Gaussian method (Helmstetter and Sornette, 2002b).
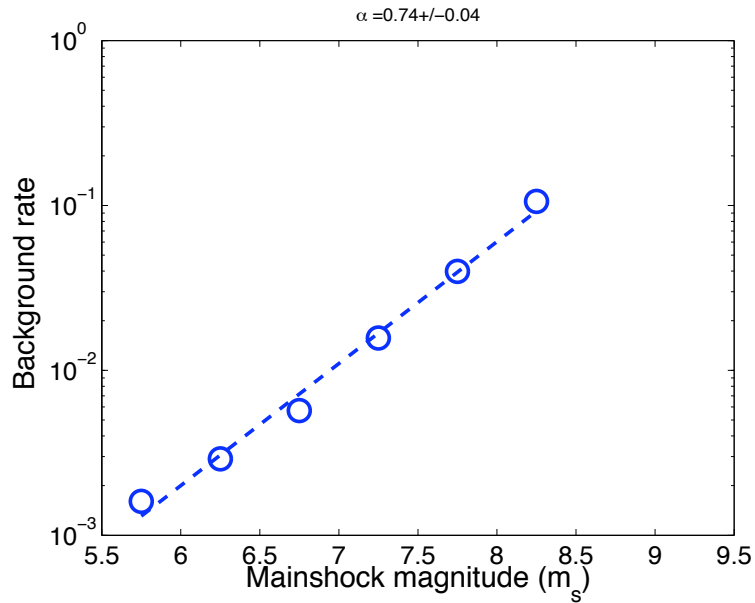
Figure 4.3: Daily background versus mainshock magnitude. Background $\sim 10^{0.80 m_m}$
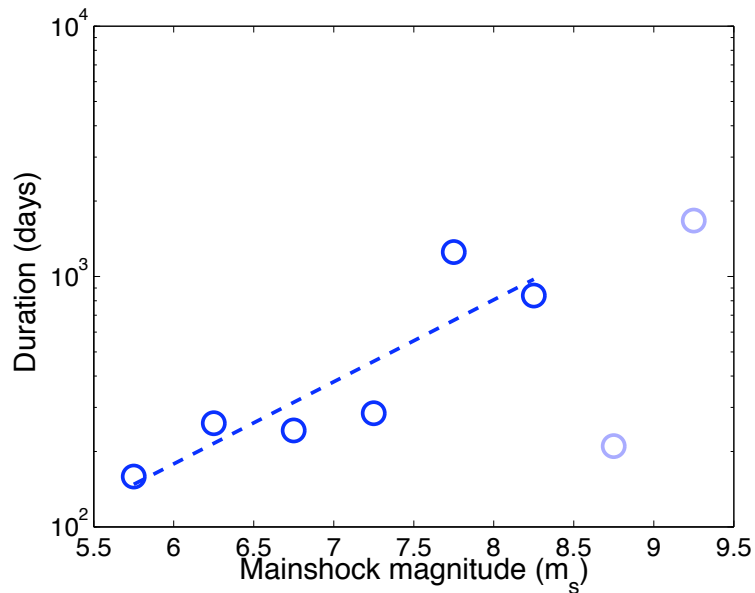
Figure 4.4: Aftershock duration versus mainshock magnitude. We only interpret data between 5.5 and 8.0 magnitude events, as events with magnitude greater 8.0 have only one mainshock in a bin. Duration $\sim 10^{0.32 m_m}$
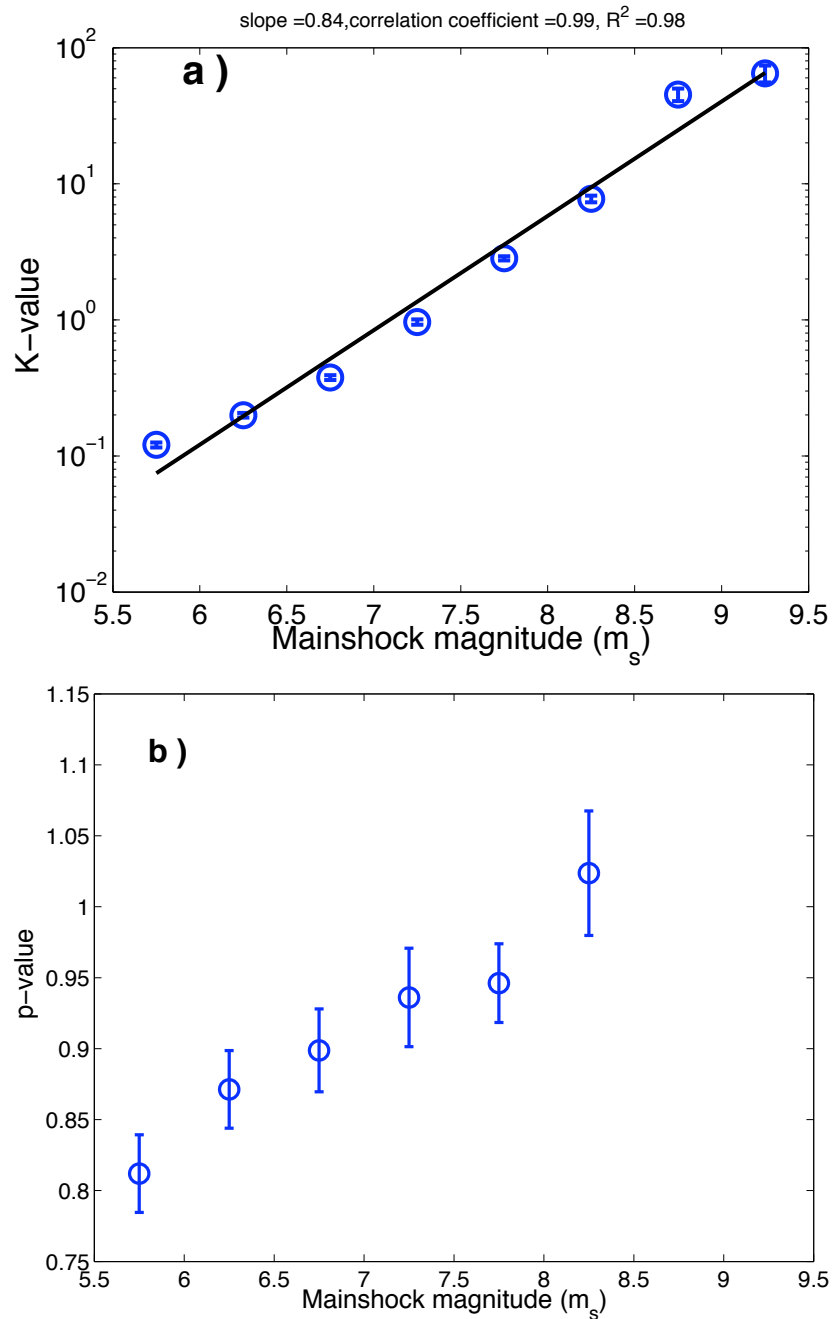
Figure 4.5: Average Omori's law parameters as a function of the triggering magnitude. Omori law fit shown in figure (4.2). (a) Average $K-value$ as function of mainshock magnitude, average rate $\sim 10^{0.84m_m}$ (b) Average $p-value$ as function of mainshock magnitude.
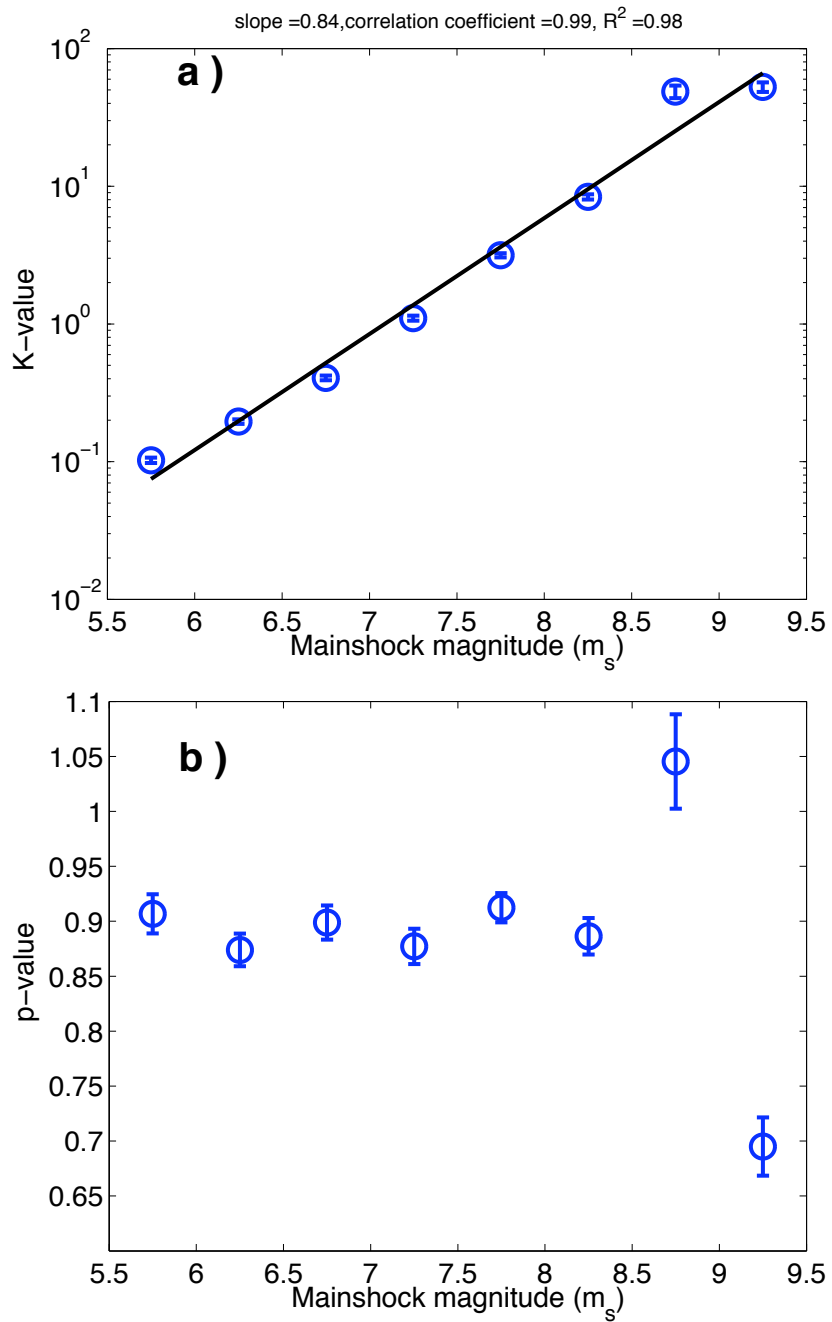
Figure 4.6: Same as figure (4.5) only Omori law fit to the data upto 80 days. (a) Average $K - value$ as function of mainshock magnitude, average rate $\sim 10^{0.84 m_m}$ (b) Average $p - value$ as function of mainshock magnitude.

4.3.4   Spatial Distribution

Linear density

Complexity in earthquake occurrence may be partly due to the earthquake triggering mechanism (Marsan and Lengliné (2010)). In this process, earthquake on one fault can trigger an event on another fault. If the triggering arises at large distance soon after the mainshock, it is considered due to the seismic waves shaking i.e., so called dynamic triggering (e.g., Kilb et al. (2000); Gomberg et al. (2001a)). This process is different from the triggering which occur at the location of stress increase due to mainshock, i.e., the static stress triggering. Linear density of earthquakes is recently used as an important tool to differentiate between the triggering mechanism (e.g., Huc and Main (2003); Felzer and Brodsky (2006); Lippiello et al. (2009a); Marsan and Lengliné (2010); Richards-Dinger et al. (2010))

We stack aftershocks following the mainshock within distance $= 10*L$ and time $= 10$ days for magnitude $\in [m,\ m+1]$, $m = 5.5,\ 6.5,\ 7.5,\ 8.5$.

Linear density of the stack sequence is being calculated by using nearest neighbor method, in which inverse of the width containing specific number (k) of aftershocks is taken as density. Power law is being fitted to the linear density by using least square method (figure 4.8). We use $k = 5\%$ of the total data so that to have same smoothing to different data.

In order to remove tentatively the effect of mainshock size on linear density, we further collapse the linear density by $10^{\sigma m}$ with $\sigma = 0.40$ (as suggested by Baiesi and Paczuski (2004); Lippiello et al. (2009a)) (figure 4.8b).
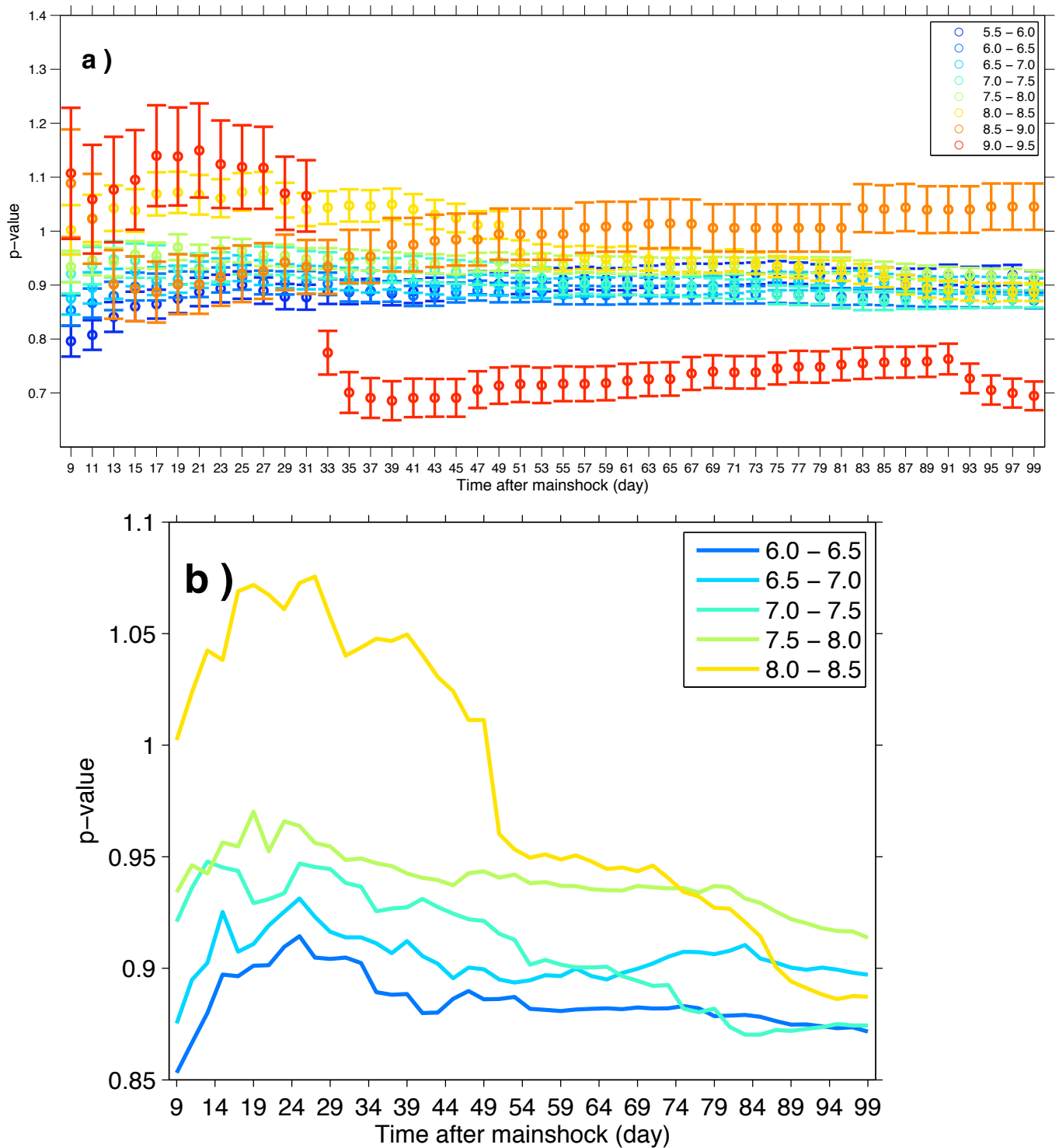
Figure 4.7: $p - value$ as function of time after the mainshock, for different values of the magnitude of the triggering earthquake increasing from 6.0 to 8.5 with a step of 0.5 from bottom to top. (a) $p - value$ calculated for different time window, with window starting time as 0.009 days and ending time varies between $[10 : 2 : 100]$ days. (b) Same as (a) but without errorbar and magnitude class with $5.5 - 6.0$, $8.5 - 9.0$ and $9.0 - 9.5$ are not considered.

Aftershocks rate through time-distance to the mainshock

Our definition of mainshock in this section is different from that used in previous sections. Instead of using all mainshock we use only those events as mainshock which has magnitude $(m_s) \geq 7.0$, but we keep same space-time window around the mainshock to avoid large shock overlap i.e., D = 5*L, time = 1 yr. Then the events following the mainshock are taken as aftershocks. For each mainshock with magnitude $< m_c + 2$, the aftershocks cannot fully expand in time and space (e.g., Helmstetter and Sornette (2003a), Tahir et al. (2011)) see in figure (4.1). Then we consider only $m_m \geq m_c + 2$ or $\alpha > 0.8$ for stress diffusion analysis.

To test the rate changes as function of distance from the mainshock, we stack aftershocks for distance classes such as $[0 : 0.5*L : 3*L]$, with mainshock taken at the center. Beyond 3*L rate is small and it is difficult to distinguish from background rate (figure 4.9). Aftershock rates are being calculated by using nearest neighbor and gaussian method (Helmstetter (2003)) as shown in figure (4.9). Duration and Omori law parameters of each stack sequence is calculated in similar way as that described in section (4.3.2) and (4.3.3) respectively.
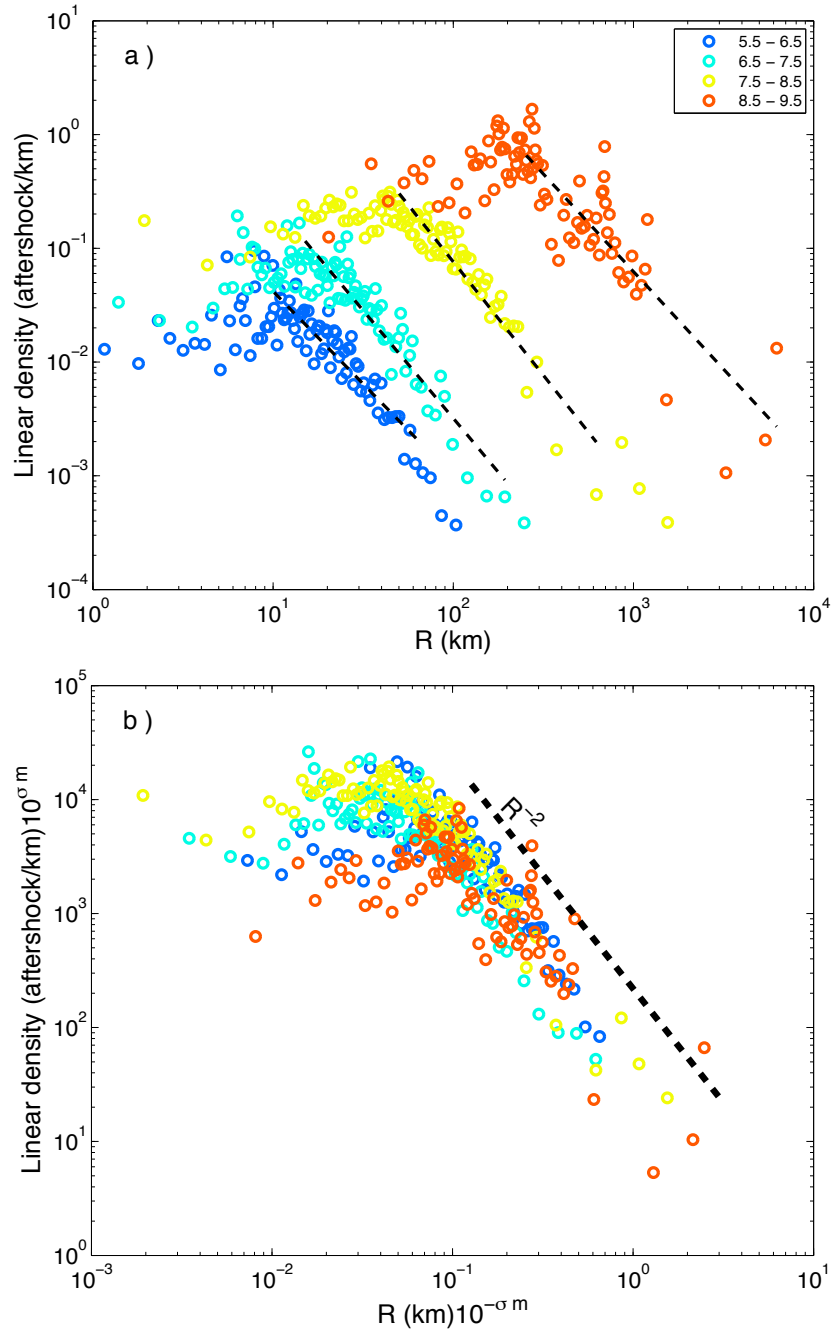
Figure 4.8: Aftershocks linear density from the mainshock as a function of distance (R), linear density for different values of the magnitude of the triggering earthquake increasing from 5.5 t o 9.5 with a step of 1 from bottom to top. Aftershock are events within $[10*L, 7 \text{ days}]$ space-time window from the mainshock. (a) Aftershock linear density for different mainshock magnitude with maximum linear density exhibit at different distance from mainshock depend on mainshock magnitude. (b) Collapse of all linear density for different magnitude class occur with $10^{\sigma m}$, $\sigma = 0.40$. Black dashed line show the decay of $F(R) \sim R^{-2}$.

4.4   Results and discussion

4.4.1   Aftershock production (N^*, $\alpha - value$)

Figure(4.1) shows average aftershocks rate of different magnitude classes, as estimated using as a proxy of aftershocks within 10 days after the mainshocks. Productivity of events with magnitude < 7.0, is smaller than that of the events with magnitude greater 7.0. This pattern is very well described by Helmstetter and Sornette (2003a) as every mainshock with magnitude $< m_c + 2$ don't trigger a complete aftershocks sequence. Mainshock with magnitude $\geq m_c + 2$ show that aftershocks productivity increase with mainshock magnitude, that is $\sim 10^{\alpha m}$, with $\alpha = 0.82 \pm 0.06$. Similar results were found by Helmstetter (2003) as $\alpha = 0.81$ for the California catalog. α value [0.66 – 1.15] are reported by Hainzl and Marsan (2008) using global earthquake data catalog of ISC. In both of these studies they have used Omori law to calculate aftershocks productivity (detail discussion in section 4.1), whereas our calculations are not dependent of any model but simply counting the number of aftershocks.

For further confirm α value of the global data, aftershock productivity are calculated for different magnitude classes by using Omori law similarly to Helmstetter (2003) and Hainzl and Marsan (2008) techniques. We resolve similar results by directly counting the number of aftershock within 10 days after the mainshock, that is aftershock productivity increases with mainshock magnitude, with $\alpha = 0.84 \pm 0.05$ (figure 4.5a). Its value is independent of time window used for Omori law fitting as shown in figure (4.5a). On this figure, Omori law parameters are estimated using 10 days of aftershocks. Figure (4.6a) show the aftershocks productivity calculated by using 80 days aftershock data, both figures give the same results. Previously α was suggested to be dependeant of the procedure used for aftershock-mainshock selection and tectonic regions (e.g, Felzer et al. (2003), Helmstetter and Sornette (2003c); Hainzl and Marsan (2008)).
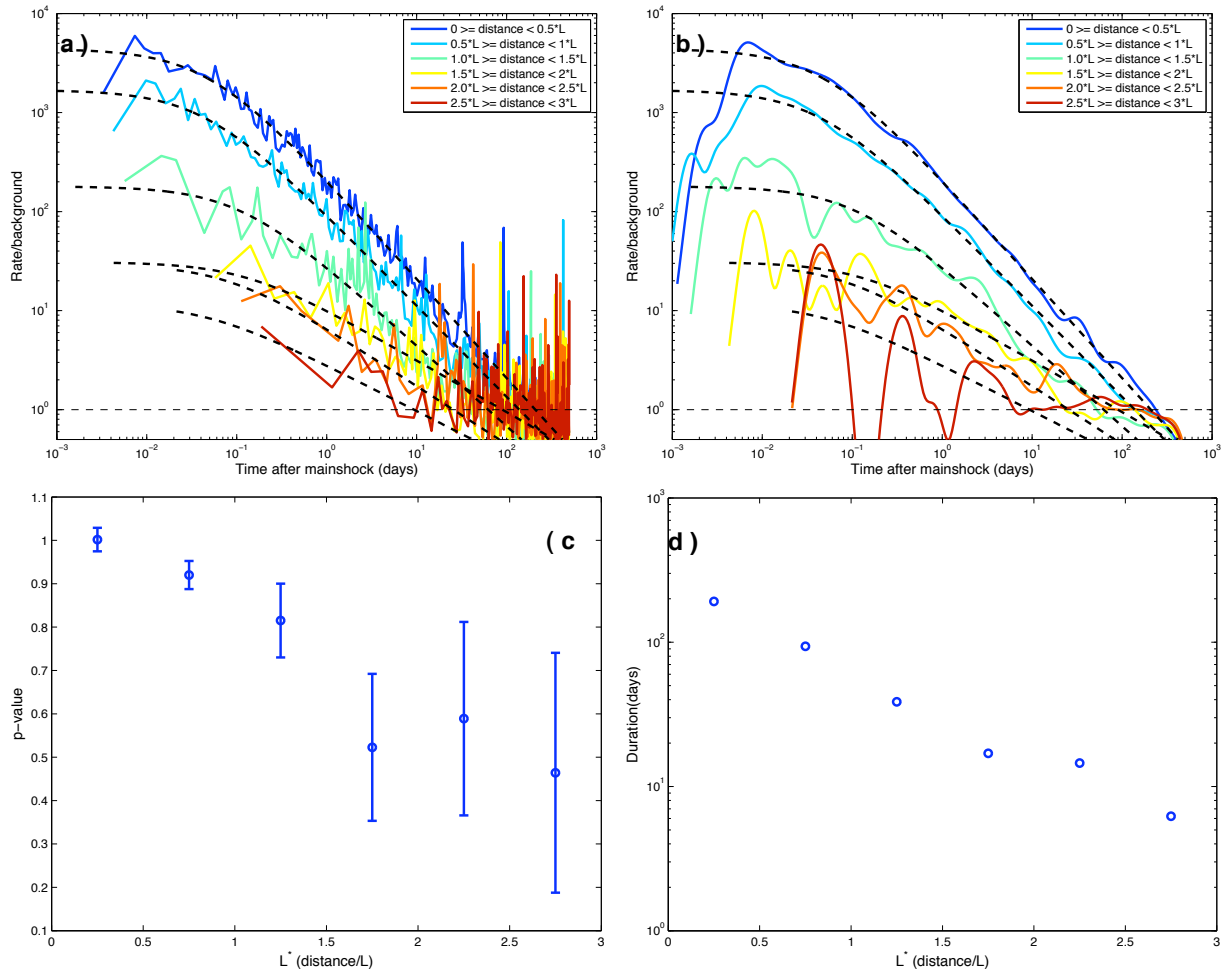
Figure 4.9: Seismicity rate for different values of distance to the mainshock. Horizontal dash line is the background rate calculated by using events within $5L$ and 5 yrs before the window mainshock. Omori law fit (black dash line) to the data upto 10 days. (a) Seismicity rate is calculated by using nearest neighbor method with k=5 % of the total data (b) rate calculated using gaussian function (c) $p-value$ correlation as function of distance from the mainshock (d) duration is function as function of distance from the mainshock.

4.4.2   Dependency of $p-value$ and duration on mainshock size

We show that $p-value$ increases with increasing mainshock magnitude (figure 4.5). Aftershocks data within time window as [0.009 – 10] days were considered for Omori law fitting. Our results are similar with that of Ouillon and Sornette (2005) for California catalog, Hainzl and Marsan (2008) for global data of ISC catalog and Ouillon et al. (2009) for California, Japan and global CMT catalog. The dependency of $p-value$ with mainshock size is well described by Ouillon and Sornette (2005) as multi-fractal model and by Hainzl and Marsan (2008) as the larger event slips, larger variability of stress changes and patches as compare to the small size events. The strong stress heterogeneity of large events is suggested to produce higher $p-value$ (Hainzl and Marsan (2008)). These authors further show that the increase of $p-value$ with mainshock size changes with stress field variability and Hurst-exponenet (H) and co-efficient of variation (CV) of the stress distribution. Afterslip have no or small effect on the correlation between $p-value$ or aftershocks productivity and mainshock size (e.g., Hainzl and Marsan (2008)).

Hainzl and Marsan (2008) use 0.1 – 100 days aftershocks data for power law fitting. When we increase the time window in the [0.009 – 80] days used for Omori's law fitting, we observed that the correlation between $p-value$ and mainshock size becomes weak for whole cascade sequence (figure 4.5b). At the sequence onset (i.e., within first few days after the mainshock as suggested by Felzer et al. (2002a, 2003); Helmstetter and Sornette (2003c)), direct aftershocks dominated but at later stages the contribution of indirect aftershocks increases which may induce changes in the aftershock production and decay rate (e.g., Felzer et al. (2003), Helmstetter and Sornette (2003c)). Furthermore we tested the effect of $p-value$ and its dependency on mainshock size for different time window after the mainshock (figure 4.7a). $p-value$ of each magnitude class is affected by time after mainshock, but the strongest effect is observed on the largest shocks. We ignore, for discussion the lower (5.5 – 6.0) and higher (> 8.5) magnitude events. The lower magnitude events are very close to the background and we cannot resolve their own aftershock sequence. The higher events magnitude classes consist only one mainshock and

no smoothed data are resolved. The $6.0 \leq m \leq 8.5$ events, show that initially $p - value$ has a small increases with time and reaches a peak value between 20 to 30 days. After peak value, $p - value$ decreases and stabilize with time. This increase in $p - value$ with time upto 30 days after the mainshock, may be driven by the occurrence of largest aftershock which is on average delayed by 40 days and with median ~ 5 days (Tahir et al. (2011)). They observed that $p - value$ of the largest aftershocks distribution is larger than regular aftershocks, with a 0.2 difference. The correlation between $p - value$ and mainshock size decreases as we consider time window > 30 days and finally becomes weak at long time window (~ 80 days). This is consistent with the results found by Marsan and Lengline (2008) for dressed aftershocks using California seismicity.

Increase of $p - value$ with time is also consistent with the result of Helmstetter and Shaw (2006) and Peng et al. (2007). They also show that $p - value$ increase with time after mainshock that is driven by heterogeneous stress distribution over fault plane. Helmstetter and Shaw (2006) and Marsan (2006) compute distribution of stress heterogeneity from aftershocks rate based on rate and state friction model. Helmstetter and Shaw (2006) show that $p - value$ increases toward 1 with increasing stress heterogeneity and time.

We find that the background rate also increase with mainshock magnitude (figure 4.3). If background level is constant then according to Omori's law lower $p - value$ and higher $K - value$ of the sequences will give the higher duration and vice versa. For first few days we find a strong correlation of $p - value$ and $K - value$ with the mainshock size. As both p and $K - value$ increases with mainshocks size will not give a correlation of duration mainshock, means duration will not increase with mainshock magnitude using small time window. But at the large time window we find weak correlation of $p - value$ with mainshock whereas correlation of $K - value$ have small effect of long time window. Which support the possibility to have higher duration with higher magnitude events because of $K - value$ has positive correlation with mainshock magnitude. Figure (4.4) is aftershock duration calculated for whole cascade sequence aftershock duration show an increases of duration with mainshock magnitude, the last two sequences that is events with magnitude in the class $8.5 - 9$ and greater than 9.0, does not goes to the average background rate.

The results of $p - value$ have no correlation and that duration and $K - value$ value increases with mainshock size is consistent with that of Omori's law and with the results of Marsan and Lengline (2008) for dressed aftershocks using california seismicity. Drakatos and Latoussakis (2001) also observed the same results by using Greece (1971–1997) catalog whereas Ziv (2006b) found that duration is smaller for small magnitude mainshock and larger for that of larger earthquakes.

4.4.3 Dependency of $p - value$ and duration on distance

Instead of temporal variation we also tested seismicity rate for different distances to the mainshock, by stacking seismicity rate at different distance from mainshock, with mainshock taken at the center. We observed that seismicity rate which is further normalized by its corresponding reference background decrease with distance from the mainshock (figure 4.9). Which is similar with the prediction of Dieterich (1994); Helmstetter and Shaw (2006) and Ziv et al. (2003). Higher seismicity rate closer to the mainshock is due to higher effective stressing rate (e.g., Ziv et al. (2003)). This is because fault patches close to the mainshock are strengthen while those away are weakened. As a results, seismicity rate decreases (Ziv et al. (2003)). They further show that secondary aftershocks of the mainshock modeled on the basis of uniform stress distribution show no change in the $p - value$ of the seismicity rate. If the stress distribution is non-uniform then secondary aftershocks modify spatial distribution of aftershocks (Ziv et al. (2003)).

Figure 4.9c supports the $p - value$ decrease upto distance 1.5*L from the mainshock and then remains stable for distance $> 1.5*L$. These results suggest that close to mainshock heterogenous stress distribution may drive higher $p - value$ of the seismicity rate and tthat its impact decreases as distance from the mainshock increases. These patterns are in agreement with Helmstetter and Shaw (2006) rate and state simulations. The decrease in $p - value$ with distance may be also due to the aftershock diffusions with distance and time as suggested by Helmstetter et al. (2003).

We also show that aftershocks duration also decreases as distance increases from the

mainshock (figure 4.9d). Again this patterb is that predicted by Dieterich (1994) model. As distance increases ratio of seismicity rate to the reference stressing rate decreases, which further decrease aftershocks duration. The similar results are suggested by Marsan (2006) with secondary aftershocks increases with distance from mainshock thus increasing the reference stress and consequently aftershocks duration decreases.

4.4.4 Aftershock linear density

Aftershocks linear density is an important tool to distinguish between dynamic and static stress triggering. In order to test the triggering mechanism of the global data we calculate aftershock linear density for different magnitude classes. We find that each magnitude classes display a maximum for linear density from the mainshock, that depends on the size of the mainshock (figure 4.8). Higher the mainshock magnitude farther away the peak linear density and vice versa. After the peak value, linear density decreases as power law from the mainshock distance with different decay exponent. We further find all curves collapse when normalize by $10^{\sigma m}, \sigma = 0.4$ with exponent decay slope as 2. It supports that global earthquake triggering is mainly driven by static stress changes, similar with the results observed for California moderate-small seismicity by Lippiello et al. (2009a).

4.5 Conclusions

We analyze spatio-temporal parameters of the global stacked earthquake data from USGS catalogue. Aftershocks productivity increases with that of mainshock magnitude $\sim 10^{\alpha m_m}$, with $\alpha = 0.82 \pm 0.06$ from direct counting number of aftershocks and $\alpha = 0.84 \pm 0.05$ from that of Omori law fitting. $p - value$ is a function of mainshock magnitude $0.009 < t < 10$ days, whereas correlation is lost for $t = [0.009 - 80]$ days. It suggests the early time aftershocks, as dominated by direct aftershocks, are the only to be impacted by the mainshock size. It is further supported by the 5 days median and 40 days mean values for the occurrence of the largest aftershocks. This later being the obvious threshold

to switch from direct to secondary aftershocks. Duration of whole sequence (direct and indirect) has a positive correlation with mainshock magnitude, i.e., duration $\sim 10^{0.32 m_m}$. Higher duration for large magnitude is driven by its larger aftershocks productivity. $p - value$ of all magnitude classes increases with time after the mainshock have maximum $p - value$ at $\sim 20 - 25$ days. In the context of rate and state friction, It suggests a change in stress field heterogeneity through time (Helmstetter et al., 2003). We further checked the rate of heterogeneity over the fault plane spatially, by observing the decrease in seismicity/background rate as a function of distance from the mainshock. $p - value$ also decreases with distance from the mainshock upto distance $< 1.5 * L$. The spatial variation of $p - value$ across the fault plane also supports the existence of heterogeneous stress distribution over the fault plane and diffusion.

Linear density of aftershocks for mainshock magnitude classes have peak values with distances that increase with the mainshock magnitude. Post peak density linear decays as a power law. Linear density of different magnitude classes collapse when normalize by $10^{\sigma m}$, with decay exponent as 2. It support that global earthquake triggering is mainly driven by static stress changes.
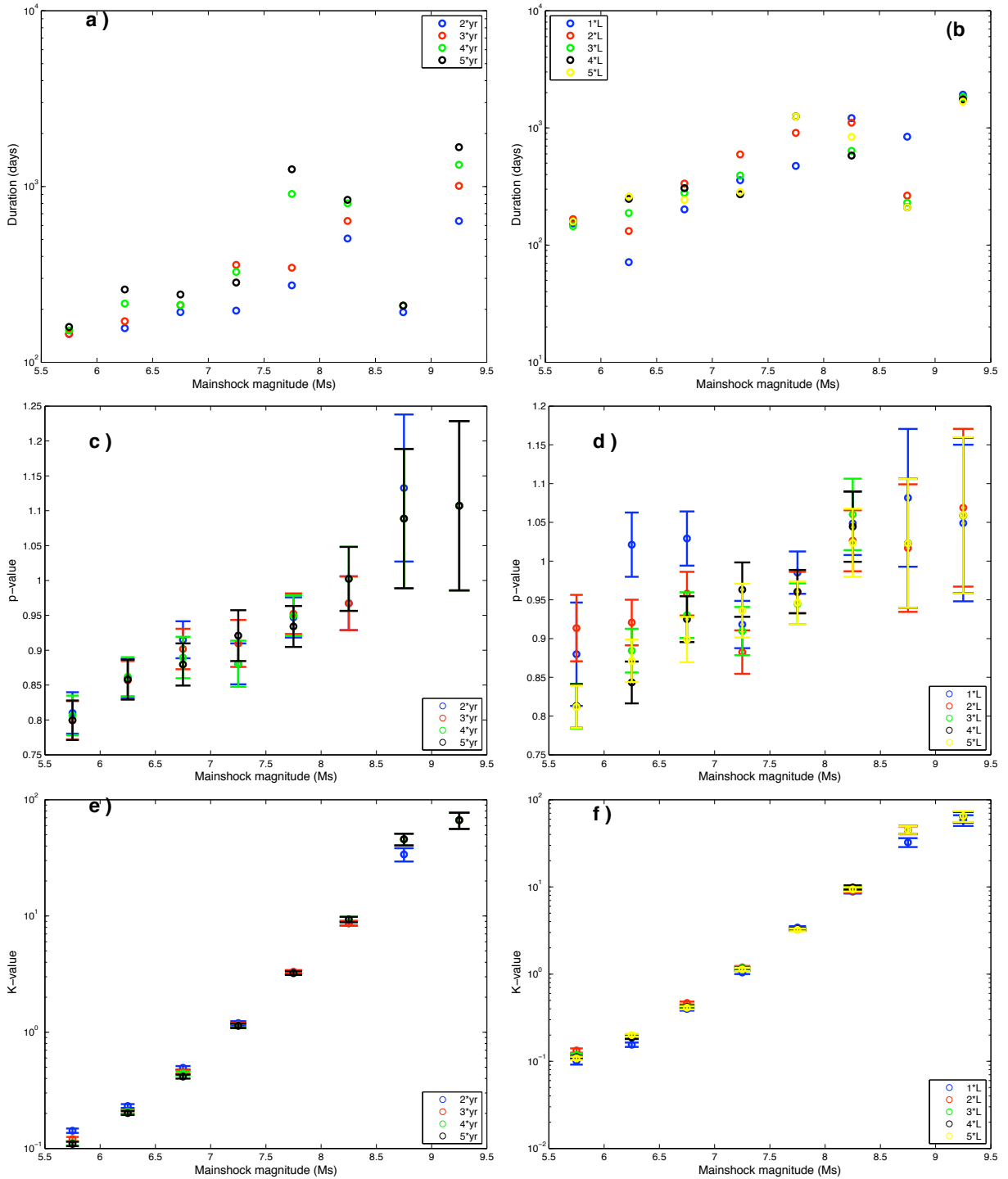
Figure 4.10: Temporal parameters such as duration, $p-value$ and $K-value$ with changing space time window for the selection of mainshock. (a, c, e) are duration, $p-value$ and $K-value$ calculated when mainshock is selected using time window = 2, 3, 4 and 5 year and distance = 5*L. (b,d,e) are duration, $p-value$ and $K-value$ calculated when mainshock is selected using distance window = 1*L, 2*L, 3*L, 4*L and 5*L and time = 5 year. The event is taken as mainshock if it not precede or followed by larger earthquake with space time window.

147

Chapter 5

Diffusion pattern of foreshocks and aftershocks: direct evidence for the respective role of direct and indirect aftershocks on diffusion regimes.

M. Tahir [1], JR Grasso[1]

[1]Institut des sciences de la Terre (ISTerre)

University Joseph Fourier - Grenoble I, FRANCE

Abstract

Interactions between earthquake triggering patterns are usually labeled as foreshocks and aftershocks. When the rate over time of both pre- and post earthquake triggered sequences are know to be well described by a Omori's power law power relaxation Omori's law ($N(t) = \frac{K}{(t+c)^p}$) a little is known on their coupled time and space evolution, i.e. the diffusion process. We observe that density rate (number/km/day) as a function of distance to the trigger shocks obey a power law ($\Phi(t) \sim \frac{1}{r^\mu}$) and diffuse with time. Aftershocks expansion toward the background is slower as compare to the foreshocks contraction towards the mainshock ($\langle\mu\rangle_{aft} > \langle\mu\rangle_{fore}$). Two regimes are observed: slow diffusion at short time scale (upto 5 days), with $H = 0.07$ and a second regime at longer time scales with $H = 0.38$. These two regimes are robust against aftershocks selection within 10 fault length, 500, 1000 km distance. We resolve the roll over between the 2 regimes, within a few days from the mainshock, is contemporary to the occurrence of the largest aftershock (4 days median value) for each sequence. Accordingly, the first regime, which corresponds to the aftershocks smaller than the largest aftershocks, is dominated by direct aftershock, i.e. those triggered by the mainshock. The second regime onset corresponds to a burst of event triggered by the largest aftershock or each sequence. It demonstrate the controls of secondary aftershocks on the second diffusion regime. These results allow to be better understand the mechanics of cascade of earthquake triggering. It allows a simple mean field picture of the cascade process.

Nous avons analysé l'exposant de loi d'Omori ($p-valeur$ de $N(t) = \frac{K}{(t+c)^p}$) et la diffusion de l'exposant (H de $R(t) = t^H$) pour des précurseurs et des répliques. La valeur p des répliques stackées est plus élevée que celle des précurseurs, alors que le même schéma est observé pour la pente de la décroissance de densité linéaire.

Auparavant, l'invariance d'échelle du tremblement de terre a été indiquée dans l'espace ou dans le temps. Le lien entre l'espace et le temps peut nous aider à mieux comprendre le mécanisme de déclenchement des systémes de failles. Nous observons que le taux de sismicité (nombre / km / jour) en fonction de la distance obéit à une loi de puissance

$(H(t) \sim \frac{1}{(D+R)}^{1+\mu})$. L'exposant μ diminue et atteind le niveau de fond à long terme ($>$ 2000 jours) avec $\mu \sim 0$. L'expansion de taux de densité de répliques (nombre / km / jour) vers le niveau de fond est plus lent comparé à la contraction des précurseurs (à partir du niveau de fond vers le choc principal). Initialement (jusqu'à 5 jours), des répliques migrent plus lentement á partir du choc principal que pour les précurseurs ($H_{aft.} = 0.07$ et de $H_{fore.} = 0.20$). Mais pour le temps ($>$ 5 jours) contemporain de l'apparition de la plus grande réplique, la migration des répliques devient rapide ($H_{aft.} = 0.38$). La diffusion linéaire des réplique est différente de celle des précurseurs, alors que la sismicité de fond à presque la même valeur dans les 2 cas.

5.1 Introduction

It has been recognized for a long time that within the specific space time window, foreshocks are the events (above the background level) preceding the large earthquake. While aftershocks are the events (above the background level) followed by the trigger shock (e.g., Felzer et al. (2004); Helmstetter et al. (2002)).

Foreshocks when averaged on many sequences appear as rate increase of earthquake toward the mainshock occurrence (Jones and Molnar (1979)). This increase in the rate is similar to the power law decay rate of aftershocks and is defined as inverse Omori law (e.g., Papazachos et al. (1967); Papazachos (1975); Kagan and Knopoff (1978); Jones and Molnar (1979); Davis and Frohlich (1991); Shaw (1993); Ogata et al. (1995); Maeda (1999); Reasenberg (1999a); Helmstetter et al. (2002)). Furthermore an inverse Omori is observed on shorter time scale (few weeks to months) than that of aftershocks (Keylis-Borok and Malinovskaya (1964)). Omori's law exponent (p'-value) of the foreshocks are equal or less than the exponent of the aftershocks ($p - value$) as shown by Maeda (1999); Helmstetter et al. (2002); Ziv (2003). The reason for smaller $p' - value$ of foreshock is not clear and the same mechanism were suggested to produce foreshocks as that of aftershocks (Yamashita and

Knopoff (1987); Shaw (1993); Helmstetter et al. (2002); McGuire et al. (2005)). Foreshocks may physically results from a fracture initiations (Mogi (1963)), subcritical weakening by stress corrosion (Yamashita and Knopoff (1989, 1992); Shaw (1993)), nucleation process of mainshock (Dodge et al. (1996)), dependent of faulting style (Reasenberg (1999b)), general damage process (Sornette et al. (1992)), stress increase (Abercrombie and Mori (1996); Maeda (1999)); dynamic stress distribution (Huang et al. (1998); Gabrielov et al. (2000); Narteau et al. (2000)) and visco-elastic response of the crust (Hainzl et al. (1999); Pelletier (2000); Bouchon et al. (2011)). For foreshocks, an emerging view of seismicity is to be able to capture any mechanical process and to consider patterns of ETAS simulation as that a null hypothesis for any mechanical models (Helmstetter et al., 2002) and Helmstetter and Sornette (2003b). They demonstrate that mainshock are aftershocks of conditional foreshocks as observed in real data and reproduce by the ETAS model. According to this perspective, any earthquake that occurs will subsequently produce other events, with the resulting number of aftershocks dependent on the size of the initial event. Consequently, smaller events should be triggered more frequently than larger ones and there is no bound on smaller events not to trigger larger events. Unfortunately, according to this conceptual view, short-term prediction may be difficult, because it implies that foreshocks are not generated during a unique period of fault activity (e.g.,Dodge et al. (1996), Helmstetter et al. (2002), Bohnenstiehl (2005)).

Aftershocks density decreases as distance increases from the mainshock (e.g., Dieterich (1994); Huc and Main (2003); Helmstetter et al. (2003); Helmstetter and Shaw (2006)). This decrease or decay of linear density with distance from mainshock have been observed to obey a range of functions, including power law and combination of power laws with constant and exponentials law (Huc and Main (2003); Felzer and Brodsky (2006); Marsan and Lengliné (2010); Richards-Dinger et al. (2010); Brodsky (2011)). These models are normally derived using fix time window and aftershocks density are calculated by counting number of aftershocks in different circular shell [r, r+dr] from the mainshock. Aftershocks spatial distributions when calculated for different time window, allow to estimate aftershock diffusion or migration. A similar type of approach has been used by Helmstetter

et al. (2003) to analysis the diffsuion of California seismicity. Previously aftershock expansion have been observed in many studies for different region of the world (e.g., Tajima and Kanamori, 1985b; Ouchi and Uekawa, 1986; Eneva and Pavlis, 1991; Dieterich, 1994; Marsan et al., 2000; Huc and Main, 2003); Helmstetter et al. (2003); Daniel et al. (2011). But a number of studies show that there is no evidence of aftershocks diffusion with time. As an example of Gasperini and Mulargia (1989) use Italian seismic catalog and found no evidence of aftershock migration. Similarly Shaw (1993) analysis spatial distribution in different time window for central and northern California seismicity, with a model based on subcritical crack growth dynamics and no expansion of aftershocks zone with time was observed. He explain the stationary spatial distribution might be due to the considering of only directly triggering events and ignore aftershocks of the aftershocks. Helmstetter et al. (2003) conclude that aftershock migration is either very small or difficult to distinguish from the background activities. Davidsen and Paczuski (2005) analyzed the spatio-temporal correlation of Southern California seismicity and found that the rate of aftershock decay does not changes with distance.

Previously diffusion was interpreted by many physical processes and related to a number of factors, e.g., a viscous relaxation process (Rydelek and Sacks (2001)), due to fluid transfer in the crust (Noir et al. (1997); Nur and Booker (1972); Hudnut et al. (1989)), by rate and state dependent friction model (Dieterich (1994)), subcritical crack grow (Das and Scholz (1981); Yamashita and Knopoff (1987)), damage or static fatigue laws (Lee and Sornette (2000)) and many other models assuming stress weakening (e.g., Mogi (1968); Imoto (1981); Chatelain et al. (1983); Tajima and Kanamori (1985b); Tajima and Kanamori (1985a); Wesson (1987); Ouchi and Uekawa (1986); Jacques et al. (1999); Helmstetter and Sornette (2002b); Godano and Pingue (2005)). Actually diffusion predicted by any model shows that stresses induced by mainshock decreases with distance from mainshock. Therefore failure time of events at larger distances increases as compare to the closer aftershocks (Helmstetter et al. (2003)). The evolution of mean distance ($R(t)$) to the mainshock with t, is express as;

$$R(t) \sim t^H \tag{5.1}$$

where H is the diffusion exponent that depends on both the exponent of Omori's law and the exponents of the spatial interactions between events i.e., $H = \frac{\theta}{\mu}$, $p = 1 \pm \theta$ (Helmstetter and Sornette (2002b)). According to ETAS model, diffusion should be observed only for the sequence with $p - value$ less than 1 (Helmstetter and Sornette (2002b)). Helmstetter and Shaw (2006) suggested an anti-correlation between p and H for the sequence with $p <$ 1. In addition Marsan et al. (1999) using mining seismicity, also proposed the dependence of H on mainshock size, which they interpret as driven by the variations in fractals or multi-fractals behavior of the fault systems. Diffusion is classified according to the value of H. For $H = 0$ no diffusion will occur, while $H = 1/2$ gives standard diffusion (Helmstetter et al. (2003)). Events with $H < 1/2$ are characterize as sub-diffusion where super-diffusion events have $H > 1/2$ (Helmstetter et al. (2003)).

In the present paper, we compare the Omori's law exponents $(p - value/p' - value)$ of foreshocks and aftershocks by using global USGS stack data. We also investigate the existence of diffusion mechanisms for both foreshocks and aftershocks by using two different techniques. First, the evolutions (time) of the linear density give the expansion of density rate with time after the mainshock. Second we estimate the diffusion exponent (H) by using average distance as a function of time after the mainshock.

5.2   Data and Methods

For this study, we analyze, $1973 - 2010$ world wide shallow (depth < 70 km) earthquakes from USGS (http://earthquake.usgs.gov) catalog. Threshold magnitude (M_c) is reported as 5 for the global data (e.g., Kagan and Knopoff (1980); Kagan (2004); Tahir et al. (2011)). To ensure the uniformity of the data, we restricted our analysis only to the $M \geq M_c$. Most of the magnitude are M_s (surface wave magnitude), but when M_s is not available then m_b (body wave magnitude) is used instead.

A number of declustering procedures are available to isolate aftershocks from background seismicity (e.g., Gardner and Knopoff, 1974; Reasenberg, 1985; Kagan, 1991; Knopoff, 2000; Felzer et al., 2004; Helmstetter et al., 2005; Marsan and Lengline, 2008), however none of them is acknowledged as being 100% robust. Instead we define a mainshock as M_s $\geq$ 7.0 event that neither precede nor followed by larger earthquake within [1 year, 5*L] window around the mainshock, L is the rupture length calculated from Wells and Coppersmith (1994) relationship. $M = 7.0$ i.e., M_c +2 is the critical value of the global data, for an aftershock sequence of the global data to be fully developed (Tahir et al. (2011)). As suggested by Helmstetter and Sornette (2003a) above M_c +2, α value ($K = K_o 10^{\alpha M}$) is larger than 0.5.

The events following the mainshock within space window as 5*L around the mainshock are taken as aftershocks whereas in the same space window the events preceding the mainshock are taken as foreshocks.

To reach on average stable estimation of spatio-temporal parameters of the global data we stack foreshocks and aftershocks time series. The stacking of the data smoothes out fluctuations associated with individual sequences and highlights the common features of all sequences (Helmstetter and Sornette (2003b); Ouillon and Sornette (2005); Yang and Ben-Zion (2009) and many others).

5.2.1   Omori Law Parameters

Omori's law describes the power decay of the aftershocks rate with time (t) from the mainshock;

$$N(t) = \frac{K}{(t+c)^p} \tag{5.2}$$

$N(t)$ is the seismicity rate, p, c and K are constants (Utsu et al. (1995); Utsu (1961)). A median $p-value$ of $\sim$1.1 is reported for the aftershock sequences in the various parts of the world, with range of $\sim$0.6 - 2.5 (Utsu et al. (1995)). K is the productivity of aftershocks sequences.

Similar to the aftershocks, foreshocks are well described by an inverse Omori's law,
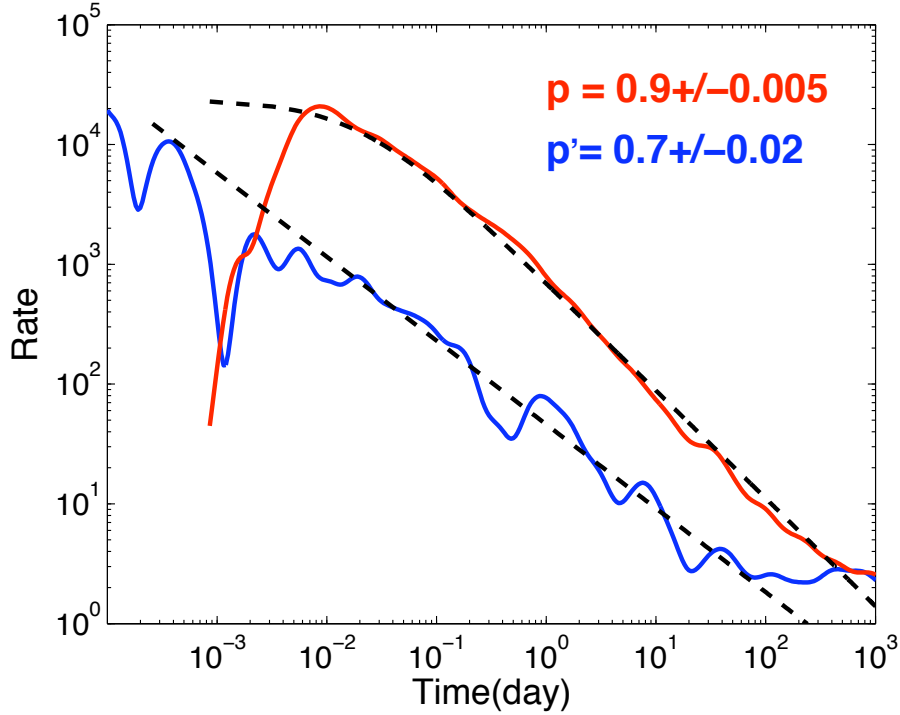
Figure 5.1: Daily rate of stack aftershocks (red) and foreshocks (blue) of the global data with modify Omori law fitting (black dotted line). Foreshock are plotted on the same side of aftershocks by multiplying with -1, so that to compare with aftershock. Note that both stack aftershock and foreshock data are smoothed with gaussian filter. p and p' are the $p-value$ of aftershocks and foreshocks respectivly. Note that 80 days seems to be duration of stacked foreshocks whereas for that of aftershocks is ~ 500 days.

$$N'(t) = \frac{K'}{(-t + c')^{p'}} \qquad (5.3)$$

$p-value$ is empirically computed using $[0.009 - 500]$ days of the stack data. Whereas for the $p'-value$ estimation we use $[0.009 - 80]$ days data (figure 5.1).

5.2.2 Forshocks/Aftershocks Diffusion

Foreshocks and aftershocks migration are analyzed by using two different methods.

First, we compute linear density of events as function of distance to mainshock for different time windows.

$$\Phi(t) \sim \frac{1}{r^{\mu(t)}} \tag{5.4}$$

where $\Phi(t)$ is the linear density and r is the distance between mainshock and aftershock (Ogata, 1999; Helmstetter et al., 2002). For the calculation of aftershocks linear density ($\Phi(t)_{aft}$), first we stack the distances of aftershocks epicenter with respect to their mainshocks epicenter (e.g., Felzer and Brodsky (2006); Lippiello et al. (2009b)). Aftershocks occurring within 10^*L space and $[1 : 1 : 50]$ days window, $[10 : 10 : 2000]$ days window around the mainshock are used in the analysis. Then the linear density of the stack sequence is calculated by using nearest neighbor method (Felzer and Brodsky (2006)). We further normalized the linear density by the corresponding duration (time window of the data) to get density rate per unit time ($\Phi(t)'_{aft} = \frac{\Phi(t)_{aft}}{duration}$). Slope of the density rate is estimated by using least square method. Least square line fit to the data between 40 to 400 km, because density rate has plateau at nearly 40 km (figure 5.2). Using the same technique foreshocks density rate ($\Phi(t)'_{fore}$) is also estimated (figure 5.2 – 5.3).

Second, we compute mean distances between aftershocks/foreshocks and mainshock for $10^{-2:0.3:3}$ day time windows. Least square line fit to the data between 5 – 1000 days, because the aftershock data trend changes after 5 days (figure 5.4). In order to compare aftershock and foreshock diffusion, we also compute the average distances between the events that occur before the mainshock. Least square line is adjusted to the data between 0.09 to 50 days (figure 5.4). To test the diffusion changes after the occurrence of largest aftershocks, we repeat the same calculations for aftershocks but stop the data upto the largest aftershock occurrence time. Then least square line fit to the data between 0.01 – 10 days.

5.3 Results

We analyzed global data foreshocks and aftershocks of the mainshock ($M_m \geq 7.0$) with using world wide USGS catalog. We consider only those events which are neither
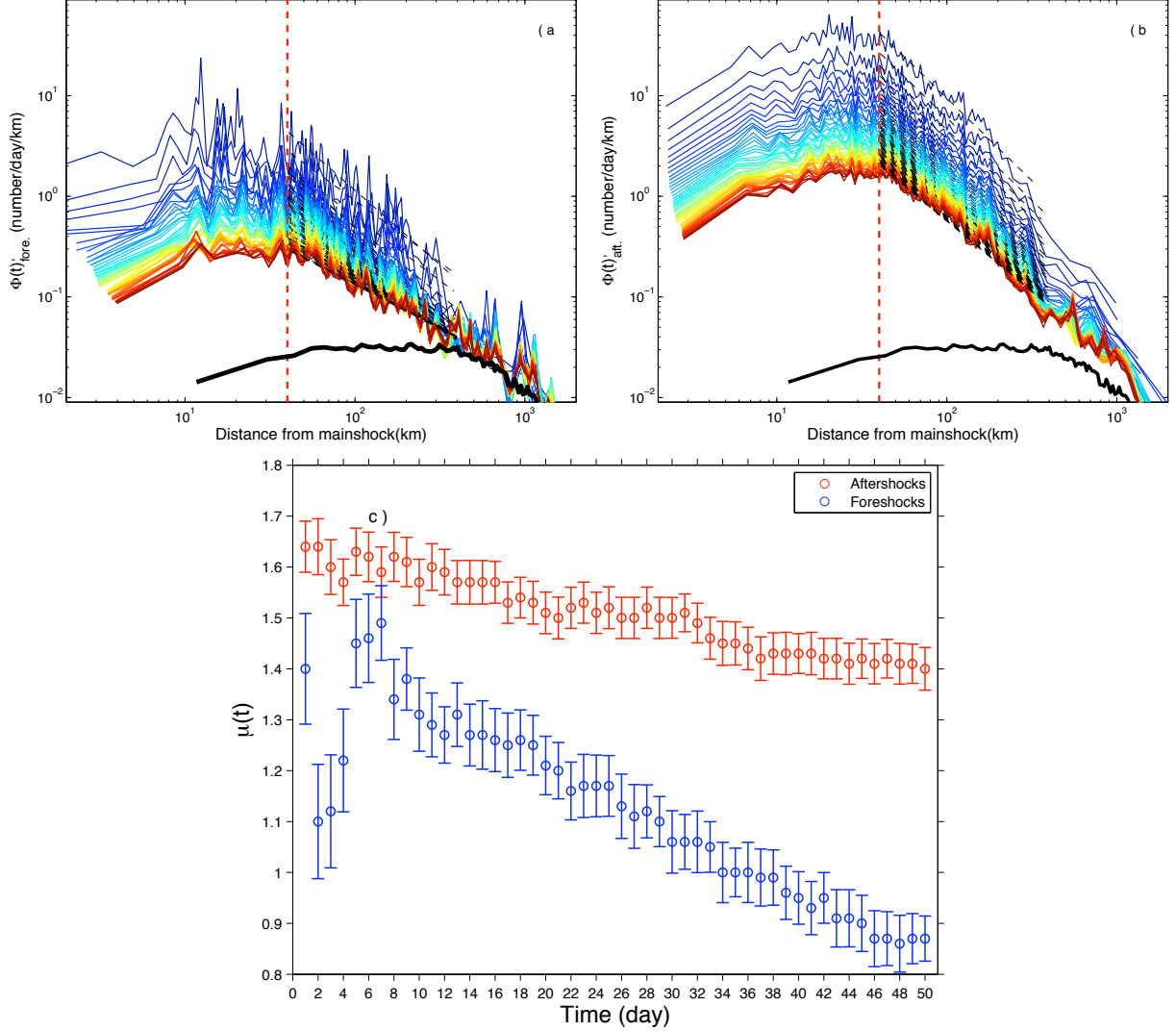
Figure 5.2: Rate $(\Phi(t)')$ of foreshocks and aftershocks of the mainshock $M_m \geq 7.0$ as function of distance for the mainshock. $\Phi(t)$ ($\Phi(t)$ from equation 5.4) is calculated for different time windows ranging from 1 (blue line at top) to 50 days (red line at bottom) with step size as 1 day for each calculation. The linear density $(\Phi(t))$ is further normalized by the duration of the time window used to estimate the seismicity rate $(\Phi(t)')$. (a) Foreshocks seismicity rate $(\Phi(t)'_{fore.})$ as a function of distance from mainshock, with least square line is fitted to the data between 40 to 400 km. (b) Aftershocks seismicity rate $(\Phi(t)'_{aft.}$ as a function of distance from mainshock, with least square line is fitted to the data between 40 to 400 km. (c) Exponent $(\mu(t))$ of the rate by fitting least square line to (a) and (b).

158
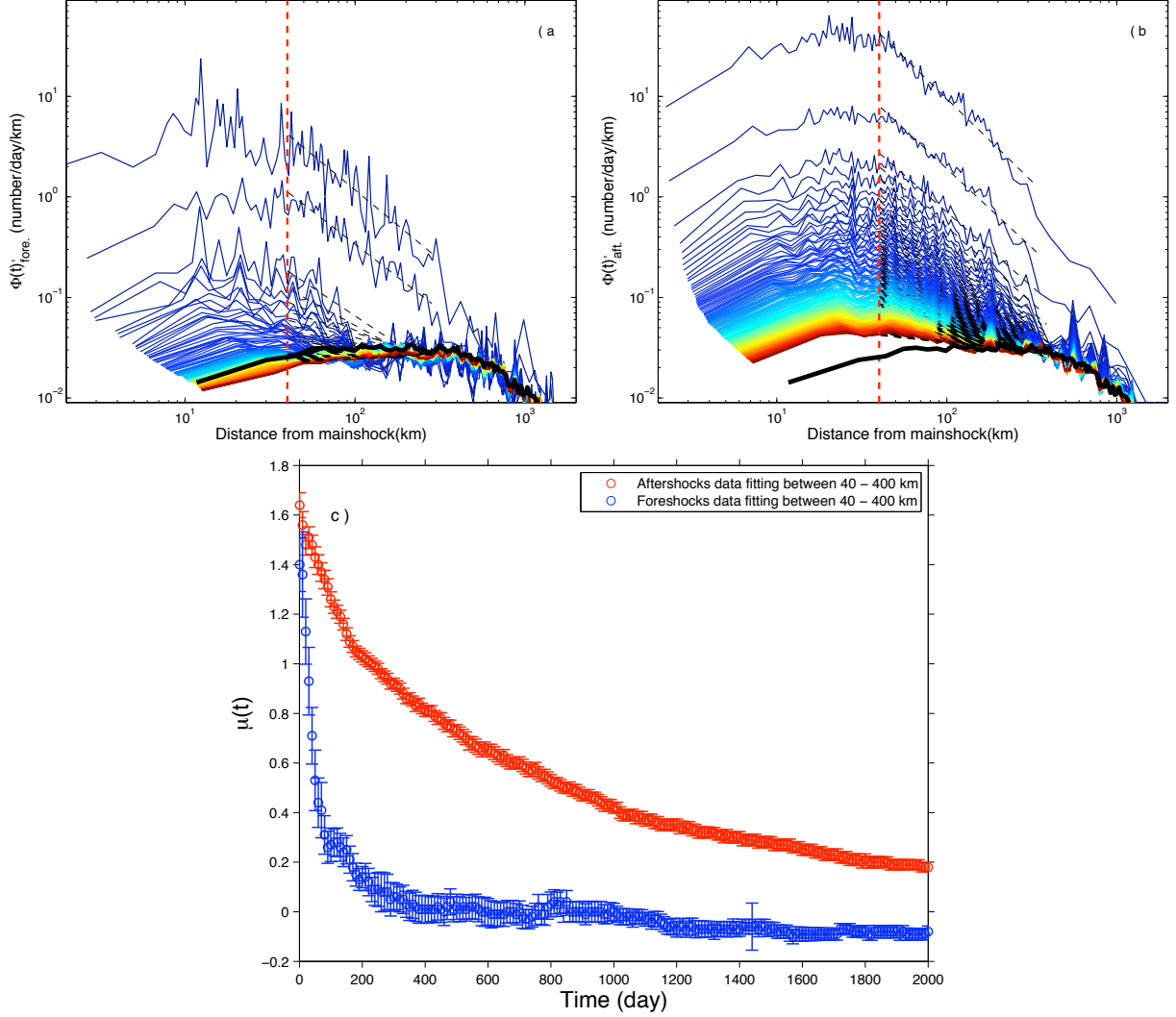
Figure 5.3: Density rate $(\Phi(t)')$ of foreshocks and aftershocks of the mainshock $M_m \geq$ 7.0 as function of distance for the mainshock. $\Phi(t)$ ($\Phi(t)$ from equation 5.4) is calculated for different time windows ranging from 1 (blue line at top) to 2000 days (red line at bottom) with step size as 10 days for each calculation. The linear density $(\Phi(t))$ is further normalized by the duration of the time window used to estimate the seismicity rate $(\Phi(t)')$. (a) Foreshocks seismicity rate $(\Phi(t)'_{fore.})$ as a function of distance from mainshock, with least square line is fitted to the data between 40 to 400 km. (b) Aftershocks seismicity rate $(\Phi(t)'_{aft.})$ as a function of distance from mainshock, with least square line is fitted to the data between 40 to 400 km. (c) Exponent $(\mu(t))$ of the rate by fitting least square line to (a) and (b).
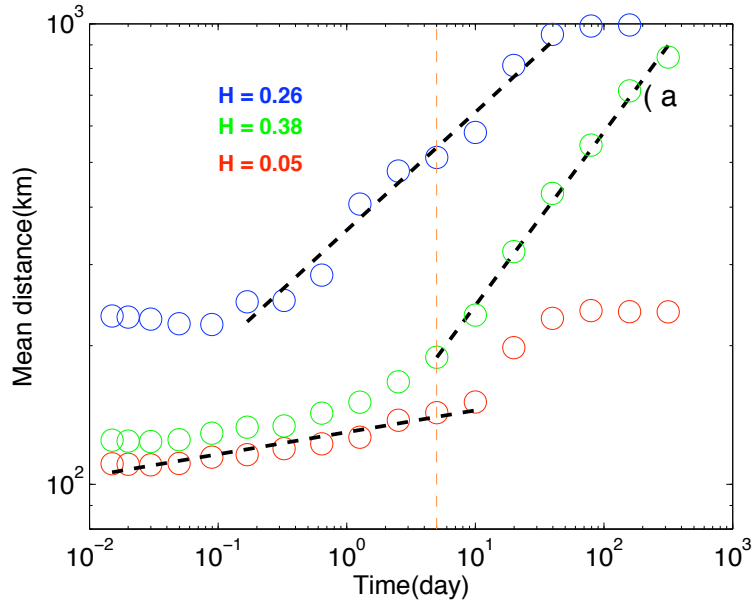
Figure 5.4: Foreshocks and Aftershocks mean $R(t)$ between mainshock $M \geq 7.0$ and its aftershocks for global data. Aftershocks and foreshocks are selected within $10L$ space window around the mainshock. All aftershocks (green) including largest aftershocks, data before the occurrence of largest aftershock (red). Foreshocks (blue) least square line fit to the data between 0.1 to 50 days, largest aftershock median time (orange)
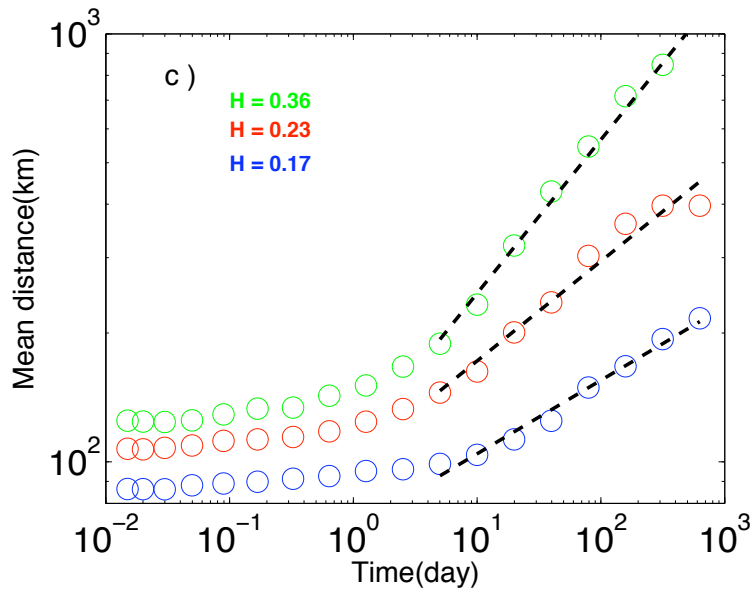
Figure 5.5: Same as figure 5.4, aftershocks select within $10*L$ (green), 1000 km (red), 500 km (blue) window from mainshock.

preceded nor followed by larger earthquake within [1 yr, 5L] time-space window around the mainshock. Aftershocks and foreshocks have been selected within time-space window T = 5 yr and $D = 5L$, where L is the rupture length calculated using Wells and Coppersmith (1994) relationship.

Omori's law exponent of the stack foreshock ($p' - value$) and aftershock ($p - value$) are computed for 80 and 400 days respectively. Stack foreshocks obey an inverse Omori's law with exponent ($p' - value = 0.7 \pm 0.02$) is smaller than that ($p - value$=0.9 $\pm$ 0.005) for aftershocks (figure 5.1). This result is similar with the results obtained previously by a number of studies with using different (e.g., Japan, California, Greece) catalogs (e.g., Papazachos et al. (1967); Papazachos (1975); Kagan and Knopoff (1978); Jones and Molnar (1979); Davis and Frohlich (1991); Shaw (1993); Ogata et al. (1995); Maeda (1999); Reasenberg (1999a); Helmstetter et al. (2002))

Figure (5.2 – 5.3) show density rate (number/day/km) of foreshocks and aftershocks as a function of a distance from mainshock. In both cases the rate has a peak value at a distance that depend on the mainshock magnitude (Lippiello et al. (2009a)). Incase of foreshocks the peak ($\sim$ 10 km) appears earlier as compare to the aftershocks ($\sim$ 30 km), but for the analyses we use the same starting of both data. Aftershocks and foreshocks rate evolve with time from the mainshock. This suggest that the aftershocks and foreshocks rate slowly diffuses with time. At large time window ($\sim$ 2000 days) the peak density vanishes and density rate becomes constant. To compare the evolution of aftershocks and foreshocks rate as function of distance, a least square line fit to data between 40 – 400 km. The data selection for line fitting is an arbitrary choice, but rate start decaying as power law started at a distance 40 km whereas the end data is tested for 400 and 3000 km. The long distance window is strongly effected by the uncorrelated activities coming from other events in the surrounding which can be observed at distance greater than 1000 km and time greater than 1000 days. So, we have used a smaller window (40 – 400 km) for data selection, in order to reduce the effect of uncorrelated activities at large space time window. $\langle \mu \rangle - value$ of foreshocks are smaller than that of aftershocks (figure (5.2 – 5.3)c).

For diffusion analysis, mean distances at different time windows are calculated. We

observed two regimes in the diffusion curve with different H (figure 5.4). First regime corresponds to the diffusion exponent ($H_{aft.}$) as 0.07 with data fit between 0.01 to 5 days after the mainshock. Whereas second regime has a faster diffusion ($H = 0.38$) observed at longer time (> 10 days). We further repeat the calculations for aftershocks occur before the occurrence of largest aftershock. We resolved that first regime is driven by aftershocks occur before largest aftershock. Foreshocks diffusion exponent ($H_{fore.}$) is 0.26 and have single diffusion regime.

5.4 Discussion and Summary

Foreshocks and aftershocks obey an Omori's law. Aftershocks duration (~ 500 days) is larger than that of foreshocks (~ 80 days). Which is similar with the results of Keylis-Borok and Malinovskaya (1964) and Bowman et al. (1998). They observed that an inverse Omori's exist for weeks to months, whereas that of direct Omori's law exist for years to decades.

$p' < p$ is first time observed for global USGS data with time span of ~ 30 years. Similar results were observed by many authors during last few decades (e.g., Papazachos et al. (1967); Papazachos (1975); Kagan and Knopoff (1978); Jones and Molnar (1979); Davis and Frohlich (1991); Shaw (1993); Ogata et al. (1995); Maeda (1999); Reasenberg (1999a); Helmstetter et al. (2002))). But the more comprehensive analysis of $p - p'$ is given by Helmstetter and Sornette (2003b) with using ETAS model and that for California seismicity. They show that the difference between the p and p' depend on aftershocks productivity (α; $K \sim 10^{\alpha M_m}$), β ($\beta = \frac{b}{1.5}$; $N \sim 10^{-bM}$) and branching ratio (n). $p - p'$ is smaller as $\frac{\alpha}{\beta}$ increases above 0.5, but for $\frac{\alpha}{\beta} < 0.5$, $p - p' = \theta \sim 0.2$ (Helmstetter et al., 2002). Since for the global data Tahir et al. (2011) observed an $\alpha \sim 0.8$ and $b = 0.96$ (figure 5.6), implies $\frac{\alpha}{\beta} \sim 0.5$. Thus $p - p' \sim 0.2$ is consistent with the ETAS model simulation (e.g., figure 6 of Helmstetter et al., 2002).

Evolution of linear density show that both foreshocks and aftershocks diffuse with time, i.e., foreshocks migrate toward the mainshock whereas aftershocks migrate away from the
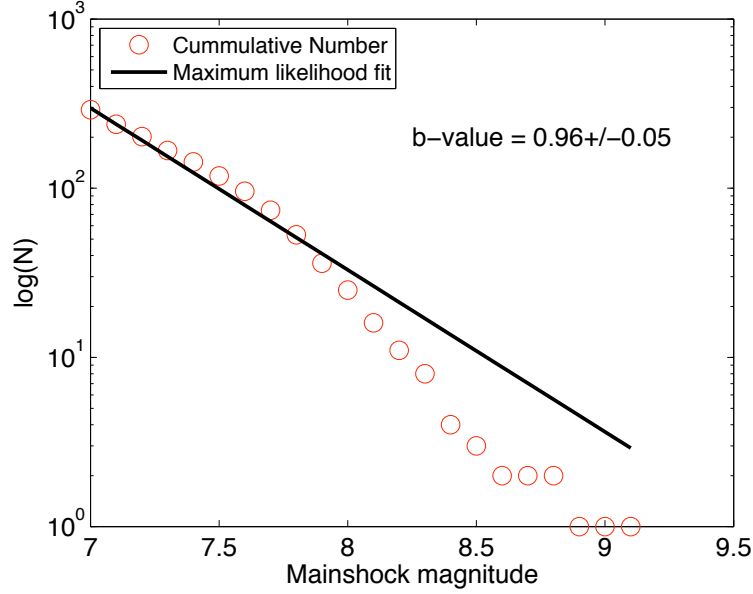
Figure 5.6: Aftershocks $b - vlaue$, calculated using maximum likelihood method (Aki (1965)).

mainshock (figure 5.3). Aftershocks diffusion is observed in many studies (e.g., Tajima and Kanamori, 1985b; Ouchi and Uekawa, 1986; Eneva and Pavlis, 1991; Dieterich, 1994; Marsan et al., 2000; Huc and Main, 2003; Marsan and Bean, 2003; Helmstetter et al., 2003; Daniel et al., 2011, many others) but the migration of foreshock is more difficult to observe. This is due to the limited number of foreshocks and to the location errors (e.g., Helmstetter et al., 2002).

We further observed that exponent ($\mu(t)$) of the density rate (number/km/day) is smaller for foreshocks than aftershocks. Using diffusion relationship of Helmstetter and Sornette (2002b) i.e., $H = \frac{\theta}{\mu}$, with $\theta = 0.2$ and $\langle\mu\rangle_{aft} > \langle\mu\rangle_{fore}$ implies faster migration of foreshocks than aftershocks.

Using H exponent we resolved two regimes for aftershocks diffusion, similar as suggested by Marsan and Bean (2003) and McKernon and Main (2005). They interpreted as the first regime is dependent on the size of the mainshock whereas second regime is driven by viscoelastic diffusion of stress in the lower crust. Aftershocks diffusion exponent ($H_{aft.}$) value in the first regime is consistent with that observed by Huc and Main (2003) as 0.06

for the global earthquakes of CMT catalog and similar with that of Helmstetter et al. (2003), analyzed 24 california aftershock sequences and concluded H as 0.08.

We further observed that first regime of the diffusion correspond to the data before the occurrence of largest aftershock. Secondary aftershocks broaden aftershocks zone and increase the diffusion process. Similarly, Ouchi and Uekawa (1986) show that diffusion is mainly due to the occurrence of large aftershocks, and to the localization of secondary aftershocks close to the largest aftershocks. Our apparent second diffusion regime emerge from cascade process, the mainshock triggers aftershocks that in turn trigger their own aftershocks, and thus lead to an expension of the aftershocks zone (Helmstetter and Sornette, 2002b).

It rejects any correlation of viscoelastic relaxation of the crust to diffuse, within a few 100 days from the mainshock. Accordingly, the two diffusions regimes are build up in correlated events, first is driven by primary aftershocks then aftershocks zone are further extended by secondary aftershocks.
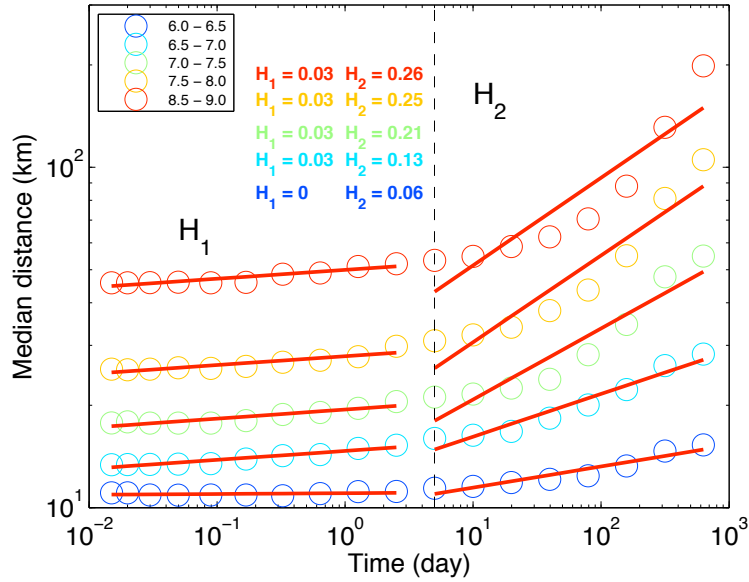
Figure 5.7: Median distances between mainshock and it corresponding aftershocks as a function of time after the mainshocks, for different values of magnitude of the mainshock (event that neither preceded nor followed by event with greater than the mainshock, with $5\ yr$, $5*L$ window) increasing from 6.0 to 8.5 with step size 0.5 from bottom to top.H_1 is the slope of the least square line fit to the data between 0.01 to 5 days, whereas H_2 is the slope of the least square line fit to the data between 6 to 1000 days.
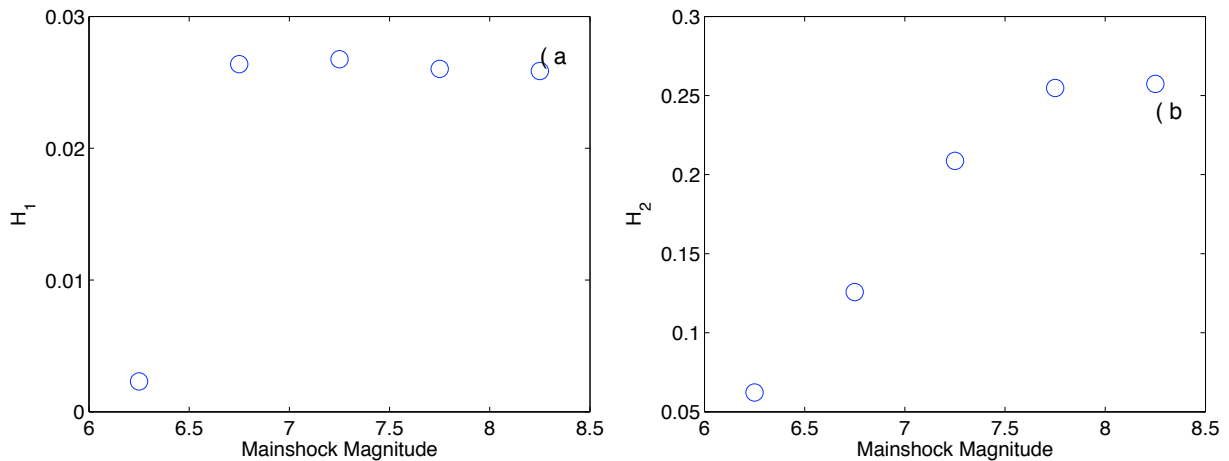
Figure 5.8: (a) H_1, (b) H_2 (H_1 is the slope of the least square line fit to the data of Figure (5.7) between 0.01 to 5 days, H_2 is the slope of the least square line fit to the data Figure (5.7) between 6 to 1000 days) as a function of mainshock size.

Conclusions and perspectives

The PhD focus on aftershock patterns. Main objectives were (1) to gain more insight in the spatial and temporal occurrence of aftershocks/foreshocks in the near-source region of seismogenic faults, (2) to improve links of spatio-temporal parameters to the underlying physics of earthquakes, (3) to understand the largest aftershock, (4) research mainly focused on understanding the origins and implications of space-time correlations and, (5) to analyze their implications for seismic hazard assessment. Therefore, we developed and used advanced statistical methods to analyze parametrics of global earthquake catalog in general and clustered sequences data in particular.

Starting with the analysis of aftershocks patterns of the Kashmir earthquake, 2005 and to compare the apparent large rate with 18 others $M \geq 7$ earthquakes within 1000 km radius. Such area, stands as the major region in which continental plates interact, worldwide. We test how Omori's law parameters, background rate, space and time patterns of the sequences interplay to produce the huge aftershock productivity for Kashmir earthquake. Normalization by earthquake sizes allow us to identify anomalies in aftershock sequence, i.e. above two times of standard deviation, for the productivity and rate of Khurgu earthquake, aftershock density for Kashmir sequences, high background rate for Southern Keriya sequence and long duration for Gazli (1976b) and Qaenat earthquakes. The other major result we robustly quantify for Western Asia $M > 7.0$ events, is the dependence of aftershock productivity on faulting styles, for all of the Omori law parameters. We resolved that the strike slip event productivity to be on average 4 times smaller than the thrust faulting productivity (Chapter 1).

We further extend and test the tectonic settings dependent triggering model that observed in Chapter 1 to a large data set and long period of global USGS and CMT catalog. In literature the role of faulting style on triggered seismicity is analyzed using $b-value$ from Gutenberg Richter law or $c-value$ from Omori law (e.g., Frohlich and Davis, 1993; Kagan, 2002b; Schorlemmer et al., 2005; Narteau et al., 2009; Gulia and Wiemer, 2010) with using Harvard CMT, Japan, Southern California (SCSN), Northern California (NCSN) and Italian Catalogs. We analyzed Omori parameters (p, $K-value$), aftershocks productivity (α) and exponent of linear density (μ) as a function of rake of the triggering earthquake.

We resolved that on average all the parameters of the Omori law (p, K, α, $N(t)$) and density rates are dependent on faulting styles (Chapter 2). Empirically we observed that thrust events have higher K, aftershocks and background rate but lower $p-value$, $\langle \mu \rangle$ and $\alpha-value$ as compare to the strike slip and normal events. Within the ETAS model strong K, N^* and low α values are driven by high branching ratio (n). We suggests that multiple interactions through higher branching ratio (n) of the thrust events drive its higher rates. Small $p-value$ and duration of the strike slip events suggests, within the rate and state context, stronger stress hetergeneity than for thrust events. In addition to provide new insight into the mechanics of earthquake interactions, our results also extends previous investigations, on importance of tectonics setting to all the parameters of both Gutenberg-Richter and Omori's laws. These findings will help, in the near future, to improve seismic hazard models.

We further investigated the effect of faulting style on the largest aftershocks. Båth's law i.e., the average size difference between mainshock and the largest aftershock is 1.2 and independent of mainshocks size, has been observed and widely discussed since the first compilation. A question of recurrent interest is whatever the law his its origin in some physical process underlying the development of aftershocks sequences, or has essentially statistical origin related to the randomness of the magnitudes. Many updates on aftershock triggering have been proposed since the 1950's for the development of empirical Båth's law. However, a comprehensive understanding of mainshock patterns in regard to size, distance and time of the largest aftershock is still unavailable. We extend Båth's law in the time

and space domains, as the largest aftershocks are closer in size (mode value : $\Delta M_r = 0.95$, $\Delta M_{ss} = 1.51$) and distance (mode value : $\Delta D_r^* = 0.11$, $\Delta D_{ss}^* = 0.22$) to the triggering shock, for ($_r$) reverse slip than for ($_{ss}$) strike slip events. Analytically using Gutenberg-richter law, we resolved that the highest thrust rate and lower $b - value$ drive the lower magnitude difference for thrust than strike slip events. The faster power law decay in time relative to regular aftershocks implies that the largest aftershocks are more prone to occur at the onset of any aftershock sequence (Chapter 3). These results, allow for a new forecast strategy for the largest aftershock occurrence.

After having clear observations of spatio-temporal parameters dependent on faulting styles, we have focused on the dependency of the seismicity patterns on the mainshock size. Aftershocks productivity increases with that of mainshock magnitude $\sim 10^{\alpha m_m}$, with $\alpha = 0.82 \pm 0.06$ from direct counting number of aftershocks and $\alpha = 0.84 \pm 0.05$ from that of Omori law fitting. $p - value$ is a function of mainshock magnitude for the time upto few days, whereas correlation is lost for time ~ 80 days. It suggests the early time aftershocks, as dominated by primary aftershocks, are the only to be impacted by the mainshock size. This later being the obvious threshold to switch from primary to secondary aftershocks. Duration of whole sequence (primary and secondary) has a positive correlation with mainshock magnitude, i.e., duration $\sim 10^{0.32 m_m}$. Higher duration for large magnitude is driven by its larger aftershocks productivity. Duration, further have an inverse correlation with the recurrence time of triggering earthquake.

We observed that $p - value$ increases with time after the mainshock and have its maximum value at $\sim 20 - 40$ days. This time we resolved in chapter 3 as correspond to the third quartile of the largest aftershocks (~ 40 days). The $p - value$ increase may correspond to stress heterogeneity increase as reproduced by simulations using Rate and State friction law. But also we show that $p - value$ decreases with distance from the mainshock. which is may be due to either the stress heterogeneity decrease with distance or due to the aftershocks diffusion occur at large time and distances. The spatial variation of $p - value$ across the fault plane also supports the decrease of heterogeneous stress distribution over the fault plane and diffusion.

Linear density of aftershocks for mainshock magnitude classes have peak values with distances that increase with the mainshock magnitude. Post peak density linear decays as a power law. Linear density of different magnitude classes collapse when normalize by $10^{\sigma m}$, with decay exponent as 2. It support that global earthquake triggering is mainly driven by static stress changes.

In the light of observations in the previous chapter 4 that stress heterogeneity of the triggering earthquake vary with time and distance from the mainshock. Also our result suggest the peak of stress heterogeneity corresponds to observed the peak stress hetrogenity correspond to the occurrence time of the largest aftershock. We investigated inter-earthquake triggering characteristics of foreshocks and aftershocks in the global USGS catalog. Omori's law exponent (p; $N(t) = \frac{K}{(t+c)^p}$) foreshocks is smaller than that of aftershocks, $p - p' = 0.2$ as predicted by ETAS model. Earthquake scale invariance are shown either in space or in time. But negligible work have been accomplished on the scale invariance of both time and space. This link between space and time would help us in better understanding the triggering mechanism of the fault systems. We observe that density rate (number/km/day) as a function of distance obeys power law ($\Phi(t) \sim \frac{1}{r^\mu}$) and diffuses with time. Aftershocks expansion toward the background is slower as compare to the foreshocks inverse expansion ($\langle \mu \rangle_{aft} > \langle \mu \rangle_{fore}$).

Two regimes are observed: slow diffusion at short time scale (upto 5 days), with $H = 0.07$ and second regime at longer time scales with $H = 0.38$. These two regimes are always observed, independently of aftershocks selection distance. First regime corresponds to the aftershocks smaller than the largest aftershocks i.e., primary aftershocks whereas second regime is mainly driven by both primary and secondary aftershocks. Secondary aftershocks broaden aftershocks zone and increase the diffusion process. Similarly, Ouchi and Uekawa (1986) show that diffusion is mainly due to the occurrence of large aftershocks, and to the localization of secondary aftershocks close to the largest aftershocks. We demonstrate the apparent two diffusion regimes of the seismicity emerge from a simple cascade process. The burst of aftershocks from the largest aftershock triggers a break in the uniform diffusion pattern.

These two regimes are only observed empirically on different data set but previously no such type of results were reported by using ETAS simulation. There is no work on the explanation of these stress regimes. Secondly, McKernon and Main (2005) observed three stress regimes, with time limits different from that of Marsan and Bean (2003) results and our study. They interpreted as the first regime is dependent on the size of the mainshock whereas third regime is driven by viscoelastic diffusion of stress in the lower crust. We observed within McKernon and Main (2005) second regime two regimes driven by the primary and secondary aftershocks respectively. Viscoelastic stress diffusion of the lower mantle if presents, should be identify after 500 days. Foreshocks as compare to the aftershocks have always one regime diffusion with limited data scaling. At small and large time from the mainshock foreshocks are stationary, while at the time between 0.01 and 30 days foreshocks migrate toward the mainshock.

Combinations of the various methods presented in my thesis provide, despite their limitations, multifold opportunities to address topics in statistical seismology, e.g., the relation of aftershock sequence properties to earthquake physics and the improvement of time-dependent seismic hazard assessment.

Conclusions et perspectives

Cette recherche se concentre sur les modèles de réplique. Les principaux objectifs étaient (1) d'obtenir plus de perspicacité dans l'occurrence spatio-temporelle des répliques / précurseurs dans la région proche-source de la faille sismogénique, (2) d'améliorer les liens spatio-temporelle des paramètres de la physique sous-jacente des tremblements de terre, (3) afin de comprendre la plus grande réplique, (4) la recherche principalement axée sur la compréhension des origines et les implications des corrélations l'espace-temps et, (5) pour analyser leurs implications pour l'évaluation des risques sismiques. Par conséquent, nous avons développé et utilisé des méthodes statistiques avancées pour analyser des catalogues sismicité mondiale en général et des données des séquences réliques en particulier.

En commençant par l'analyse des modèles répliques du tremblement de terre du Cachemire en 2005 et de comparer son taux apparemment élevé de réliques, avec 18 autres M ≥ 7 tremblements de terre à moins de 1000 km de rayon. Cette zone, se présente comme la principale région dans laquelle interagissent les plaques continentales. Nous testons la manière dont la loi d'Omori, taux de sismicite de fond, l'interaction des séquences peut produire la productivité de réplique énorme telle pu observé pour le séisme au Cachemire. La normalisation par la taille du tremblement de terre nous permette d'identifier les anomalies dans la séquence réplique, c'est à dire plus de deux fois l'écart-type, pour la productivité et le taux de tremblement de terre Khurgu, la densité réplique pour les séquences du Cachemire, le taux une sismicite de fond élevé pour le séquence sud de Keria et la durée longue pour Gazli (1976b) et les tremblements de terre du Qaenat. L'autre résultat majeur robuste pour l'Asie occidentale, est la dépendance de la productivité des répliques

aux types de failles, pour tous les paramètres de la loi d'Omori. Nous avons résolu que la productivité des seismes en coulissage en moyenne 4 fois plus petite que productivité des failles inverses (chapitre 1).

Nous avons en outre tester cette dépendance des autres paramètres tectoniques modèl de déclenchement que l'on observe dans le chapitre 1 à un grand ensemble de données et sur les catalogues mondiaux de l'USGS et CMT. Dans la littérature, l'impact du types des failles sur la sismicité déclenchée est analysé en utilisant la valeur b de la loi Gutenberg Richter ou la valeur c de la loi Omori (e.g., Frohlich and Davis, 1993; Kagan, 2002b; Schorlemmer et al., 2005; Narteau et al., 2009; Gulia and Wiemer, 2010). Nous avons analysé les paramètres Omori (p, K), la productivité des répliques (α) et l'exposant de la densité linéaire (μ) en fonction du orientation des glissement sismique pour chaque du tremblement de terre.

Nous avons résolu en évaluant la moyenne de tous les paramètres de la loi d'Omori (p, K, α, $N(t)$) et les taux de densité que dépendent tous du type des failles (chapitre 2). Empiriquement, nous avons observé que les séismes de failles inverses ont des valeurs de K et les sismicité de fond plus élevés, mais les valeurs de p, $\langle\mu\rangle$ et α sont inférieures en comparaison avec la coulissage. Dans le modèle ETAS, K et N^* forts et les valeurs α faibles sont entraînés par un ratio branchement élevé (n). Nous suggérons que les interactions multiples liées à un branchement élevé (n) pour les séismes de faille inverse entraînement des taux plus élevés. La petite valeur de p et la durée des sismique en coulissage suggèront une hétérogénéité de contrainte plus grande par rapport du séisme de faille inverses. Pour donner un nouveau point de vue sur les interactions dans mécanique des tremblement de terre, nos résultats s'étendent á tous les paramètres, des lois de Gutenberg-Richter et les lois d'Omori. Ces résultats permettront, dans un proche avenir, d'améliorer les modèles d'aléa sismique.

Nous avons également étudié l'effet du type de la faille sur les répliques de grande magnitude. Lois Båth, i.e., la différence moyenne de la magnitude entre le choc principal et la plus grande réplique est de 1.2 et indépendement de la taille de mainshocks, a été observée et largement discutée depuis la première compilation en 1950. Une question

174

récurrente concerne la signification physique pour de cette loi développement déterministe de séquences de répliques, ou d'origine essentiellement statistique liée à l'aspect aléatoire des magnitudes. Plusieurs mises à jour sur la réplique déclenchement ont été proposés depuis les années 1950 pour le développement de la loi empirique Båth. Cependant, une compréhension globale de role choc principal pour la taille, la distance et le temps de la plus grande réplique est toujours indisponible. Nous étendons loi Båth dans les domaines du temps et de l'espace. Les plus grandes répliques sont plus proches de choc principal en magnitude (valeur mode: $\Delta M_r = 0.95$, $\Delta M_{ss} = 1.51$) et la distance (valeur mode: $\Delta D*_r = 0.11$, $\Delta D*_{ss} = 0.22$) pour le choc déclencheur, $(_r)$ pour inverse, $(_{ss})$ pour coulissage. La décroissance en loi de puissance dans le temps par rapport aux répliques régulières implique que les plus grand répliques sont plus enclins à se produire au début de n'importe quelle séquence de répliques (chapitre 3). Ces résultats, permettent d'adopter une stratégie nouvelle de prévision pour l'apparition des réplique de plus grande magnitudes.

Après cette analyse de dépendences spatio-temporelle une type de faille, nous nous sommes concentrés sur la dépendance des modèls de sismicité à la taille du choc principal. La productivité des répliques augments de magnitude avec les magnitudes du choc principal $\sim 10^{\alpha m_m}$, avec $\alpha = 0.82 \pm 0.06$. La valeur p est fonction de la magnitude du choc principal pour une durée jusqu'à quelques jours, alors que la corrélation est perdue pour ~ 80 jours. Cela suggère que de la période de l'après choc pour les premiéres répliques sont les seules infuencées la magniutde du choc principal. Cette dernière étant une évidence du seul qui permet de passer des réliques primaires aux secondaires. La durée de la séquence entière (primaire et secondaire) a une corrélation positive avec le magnitude du choc principal (la durée $\sim 10^{0.32 m_m}$). La durée, aussi a une corrélation inverse avec le temps de récurrence du déclenchement du séisme.

Nous avons observé que la valeur p augmente avec le temps après le choc principal et valeur maximale est de l'ordre de ~ 20 - 40 jours. L'augmentation de la valeur p peut correspondre à l'augmentation l'hétérogénéité des contraintes telle que reproduite par les simulations à l'aide du taux et la loi de rate and state. Mais aussi, nous montrons que la valeur p diminue avec la distance au choc principal. Ce qui est peut être due soit à la baisse

d'hétérogénéité des contraintes avec la distance ou à cause de la diffusion des répliques.

Les observations du chapitre précédent montrent que les hétérogénéités de contrainte varient avec le temps et la distance au choc principal. Nous avons étudié les caractéristiques du tremblement de terre entre le déclenchement de précurseurs et les répliques dans le catalogue global USGS. L'exposant de loi d'Omori (p, $N(t) = \frac{K}{(t+c)^p}$) pour les précurseurs est plus petit que celui des répliques, le $p - p' = 0.2$ comme prédit par le modèle ETAS. L'invariance d'échelle sismique est montrée dans l'espace ou dans le temps. Mais peu de travail a été accompli sur l'invariance d'échelle en temps et en d'espace simultanément. Ce lien entre l'espace et le temps pourait nous aider à mieux comprendre le mécanisme de déclenchement des systèmes de faille. Nous observons que le taux de densité (nombre / km / jour) en fonction de la distance obéit à la loi puissance ($\phi(\theta) \sim \frac{1}{r^\mu}$) et diffuse dans le temps. L'expansion des répliques est plus lente comparé à l'expansion les précurseurs inverse ($\langle \mu \rangle_{aft.} < \langle \mu \rangle_{fore.}$).

Deux régimes sont observés: la diffusion lente à courte terme (jusqu'à 5 jours), avec $H = 0.07$ et un second régime, à plus long terme avec $H = 0.38$. Ces deux régimes sont toujours observés, indépendamment de la sélection des répliques. Le transition entre les 2 régimes correspond à l'occurrence de la plus grande réplique, tandis que le deuxième régime est principalement controlé par les répliques secondaires. Les répliques secondaires élargissent la zone de répliques et augmentent le processus de diffusion. De même, Ouchi and Uekawa (1986) montrent que la diffusion est principalement due à l'occurrence de grandes répliques, et à la localisation des répliques secondaires à proximité des plus grande répliques. Nous démontrons que les deux régimes de diffusion apparents de la sismicité émergent d'un simple processus de cascade .

Ces deux régimes sont observés empiriquement sur des données différentes, mais auparavant aucun résultats de ce type n'a ont été rapporté en utilisant la simulation ETAS. Il n y a pas de travaux sur l'explication de ces régimes de diffusion. McKernon and Main (2005) ont observé trois régimes de contrainte, avec des délais différents des résultats de Marsan and Bean (2003) et de notre étude. Ils ont interprété, leur résultats comme le premier régime dépendant de la taille du choc principal tandis que le troisième régime est piloté

par la diffusion viscoélastique de contrainte dans la croûte inférieure. Nous avons observé au sein du second régime de McKernon and Main (2005) deux régimes controlés respectivement par les répliques primaires et secondaires. La diffusion de contrainte viscoélastique du manteau inférieur, si elle est présente, doit tre identifié, après 500 jours. Les précurseurs, comparés aux répliques, ont toujours un régimede diffusion avec une mise à l'échelle liées à des données limitées.

Les combinaisons des différentes analyses présentées dans cette thèse fournissent, malgré leurs limites, de nouvelles possibilités pour traiter en sismologie statistique. Les propriétés des séquences de répliques avec la physique du tremblement de terre, et ainsi améliorer de l'évaluation du risque sismique dépendant du temps.

177

Appendices

Appendix A

Aftershocks patterns in the Asian continental collision belt and the Muzafffarabad, Kashmir, 2005, sequence.

A Mainshocks and Tectonics setting

Tectonically, the study area is located on the Himalayan arc and Karakorum range, where the current tectonic activity is driven by the continental collision between India, Eurasia and Arabia. Our selected region is bounded by Tien Shan Fold belt (Tarim block) to the N and NE, by Tibetan Plateau Eastward, by Burman arc to SE, by Indian shield to the S, Zagros to the SW end, Kopet-Dagh seismic belt and Central Iranian (Lut block and Tabas block) to the W and Siberian platform in the NW (Molnar et al. (1973); Haghipour and Amidi (1980); Bossu et al. (1996)). Low seismicity through most of Siberian platform and northwestern Asia show that the stability of this region but the Southern boundary of the Eurasian plate is still active. Geologically it includes several Paleozoic and Mesozoic fold belt that experienced more deformations but it is surrounded by stable blocks since Precambrian era. Earthquakes tend to be more frequent on these belts rather than in stable blocks. The compressional stresses driven by the convergence of the Indian and Eurasian plates appear to be transmitted over broad zone, causing deformation along old zone of weakness (Molnar and Tapponnier (1975); Thomas et al. (1999b); Thomas et al. (1999a)). Seismicity show that most of the active deformation of this region is partitioned between thrusting in mountain belts and sliding along great strike slip faults (Avouac and Tapponnier (1993)). The strike slip fault pattern has long been interpreted to result from extrusion due to indentation of India into Asia (Tapponnier and Molnar (1977)).

Gazli (Uzbekistan) earthquakes, 1976a, 1976b and 1984 that are event # 2, # 3 and # 9 (figure (1.1, 1.2)) occurred in low seismic area, where the low regional tectonics are suggested to be associated with both the Arabia and India collisions into Asia (Amorese et al. (1995); Bossu et al. (1996); Thomas et al. (1999b); Thomas et al. (1999a)). Tectonically the Gazli area is bounded by major and active tectonic zones such as Tien Shan fold belt and Kopet-Dagh seismic belt. Tien Shan suture, reactivated during Tertiary age, is suggested to localize Gazli seismic sequence in an intracontinental and low seismic region (Bossu et al. (1996)). A possible connection with oil and gas recovery may also exist (Simpson and Leith (1985); Grasso (1992); McGarr et al. (2002)).

Event 11 and 5 are located in Tien Shan fold belt, which is subjected to horizontal compressive stress field, due to the convergence of Indian and Eurasian plates (Arrowsmith and Strecker (1999); Ulomov (2004)). Much of that convergence is absorbed farther north, with nearly 20 mm/yr across the Western Tien Shan (Abdrakhmatov et al. (1996)).

The Arabia-Eurasia plate convergence occurs in the NE of the Zagros, across the Iranian Plateau and surroundings, which results in crustal thickening and mountain building. Some of the convergence is absorbed by lateral transfer of material out of the paths of Arabia. The oblique convergence of Arabia with Eurasia at the NW trending Zagros induces right-lateral shear across the NW Zagros, which in turn transforms into Westward translation of crust in NW Iran and Turkey (McClusky et al. (2000); Reilinger et al. (2006)). Most Zagros events are reverse faulting (figure 1.2), number 7, 13 events occur in Central Iran (NE corner of the Lut Block), as a fragments broken from Gondwana in late Paleozoic time and successively added to the Southern margin in early Mesozoic time (e.g., Stocklin (1968); Sengor (1979); Sengor et al. (1984); Sengor et al. (1988)), show strike slip faulting associated with segments of the Kazerun fault system (Talebian and Jackson (2004); Hatzfeld and Molnar (2010)). Which (Kazerun fault) transfers right-lateral slip on the Main Recent fault into a component in the Southeastern Zagros (e.g., Authemayou et al. (2009); Tavakoli et al. (2008)), where event 4 occurred. Thus, most moderate earthquakes reflect straining of the subducting Arabian plate, not the underthrusting of that plate beneath the mountain belt (Hatzfeld and Molnar (2010)).

Bhuj 2001 (# 15) earthquake is an intracontinental earthquake, located 300-400 km from triple junction that joins the Owen fracture zone (sinistral slip between the Indian and Arabian plates), the Chaman transform (sinistral slip between the Indian and Eurasian plates) and Makran convergent zone between the Arabian and Eurasian plates (Molnar and Tapponnier (1975); Bodin and Horton (2004)). The Rann Kutch is the major seismic zone in this area (Chung and Gao (1995)).

Quetta earthquake (# 12) 1997, occurred in Baluchistan arc which is also different and away from Himalayan Arc. It is an extension of the Zagros Makran belt under which the Arabian plate is underthrusting. The deformation in this region is due to the Sulaiman

and Kirthar Shear zone (Molnar and Tapponnier (1975); Tahir et al. (2009)).

Kashmir earthquake 2005, occurred in the Himalayan Arc which is the northern edge of the Indian plate, where the Indian plate is underthrusting beneath the Tibetan plateau. This event was close to the main frontal thrust (MFT) that marks the southern margin of the Himalayan range (e.g., Avouac et al. (2006); Kaneda et al. (2008)).

Earthquakes within Tibet show a mixture of normal (# 18) and strike-slip faulting (# 14, 16) with both having an EW extension (Molnar and Tapponnier (1978); Ni and York (1978); Molnar and Chen (1983); Molnar and Lyon-Caent (1989); Langin et al. (2003)). A summation of moment tensors of earthquakes within Tibet suggests that EW extension occurs at roughly twice the rate of NS compression (e.g., Molnar and Chen (1983); Molnar and Lyon-Caent (1989)). Normal faulting leads to vertical compression (crustal thinning), and the conjugate strike-slip faulting, with right-lateral slip on NE-striking planes and left-lateral on NW-striking planes, contributes NS shortening (Molnar and Lyon-Caent (1989); Lin et al. (2002)). North of the Tibet is a Tarim basin, where # 1, 10 events are located, which is also considered as fragment broken from Gondwana in late Paleozoic (Sengor (1979); Sengor et al. (1984); Sengor et al. (1988); Stocklin (1968)).

Appendix B

The largest aftershock: how strong, how far away, how delayed?

A   Largest aftershock size: $\langle \Delta M \rangle$

$\langle \Delta M \rangle$ of randomly reshuffled size data, increases with that of mainshock magnitude. Data with aftershock selected at large space time window (time = 5 year, $D^* = 5$) behave similarly to the reshuffled magnitude catalogue (figure B.1 a). At these space - time windows, the probability of picking the largest aftershock from the uncorrelated background seismicity increases. It is confirmed by the estimated aftershocks productivity decrease from 0.91 $\pm$ 0.03 to 0.71 $\pm$ 0.09 as we change space time window from [1 year, D^*=1] to [5 year, $D^* = 5$] (figure 3.1 a). Apparent productivity decreases can also be observed in all cases of randomly reshuffle catalogue i.e., $\alpha - value$ decreases to 0.34 $\pm$ 0.08 or smaller (as shown in figure (3.1) a). The α value change drives on the apparent $\langle \Delta M \rangle$ increases with mainshock magnitude as suggested by (Helmstetter and Sornette, 2003a). Thus Båth's law can only be observed for the sequences which are clustered in space, time and mainshock with its corresponding largest aftershock belongs to same sequence.

QQ plot (figure (3.2 d)) of ΔM distribution demonstrate with fat tail distribution, which support ΔM distribution is a positive skew i.e., semi-log distribution. It argues for the Gutenberg-Richter relationship holds in figure (B.1 b) as semi-log distribution.
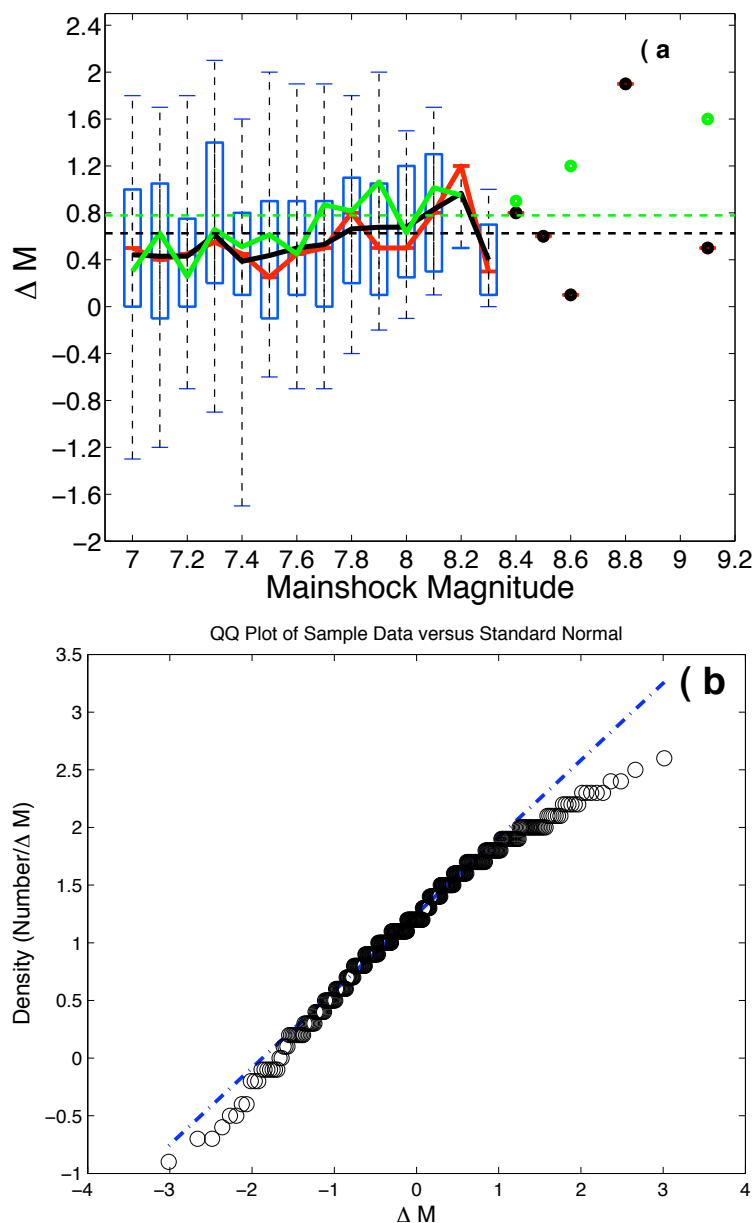
Figure B.1: (a) ΔM distribution as function of mainshock magnitude with aftershocks, 5 year and $D^* = 5$ window used. Average ΔM (black), median ΔM (red) and average ΔM for reshuffled magnitude (green). Dotted lines are global average $\langle \Delta M \rangle$, 0.63 and 0.78 for data and reshuffled magnitude respectively. (b) QQ plot for data, aftershock selection time = 1 year and $D^* = 1$.

B   Largest aftershock distance: $\langle \Delta D^* \rangle$

ΔD^* calculated using time = 5 yr, $D^* = 5$
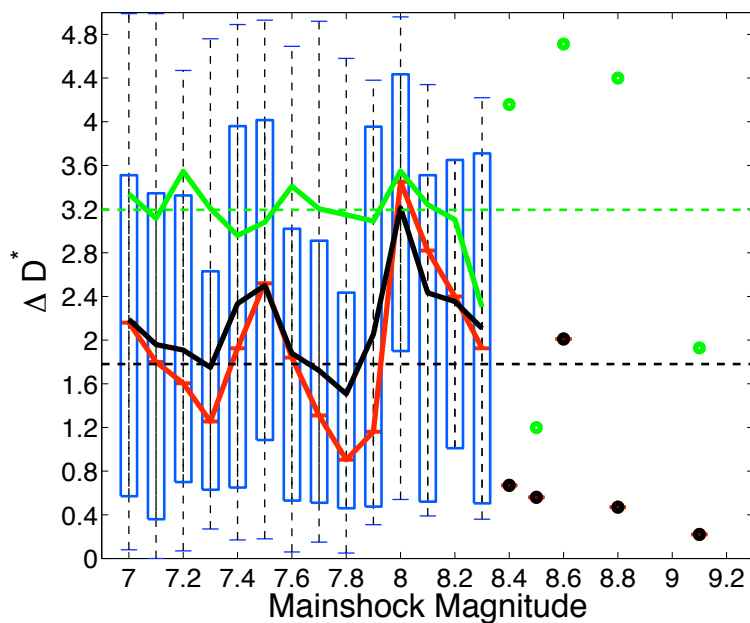
Figure B.2: Normalized difference between mainshock and its corresponding largest after-shock within time = 5 year and $D^* = 5$ as a function of mainshock magnitude. Average (black), median (red) and average ΔD^* for reshuffled location (green). Dotted lines are global average $\langle \Delta D^* \rangle$, 1.78 and 3.19 for data and reshuffled location respectively.

C   Largest aftershock time: $\langle \Delta T \rangle$

ΔT calculated using time = 5 yr, $D^* = 5$, shows In case of large space time window both real and reshuffled data merge together for median and average values (figure B.3).

Figure B.3: Time difference between mainshock and its corresponding largest aftershock within time = 5 year and $D^* = 5$ as a function of mainshock magnitude. Average (black), median (red) and average ΔT for reshuffled time (green). Dotted lines are global average $\langle \Delta T \rangle$, 542.85 day and 714.44 day for data and reshuffled time respectively.

Bibliography
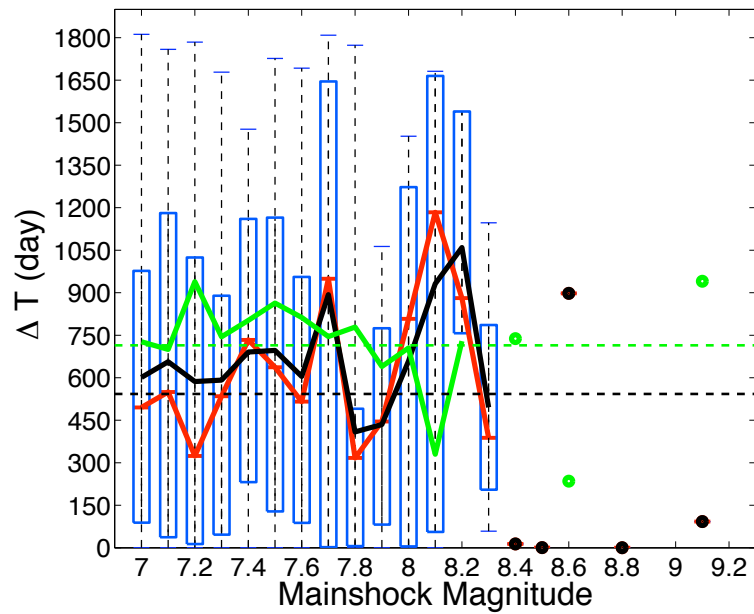
K.Y. Abdrakhmatov, SA Aldazhanov, BH Hager, MW Hamburger, TA Herring, KB Kalabaev, VI Makarov, P. Molnar, SV Panasyuk, MT Prilepin, et al. Relatively recent construction of the tien shan inferred from gps measurements of present-day crustal deformation rates. *Nature*, 384(6608):450–453, 1996.

R.E. Abercrombie and J. Mori. Occurrence patterns of foreshocks to large earthquakes in the western united states. *Nature*, 381:303 – 307, 1996.

H. Adeli. The sirch (kerman, iran) earthquake of 28 july 1981–a field investigation. *Bull. Seismol. Soc. Am.*, 72(3):841 – 861, 1982.

K. Aki. Maximum likelihood estimate of b in the formula logn = a – bm and its confidence limits. *Bull. Earthquake Res. Inst*, 43:237 –239, 1965.

K. Aki and P.G. Richards. *Quantitative seismology*. Univ. Sci. Books, Sausalito, Calif., 2nd edition, 2002. ISBN 0935702962.

D. Amorese, J.R. Grasso, LM Plotnikova, BS Nurtaev, and R. Bossu. Rupture kinematics of the three gazli major earthquakes from vertical and horizontal displacements data. *Bull. Seismol. Soc. Am.*, 85(2):552 – 559, 1995.

J.R. Arrowsmith and MR Strecker. Seismotectonic range-front segmentation and mountain-belt growth in the pamir-alai region, kyrgyzstan (india-eurasia collision zone). *Geol. Soc. Am. Bull.*, 111(11):1665 – 1683, 1999.

C. Authemayou, O. Bellier, D. Chardon, L. Benedetti, Z. Malekzade, C. Claude, B. Angeletti, E. Shabanian, and M.R. Abbassi. Quaternary slip-rates of the kazerun and the main recent faults: active strike-slip partitioning in the zagros fold-and-thrust belt. *Geophys. J. Int.*, 178(1):524–540, 2009.

J.-P. Avouac, F. Ayoub, S. Leprince, O. Konca, and D. V. Helmberger. The 2005, mw 7.6 kashmir earthquake: Sub-pixel correlation of aster images and seismic waveforms analysis. *Earth Planet. Sci. Lett.*, 249:514–528, 2006.

J.P. Avouac and P. Tapponnier. Kinematic model of active deformation in central asia. *Geophys. Res. Lett.*, 20(10):895–898, 1993.

M. Baiesi and M. Paczuski. Scale-free networks of earthquakes and aftershocks. *Phys. Rev. E.*, 69(6):066106, 2004.

P. Bak and C. Tang. Earthquakes as a self-organized critical phenomenon. *J. Geophys. Res.*, 94(B11):15635–15637, 1989.

P. Bak, K. Christensen, L. Danon, and T. Scanlon. Unified scaling law for earthquakes. *Phys. Rev. Lett.*, 88(17):178501, 2002.

M. Båth. Lateral inhomogeneities of the upper mantle. *Tectonophysics*, 2(6):483–514, 1965.

Y. Ben-Zion. Collective behavior of earthquakes and faults: Continuum-discrete transitions, progressive evolutionary changes, and different dynamic regimes. *Rev. Geophys.*, 46(4):RG4006, 2008.

Y. Ben-Zion and V. Lyakhovsky. Analysis of aftershocks in a lithospheric model with seismogenic zone governed by damage rheology. *Geophys. J. Int.*, 165(1):197–210, 2006.

H. Benioff. Earthquakes and rock creep, part i. *Bull. Seism. Soc. Am*, 41:31 – 62, 1951.

M. Berberian. Earthquake faulting and bedding thrust associated with the tabas-e-golshan (iran) earthquake of september 16, 1978. *Bull. Seism. Soc. Am*, 69:1861–1887, 1979.

M. Berberian and R.S. Yeats. Patterns of historical earthquake rupture in the iranian plateau. *Bull. Seismol. Soc. Am.*, 89(1):120 – 139, 1999.

J. Boatwright and M. Cocco. Frictional constraints on crustal faulting. *J. Geophys. Res.-Solid Earth*, 101(B6):13895–13909, 1996.

P. Bodin and S. Horton. Source parameters and tectonic implications of aftershocks of the mw 7.6 bhuj earthquake of 26 january 2001. *Bull. Seismol. Soc. Am.*, 94(3):818 – 827, 2004.

D.W.R. Bohnenstiehl. A different kind of foreshock. *Nature: International Weekly Journal of Science*, 2005.

R. Bossu, JR Grasso, LM Plotnikova, B. Nurtaev, J. Frechet, and M. Moisy. Complexity of intracontinental seismic faultings: The gazli, uzbekistan, sequence. *Bull. Seismol. Soc. Am.*, 86(4):959 – 971, 1996.

M. Bouchon and H. Karabulut. The aftershock signature of supershear earthquakes. *science*, 320:1323–1325, 2008.

M. Bouchon and M. Vallée. Observation of long supershear rupture during the magnitude 8.1 kunlunshan earthquake. *Science*, 301(5634):824 – 826, 2003.

M. Bouchon, H. Karabulut, M. Aktar, S.
  "Ozalaybey, J. Schmittbuhl, and M.P. Bouin. Extended nucleation of the 1999 mw 7.6
  izmit earthquake. *Science*, 331(6019):877, 2011.

DD Bowman, G. Ouillon, CG Sammis, A. Sornette, and D. Sornette. An observational
  test of the critical earthquake concept. *J. Geophys. Res.*, 103:24359 – 24372, 1998.

E.E. Brodsky. The spatial density of foreshocks. *Geophys. Res. Lett.*, 38(10):L10305, 2011.

J.L. Chatelain, R.K. Cardwell, and B.L. Isacks. Expansion of the aftershock zone following
  the vanuatu (new hebrides) earthquake on 15 july 1981. *Geophys. Res. Lett.*, 10(5):385–
  388, 1983. ISSN 0094-8276.

W.Y. Chung and H. Gao. Source parameters of the anjar earthquake of july 21, 1956,
  india, and its seismotectonic implications for the kutch rift basin. *Tectonophysics*, 242
  (3-4):281–292, 1995.

R. Console and F. Catalli. A physical model for aftershocks triggered by dislocation on a
  rectangular fault. *Arxiv preprint physics/0505033*, 2005.

R. Console, A.M. Lombardi, M. Murru, and D. Rhoades. Båth's law and the self-similarity
  of earthquakes. *J. Geophys. Res.*, 108(B2):2128, 2003a.

R. Console, M. Murru, and A.M. Lombardi. Refining earthquake clustering models. *J.
  Geophys. Res.*, 108(B10):2468, 2003b.

G. Daniel, D. Marsan, and M. Bouchon. Earthquake triggering in southern iceland following
  the june 2000 ms 6.6 doublet. *J. Geophys. Res*, 113(B5):B05310, 2008.

G. Daniel, E. Prono, F. Renard, F. Thouvenot, S. Hainzl, D. Marsan, A. Helmstetter,
  P. Traversa, JL Got, L. Jenatton, et al. Changes in effective stress during the 2003–2004
  ubaye seismic swarm, france. *J. Geophys. Res*, 116:B01309, 2011.

S. Das and CH Scholz. Theory of time-dependent rupture in the earth. *J. Geophys. Res.*,
  86(87):6039–6051, 1981.

J. Davidsen and M. Paczuski. Analysis of the spatial distribution between successive
  earthquakes. *Phys. Rev. Lett.s*, 94(4):48501, 2005. ISSN 1079-7114.

S.D. Davis and C. Frohlich. Single-link cluster analysis of earthquake aftershocks: decay
  laws and regional variations. *J. Geophys. Res.*, 96(B4):6335–6350, 1991.

J. Dieterich. A constitutive law for rate of earthquake production and its application to
  earthquake clustering. *J. Geophys. Res.*, 99:2601–2618, 1994.

J. Dieterich, V. Cayol, and P. Okubo. The use of earthquake rate changes as a stress meter
  at kilauea volcano. *Nature*, 408(6811):457–460, 2000.

J.H. Dieterich. A model for the nucleation of earthquake slip. *Earthquake source mechanics*, 37:37–47, 1986.

D.A. Dodge, G.C. Beroza, and WL Ellsworth. Detailed observations of california foreshock sequences: Implications for the earthquake initiation process. *J. Geophys. Res.*, 101 (B10):22371, 1996. ISSN 0148-0227.

G. Drakatos and J. Latoussakis. A catalog of aftershock sequences in greece (1971–1997): Their spatial and temporal characteristics. *J. Seismol.*, 5(2):137–145, 2001.

B. Enescu and K. Ito. Spatial analysis of the frequency-magnitude distribution and decay rate of aftershock activity of the 2000 western tottori earthquake. *Earth, Planets and Space*, 54(8):847–859, 2002. ISSN 1343-8832.

M. Eneva and G.L. Pavlis. Spatial distribution of aftershocks and background seismicity in central california. *Pure Appl. Geophys.*, 137(1):35–61, 1991. ISSN 0033-4553.

W. Feller. *An Introduction to Probability Theory and Applications.*, volume 2. Wiley, New York, 1966.

K.R. Felzer, T.W. Becker, R.E. Abercrombie, G. Ekström, and J.R. Rice. Triggering of the 1999 mw 7.1 hector mine earthquake by aftershocks of the 1992 mw 7.3 landers earthquake. *J. Geophys. Res.*, 107:2190, 2002a.

K.R. Felzer, T.W. Becker, R.E. Abercrombie, G. Ekström, and J.R. Rice. Triggering of the 1999 mw 7.1 hector mine earthquake by aftershocks. *J. Geophys. Res.*, page 2190, 2002b.

K.R. Felzer, R.E. Abercrombie, and G. Ekström. Secondary aftershocks and their importance for aftershock forecasting. *Bull. Seismol. Soc. Am.*, 93(4):1433 – 1448, 2003. ISSN 0037-1106.

K.R. Felzer, R.E. Abercrombie, and G. Ekström. A common origin for aftershocks, foreshocks, and multiplets. *Bull. Seismol. Soc. Am.*, 94(1):88–99, 2004. ISSN 0037-1106.

R. Felzer and E.E. Brodsky. Decay of aftershock density with distance indicates triggering by dynamic stress. *Nature*, 441:735–738, 2006.

A.M. Freed. Earthquake triggering by static, dynamic, and postseismic stress transfer. *Annu. Rev. Earth Planet. Sci.*, 33:335–367, 2005.

A.M. Freed and J. Lin. Delayed triggering of the 1999 hector mine earthquake by viscoelastic stress transfer. *Nature*, 411(6834):180–183, 2001.

C. Frohlich and S.D. Davis. Teleseismic b values; or, much ado about 1.0. *J. Geophys. Res.*, 98(B1):631–644, 1993. ISSN 0148-0227.

C. Frohlich and R.J. Willemann. Statistical methods for comparing directions to the orientations of focal mechanisms and wadati-benioff zones. *Bull. Seismol. Soc. Am.*, 77 (6):2135 – 2142, 1987. ISSN 0037-1106.

A. Gabrielov, I. Zaliapin, W.I. Newman, and V.I. Keilis-borok. Colliding cascades model for earthquake prediction. *Geophys. J. Int.*, 143(2):427–437, 2000. ISSN 1365-246X.

JK Gardner and L. Knopoff. Is the sequence of earthquakes in southern california, with aftershocks removed, poissonian. *Bull. Seism. Soc. Am*, 64(5):1363–1367, 1974.

P. Gasperini and F. Mulargia. A statistical analysis of seismicity in italy: the clustering properties. *Bull. Seismol. Soc. Am.*, 79(4):973, 1989. ISSN 0037-1106.

S. Ghose, R.J. Mellors, A.M. Korjenkov, M.W. Hamburger, T.L. Pavlis, G.L. Pavlis, M. Omuraliev, E. Mamyrov, and AR Muraliev. The ms= 7.3 1992 suusamyr, kyrgyzstan, earthquake in the tien shan: 2. aftershock focal mechanisms and surface deformation. *Bull. Seismol. Soc. Am.*, 87(1):23, 1997.

C. Godano and F. Pingue. Multiscaling in earthquakes diffusion. *Geophys. Res. Lett.*, 32 (18):L18302, 2005. ISSN 0094-8276.

J. Gomberg, NM Beeler, ML Blanpied, and P. Bodin. Earthquake triggering by transient and static deformations. *J. Geophys. Res.*, 103:24411–24426, 1998.

J. Gomberg, N. Beeler, and ML Blanpied. On rate-state and coulomb failure models. *J. Geophys. Res*, 105(14):7857–7872, 2000.

J. Gomberg, PA Reasenberg, P. Bodin, and RA Harris. Earthquake triggering by seismic waves following the landers and hector mine earthquakes. *Nature*, 411(6836):462–466, 2001a.

J. Gomberg et al. The failure of earthquake failure models. *J. Geophys. Res*, 106(B8): 16253–16263, 2001b.

J.R. Grasso. Mechanics of seismic instabilities induced by the recovery of hydrocarbons. *Pure Appl. Geophys.*, 139(3):507–534, 1992.

J.R. Grasso and M.N. Mughal. Extended abstracts: International conference on earthquake in pakistan; its implications and hazard mitigation. page 28, 2006.

L. Gulia and S. Wiemer. The influence of tectonic regimes on the earthquake size distribution: A case study for italy. *Geophys. Res. Lett.*, 37(10):L10305, 2010. ISSN 0094-8276.

Z. Guo and Y. Ogata. Statistical relations between the parameters of aftershocks in time, space, and magnitude. *J. Geophys. Res.*, 102(B2):2857–2873, 1997. ISSN 0148-0227.

B. Gutenberg and CF Richter. Frequency of earthquakes in California. *Bull. Seismol. Soc. Am.*, 34(4):185–188, 1944. ISSN 0037-1106.

B. Gutenberg and CF Richter. *Seismicity of the Earthand Associated Phenomena.* Number 310 pp. Princeton Univ. Press, Princeton, NJ., 310 pp, 1954.

A. Haghipour and M. Amidi. The november 14 to december 25, 1979 ghaenat earthquakes of northeast iran and their tectonic implications. *Bull. Seismol. Soc. Am.*, 70(5):1751 – 1757, 1980.

S. Hainzl and D. Marsan. Dependence of the omori-utsu law parameters on main shock magnitude: Observations and modeling. *J. Geophys. Res.*, 113(B10):B10309, 2008. ISSN 0148-0227.

S. Hainzl, G. Zoller, and J. Kurths. Similar power laws for foreshock and aftershock sequences in a spring-block model for earthquakes. *J. Geophys. Res.*, 104(B4):7243–7253, 1999. ISSN 0148-0227.

S. Hainzl, F. Scherbaum, and C. Beauval. Estimating background activity based on interevent-time distribution. *Bull. Seismol. Soc. Am.*, 96(1):313 – 320, 2006.

S. Hainzl, G.B. Brietzke, and G. Zöller. Quantitative earthquake forecasts resulting from static stress triggering. *J. Geophys. Res. (Solid Earth)*, 115(B14):11311, 2010a.

S. Hainzl, G. Zöller, R. Wang, N. Brantut, A. Schubnel, J. Corvisier, J. Sarout, T. Hirono, Y. Hamada, A. Chulliat, et al. Impact of the receiver fault distribution on aftershock activity. *J. Geophys. Res*, 115(B05315):B05315, 2010b.

R.A. Harris. Introduction to special section: Stress triggers, stress shadows, and implications for seismic hazard. *J. Geophys. Res.*, 103(24):347–358, 1998.

R.A. Harris, R.W. Simpson, and P.A. Reasenberg. Influence of static stress changes on earthquake locations in southern california. *Nature*, 375:221–224, 1995.

D. Hatzfeld and P. Molnar. Comparisons of the kinematics and deep structures of the zagros and himalaya and of the iranian and tibetan plateaus, and geodynamic implications. *Rev. Geophys.*, 48:RG2005, 2010.

A. Helmstetter. Is earthquake triggering driven by small earthquakes? *Phys. Rev. Lett.*, 91(5):58501, 2003.

A. Helmstetter and B.E. Shaw. Relation between stress heterogeneity and aftershock rate in the rate-and-state model. *J. Geophys. Res.*, 111:B07304, 2006.

A. Helmstetter and D. Sornette. Sub-critical and super-critical regimes in epidemic models of earthquake aftershocks. *J. Geophys. Res.*, 107:2237, 2002a.

A. Helmstetter and D. Sornette. Diffusion of epicenters of earthquake aftershocks, omoris law, and generalized continuous-time random walk models. *Phys. Rev. E*, 66(6):61104, 2002b. ISSN 1550-2376.

A. Helmstetter and D. Sornette. Bath's law derived from the gutenberg-richter law and from aftershock properties. *Geophys. Res. Lett.*, 30(20):2069 – 2072, 2003a.

A. Helmstetter and D. Sornette. Foreshocks explained by cascades of triggered seismicity. *J. Geophys. Res.*, 108(B10):2457, 2003b. ISSN 0148-0227.

A. Helmstetter and D. Sornette. Importance of direct and indirect triggered seismicity. *Geophys. Res. Lett.*, 30:1576, 2003c.

A. Helmstetter, D. Sornette, and J.R. Grasso. Mainshocks are aftershocks of conditional foreshocks: How do foreshock statistical properties emerge from aftershock laws. *J. Geophys. Res.*, 108(B1):2046, 2002.

A. Helmstetter, G. Ouillon, and D. Sornette. Are aftershocks of large californian earthquakes diffusing? *J. Geophys. Res.*, 108:2483, 2003.

A. Helmstetter, Y.Y. Kagan, and D.D. Jackson. Importance of small earthquakes for stress transfers and earthquake triggering. *J. Geophys. Res.*, 110(B5):B05S08, 2005.

DP Hill, PA Reasenberg, A. Michael, WJ Arabaz, G. Beroza, D. Brumbaugh, JN Brune, R. Castro, S. Davis, D. DePolo, et al. Seismicity remotely triggered by the magnitude 7.3 landers, california, earthquake. *Science*, 260(5114):1617 – 1623, 1993.

Y. Huang, H. Saleur, C. Sammis, and D. Sornette. Precursors, aftershocks, criticality and self-organized criticality. *Europhys. Lett.*, 41:43 – 48, 1998.

M. Huc and I.G. Main. Anomalous stress diffusion in earthquake triggering: Correlation length, time dependence, and directionality. *J. Geophys. Res.*, 108:2324, 2003.

KW Hudnut, L. Seeber, and J. Pacheco. Cross-fault triggering in the november 1987 superstition hills earthquake sequence, southern california. *Geophys. Res. Lett.*, 16(2): 199–202, 1989. ISSN 0094-8276.

M. Imoto. On migration phenomena of aftershocks following large thrust earthquakes in subduction zones. *Report of the National Research Center for Disaster Prevention*, 25: 29–71, 1981.

E. Jacques, JC Ruegg, JC Lépine, P. Tapponnier, GCP King, and A. Omar. Relocation of m 2 events of the 1989 dôbi seismic sequence in afar: evidence for earthquake migration. *Geophys. J. Int.*, 138(2):447–469, 1999. ISSN 1365-246X.

S.C. Jaume and L.R. Sykes. Changes in state of stress on the southern san andreas fault resulting from the california earthquake sequence of april to june 1992. *Science*, 258 (5086):1325, 1992.

L.M. Jones and P. Molnar. Some characteristics of foreshocks and their possible relationship to earthquake prediction and premonitory slip on faults. *J. Geophys. Res.*, 84(B7):3596– 3608, 1979. ISSN 0148-0227.

LM Jones, R. Console, F. Di Luccio, and M. Murru. Are foreshocks mainshocks whose aftershocks happen to be big. *EOS*, 76(abstract):388, 1995.

Y. Kagan and L. Knopoff. Statistical study of the occurrence of shallow earthquakes. *Geophysical Journal of the Royal Astronomical Society*, 55(1):67–86, 1978. ISSN 1365-246X.

YY Kagan. Likelihood analysis of earthquake catalogues. *Geophys. J. Int.*, 106(1):135–148, 1991. ISSN 1365-246X.

YY Kagan. Statistics of characteristic earthquakes. *Bull. Seismol. Soc. Am.*, 83(1):7, 1993.

Y.Y. Kagan. Aftershock zone scaling. *Bull. Seismol. Soc. Am.*, 92(2):641 – 655, 2002a.

Y.Y. Kagan. Seismic moment distribution revisited: I. statistical results. *Geophys. J. Int.*, 148(3):520–541, 2002b. ISSN 1365-246X.

Y.Y. Kagan. Short-term properties of earthquake catalogs and models of earthquake source. *Bull. Seismol. Soc. Am.*, 94(4):1207, 2004.

Y.Y. Kagan and D.D. Jackson. Spatial aftershock distribution: Effect of normal stress,. *J. Geophys. Res.*, 103(B10),:24,453–24,467, 1998.

YY Kagan and L. Knopoff. Dependence of seismicity on depth. *Bull. Seismol. Soc. Am.*, 70(5):1811, 1980.

YY Kagan and L. Knopoff. Stochastic synthesis of earthquake catalogs. *J. Geophys. Res.*, 86(B4):2853–2862, 1981. ISSN 0148-0227.

H. Kanamori and E.E. Brodsky. The physics of earthquakes. *Rep. Prog. Phys.*, 67:1429–1496., 2004.

H. Kaneda, T. Nakata, H. Tsutsumi, H. Kondo, N. Sugito, Y. Awata, S.S. Akhtar, A. Majid, W. Khattak, A.A. Awan, et al. Surface rupture of the 2005 kashmir, pakistan, earthquake and its active tectonic implications. *Bull. Seismol. Soc. Am.*, 98(2):521 – 557, 2008.

VI Keylis-Borok and LN Malinovskaya. One regularity in the occurrence of strong earthquakes. *J. Geophys. Res.*, 69(14):3019–3024, 1964.

D. Kilb, J. Gomberg, and P. Bodin. Triggering of earthquake aftershocks by dynamic stresses. *Nature*, 408(6812):570–574, 2000.

D. Kilb, J. Gomberg, and P. Bodin. Aftershock triggering by complete coulomb stress changes. *J. Geophys. Res*, 107(B4):2060, 2002.

GCP King and M. Cocco. Fault interaction by elastic stress changes: new clues from earthquake sequences. *Adv. Geophys.*, 44:1–38, 2001. ISSN 0065-2687.

G.C.P. King, R.S. Stein, and J. Lin. Static stress changes and the triggering of earthquakes. *Bull. Seismol. Soc. Am.*, 84(3):935–953, 1994.

C. Kisslinger. Aftershocks and fault-zone properties. *Adv. Geophys.*, 38:1–36, 1996. ISSN 0065-2687.

C. Kisslinger and L.M. Jones. Properties of aftershock sequences in southern california. *J. Geophys. Res.*, 96(B7):11947, 1991.

F.W. Klein, T. Wright, and J. Nakata. Aftershock decay, productivity, and stress rates in hawaii: Indicators of temperature and stress from magma sources. *J. Geophys. Res.*, 111(B7):B07307, 2006. ISSN 0148-0227.

L. Knopoff. The magnitude distribution of declustered earthquakes in southern california. *Proc. Natl. Acad. Sci. USA*, 97(22):11880–11884, 2000.

W.R. Langin, L.D. Brown, and E.A. Sandvol. Seismicity of central tibet from project indepth iii seismic recordings. *Bull. Seismol. Soc. Am.*, 93(5):2146 – 2159, 2003.

Kanamori H Jennings PC Kisslinger C. Lee, W.H.K. *International handbook of earthquake and engineering seismology.* Academic Press, New York, 2003. ISBN 0124406580.

MW Lee and D. Sornette. Novel mechanism for discrete scale invariance in sandpile models. *Euro. Phys. J. B.*, 15(1):193–197, 2000. ISSN 1434-6028.

V.C. Li, S.H. Seale, and T. Cao. Postseismic stress and pore pressure readjustment and aftershock distributions. *Tectonophysics*, 144(1-3):37–54, 1987. ISSN 0040-1951.

A. Lin, B. Fu, J. Guo, Q. Zeng, G. Dang, W. He, and Y. Zhao. Co-seismic strike-slip and rupture length produced by the 2001 ms 8.1 central kunlun earthquake. *Science*, 296 (5575):2015 – 2017, 2002.

J. Lin and R.S. Stein. Stress triggering in thrust and subduction earthquakes and stress interaction between the southern san andreas and nearby thrust and strike-slip faults. *J. Geophys. Res.*, 109:B02303, 2004.

E. Lippiello, L. de Arcangelis, and C. Godano. The role of static stress diffusion in the spatio-temporal organization of aftershocks. *Phys. Rev. Lett.*, 103:038501–04, 2009a.

E. Lippiello, L. De Arcangelis, and C. Godano. Role of static stress diffusion in the spatiotemporal organization of aftershocks. *Phys. Rev. Lett.*, 103(3):38501, 2009b.

K. Maeda. Time distribution of immediate foreshocks obtained by a stacking method. *Pure Appl. Geophys.*, 155(2):381–394, 1999. ISSN 0033-4553.

I.G. Main. Earthquakes as critical phenomena: implications for probabilistic seismic hazard analysis. *Bull. Seismol. Soc. Am.*, 85(5):1299–1308, 1995.

B.B. Mandelbrot. *The fractal geometry of nature*. W.H. Freeman, New York, 1983.

ST Maqsood and J. Schwarz. Comparison of seismic vulnerability of buildings before and after 2005 kashmir earthquake. *Seismol. Res. Lett.*, 81(1):85, 2010. ISSN 0895-0695.

D. Marsan. Triggering of seismicity at short timescales following californian earthquakes. *J. Geophys. Res*, 108(B5):2266, 2003.

D. Marsan. The role of small earthquakes in redistributing crustal elastic stress. *Geophys. J. Int.*, 163(1):141–151, 2005. ISSN 1365-246X.

D. Marsan. Can coseismic stress variability suppress seismicity shadows? Insights from a rate-and-state friction model. *J. Geophys. Res*, 111, 2006.

D. Marsan and C.J. Bean. Seismicity response to stress perturbations, analysed for a world-wide catalogue. *Geophys. J. Int.*, 154(1):179–195, 2003.

D. Marsan and O. Lengline. Extending earthquakes' reach through cascading. *Science*, 319(5866):1076–1079, 2008.

D. Marsan and O. Lengliné. A new estimation of the decay of aftershock density with distance to the mainshock. *J. Geophys. Res.*, 115(B9):B09302, 2010. ISSN 0148-0227.

D. Marsan, C.J. Bean, S. Steacy, and J. McCloskey. Spatio-temporal analysis of stress diffusion in a mining-induced seismicity system. *Geophys. Res. Lett*, 26(24):3697–3700, 1999.

D. Marsan, C.J. Bean, S. Steacy, and J. McCloskey. Observation of diffusion processes in earthquake populations and implications for the predictability of seismicity systems. *J. Geophys. Res.*, 105:28–081, 2000.

S. McClusky, S. Balassanian, A. Barka, C. Demir, S. Ergintav, I. Georgiev, O. Gurkan, M. Hamburger, K. Hurst, H. Kahle, et al. Global positioning system constraints on plate kinematics and dynamics in the eastern mediterranean and caucasus. *J. Geophys. Res.*, 105(B3):5695–5719, 2000.

A. McGarr, D. Simpson, and L. Seeber. 40 case histories of induced and triggered seismicity. *International Geophysics*, 81:647–661, 2002.

J.J. McGuire, M.S. Boettcher, and T.H. Jordan. Foreshock sequences and short-term earthquake predictability on east pacific rise transform faults. *Nature*, 434(7032):457–461, 2005.

C. McKernon and I.G. Main. Regional variations in the diffusion of triggered seismicity. *J. Geophys. Res.*, 110:B05S05, 2005.

C. Mendoza and S.H. Hartzell. Aftershock patterns and main shock faulting. *Bull. Seismol. Soc. Am.*, 78(4):1438 – 1449, 1988.

A.J. Michael. Spatial patterns of aftershocks of shallow focus earthquakes in california and implications for deep focus earthquakes. *J. Geophys. Res.*, 94(B5):5615–5626, 1989. ISSN 0148-0227.

T. Mikumo and T. Miyatake. Earthquake sequences on a frictional fault model with non-uniform strengths and relaxation times. *Geophys. J. Roy. Astron. Soc.,*, 59(3):497–522, 1979.

K. Mogi. Study of elastic shocks caused by the fracture of heterogeneous materials and its relations to earthquake phenomena. *Bull. Earthq. Res. Inst. Univ. Tokyo*, 40:125 – 173, 1962.

K. Mogi. Some discussions on aftershocks, foreshocks and earthquake swarms: the fracture of a semi-infinite body caused by an inner stress origin and its relation to the earthquake phenomena (third paper). *Bull. Earthq. Res. Inst. Univ. Tokyo*, 41:615–658, 1963. ISSN 0040-8972.

K. Mogi. Earthquakes and fractures. *Tectonophysics*, 5(1):35–55, 1967.

K. Mogi. Sequential occurrences of recent great earthquakes. *J. Phys. Earth*, 16(1):30–36, 1968.

GM Molchan and OE Dmitrieva. Aftershock identification: methods and new approaches. *Geophys. J. Int.*, 109(3):501–516, 1992. ISSN 1365-246X.

P. Molnar and W.P. Chen. Focal depths and fault plane solutions of earthquakes under the tibetan plateau. *J. Geophys. Res.*, 88(B2):1180–1196, 1983.

P. Molnar and H. Lyon-Caent. Fault plane solutions of earthquakes and active tectonics of the tibetan plateau and its margins. *Geophys. J. Int.*, 99(1):123–154, 1989.

P. Molnar and P. Tapponnier. Tectonics of asia: Consequences and implications of a continental collision. *Science*, 189:419–426, 1975.

P. Molnar and P. Tapponnier. Active tectonics of tibet. *J. Geophys. Res.*, 83(B11):5361–5375, 1978.

P. Molnar, T.J. Fitch, and FT Wu. Fault plane solutions of shallow earthquakes and contemporary tectonics in asia. *Earth Planet. Sci. Lett*, 19(2):101–112, 1973.

K. Nanjo, H. Nagahama, and M. Satomura. Rates of aftershock decay and the fractal structure of active fault systems. *Tectonophysics*, 287(1-4):173–186, 1998.

C. Narteau, P. Shebalin, M. Holschneider, J.L. Le Mouel, and CJ Allegre. Direct simulations of the stress redistribution in the scaling organization of fracture tectonics (soft) model. *Geophys. J. Int.*, 141(1):115–135, 2000. ISSN 1365-246X.

C. Narteau, P. Shebalin, and M. Holschneider. Temporal limits of the power law aftershock decay rate. *J. Geophys. Res*, 107:2359, 2002.

C. Narteau, S. Byrdina, P. Shebalin, and D. Schorlemmer. Common dependence on stress for the two fundamental laws of statistical seismology. *Nature*, 462(7273):642–645, 2009. ISSN 0028-0836.

J. Ni and J.E. York. Late cenozoic tectonics of the tibetan plateau. *J. Geophys. Res.*, 83: 5377–5384, 1978.

J. Noir, E. Jacques, S. Bekri, PM Adler, P. Tapponnier, and GCP King. Fluid flow triggered migration of events in the 1989 dobi earthquake sequence of central afar. *Geophys. Res. Lett.*, 24(18):2335–2338, 1997. ISSN 0094-8276.

A. Nur and J.R. Booker. Aftershocks caused by pore fluid flow? *Science*, 175:885–887, 1972.

Y. Ogata. Estimation of the parameters in the modified omori formula for aftershock frequencies by the maximum likelihood procedure. *J. Phys. Earth*, 31:115–124, 1983.

Y. Ogata. Seismicity analysis through point-process modeling: A review. *Pure Appl. Geophys.*, 155:471 – 507, 1999.

Y. Ogata. Statistical model for standard seismicity and detection of anomalies by residual analysis. *Tectonophysics*, 169(1-3):159–174, 1989. ISSN 0040-1951.

Y. Ogata. Detection of precursory relative quiescence before great earthquakes through a statistical model. *J. Geophys. Res.*, 97(B13):19845, 1992. ISSN 0148-0227.

Y. Ogata, T. Utsu, and K. Katsura. Statistical features of foreshocks in comparison with other earthquake clusters. *Geophys. J. Int.*, 121(1):233–254, 1995. ISSN 1365-246X.

Y. Okada. Internal deformation due to shear and tensile faults in a half-space. *Bull. Seismol. Soc. Am.*, 82(2):1018 – 1040, 1992. ISSN 0037-1106.

P.G. Okubo and K. Aki. Fractal geometry in the san andreas fault system. *J. Geophys. Res.*, 92(B1):345–355, 1987.

F. Omori. Investigation of aftershocks. *Rep. Earthquake Inv. Comm*, 2:103–139, 1894.

D.H. Oppenheimer, P.A. Reasenberg, and R.W. Simpson. Fault plane solutions for the 1984 morgan hill, california, earthquake sequence: Evidence for the state of stress on the calaveras fault. *J. Geophys. Res.*, 93(B8):9007–9026, 1988. ISSN 0148-0227.

T. Ouchi and T. Uekawa. Statistical analysis of the spatial distribution of earthquakes–variation of the spatial distribution of earthquakes before and after large earthquakes. *Phys. Earth Planet. In.*, 44(3):211–225, 1986. ISSN 0031-9201.

G. Ouillon and D. Sornette. Magnitude-dependent omori law: Theory and empirical study. *J. Geophys. Res.*, 110(B4):B04306, 2005. ISSN 0148-0227.

G. Ouillon, D. Sornette, and E. Ribeiro. Multifractal omori law for earthquake triggering: new tests on the california, japan and worldwide catalogues. *Geophys. J. Int.*, 178(1): 215–243, 2009.

B. Papazachos, N. Delibasis, N. Liapis, G. Moumoulidis, and G. Purcaru. Aftershock sequences of some large earthquakes in the region of greece. In *Papers presented at the Ninth Assembly of the European Seismological Commission held 1-7 August 1966 in Copenhagen*, page 313. Akademisk Forlag,(DBK), 1967.

BC Papazachos. Foreshocks and earthquake prediction. *Tectonophysics*, 28(4):213–226, 1975. ISSN 0040-1951.

T. Parsons. Global omori law decay of triggered earthquakes: Large aftershocks outside the classical aftershock zone. *J. Geophys. Res.*, 107(10.1029), 2002.

T. Parsons and A.A. Velasco. On near-source earthquake triggering. *J. Geophys. Res*, 114: B10307, 2009.

T. Parsons, R.S. Stein, R.W. Simpson, and P.A. Reasenberg. Stress sensitivity of fault seismicity- a comparison between limited-offset oblique and major strike-slip faults. *J. Geophys. Res.*, 104:20,183–20,202, 1999.

T. Parsons, R.S. Yeats, Y. Yagi, and A. Hussain. Static stress change from the 8 october, 2005 m= 7.6 kashmir earthquake. *Geophys. Res. Lett*, 33(6), 2006.

E. Pathier, E. J. Fielding, T. J. Wright, R. Walker, B. E. Parsons, and S. Hensley. Displacement field and slip distribution of the 2005 kashmir earthquake from sar imagery. *Geophys. Res. Lett.*, 33:L203, 10 2006.

G. Pegler and S. Das. Analysis of the relationship between seismic moment and fault length for large crustal strike-slip earthquakes between 1977-92. *Geophys. Res. Lett.*, 23 (9):905–908, 1996.

T.P. Peixoto, K. Doblhoff-Dier, and J. Davidsen. Spatiotemporal correlations of aftershock sequences. *J. Geophys. Res.*, 115:B10309, 2010.

J.D. Pelletier. Spring-block models of seismicity: Review and analysis of a structurally heterogeneous model coupled to a viscous asthenosphere. *Geocomplexity and the Physics of Earthquakes*, pages 27–42, 2000.

G. Peltzer and F. Saucier. Present-day kinematics of asia derived from geologic fault rates. *J. Geophys. Res.*, 101(27):943–27956, 1996.

Z. Peng, J.E. Vidale, C. Marone, and A. Rubin. Systematic variations in recurrence interval and moment of repeating aftershocks. *Geophys. Res. Lett*, 32:15, 2005.

Z. Peng, E. Vidale, M. Ishii, and A. Helmstetter. Seismicity rate immediately before and after mainshock rupture from high-frequency waveforms in japan. *J. Geophys. Res.*, 112: B03306, 2007.

H. Perfettini, J. Schmittbuhl, and A. Cochard. Shear and normal load perturbations on a two-dimensional continuous fault: 2. dynamic triggering. *J. Geophys. Res*, 108:2409, 2003.

A. Piersanti, G. Spada, R. Sabadini, and M. Bonafede. Geobal post-seismic deformation. *Geophys. J. Int.*, 120(3):544–566, 1995.

A. Piersanti, G. Spada, and R. Sabadini. Global postseismic rebound of a viscoelastic earth: Theory for finite faults and application to the 1964 alaska earthquake. *J. Geophys. Res.-ALL SERIES-*, 102:477–492, 1997.

F.F. Pollitz and I. Selwyn Sacks. The 1995 kobe, japan, earthquake: A long-delayed aftershock of the offshore 1944 tonankai and 1946 nankaido earthquakes. *Bull. Seism. Soc. Am*, 87(1):1–10, 1997.

P. Reasenberg. Second-order moment of central california seismicity, 1969–1982. *J. Geophys. Res.*, 90(B7):5479–5495, 1985. ISSN 0148-0227.

P. Reasenberg and WL Ellsworth. Aftershocks of the coyote lake, california, earthquake of august 6, 1979'a detailed study. *J. Geophys. Res.*, 87:10,637–10,655, 1982.

P. A. Reasenberg and R. W. Simpson. Response of regional seismicity to the static stress changes produced by the loma prieta earthquake. *Science*, 255:1687–1690, 1992a.

P.A. Reasenberg. Foreshock occurrence before large earthquakes. *J. Geophys. Res.*, 104 (B3):4755–4768, 1999a. ISSN 0148-0227.

P.A. Reasenberg. Foreshock occurrence rates before large earthquakes worldwide. *Pure Appl. Geophys.*, 155(2):355–379, 1999b. ISSN 0033-4553.

P.A. Reasenberg and R.W. Simpson. Response of regional seismicity to the static stress change produced by the loma prieta earthquake. *Science*, 255(5052):1687, 1992b.

R. Reilinger, S. McClusky, P. Vernant, S. Lawrence, S. Ergintav, R. Cakmak, H. Ozener, F. Kadirov, I. Guliev, R. Stepanyan, et al. Gps constraints on continental deformation in the africa-arabia-eurasia continental collision zone and implications for the dynamics of plate interactions. *J. Geophys. Res.*, 111(B5):B05411, 2006.

A. Replumaz. *Reconstruction de la zone de collision Inde-Asie: etude centrée sur l'Indochine.* PhD thesis, PhD thesis, 1999.

J.R. Rice and M.P. Cleary. Some basic stress diffusion solutions for fluid-saturated elastic porous media with compressible constituents. *Rev. Geophys. Space Phys*, 14(2):227–241, 1976.

K. Richards-Dinger, R.S. Stein, and S. Toda. Decay of aftershock density with distance does not indicate triggering by dynamic stress. *Nature*, 467(7315):583–586, 2010.

C.F. Richter. *Elementary seismology*. W. H. Freeman and Co., San Francisco, 1958.

B. Romanowicz. Spatiotemporal patterns in the energy release of great earthquakes. *Science*, 260(5116):1923, 1993.

J.B. Rundle, D.L. Turcotte, R. Shcherbakov, W. Klein, C. Sammis, et al. Statistical physics approach to understanding the multiscale dynamics of earthquake fault systems. *Rev. Geophys.*, 41(4):1019, 2003.

P.A. Rydelek and I.S. Sacks. Migration of large earthquakes along the san jacinto fault; stress diffusion from the 1857 fort tejon earthquake. *Geophys. Res. Lett.*, 28(16):3079–3082, 2001. ISSN 0094-8276.

A. Saichev and D. Sornette. Distribution of the largest aftershocks in branching models of triggered seismicity: Theory of the universal båth law. *Phys. Rev. E.*, 71(5):056127, 2005.

D.P. Schaff, G.C. Beroza, and B.E. Shaw. Postseismic response of repeating aftershocks. *Geophys. Res. Lett*, 25(24):4549–4552, 1998.

CH Scholz. Microfractures, aftershocks, and seismicity. *Bull. Seismol. Soc. Am.*, 58(3):1117 – 1130, 1968.

C.H. Scholz. *The mechanics of earthquakes and faulting*. Number pp. 471. Cambridge Univ Pr, 2002.

D. Schorlemmer, S. Wiemer, and M. Wyss. Variations in earthquake-size distribution across different stress regimes. *Nature*, 437(7058):539–542, 2005. ISSN 0028-0836.

AMC Sengor. The north anatolian transform fault: its age, offset and tectonic significance. *Journal of Geological Society*, 136(3):269 – 282, 1979.

AMC Sengor, Y. Yilmaz, and O. Sungurlu. Tectonics of the mediterranean cimmerides: nature and evolution of the western termination of palaeo-tethys. *Geol. Soc. Spec. Pub.*, 17(1):77 – 112, 1984.

AMC Sengor, D. Altiner, A. Cin, T. Ustaomer, and KJ Hsu. Origin and assembly of the tethyside orogenic collage at the expense of gondwana land. *Geol. Soc. Spec. Pub.*, 37(1):119 – 181, 1988.

B.E. Shaw. Generalized omori law for aftershocks and foreshocks from a simple dynamics. *Geophys. Res. Lett.*, 20(10):907–910, 1993. ISSN 0094-8276.

R. Shcherbakov, D.L. Turcotte, and J.B. Rundle. Scaling properties of the parkfield aftershock sequence. *Bull. Seismol. Soc. Am.*, 96(4B):S376–S384, 2006. ISSN 0037-1106.

BW Silverman. *Density estimation for statistics and data analysis*. Chapman & Hall/CRC, 1986.

D.W. Simpson and W. Leith. The 1976 and 1984 gazli, ussr, earthquakes–were they induced? *Bull. Seismol. Soc. Am.*, 75(5):1465 – 1468, 1985.

SK Singh and G. Suarez. Regional variation in the number of aftershocks (mb greater double equals 5) of large, subduction-zone earthquakes (mw greater double equals 7.0). *Bull. Seismol. Soc. Am.*, 78(1):230 – 242, 1988. ISSN 0037-1106.

SL Solovev and ON Soloveva. Exponential distribution of the total number of an earthquakes aftershocks and the decrease of their mean value with increasing depth. *Bull. Acad. Sci. USSR, Ser. Geophys*, pages 1053–1060, 1962.

D. Sornette and A Sornette. Self-organised criticality and earthquakes. *Europhys. Lett.*, 9: 197–202, 1989.

D. Sornette, C. Vanneste, and L. Knopoff. Statistical model of earthquake foreshocks. *Phys. Rev. A*, 45(12):8351–8357, 1992. ISSN 1094-1622.

S. Steacy, J. Gomberg, and M. Cocco. Introduction to special section: Stress transfer, earthquake triggering, and time-dependent seismic hazard. *J. Geophys. Res.-SOLID EARTH*, 110(B5):B05S01, 2005.

R.S. Stein. The role of stress transfer in earthquake occurrence. *Nature*, 402(6762):605–609, 1999.

R.S. Stein. Earthquake conversations. *Scientific American*, 288(1):72, 2003.

R.S. Stein and M. Lisowski. The 1979 homestead valley earthquake sequence, california: Control of aftershocks and postseismic deformation. *J. Geophys. Res.*, 88(B8):6477–6490, 1983. ISSN 0148-0227.

R.S. Stein, G.C.P. King, and J. Lin. Change in failure stress on the southern san andreas fault system caused by the 1992 magnitude= 7.4 landers earthquake. *Science*, 258(5086): 1328, 1992.

R.S. Stein, A.A. Barka, and J.H. Dieterich. Progressive failure on the north anatolian fault since 1939 by earthquake stress triggering. *Geophys. J. Int.*, 128(3):594–604, 1997.

J. Stocklin. Structural history and tectonics of iran: a review. *AAPG Bulletin*, 52(7): 1229–1258, 1968.

M. Tahir and JR Grasso. Triggered earthquakes and earthquake interactions: the role of the focal mechanisms. In *AGU Fall Meeting Abstracts*, page 1438, 2009.

M. Tahir and JR. Grasso. How much does the seismic slip orientation control the aftershocks patterns ? worldwide earthquake catalogue analysis. *JGR*, (submitted), 2011.

M. Tahir, M.A. Shah, JR Grasso, M. Qaisar, and J. Iqbal. Probabilistic seismic hazard assessment for quetta and surrounding region. ASCE, 2009.

M. Tahir, JR. Grasso, and D Amorèse. The largest aftershock: how strong, how far away, how delayed? *Geophys. Res. Lett.*, submitted, 2011.

F. Tajima and H. Kanamori. Aftershock area expansion and mechanical heterogeneity of fault zone within subduction zones. *Geophys. Res. Lett.*, 12(6):345–348, 1985a. ISSN 0094-8276.

F. Tajima and H. Kanamori. Global survey of aftershock area expansion patterns. *Phys. Earth Planet. In.*, 40:77–134, 1985b. ISSN 0031-9201.

M. Talebian and J. Jackson. A reappraisal of earthquake focal mechanisms and active shortening in the zagros mountains of iran. *Geophys. J. Int.*, 156(3):506–526, 2004.

P. Tapponnier and P. Molnar. Active faulting and tectonics in china. *J. Geophys. Res.*, 82 (20), 1977.

F. Tavakoli, A. Walpersdorf, C. Authemayou, HR Nankali, D. Hatzfeld, M. Tatar, Y. Djamour, F. Nilforoushan, and N. Cotte. Distribution of the right-lateral strike-slip motion from the main recent fault to the kazerun fault system (zagros, iran): evidence from present-day gps velocities. *Earth Planet. Sci. Lett.*, 275(3-4):342–347, 2008.

JC Thomas, PR Cobbold, VS Shein, and S. Le Douaran. Sedimentary record of late paleozoic to recent tectonism in central asia—analysis of subsurface data from the turan and south kazak domains. *Tectonophysics*, 313(3):243–263, 1999a.

J.C. Thomas, J.R. Grasso, R. Bossu, J. Martinod, and B. Nurtaev. Recent deformation in the turan and south kazakh platforms, western central asia, and its relation to arabia-asia and india-asia collisions. *Tectonics*, 18(2):201 – 214, 1999b.

S. Toda and R.S. Stein. Did stress triggering cause the large off-fault aftershocks of the 25 march 1998 m˜ w= 8.1 antarctic plate earthquake? *Geophys. Res. Lett.*, 27(15): 2301–2304, 2000.

S. Toda and R.S. Stein. Response of the san andreas fault to the 1983 coalinga-nunez earthquakes: An application of interaction-based probabilities for parkfield. *J. Geophys. Res*, 107:2126, 2002.

S. Toda, RS Stein, PA Reasenberg, and JH Dieterich. Stress transferred by the mw= 6.5 kobe, japan, shock: Effect on aftershocks and future earthquake probabilities. *J. Geophys. Res*, 103(24):54324, 1998.

S. Toda, R.S. Stein, K. Richards-Dinger, and S. Bozkurt. Forecasting the evolution of seismicity in southern california: Animations built on earthquake stress transfer. *J. Geophys. Res.*, 110(10.1029), 2005.

P. Tosi, V. De Rubeis, V. Loreto, I. Centro, L. Pietronero, et al. Space-time combined correlation integral and earthquake interactions. *Ann. Geophys.*, 47:1849, 2004.

VI Ulomov. Implication of horizontal tectonic movements for seismogeodynamics and seismic hazard prediction. *Izvestiya Physics of the Solid Earth*, 40(9):710–724, 2004.

T. Utsu. A statistical study on the occurrence of aftershocks. *Geophys. Mag*, 30(4):521–605, 1961.

T. Utsu. Aftershocks and earthquake statistics (1): Some parameters which characterize an aftershock sequence and their interrelations. *Journal of the Faculty of Science, Hokkaido University. Series 7, Geophysics*, 3(3):129–195, 1970.

T. Utsu. Statistical features of seismicity, international handbook of earthquake and engineering seismology, 81a. elservier. pages 719–732., 2002.

T. Utsu and A. Seki. A relation between the area of aftershock region and the energy of main shock. *J. Seism. Soc. Japan*, 7:233–240, 1954.

T. Utsu, Y. Ogata, and RS Matsu'ura. The centenary of the omori formula for a decay law of aftershock activity. *J. Phys. Earth*, 43(1):1–33, 1995.

D. Vere-Jones. A note on the statistical interpretation of bath's law. *Bull. Seismol. Soc. Am.*, 59(4):1535–1541, 1969. ISSN 0037-1106.

D. Vere-Jones. A limit theorem with application to båth's law in seismology. *Adv. Appl. Probab.*, 40(3):882–896, 2008.

C. Voisin. Dynamic triggering of earthquakes: the nonlinear slip-dependent friction case. *J. Geophys. Res.*, 107(B12):2356, 2002.

D. L. Wells and K. J. Coppersmith. New empirical relationships among magnitude, rupture length, rupture width, rupture area, and surface displacement. *Bull. Seismol. Soc. Am.*, 84(4):974–1002, 1994.

R.L. Wesson. Modelling aftershock migration and afterslip of the san juan bautista, california, earthquake of october 3, 1972. *Tectonophysics*, 144(1-3):215–229, 1987. ISSN 0040-1951.

S. Wiemer and K. Katsumata. Spatial variability of seismicity parameters in aftershock zones. *J. Geophys. Res.*, 104(B6):13135, 1999.

S. Wiemer and M. Wyss. Minimum magnitude of completeness in earthquake catalogs: examples from alaska, the western united states, and japan. *Bull. Seismol. Soc. Am.*, 90 (4):859 – 869, 2000.

J. Woessner and S. Wiemer. Assessing the quality of earthquake catalogues: estimating the magnitude of completeness and its uncertainty. *Bull. Seismol. Soc. Am.*, 95(2):684–698, 2005.

Y. Yamanaka and K. Shimazaki. Scaling relationship between the number of aftershocks and the size of the main shock. *J Phys Earth*, 38(4):305–324, 1990. ISSN 0022-3743.

T. Yamashita and L. Knopoff. Models of aftershock occurrence. *Geophys. J. Roy. Astron. Soc.*, 91(1):13–26, 1987.

T. Yamashita and L. Knopoff. A model of foreshock occurrence. *Geophys. J. Int.*, 96(3): 389–399, 1989. ISSN 1365-246X.

T. Yamashita and L. Knopoff. Model for intermediate-term precursory clustering of earthquakes. *J. Geophys. Res.*, 97(B13):19873, 1992. ISSN 0148-0227.

W. Yang and Y. Ben-Zion. Observational analysis of correlations between aftershock productivities and regional conditions in the context of a damage rheology model. *Geophys. J. Int.*, 177(2):481–490, 2009.

Y. Zeng. Viscoelastic stress-triggering of the 1999 hector mine earthquake by the 1992 landers earthquake. *Geophys. Res. Lett.*, 28(15):3007–3010, 2001. ISSN 0094-8276.

J. Zhuang, Y. Ogata, and D. Vere-Jones. Analyzing earthquake clustering features by using stochastic reconstruction. *J. Geophys. Res.*, 109(B5):B05301, 2004. ISSN 0148-0227.

A. Ziv. Foreshocks, aftershocks, and remote triggering in quasi-static fault models. *J. Geophys. Res*, 108(2498):10–10, 2003.

A. Ziv. What controls the spatial distribution of remote aftershocks? *Bull. Seismol. Soc. Am.*, 96(6):2231 – 2241, 2006a.

A. Ziv. Does aftershock duration scale with mainshock size? *Geophys. Res. Lett*, 33: L17317, 2006b.

A. Ziv, AM Rubin, and D. Kilb. Spatiotemporal analyses of earthquake productivity and size distribution: observations and simulations. *Bull. Seismol. Soc. Am.*, 93(5):2069, 2003.

S. Hainzl M. Holschneider Zöller, G. and Y. Ben-Zion. Aftershocks resulting from creeping sections in a heterogeneous fault. *Geophys. Res. Lett.*, 32, 2005.